Soil Forensics

Mariano Mercurio
Alessio Langella
Rosa Maria Di Maggio
Piergiulio Cappelletti *Editors*

Mineralogical Analysis Applied to Forensics

A Guidance on Mineralogical Techniques and Their Application to the Forensic Field

Springer

Soil Forensics

Series Editor
Patrick Randolph-Quinney, Dept. of Appl. Sc., Fac. of Health & L.S,
Northumbria University, Newcastle-upon-Tyne, UK

Soil Forensics aims to provide a transdisciplinary overview of all relevant forensic fields which interact with the soil environment and Earth-system processes. This includes disciplines such as forensic archaeology, forensic taphonomy and anthropology, geophysics and remote sensing, forensic geology and soil science, forensic ecology, and environmental forensics. Volumes in the series are intended to stimulate multidisciplinary and transdisciplinary approaches at the interface of forensics and the many sub-disciplines in Earth Sciences, Archaeology and others, such as traditional soil science, palynology, geochemistry, biogeochemistry, sedimentology, field archaeology, archaeological prospection, and taphonomy. The series will include investigation into:

- Human taphonomy and experimental decomposition studies
- Experimental standards development and validation
- Violation of the environment (chemical exposure, pollution, illegal mining)
- Search, detection, identification, and recovery of human remains in soil context
- New methods and techniques in soil forensics such as proteomics, magnetic surveys, electrical imaging techniques, and UAV-based spectroscopy and remote sensing
- Application of AI and Machine learning approaches to complex forensic issues
- 3D and 4D modelling, visualization, and spatial analyses (including the use of Geographical Information Systems)
- Stratigraphy, stratification and soil context
- Linking research-based knowledge to the community of action, with a focus on knowledge transfer and practice-informed research
- Degradation studies of organic and inorganic anthropogenic materials in soils.

The Soil Forensics Series was originally developed by the late Professor Henk Kars from the Institute of Geo- and Bioarchaeology at VU University Amsterdam. The current Series Editor and Editorial Board will continue to adhere to the interdisciplinary interplay between the sciences and humanities that distinguished Professor Kars' academic career.

Mariano Mercurio • Alessio Langella
Rosa Maria Di Maggio • Piergiulio Cappelletti
Editors

Mineralogical Analysis Applied to Forensics

A Guidance on Mineralogical Techniques and Their Application to the Forensic Field

Springer

Editors
Mariano Mercurio
Department of Science & Technology
Sannio University
Benevento, Italy

Rosa Maria Di Maggio
Forensic Geoscience Italy
Geoscienze Forensi Italia®
Roma, Italy

Alessio Langella
Department of Earth, Environmental and Resources Sciences (DiSTAR)
Federico II University
Napoli, Italy

Piergiulio Cappelletti
Department of Earth, Environmental and Resources Sciences (DiSTAR)
Federico II University
Napoli, Italy

ISSN 2214-4293 ISSN 2214-4315 (electronic)
Soil Forensics
ISBN 978-3-031-08833-9 ISBN 978-3-031-08834-6 (eBook)
https://doi.org/10.1007/978-3-031-08834-6

This Springer imprint is published by the registered company Springer Nature Switzerland AG
The registered company address is: Gewerbestrasse 11, 6330 Cham, Switzerland

Preface

This book, edited by an experienced group of scientists from a diverse and complementary range of backgrounds, is a wonderful collection of papers from a range of very important areas in the application of minerals pertaining to the law. It discusses the main approaches which can be used in the examination, characterisation and comparison of minerals, whether as part of a rock sample or minerals within a soil.

Soil forensic investigations often involves the collection of soil samples from a crime scene location and the recovery of soil from a questioned item, such as boots, vehicles or tools, followed by a process of soil description, characterisation and the application of appropriate analysis. Integration and extrapolation of the soil information can then be scaled up to build a coherent model of soil information – from the initial trace sample observations to the landscape scale, which often involves soil/geological/land cover maps and geographical information systems (GIS) and appropriate evaluation of the ensuing results. Established concepts and standardised approaches in geology and mineralogy are vitally important in the appropriate application of geology within the criminal justice systems worldwide, and our global safety and security depends upon the sharing of best practices and collaboration. Such quality best practice approaches can also apply to the application of forensic mineralogy in field, wildlife, art, ballistics and drug crime.

This book features both advantages and disadvantages of a range of inorganic methods that can be adopted and recommends when and where to use the different approaches. Type of sample, size and type of analysis method, whether the method is destructive or non-destructive, sampling procedures, and analytical conditions and accreditation are discussed. The chapters focus on analytical approaches using optical microscopy, X-ray diffraction, electron microscopy, infrared spectroscopy, Raman spectroscopy, X-ray fluorescence, STA[1] and much more. In addition, this book illustrates the academic text with actual case examples, putting into context many of the procedures recommended. Studies on criminal offenses against persons, environment and cultural heritage are illustrated.

[1] Simultaneous thermal analysis.

This book is primarily of use to the academic population, as well as practising geo scientists, with some information also of use for servants of the criminal justice system, in particular, in those countries with an inquisitorial system.

This well-written publication illustrates how excellent strategic science applied across many scientific disciplines can assist in both the investigation of crime and its use as evidence in court, and can make our criminal justice systems safer, no matter which legal jurisdiction or which part of the world we live in. A 'must have' volume for the shelves of a forensic geologist's library.

The James Hutton Institute, Aberdeen, Scotland - IUGS Initiative on Forensic Geology
Aberdeen, Scotland

Lorna Dawson

Contents

Contributors

Pasquale Acquafredda Dipartimento di Scienze della Terra e Geoambientali, Università degli Studi di Bari Aldo Moro, Bari, Italy

Centro Interdipartimentale "Laboratorio di Ricerca per la Diagnostica dei Beni Culturali", Campus Universitario, Bari, Italy

Ilenia Arienzo Sezione Osservatorio Vesuviano, Istituto Nazionale di Geofisica e Vulcanologia (INGV), Sez. Osservatorio Vesuviano, Napoli, Italy

Giuseppina Balassone Dipartimento di Scienze della Terra, dell'Ambiente e delle Risorse (DiSTAR), Università Federico II, Napoli, Italy

Donatella Barca Dipartimento di Biologia, Ecologia e Scienze della Terra, Università della Calabria, Cosenza, Italy

Fabio Bellatreccia Dipartimento di Scienze, Sez. Scienze Geologiche, Università Roma Tre, Roma, Italy

Anton Beran Institut für Mineralogie und Kristallographie, Universität Wien, Wien, Austria

David L. Bish Molecular Structure Center, Indiana University, Bloomington, IN, USA

Geoffrey D. Bromiley School of Geosciences, University of Edinburgh, Grant Institute, Edinburgh, UK

Piergiulio Cappelletti Dipartimento di Scienze della Terra, dell'Ambiente e delle Risorse (DiSTAR), Università Federico II di Napoli, Napoli, Italy

Massimo D'Antonio Dipartimento di Scienze della Terra, dell'Ambiente e delle Risorse (DiSTAR), Università Federico II, Napoli, Italy

Fábio Augusto da Silva Salvador Federal Police of Brazil, Curitiba, Brazil

IUGS Initiative on Forensic Geology, Curitiba, Brazil

Monica Alvarez de Buergo Instituto de Geociencias IGEO, Consejo Superior de Investigaciones Científicas (CSIC) and Universidad Complutense de Madrid (UCM), Madrid, Spain

Roberto De Gennaro Dipartimento di Scienze della Terra, dell'Ambiente e delle Risorse (DiSTAR), Università Federico II, Napoli, Italy

Rosa Maria Di Maggio Geoscienze Forensi Italia® – Regional Officer for Europe of IUGS Initiative on Forensic Geology, Roma, Italy

Valeria Di Renzo Dipartimento di Scienze della Terra, dell'Ambiente e delle Risorse (DiSTAR), Università Federico II, Napoli, Italy

G. Diego Gatta Dipartimento di Scienze della Terra, Università degli Studi di Milano, Milano, Italy

Chiara Germinario Department of Sciences and Technologies, University of Sannio, Benevento, Italy

Sossio Fabio Graziano Dipartimento di Farmacia, Università Federico II di Napoli, Napoli, Italy

Celestino Grifa Department of Sciences and Technologies, University of Sannio, Benevento, Italy

F. Javier Huertas Instituto Andaluz de Ciencias de la Tierra CSIC – Universidad de Granada, Granada, Spain

Francesco Izzo Dipartimento di Scienze della Terra, dell'Ambiente e delle Risorse (DiSTAR), Università Federico II, Napoli, Italy

Alessio Langella Dipartimento di Scienze della Terra, dell'Ambiente e delle Risorse (DiSTAR), Università Federico II, Napoli, Italy

Mauro Francesco La Russa Dipartimento di Biologia, Ecologia e Scienze della Terra, Università della Calabria, Cosenza, Italy

Luciana Mantovani Dipartimento di Scienze Chimiche della Vita e della Sostenibilità Ambientale, Università di Parma, Parma, Italy

Mariano Mercurio Dipartimento di Scienze e Tecnologie, Università degli Studi del Sannio, Benevento, Italy

Paola Petrosino Dipartimento di Scienze della Terra, dell'Ambiente e delle Risorse (DiSTAR), Università Federico II, Napoli, Italy

Duncan Pirrie School of Applied Science, Faculty of Computing, Engineering and Science, University of South Wales, Pontypridd, UK

IUGS Initiative on Forensic Geology, Pontypridd, UK

Silvestro Antonio Ruffolo Dipartimento di Biologia, Ecologia e Scienze della Terra, Università della Calabria, Cosenza, Italy

Licia Santoro Dipartimento di Scienze della Terra, Università di Torino, Torino, Italy

Binoy Sarkar Future Industries Institute, University of South Australia, Mawson Lake, Australia

Dominik Talla Institut für Mineralogie und Kristallographie, Universität Wien, Wien, Austria

David Widory Département des Sciences de la Terre et de l'Atmosphère, Université du Québec à Montréal, Montréal, Canada

Chapter 1
Optical Microscopy Applied to Forensics

Rosa Maria Di Maggio and Fábio Augusto da Silva Salvador

Abstract Optical microscopy is suitable for numerous applications ranging from various fields of research such as mineralogy, entomology, botany, medicine, surgery, and various sectors of industrial production. As far as forensic applications are concerned, it maintains a prominent position as an important tool for the examination of the evidence. Actually, optical microscopy has always been a key application in judicial investigations and, until the early 1900s, it has been the forensic scientists' main tool. At present, although highly advanced analytical techniques support forensic scientists for characterizing and identifying traces linked to a particular offence, optical microscopy continues to play an important role, especially in the early stages of laboratory investigation. Optical microscopy can provide direct information when there are comparative materials associated with suspects, or indirect information when compared with databases dedicated to forensic science applications. The most used optical microscopy tools for forensic purposes on a wide range of materials are the stereoscopic microscope and the polarized light microscope (PLM).

Keywords Optical microscopy · Stereoscopic microscope · Polarizing light microscope · Forensic science · Geological materials

R. M. Di Maggio (✉)
Geoscienze Forensi Italia® – Regional Officer for Europe of IUGS Initiative on Forensic Geology, Rome, Italy
e-mail: dimaggio@geologiaforense.com

F. A. da Silva Salvador
Federal Police of Brazil, Curitiba, Brazil

IUGS Initiative on Forensic Geology, Curitiba, Brazil

M. Mercurio et al. (eds.), *Mineralogical Analysis Applied to Forensics*, Soil Forensics, https://doi.org/10.1007/978-3-031-08834-6_1

In the collective imaginary, the forensic scientist has always been inextricably linked to the microscope. Just consider the famous investigator Sherlock Holmes, the central character of the works of Sir Arthur Conan Doyle, who is portrayed with his microscope and magnifying glass.

Effectively, optical microscopy has always played a key role in judicial investigations and, before the great technological developments experienced since the early 1900s, it was the only investigative tool used by forensic scientists (Fig. 1.1).

The journal *Scientific American*, in its edition "Science and Art: Curious use of the microscope" (1856), records the earliest use of microscopy for analysing sediments for forensic purposes, whereby Christian Ehrenberg, the famous Berlin professor, was asked to analyse some sand. Along the Prussian railway, barrels containing silver coins were emptied and filled with sand, somewhere between the departure and final destination. The case of substitution, where the coins were replaced by sand, was discovered only at the final destination. With the help of a microscope, Ehrenberg compared the sand collected from each intermediate stop of

Fig. 1.1 Powell and Lealand No. 1 monocular microscope, dated 1908, very popular at the time when Sherlock Holmes' stories were published. (Courtesy of Dr. Allan Wissner, www.antique-microscopes.com)

the train with the sand contained in the barrels and indicated the station where the swap had been made. Interviews by the police established a possible suspect, who later confessed (Ruffell 2009).

Optical microscopy has played an integral part in forensic science since the early part of the last century. In 1928, E. Locard established the practical and theoretical underpinnings of the microscopic examination to trace the amounts of evidence (Houck 1992). The "exchange principle of evidence" was so developed: *whenever two objects come into contact, there is always a transfer of material. The methods of detection may not be sensitive enough to demonstrate this or the decay rate may be so rapid that all evidence of transfer has vanished after a given time; nonetheless, the transfer had taken place*. At present, although highly advanced analytical techniques support forensic scientists for characterizing and identifying traces linked to a particular offence, optical microscopy continues to play an important role, especially in the early stages of laboratory investigation.

The most used optical microscopy tools for forensic purposes on a wide range of materials are the stereoscopic microscope and the polarized light microscope (PLM). These two are employed with different pieces of equipment and configurations. Generally, the optical microscopes have an upper structure for the photographic connection, which allows the microscopes to be interfaced with a camera or video camera, or a built-in digital camera (CCD or CMOS) interfaced with a computer. Each camera has its operating software that acquires images and videos and carries out image processing and analysis, angular, linear and areal measurements (see Chap. 10).

1.1 Stereoscopic Microscope: Instrumentation and Analysis Procedures

The stereoscopic microscope, or stereo-microscope, is an instrument designed to provide a spatial and "realistic" view of the sample under examination. For this purpose, the instrument is provided with two separate and differently aligned optical paths to return differently angled images for the right and left eyes. The determinations in stereoscopic microscopy help to study the surfaces of solid samples and to inspect details that are not visible to the naked eye or at low magnification.

Microscopes are generally made up of structural parts for holding and supporting the microscope and its components, and the optical parts which are used for magnification and viewing of the specimen images (Fig. 1.2):

– The stage (or base), where the specimen is placed for viewing, generally equipped with stage clips;
– The arm, where the adjustments knobs are placed. The knobs are used to change the focus of the microscope. These are of two types: fine adjustment knobs and coarse adjustment knobs. The arm connects the base to the head and gives

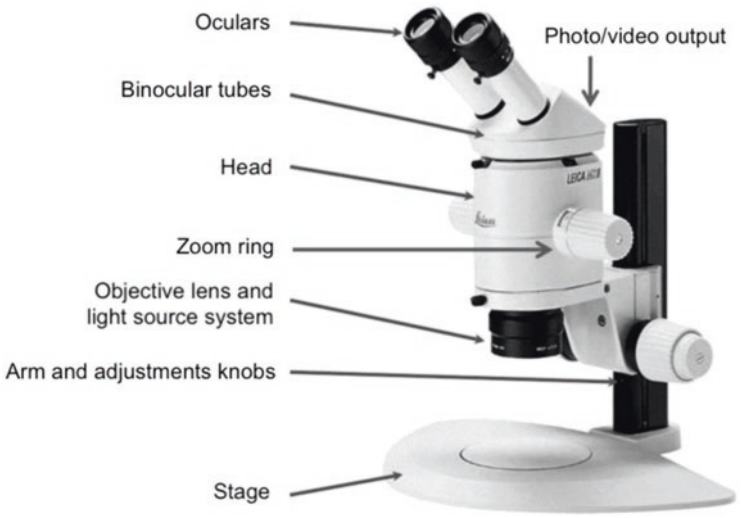

Fig. 1.2 Stereoscopic microscope and its components. (Courtesy of Dr. Luca Pascucci, Leica Microsystems)

support to the head of the microscope. High-quality microscopes have an articulated arm with more than one joint allowing more movement of the microscopic head for better viewing;

– The head (also known as the body) contains in the lower part the objective lens and the light source system, in the medium part the zoom ring, and in the upper part the eyepiece tubes;
– The objective lens has a fixed magnification power (generally 1×). The fixed objective can be replaced with other objectives with different magnification, generally 0.3×, 0.5×, 1.5×, and 2.0×. These adjunctive objectives vary the total magnification and the working distance, which is the distance between the specimen and the objectives. In microscopes with two objectives, a revolver holds the objectives and allows to align the selected objective with the optical path;
– The light source system is a cold light annular lighting system (or close to the color temperature of daylight) that can be fluorescent or LED. It illuminates the specimen without creating shadow spots;
– The zoom ring allowing further magnification determined by the objective and the eyepieces is graduated and has a click-stop accordingly with the main step of magnification (generally from 0.65× to 4.5×);
– The eyepieces and the eyepiece tubes, also known as the oculars, have diopter adjustment (the eyepiece tube is flexible and can be rotated for maximum visualization, for variance in distance) and blinders. The standard eyepieces have 10 magnifications but they can be replaced with eyepieces of 15×, 20×, 25× or 30×, with the consequent increase of total magnification with the same work distance;

– The photo/video output is placed on the upper side of the head, behind the eyepieces. Many of the stereomicroscopes are equipped with a third optical output to a camera or a video camera (eventually USB) interfaced with a computer for taking digital photos and/or measurements using image analysis programs.

1.1.1 Magnification

The microscope's total magnification is given by the mathematical product between the magnification of the eyepieces and the magnification of the objective; for example, with 10× eyepieces and 1× objective, total magnifications are 10×. The stereomicroscope allows the use of different magnifications and zooms, ranging from 7× to 180× and can reach up to 250× in the case of more advanced instruments for professional purposes; however, it must always be borne in mind that very high magnifications do not permit to have a large depth of field, therefore their use is recommended for the observation of objects with flat surfaces and regular morphology.[1] The optimal magnification range of the stereomicroscope is typically between 8× and 50×, lower magnifications respect those of the biological microscope. Although the lower magnification of the stereomicroscope as compared to the biological microscope may appear to be a limitation, it has its advantages. It is suitable for observing objects without necessarily making sample preparations.

1.1.2 Lighting System

The specimen is illuminated by incident light, with LED technology, which allows the study of thick or opaque objects. Therefore, in a stereoscopic microscope, the light reflected from the sample is observed. However, for the observation of transparent three-dimensional objects, modern stereomicroscopes can be configured to operate with transmitted lighting using a lamp or mirror underneath a transparent support placed below the object.

Generally, some microscopes are accompanied by separated cold light optical fibres illuminators, adjustable in intensity, and with flexible light conductors. These are useful for intensely lighting up even very small objects, up close and without heat development. It also helps in carrying out observations with different angles of light, up to the condition of raking light.

Almost all laboratory brightfield microscopes can be easily converted for use with darkfield illumination, using a special condenser, which allows only oblique

[1] 3D measurements are achieved with a digital microscope by image stacking. Using a stepping motor, the system takes images from the lowest focal plane in the field of view to the highest focal plane. The images are reconstructed into a contrast-based 3D model to provide a 3D color image of the sample.

light rays to illuminate the specimen on the microscope stage. Through the condenser, the image is formed by light rays diffused by the sample and captured by the lens, while the light that is directly reflected does not give any contribution to the formation of the image. Darkfield microscopy is ideal for detecting edges, margins, boundaries, refractive index gradients, which often cannot be appreciated in brightfield analysis and is particularly useful for observing minerals, gems, chemical crystals, colloidal particles, inclusions and porosities of glass, ceramics and thin sections of polymers.

1.1.3 Diagnostic Characteristics for the Study of Various Materials

The physical characteristics of the materials observable under a stereoscopic microscope are the shape, size, morphology of the surfaces, brightness, colour and structure.

The study of the shapes and morphology of the surfaces can provide useful information depending on the material observed (for example, the study of the shape of the clasts provides information on the environmental processes of erosion, transport, and sedimentation. See Sect 1.3.2.1). The study of the relative dimensions and geometries can be carried out with dedicated software for image analysis. The description of brightness and structure generally includes qualitative terms based on mere observation.

1.2 Polarized Light Microscope: Instrumentation and Analysis Procedures

The polarized light microscope (PLM) is an instrument designed for recognising birefringent materials at a micro-scale, observed in thin sections. The observation is based on birefringence, a physical phenomenon consisting of the decomposition of light into two different rays (ordinary and extraordinary rays) that occurs when it passes through particular anisotropic materials, depending on the polarization of the light.[2] The recognition at the microscopic scale is based on the observation of the constituents and the structure, and of some specific optical properties of the birefringent materials, when they are crossed by the polarized light.

The main components of a polarizing microscope are illustrated in Fig. 1.3:

– The transmitted light source system, consisting of an incandescent bulb or a LED light, whose luminous intensity can be suitably adjusted;

[2] Please refer to dedicated didactic texts for the birefringence of anisotropic materials.

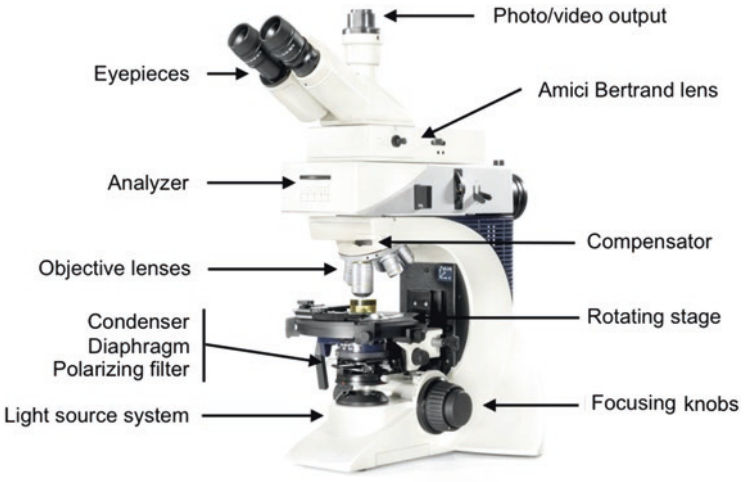

Fig. 1.3 Polarizing light microscope and its components

- The polarizing filter (or nicol). The light that passes through this element undergoes a modification: it becomes polarized from simple natural light, and the polarization plane is usually horizontal;
- The diaphragm, which has the function of regulating the quantity of light that passes through the specimen under observation;
- The condenser, placed above the diaphragm, that, when suitably inserted, determines a variation in the propagation of the light rays, which pass from parallel to convergent. This assessment allows conoscopic observations as opposed to orthoscopic observations in parallel light;
- The rotating stage, where the specimen under examination is placed. The stage, equipped with clips, can be raised or lowered utilizing two focusing knobs (coarse and fine). It can be rotated around a vertical axis and is equipped with a goniometer (with 360 degrees marked in 1-degree increments around the edge of the stage) and a vernier for angular measurements;
- The objective lenses, mounted on a revolver, through which choosing the most suitable objective for the observations is possible. Usually, the most common objectives are 2.5×, 4×, 10×, 20×, 40× and 60× (or 63×) magnification, but each microscope can have a different configuration, customizable by the user;
- The compensator, a specially-cut oriented filter of biaxial minerals (generally a gypsum plate) inserted in a slot at 45°, that is devoted to determining optical sign of minerals and, in extreme cases, the mineral order when needed;
- The analyzer (a second polarizer/nicol) with the polarization plane at 90° (usually vertical) with respect to the polarizing filter. The observation of specimen at nicols arrangement is parallel without an inserted analyzer and crossed with it;
- The Amici-Bertrand lens is located between the objective and the eyepiece. It is a small convergent lens used for the conoscopic analysis of thin sections and examination of the interference figure, a feature useful for the identification of

the studied minerals. This lens focuses an image of the upper focal plane of the objective in the focal plane of the eyepiece. It is also used to quickly verify an aperture's center, size, and uniform illumination;
– The eyepieces, equipped with a crucifix consisting of two graduated lines (useful for linear measurements) oriented vertically and horizontally, exactly like the polarization planes of the analyzer and polarizer;
– Photo/video output aimed at interfacing the microscope with a computer for taking digital photos and/or measurements utilizing image analysis programs.

1.2.1 Sample Preparation

The study of materials with the polarizing microscope is carried out on special preparations called thin sections that permit the polarized light to pass through the material under examination. Thin sections are very small slices with a thickness fixed at about 30 μm and glued to a support microscope glass slide.

The preparation of the thin sections takes place in several stages. The first stage is the cutting of the material with a circular saw consisting of a diamond blade to create a block of about 2 × 3 cm area and 0.5–1 cm thickness. Unconsolidated materials, such as sands or soils, are previously incorporated in epoxy resin to obtain coherent and solid cylinders which are cut into sheets of about 100 μm thickness using microtomes. The block and/or sheets are sanded and polished with silicon carbide abrasive pastes with decreasing granulometry (generally from 100, 60 and 12 μm) until a perfectly flat and shiny surface is obtained. They are then glued to the support slide usually using an epoxy resin with refractive index similar to that of quartz, equal to about 1.544–1.553. Subsequently, the free surface of the block and/or the sheet are progressively sanded and polished using abrasive pastes with decreasing grain to reach the required thickness of 30 μm and protected with a coverslip (Cucciniello et al. 2019).

1.2.2 Different Light Arrangements and Optical Diagnostic Characteristics of Anisotropic Materials[3]

The polarized light determinations for a thin section of material follow a logical operational sequence. The first observations to be made are those in which the propagative direction of the polarized light is parallel to the axis of the microscope (orthoscopic conditions).

[3] Please refer to dedicated didactic texts regarding the optical behaviour of minerals and their recognition.

In orthoscopic conditions, there are two possible arrangements of light: polarizer only or crossed polarizers. In the first case, only the polarizer is in the optical path of the microscope; this setup allows the following evaluations: shape,[4] habit,[5] refractive index, color and pleochroism,[6] presence of inclusions, degree of alteration, traces of corrosion, type of fracture, and flaking.[7] The crossed polarizers arrangement involves the use of the analyzer, whose vibration plane is at right angles to that of the polarizer. Crossed polarizers observations allow the analysis of all light interference phenomena that occur inside the material when the polarized light passing through is broken down in two vibration directions (ordinary and extraordinary rays). Employing this arrangement, birefringence,[8] determination of the optical and crystallographic orientations, mineral extinction types, eventual mineral zoning,[9] and crystal twinning[10] can be analysed.

Subsequent determinations are carried out in conoscopic conditions, where the polarized light beams are made convergent by the use of an additional lens, the condenser. A further lens (Amici-Bertrand lens) inserted along the optical path produces an interference figure that provides further data on the optical features of the investigated mineral, such as the optic indicatrix, optical sign, as well as the angle between the optical axes (Di Maggio and Barone 2017).

[4] The shape represents the degree of crystallinity of a mineral, which depends mainly on the growth conditions. The shape of minerals in a thin section is not a particularly diagnostic property as they are conductive to its growth, rather than on the intrinsic characteristics of the mineral.

[5] The habit is the morphology of a mineral and depend on its degree of symmetry. In thin section, it is not always easy to trace the morphology of a three-dimensional mineral through the observation of the two-dimensional morphologies.

[6] Pleochroism depends on the fact that some colored and optically anisotropic minerals are characterized by a different absorption of light according to their orientation with respect to the incident light.

[7] The flaking traces can be relevant for diagnostic purposes as well as the angle of intersection between two or more cleavage systems in the same mineral. It is important to be very careful and not confuse the traces of flaking with any fractures that may be present in a mineral subjected to mechanical stress. The key difference is that the fracture surfaces are usually very irregular.

[8] Birefringence is a quantitative measure of double refraction. In crossed nicol observations, birefringence produces the appearance of particular colors, called interference colors, which depend on the difference existing in the propagation speed of ordinary and extraordinary rays.

[9] Zoning is a property that can be observed in some minerals when the chemical composition does not remain constant throughout the mineral. Areas with different composition have a different optical behaviour showing different interference colors and extinguishing at different angles as the stage rotates.

[10] Twinning is a property observable when a single mineral appears to be made up of two or more individuals showing a generally symmetrical arrangement between them. The individuals that make up a geminate usually have a different orientation of the crystallographic axes and therefore show different interference colors.

1.2.3 Semi-quantitative Analysis

Polarizing microscope observations of geo-materials also allow semi-quantitative analysis of the sample components. This analysis is performed with the aid of an integrator table mounted on the rotating stage and applied on the sample, which allows micrometric linear displacements according to the two fundamental x, y directions on a Cartesian plane. Using these movements, it is possible to perform a count, manual or electronic, of granules' number of each mineralogical species (from 1000 to 2000 units). The granules of each species are counted separately so that there are as many partial sums as mineral phases observed. The next stage is the calculation of the volumetric percentages with which each mineral is present in the thin section. This methodology is appropriately applied when the size of minerals is fairly homogeneous. However, if the section presents minerals of significantly different sizes then some corrective factors can be applied to the calculations.

1.3 Applications of Optical Microscopy to Forensic Sciences

Optical microscopy is suitable for numerous applications ranging from various fields of research such as mineralogy, entomology, botany, medicine, surgery, and various sectors of industrial production. In forensic applications, optical microscopy maintains a prominent position as an important tool for the examination of the evidence. Optical microscopy can provide direct information when there are comparative materials associated with suspects, or indirect information when compared with databases dedicated to forensic science applications.

The stereoscopic microscope showed numerous applications in the forensic field because it is suitable for the observation of various types of opaque and glossy materials. Because of its low magnification, wide field of view, large working distance, and stereoscopic vision, stereomicroscope is mainly used for preliminary evaluations. These are aimed at locating, detecting, isolating, identifying, and comparing samples and traces. It also allows comparative examinations of evidence such as physical matches and impression evidence (Wheeler and Wilson 2011).

Furthermore, stereoscopic microscopy observation is a repeatable analysis as does not require any specimen preparation that could modify the features of the sample under examination. This is a prerogative that covers an important aspect of the applications in the forensic field. When carrying out technical analysis on things, places, or people, during the investigative phases, all the technical operators involved in the investigation must know whether the analysis is repeatable or unrepeatable. In the cases where only a few quantities of the sample are available for the analysis and/or the sample is subject to modification during the performance of a specific analysis, ad hoc analytical procedures need to be assessed to obtain maximum

information (Di Maggio 2019). Furthermore, the unrepeatable analysis of a sample evidence requires a dedicated legal procedure provided for in most of the Codes of Criminal Procedure of different states.[11]

The materials most observed under stereoscopic microscope in forensic field are of various organic and inorganic nature: banknotes, documents, ballistic objects (cartridges and bullets), natural and artificial fibres (Fig. 1.4a), fabrics,

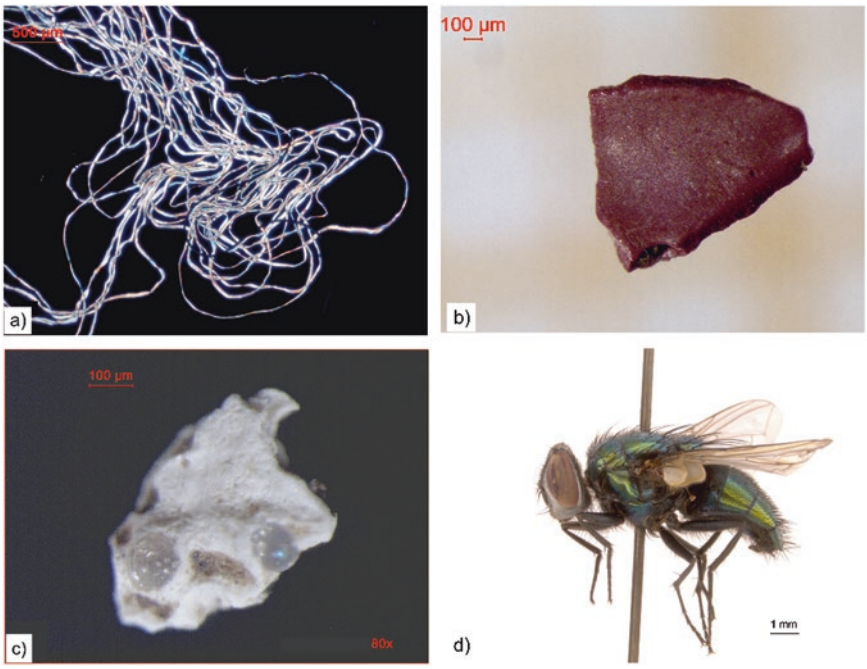

Fig. 1.4 Materials involved in forensic cases observed at the stereoscopic microscope: (**a**) Natural fibres; (**b**) Tile's fragment; (**c**) Fragment of reflective paint for road markings; (**d**) Adult specimen of *Lucilia Sericata,* dipterous of Calliphoridae family. (Courtesy of Dr. Giorgia Giordani, Department of Pharmacy and Biotechnology – FABIT, University of Bologna)

[11] By way of example, for the Italian Code of Criminal Procedure, the repeatable technical assessments do not require particular formalities to be respected, other than those imposed by law for the type of technical assessment that must be performed. However, the case of non-repeatable technical assessments is different: the art. 360 c.p.p. provides for a discipline according to which if the cross-examination is not respected in carrying out the investigations, it does not have any probative effect. Non-repeatability is closely linked to the modification of things, places and people, which is also extended to technical assessments. If carried out, it would determine the "modifications of things, places or people such as to make the act non-repeatable". In this case, the act becomes unrepeatable, precisely through and because of the completion of the technical assessment. Even if things, places and people were not themselves susceptible to modification, the assessment itself involves or may involve their alteration and modification, which requires the adoption of the precautions provided in the art. 360 c.p.p. (Valli 2013).

odontological materials and those related to forensic medicine, industrial and building materials (Fig. 1.4b), paints and pigments (Fig. 1.4c), botanical and entomological materials (Fig.1.4d), and a wide range of geological materials (Wilson and Wheeler 2009).

Furthermore, stereoscopic analysis allows observation of a wide range of tool marks, cut marks, and marks of transferred materials. Frequently, in forensic cases is necessary to understand and note what kind of tip has left its mark in the plaster, wood, or metal. The streaks and scratches that can be impressed by a knife, a screwdriver, or a drill reveal the shape and size of the tool as well as its defects and irregularities. These marks can be of three types: compression (impressed on a softer surface than the tool), sliding (when streaks are formed due to scraping), or cutting (a track where compression and sliding coexist).

In a forensic investigation, potentially relevant information can be provided by both inorganic and organic micro-traces adhering to fabrics. Given their particular physical structure, fabrics incorporate micro-particles in their wefts that can remain in place even for a long time. Fabrics of investigative interest can be clothing, shoes, car upholstery, but also all those fabrics devoted to technical or industrial use, such as packaging. The micro-particles found on fabrics can be of natural origin, such as microcrystals, soil particles, and pollens, or of anthropogenic origin, such as glass fragments, dust, fibers extraneous to the fabric, plastic fragments, and building materials, such as lime (Fig. 1.5). These micro-traces can provide geographical data (e.g., about the transit of a person or vehicles in certain areas), indication on work activities, or information relating to particular dynamics that lead to having a contact with unusual material.

In forensic geoscience, observation under the stereomicroscope is carried out on all those geological materials that are the object of illegal acts. For this purpose, it is useful to study their morphological, geometric, and microscopic features, and to perform all the preliminary characterizations. Observation under a stereomicroscope, in addition to being functional in determining numerous characteristics of the materials for their identification and/or comparison, is extremely useful for planning subsequent analytical procedures of mineralogical, petrographic and chemical nature, required to better characterize the samples.

In forensic applications, observations under the polarized microscope are often helpful for other investigation methodologies (Pye and Croft 2004). They are almost unlimited and are applied on different birefringent materials of interest to different fields of forensic science. The main advantage of the polarizing light microscope is in the identification and comparison of samples, offering higher magnification and providing information on the morphological, optical, chemical, and physical properties of the sample (Wilson and Wheeler 2009).

From a strictly forensic procedural point of view, although the observation of the sample with PLM is a repeatable activity, the preparation of the sample assumes a non-repeatable character as the realization of the thin section presupposes a modification of the evidence.[12]

[12] It should be remembered that in many international Codes of Criminal Procedure, non-repeatability linked to the modification of things is also extended to technical assessments.

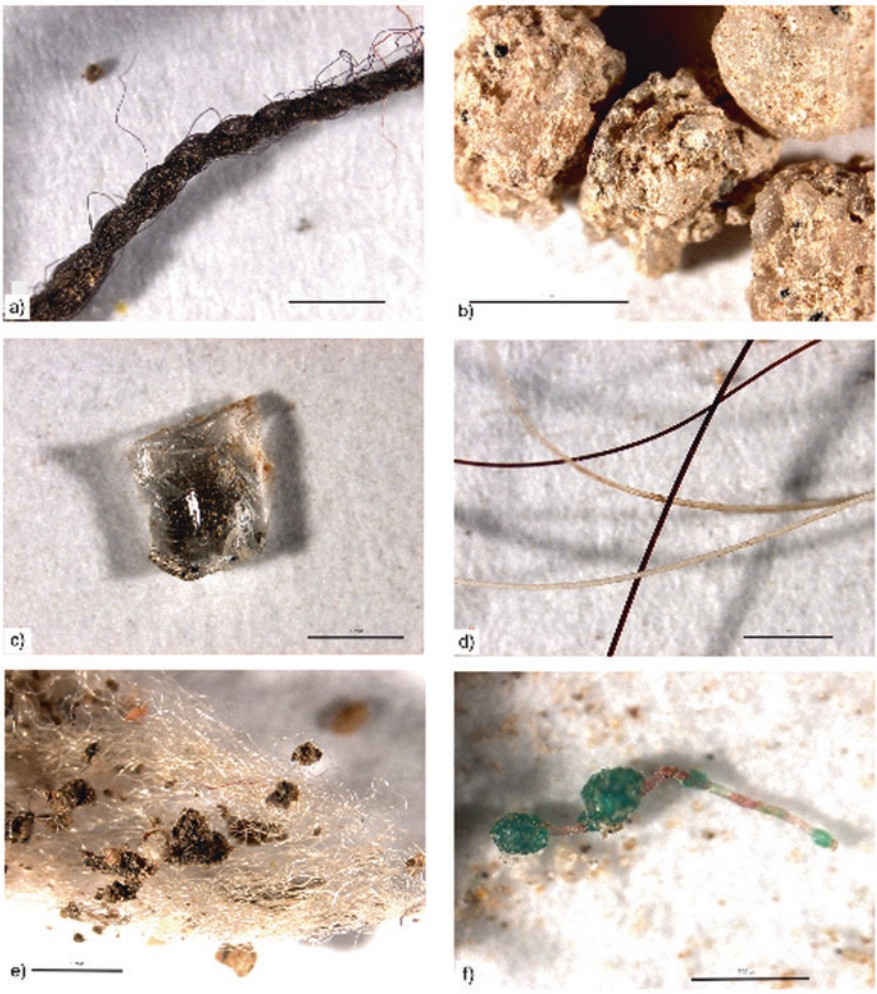

Fig. 1.5 Micro-traces of different materials found on fabrics, under the stereoscopic microscope: (**a**) Plastic fiber; (**b**) Soil particles found on the floor mat of a vehicle; (**c**) Plastic fragment on clothing; (**d**) Artificial fibers on cotton garments; (**e**) Mineral fragments on fabric tufts; (**f**) Overheated synthetic fiber

Marijuana Tablets

A seizure of marijuana tablets at the airport of Manaus, capital of the Amazon State, Brazil, was indicated as possibly coming from Europe by the Brazilian Federal Police investigation. This hypothesis was corroborated by the appearance of weed which is very different from those normally seized in Brazil (Fig. 1.6a). The packaging, the visual appearance of the cannabis tablets, and the extremely high THC content measured in the laboratory made the police believe in the foreign origin of weed. It was grown in controlled environments for the germination of the most potent marijuana, commonly known as "skunk". The fact that the material was seized at the Manaus airport, with a traveller who would have continued his journey to the interior of the country, also led to believe in the international origin of the drug.

A detailed observation under a stereoscopic microscope was carried out on the seized marijuana to search for micro-traces that could indicate its origin. The sample did not have any dirt residues that are normally associated with marijuana tablets. However, a complete body of an insect was identified (Fig. 1.6b) and, through the entomological taxonomic analysis, it was classified as the species *Euschistus heros*, endemic to the Neotropical Region, present in South America and, possibly, in Panama (first observed in soybeans in Argentina, in the Province of Entre Ríos – 2011) (Fig. 1.6c).

Forensic entomology and detailed protocols for the search for micro-traces through stereomicroscopy made it possible to discard the European origin of the seized marijuana. New investigations, now aimed at finding illegal laboratories associated with soybean plantations, pointed to real possibility of it belonging to the neighboring state of Pará, in the Amazon region.

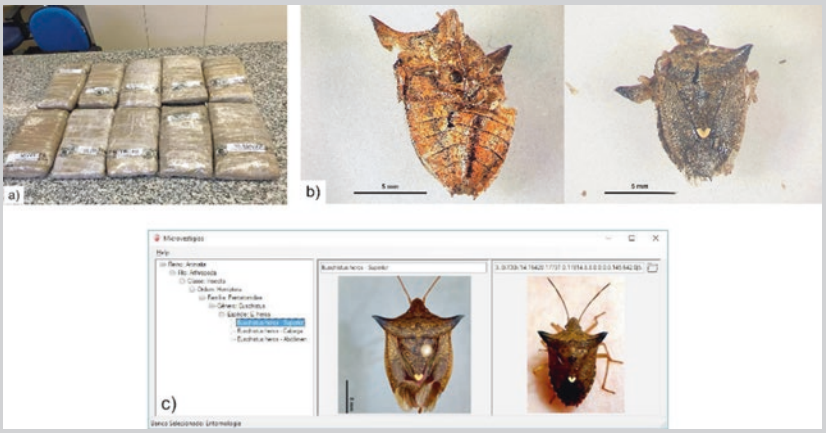

Fig. 1.6 (**a**) Sample of seized marijuana tablet; (**b**) Insect found in the marijuana tablet observed under a stereoscopic microscope; (**c**) Entomological classification through dedicated software: *Euschistus heros*

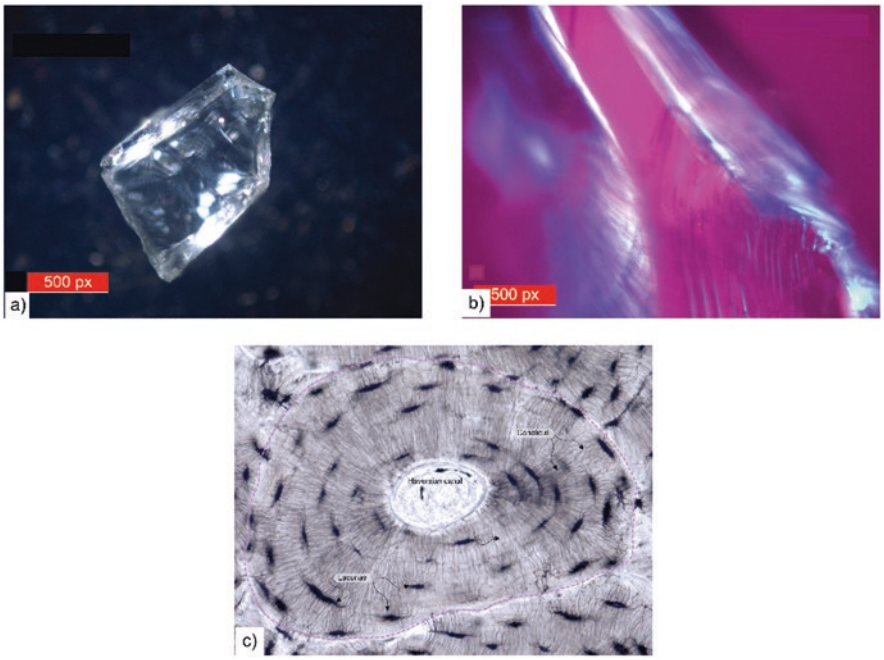

Fig. 1.7 Birefringent materials involved in forensic cases observed under PLM: (**a**) Fragment of tempered glass parallel nicols (40×) and (**b**) Crossed nicols and compensator inserted (60×). High birefringence is caused by tempering treatment (Courtesy of Dr. Leonardo Nuccetelli, former Servizio Polizia Scientifica); (**c**) Human bone (160×). In the single osteon (dashed in pink) the concentric lamellar system surrounding the Haversian canal is highlighted. (Courtesy of Dr. Amleto De Santanna, Department of Experimental Medicine, University of Genoa)

Various inorganic and organic materials are most commonly observed under PLM in the forensic field. In the forensic analysis of industrial materials, polarized light microscopy is used for the technology of glass (Fig. 1.7a, b), ceramic and a wide range of building materials, the study of food and pharmaceutical products, as well as for the technology of textile fibers, paper and related objects. The strong birefringence of many components of fabrics and vegetable fibers, such as cellulose, lignin, starch is well known (Sini 2006) and widely analysed as well.

In biological and forensic medicine applications, relevant information can be provided by polarized light microscopy performed for the study of birefringent living structures containing inclusions of isolated crystals or non-living microcrystalline masses attributable to pathological diseases such as crystals of waste products, dyes, pigments.[13] Many organic structures are birefringent due to their oriented arrangement of the macromolecules or micelles and have a submicroscopic organization as compared to that of crystals. This is particularly evident for skin structures such as cellular and nuclear membranes with layers of oriented lipid molecules, and

[13] A typical example are the crystalline fragments of quartz embedded in the lung tissues of silicosis patients.

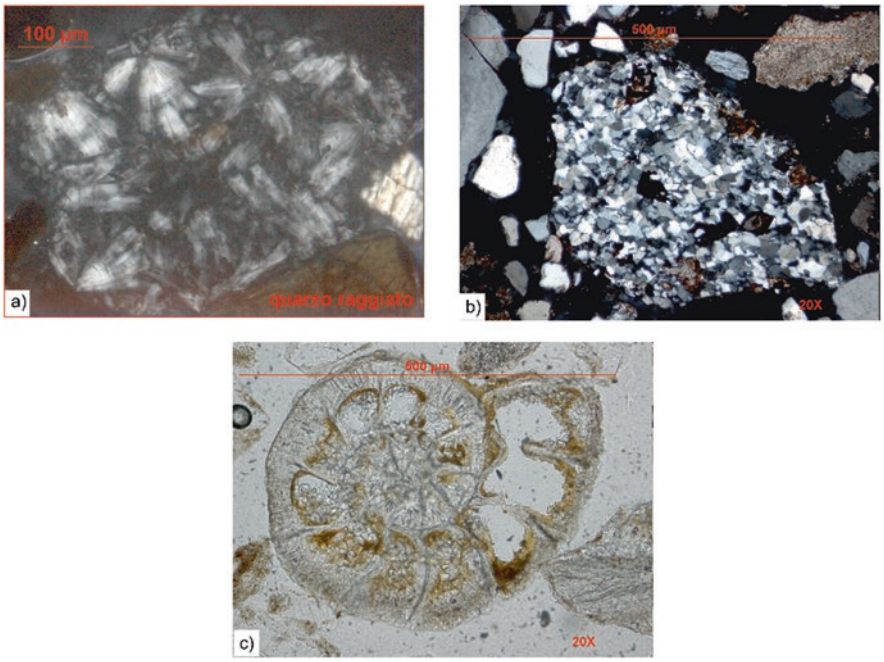

Fig. 1.8 (**a**) Radial quartz at crossed nicols (40×); (**b**) Sandstone at crossed nicols (20×); (**c**) Foraminiferal microfossil *Ammonia beccarii* at parallel nicols (20×)

for fibrillar structures such as nerve, connective, and muscular fibers. Furthermore, keratinized horny formations such as hair, nails, and stratum corneum of the epidermis are birefringent (Sini 2006). Mineralized tissues such as bones and teeth are strongly birefringent; in particular, the polarized light observation of bone tissue sections (usually femur) allows the study of osteons[14] and "Haversian canals"[15] (Fig. 1.7c). It also helps in obtaining indications on the age and some anthropometric parameters of the individual, and the possible pathologies suffered.

In forensic geoscience, observation under polarized light microscope is one of the main techniques used for carrying out an accurate identification of the minerals and rock fragments constituting soil particles. This also includes individual geological materials such as minerals, rocks, fossils, and microfossils (Fig. 1.8), and the study of all those materials of geological origin such as concrete, cements, bricks, mortars, plasters, and ceramics. The latter type of materials is often analysed whenever present in soil as anthropogenic fragments, in cases of crimes against cultural heritage, and in the field of forensic engineering to assess the quality of building materials.

[14] The osteon is the functional unit of compact bone tissue. It has a cylindrical shape with a diameter of about 0.2 mm and a length of a few millimetres.

[15] Haversian canals are vascular canals that run through the compact lamellar bone tissue of flat bones and into the diaphyses of long bones. The Havers canal is the innermost part of the osteon and is surrounded by concentric lamellae, in a variable number, which have the function of carrying nutrients. Nerve fibers, blood vessels and lymphatic vessels run along the Haversian canals.

Graminaceae

A woman was found strangled in her apartment. The analysis of the crime scene allowed for to hypothesize that the woman had been killed in another place, presumably outdoor: the house was in order (there were no signs of a struggle), the victim's shoes had soil, on the floor there were footprints with soil and plant fragments left by shoes that were different from those worn by the victim, and plant fragments were on the corpse.

If both the soils from the footprints and from the victim's shoes had a moderately-strong degree of comparability, they did not have peculiarities that would permit to circumscribe a specific area of origin. Both plant fragments from the victim and the footprints were then analysed. They were initially observed in optical microscopy. The observation under the PLM showed that the fragments had tissue and cellular characteristics of monocotyledons, which include numerous species of industrial, food, and economic interest, such as *Graminaceae* (Fig. 1.9).

Although the molecular analysis of the plastidial genetic material is the only technique for identifying the species of plant fragments, preliminary optical microscopy analysis allowed them to be classified as belonging to the family of Graminaceae and to confirm the hypothesized criminal narrative: the corpse was moved after the killing in an outdoor environment to obliterate the traces attributable to the murderer.

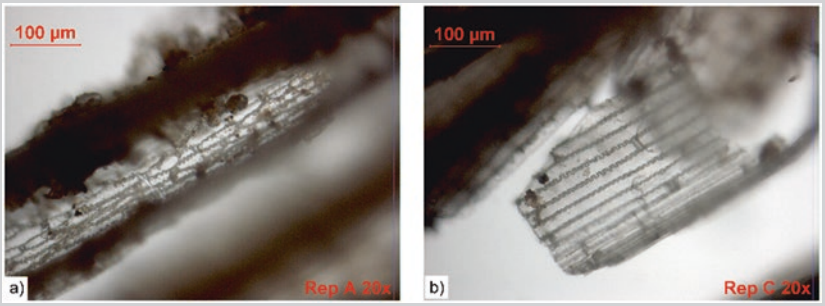

Fig. 1.9 Plant fragments from the footprints (**a**) and from the victim (**b**) under the PLM. The cells of the epidermal tissue, that act as the integument of the leaves, are clearly visible. The linear leaves of monocotyledons have elongated epidermal cells, with a rectangular shape and lateral cell walls with toothed morphology. (Garuba et al. 2014; Gray et al. 2020)

It is impossible to avoid highlighting the application of optical microscopy and the use of the comparison microscope for carrying out physical comparative examinations of evidence such as paint, firearm ammunitions, questioned documents, banknotes, graphological signs, as well as a wide range of tool-marks and impression evidence.

The comparison microscope essentially consists of two microscopes with identical objectives connected by an optical bridge, containing a combination of prisms that convey the images to a single eyepiece. It is thus possible to observe two separate objects in the same field and to compare them visually by juxtaposing each of them. Objects appear in a circular field of view divided in the center by a thin vertical line.

It is the tool of excellence used in ballistic investigations that permits easy comparison of tool-marks on ballistic objects. In the case of bullets fired from the same weapon, it is often possible to make the "groove and land" micro-impressions present in the marks left by the rifling of the barrel that coincide along the dividing line as well as in the cartridges, the tool marks left by the firing pin and the ejector in semi and fully automatic firearms.

The following paragraphs describe optical microscopy observations of various geological materials that are frequently analysed as evidence in forensic applications.

1.3.1 Minerals and Rocks

Minerals are the fundamental constituents of geological materials, including those of forensic interest. They are present in unconsolidated materials, such as sands and soils, as well as in rocks. Furthermore, most known gems are made of rare minerals with particular properties of beauty and hardness.

Minerals are essential materials used in those human activities for which they have always represented a primary resource. Some minerals are used as they are, such as talc, silver, or asbestos; others are treated to obtain usable materials in the most varied fields of application. Their use in electronic and mechanical components, building materials and ceramics, paints and pigments, cosmetics, pharmaceuticals, and so on is critical. In addition, the crystal structures produced in nature throughout geological time represent a source of inspiration for undertaking synthesis, for the artificial reproduction of technologically advanced materials.

Rocks are geological materials that are often involved in crime narratives, both because they are present as fragments in soil and because they are frequently used as blunt instruments or ballistic objects. Furthermore, their analysis is useful for all those crimes against cultural heritage and for a wide range of litigations about building structures. This is because they represent the primary source of buildings materials, for which they are used as they are, such stone materials, or used as components for bricks, concrete, and cement.

The study of minerals and rocks, their structure and composition, therefore, is of forensic interest not only for investigations involving the geosciences but also for all those criminal investigation sciences that have the purpose of identifying every type of material, regardless of its natural or synthetic nature (Di Maggio et al. 2013).

Salt Crystals on Fabric

Early in the morning a boy was found dead after jumping from the top floor of a building. According to numerous witnesses, the boy spent the night before at a nightclub on the beach. Therefore, investigators wanted to reconstruct the last hours of the victim's life to understand if the death was due to suicide or murder. The victim's jeans were wet, so they were analysed to understand if the boy had been into the sea dressed during the night. If the jeans had been soaked in seawater, the fabric would have had micro-crystals of marine salt.

The jeans were preliminary observed under a stereoscopic microscope, at different magnifications, to verify the presence of any salt crystals. The jeans fabric featured numerous white micro-crystals, vitreous and oily sheen, and translucent opacity with irregular morphology. The crystals were dispersed among the fibers with greater concentrations near the hems of the pockets and legs, where the fabric is thicker (Fig. 1.10a), and near the rivets. Assuming

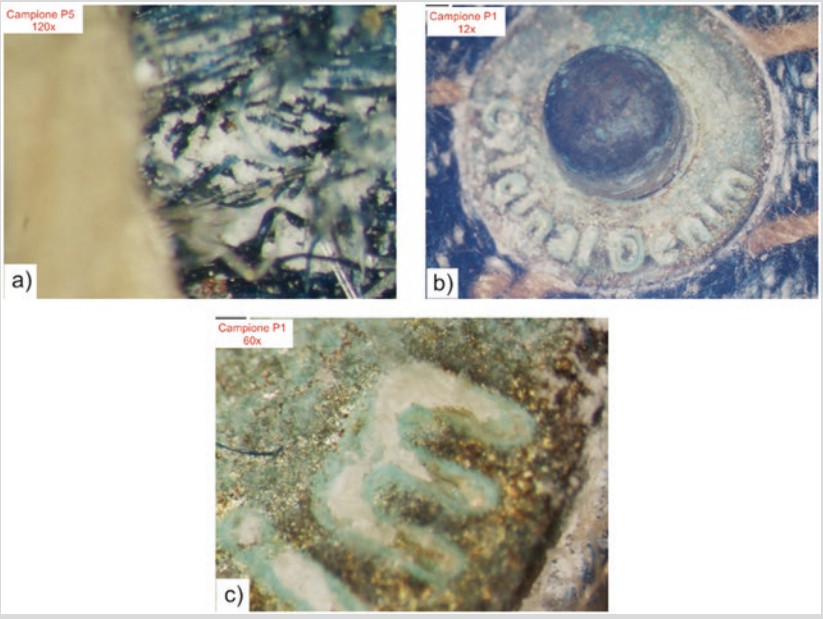

Fig. 1.10 Victim's jeans observed under a stereoscopic microscope: (**a**) White micro-crystals near the hems of the pockets (120×); (**b**) Metal rivet with white micro-crystals along the rivet circumference and in the engraved inscriptions (12×); (**c**) Particular of white micro-crystalline patina inside the engraved letter (60×). (Courtesy of SCARLabs srl, Caserta, Italy)

(continued)

that the jeans had been soaked in seawater, these portions of fabric would likely have a slower chance to air-dry than others, allowing for a greater concentration of any salt crystals precipitated during evaporation. Furthermore, the rivets showed a high oxidation stage of the metal and had numerous white micro-crystals, mainly arranged along their circumference, between the rivet and the jeans fabric, and inside the inscriptions engraved on their surface (Fig. 1.10b, c).

Stereoscopic observation allowed the performance of subsequent analysis using a scanning electron microscope and x-ray microanalysis (SEM-EDX) in the most representative areas of the jeans to identify the presence of any precipitated salt crystals through qualitative and semi-quantitative analysis. This spectroscopic technique confirmed that the micro-crystals were composed of sodium chloride (NaCl – halite), the main constituent of sea salt.

Stony Splinter

During a shooting between criminal gangs in a neighbourhood of Naples, a person, extraneous to gangs, was killed by a stray bullet. During the autopsy examination, the coroner found a small splinter of presumably stony material embedded in the victim's flesh. A stone bollard was present at the scene of the shooting, so the investigators hypothesized that the bullet had been deflected by the impact with the bollard and consequently hit the person who was not on the trajectory of target.

Both the splinter found on the victim and a sample taken from the stone bollard present at the scene of the shooting were analysed under the polarizing light microscope. This technique allowed us to observe that both samples were an artificial conglomerate consisting of volcanic rocks fragments cemented by an optically isotropic glue (Fig. 1.11). The rock fragments had a typical angular morphology, with a low degree of sphericity, due to a possible industrial grinding. The volcanic rocks were highly altered leucitites with a microcrystalline groundmass consisting of plagioclase and potassium feldspar, and phenocrysts of clinopyroxene, leucite, iron oxides, and olivine. The rock fragments identified in the splinter found on the victim and in the sample taken from the bollard were typical of the alkaline potassium volcanism of the Tyrrhenian margin, and in particular, linked to the volcanic activity of the Vesuvius. These rocks are often quarried to provide loose material to be used in the construction of urban artefacts and of building materials with low breaking strength.

The observation under polarizing microscope highlighted that the fragment found on the victim was of the same nature as the material used to make the bollard and probably had detached from the bollard due to the impact of the bullet and intercepted the trajectory of the bullet deviated from the impact.

(continued)

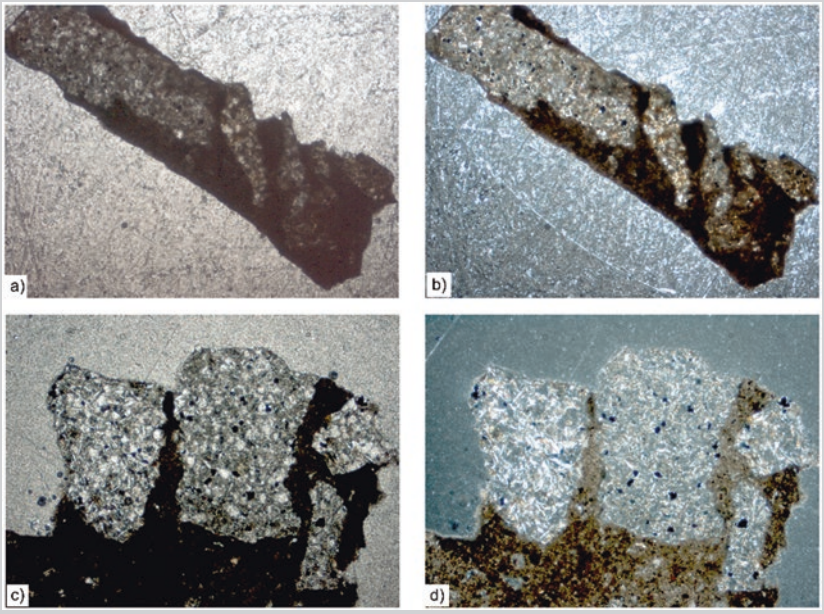

Fig. 1.11 (**a**) Stony splinter found on the victim observed under parallel nicols, and (**b**) Under crossed nicols (60×); (**c**) Sample taken from the bollard under parallel nicols, and (**d**) Under crossed nicols (20×). Both specimens have leucitite fragments immersed in an optical isotropic cement/paste

1.3.2 Pedological Materials

Forensic pedology studies and analyzes traces of geological debris and loose materials connected to a crime in order to provide assistance to the judicial police activities and to obtain conclusive evidence useful to investigation. In the context of forensic analysis, such materials are commonly referred to by the term 'soil' and include sand, mud, soil in the strict sense, etc.

Soils are multi-component systems. The characterization of these systems and the identification of their components require the use of different analytical techniques. These include colorimetric, sedimentological, morphological, mineralogical, petrographic, chemical, physical, and biological techniques. The degree of comparability between soil samples is estimated by comparing, from qualitative and quantitative point of view, numerous geological, physical and chemical data (Di Maggio and Barone 2017).

In forensic pedology, stereoscopic observation allows the study of the morphological characters of soil particles, determining their color, degree of angularity or sphericity, brightness, shape, the appearance of the surfaces, and any other evident feature. Furthermore, during stereoscopic observation, any organic and anthropogenic components are observed, described, and separated to carry out detailed analytical procedures aimed at their characterization and identification (Fig. 1.12a). Generally, stereoscopic observation is performed several times during the succession of the analytical phases. Actually, the samples are first observed as they are, without carrying out any preliminary treatment, to evaluate their main characters; subsequently, they are examined after washing in an ultrasonic bath and sieving. In this phase, the observation of each particle size fraction is aimed at studying the detailed characteristics of the individual particles and at separating the peculiar elements (Di Maggio et al. 2013).

Soil observations under the polarizing light microscope are carried out on thin sections suitably prepared following procedures dedicated to unconsolidated materials (see Sect. 1.2.1). The use of polarizing microscopy allows a detailed identification of single grains of soil composed of fragments of minerals and rocks, and of all those birefringent materials of organic and anthropogenic origin (Fig. 1.12b). Depending on the amount of sample available, more thin sections are prepared for each particle size class obtained by the sieving separation. This allows observation of the greatest number of types of sample components. Generally, the particle size class that can be better described under a polarizing light microscope is sand, with dimensions ranging between 1 millimetre and 63 micron. Particles smaller than 63 micron are observed and analysed with spectroscopic techniques such as the scanning electron microscope.

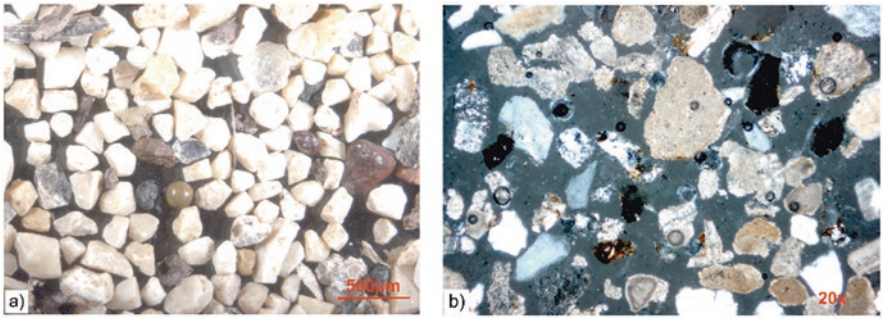

Fig. 1.12 (**a**) Soil washed in ultrasonic bath, observed under a stereoscopic microscope, composed of various types of inorganic particles and some fragments of organic origin; (**b**) Thin section of a soil under PLM at crossed nicols where minerals such as quartz, feldspar, plagioclase and calcite, rock fragments of meta-granite, sandstone, micritic limestone and sparite, and microfossils are present

The New Red Brigates

During the nineties of the last century, a criminal group, which claimed the paternity of Red Brigades that was active in the seventies, committed a series of violent crimes. They conducted armed robbery, terrorist outrages, and homicides with a political background. At the end of the first decade of this century, the investigators arrested the group members. In one of the dens of the terrorist group in Rome, gardening tools with soils were found. The investigators supposed that the criminals had hidden firearms and explosives. Comparison analysis between the soil found on the tools (questioned sample) and some control soil samples, collected at several sites linked to the criminal group members, was requested.

The comparison did not provide any useful information, as the questioned soil from the den did not have any meaningful similarity with the control soil samples, just a slight resemblance with one control sample collected from an area north of Rome. A deep mineralogical and petrographic analysis of numerous lava fragments was performed by observation of soil thin sections under the polarized light microscope. The geologists inferred that both questioned sample and the control sample from north of Rome were likely to come from volcanic alkaline-potassic deposits of the Roman Comagmatic Province (Fig. 1.13). Nevertheless, total absence of mineral sanidine in questioned soil, both as singular particles and as phenocrysts in the lavas (Fig. 1.14a), supplied indications on their probable origin: sanidine widely present in the volcanic deposits of the Sabatini Volcano District, which are spread throughout the area north of Rome (Fig. 1.14b) is not present in the volcanic rocks of the Alban Hills Volcano District, deposited in the area south of Rome. Furthermore, presence of unalterated leucite in the questioned sample pemitted the recognition of a specific outcrop of the Alban Hills Volcano deposits where this type of leucite is well represented (Fig. 1.14c). Control soil samples collected at this outcrop in the southern area of Rome, were compared with the questioned sample from the den and the control sample from the north of Rome. Soil samples from the south of Rome (Fig. 1.14d) proved to be extremely comparable with soil from the den. Even though the soils from north of Rome and south of Rome show typical features of alkaline-potassic rocks, they had substantial differences in granulometry, color, crystalline phases, and leucite alteration. These different soils have been generated by volcanic deposits which have had different petrogenesis, different depth of magmatic chamber, different substratum of rocks, and different pedogenesis.

The accurate mineralogical and petrographic analysis of volcanic particles by means of PLM and supported by a scrupulous geological study of the territory allowed to delimit an area, where the investigators carried out inquiries and found a new den with further pieces of evidence linked to the criminal group activities.

(continued)

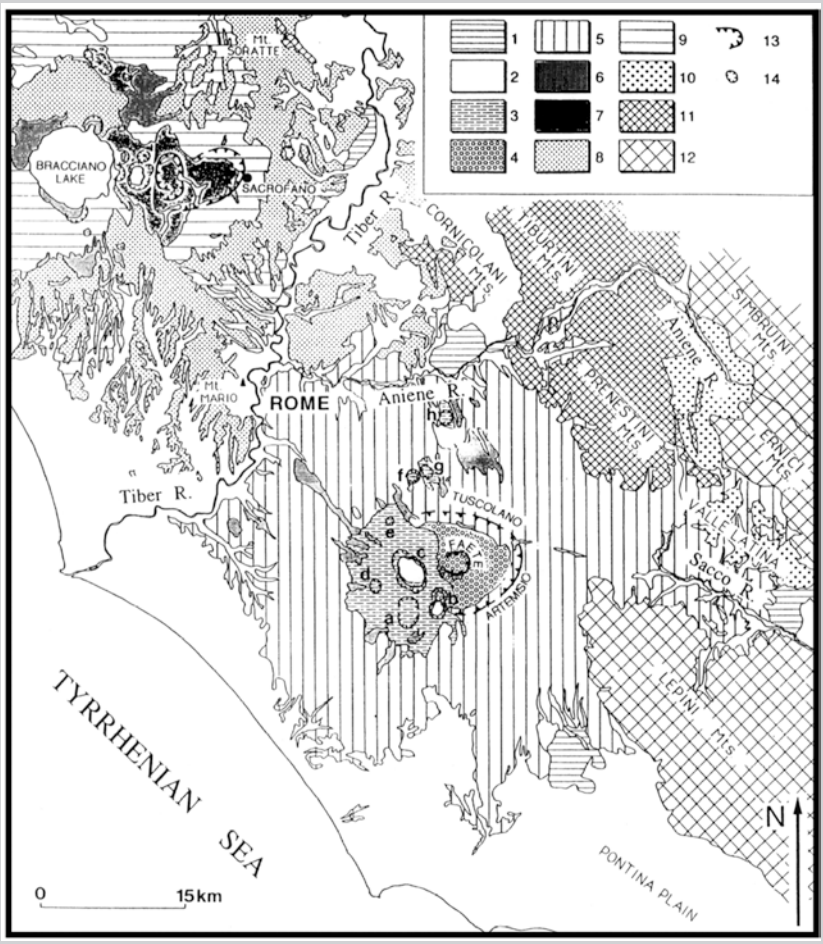

Fig. 1.13 Geological map of Roman Comagmatic Province: (1) Travertine; (2) Plio-Pleistocene sediments; (3), (4), (5) Volcanic rocks of Alban Hills District, south of Rome; (6) Main lava flow; (7), (8), (9) Volcanic rocks of Sabatini District, north of Rome; (10) Tortonian sedimentary units; (11), (12) Carbonate units; (13) Caldera rims; (14) Crater rims

(continued)

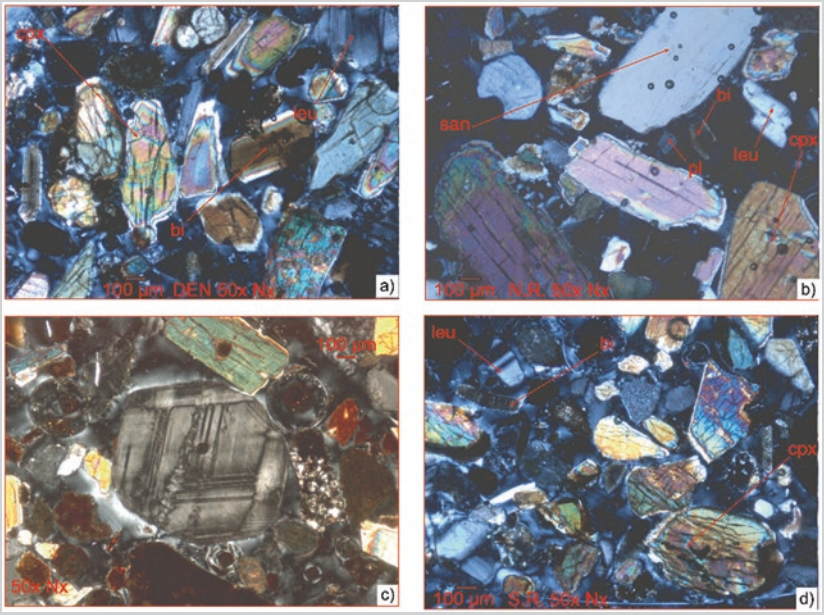

Fig. 1.14 Thin sections of soil samples under PLM (crossed nicols, 50×); (**a**) Questioned soil from the den; (**b**) Control soil sample from north of Rome; (**c**) Unalterated leucite in the questioned sample from the den where polysynthetic twinning is visible; (**d**) Control soil sample from south of Rome. Legend: *san* sanidine, *pl* plagioclase, *leu* leucite, *bi* biotite, *cpx* clinopyroxene

1.3.2.1 Diagnostic Physical Characteristics for the Study of Soil Particles

Physical characteristics of soil particles that are observable through optical microscopy are morphoscopy, morphometry, size, morphology of the surfaces, brightness, color and structure, and birefringence.

In sedimentology, morphoscopy is the qualitative study of particles' shape of sediment, while morphometry is the measure of their shape. The more current meaning of the term morphoscopy refers to the appearance of clasts' surface, regardless of the other morphological characteristics (Angelucci 1989). In forensic pedology, morphoscopy and morphometry are applied for the study of inorganic particles present in soil samples.

The shape and surface appearance of soil particles are mainly conditioned by their mineralogical and textural characteristics and by the size and shape of initial fragments. With the same initial conditions, the duration and modality of erosion and transport, the sedimentation conditions, and the chemical-physical alterations subsequent to deposition affect the shape and the surface appearance. Therefore, the shape

and surface appearance of particles are properties that can give important information on their transport and deposition environment and can be used as a term of comparison between different soil samples and for understanding their origin, even with the same mineralogical-petrographic composition and the same particle size.

A careful description of the shape of the granules includes angular and linear measurements of their edges and axes as clearly described in Fig. 1.15.

The indices based on the elaboration of two axes express the two-dimensional shape which is generally related to the transport modes of the clasts and the degree of alteration due to atmospheric agents. The two-dimensional shape can be defined by:

– Roundness, which indicates how close the particle outline is to a circle;
– Angularity, which indicates the irregularity of the particle outline;
– Elongation, given by the ratio between the major axis *a* and the minor axis *c*.

The indices based on the elaboration of three axes express the three-dimensional shape that is generally conditioned by the lithological or mineralogical composition of the clasts. The three-dimensional shape can be defined by:

– Sphericity, which indicates how close the particle is to the sphere;
– Shape, which expresses the similarity of the particle to a regular geometric solid;
– Flattening, given by the ratio between the minor axis and the two major axes of the particle.

Some authors have developed formulas to indicate both two-dimensional and three-dimensional shape indices (Table 1.1).

Generally, the soils of forensic interest mainly consist of particles with dimensions of sand, silt and clay. When measuring the axes (and therefore the shape indices) of the sandy particles, various difficulties can be encountered. Therefore, for the study of their shape, it is sometimes suggested to rely on different diagrams by which the measurement is carried out by visual comparison. The most used are the Krumbein roundness chart (Fig. 1.16a) and the Powers comparison chart (Fig. 1.16b). The advantages of these diagrams are speed and accuracy, the latter not less than that obtained by the other indices indicated in Table 1.1.

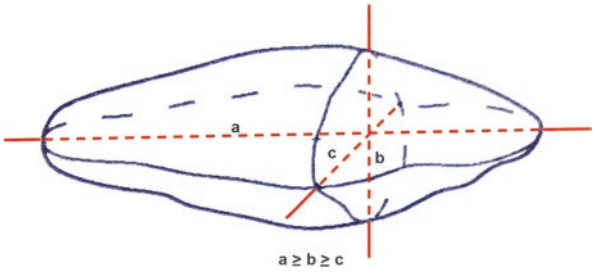

Fig. 1.15 Main axes of a clast used for the evaluation of its dimension and shape. (Angelucci 1989, modified)

Table 1.1 Main two-dimensional and three-dimensional shape indices used in literature: a, b and c indicate the axes of the particles (Fig. 1.15); r is the radius of the circle inscribed in the most acute angle of the plane of maximum projection of the particle (1989, modified)

Two-dimensional	roundness Cailleux: $2r/a$; visual by Krumbein or Powers (Fig. 1.16) angularity $a/2r$ elongation a/c
Three-dimensional	Shape Zingg: b/a, c/b Sphericity Krumbein: $\sqrt[3]{(bc/a^2)}$ Flattening Cailleux: $(a + b)/2c$

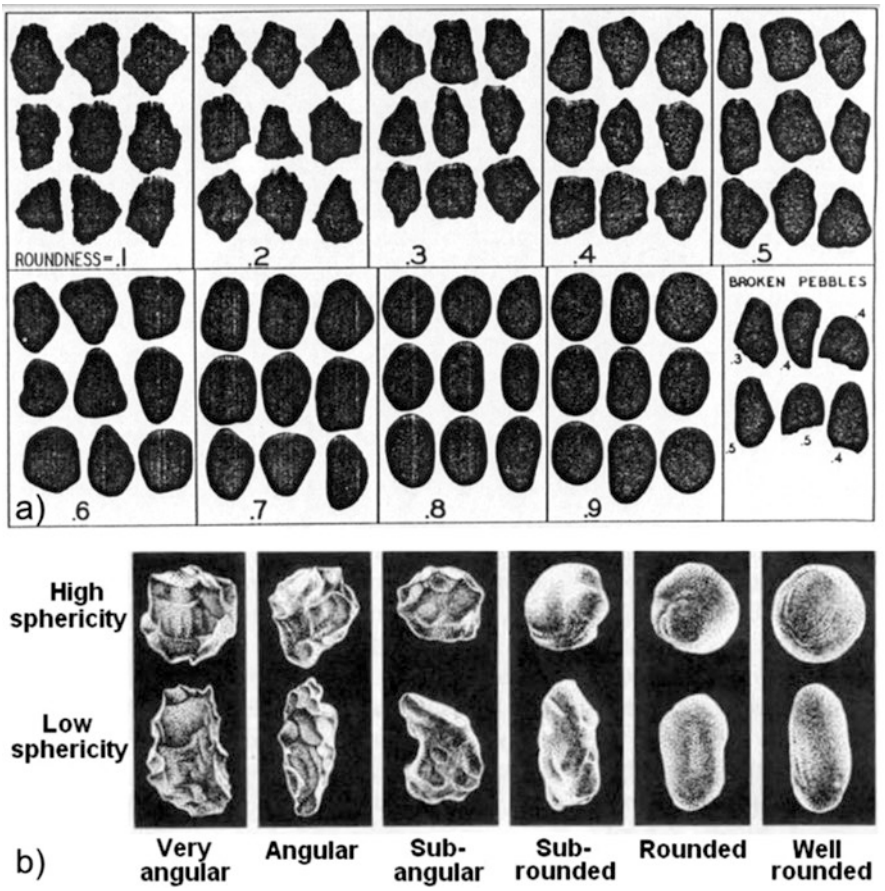

Fig. 1.16 (**a**) Krumbein diagram for the visual classification of the roundness of the clasts in ascending order from class 1 to 9 (Krumbein 1941); (**b**) Powers visual comparison chart for estimating the roundness of sand grains. (Powers 1953)

The study of granules surface contemplates visual observation and the use of one or more qualitative terms such as rough, shiny, frosted, opaque, fractured, striated, stepped, with characteristic marks, with cavities, etc. The observation of the surface and shape of the granules can be carried out with different means of investigation depending on the size of the examined particles. The largest particles are observed with the stereoscopic microscope interfaced with software that enables linear and angular measurements. For smaller particles, it is necessary to use the scanning electron microscope (SEM).

In general, the color is not an identifying character of soil clasts. However, it is detected to divide the particles into diagnostic classes whose compositions are subsequently identified through detailed mineralogical analysis.

The description of brightness and structure includes qualitative terms based on mere observation. Different types of brightness (vitreous, opaque, metallic, oily, etc.) can be associated with a structure that can be defined as compact, crumbly, pumiceous, etc.

1.3.2.2 Organic and Anthropogenic Fragments in Forensic Soil

Forensic soils are composed of three types of components present with strongly variable reciprocal ratios: the inorganic fraction, the organic fraction, and the anthropogenic fraction, the latter representing a set of various materials whose presence in the soil is attributable to human activities. The organic and anthropogenic components can be extremely qualifying for those soil samples originated from an area with limited extension, and quasi-homogeneous soil and/or geological characteristics. For this reason, in the preliminary phase of observation in optical microscopy, it is of primary importance to detect the presence of such materials and separate them for subsequent identification (Di Maggio 2019).

The organic fraction consists of plants and animal organisms, both living and dead, in various stage of decomposition or fossilization, and the complex of humus substances. The quantity and nature of the organic fraction are indicative of the environmental features that have presided over the formation and evolution of soil, regarding both the regional and micro-environmental levels. For this reason, the identification and classification of the species of animal and plant organisms in soil is a further and useful method of comparison between the samples and a valid tool for determining their origin. The plant component includes fragments of leaves and barks, seeds, inflorescences, algae such as diatoms,[16]

[16] Diatoms are unicellular siliceous algae that colonize all aquatic environments with a large number of genera and species. Diatoms are useful in the comparison of soil samples for forensic purposes; in fact, their presence in the lungs, liver or kidneys of corpses helps to diagnose death by drowning.

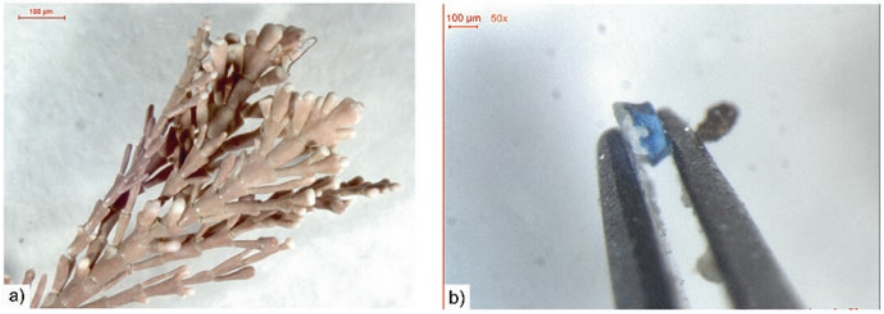

Fig. 1.17 (**a**) Organic fragment in a sandy sample found on a victim of homicide; (**b**) Paint fragment in a soil sample gathered from a suspect's shoes

pollens,[17] fungi, spores, phytoliths[18] (Fig. 1.17a). The animal remains include fragments of marine and terrestrial shells, insects, and microorganisms such as bacteria, protozoa, protists and metazoans. Although the study of insects in the context of criminal investigation plays an important role in taphonomic studies, their presence or their biological activity in the soil can provide useful information on the origin of a sample.

The anthropogenic component includes all those fragments or traces of materials and substances, whose presence in soil is attributable to human activity. This component consists of fragments of various materials such as paper, plastic, glass, paints, fibers, metals, ceramics, and chemicals, including precipitates, solvents and slag (Fig. 1.17b) (Di Maggio et al. 2013). Also, there is a considerable variety of man-made materials that can be regarded as artificial rocks. These are building materials that include cement, mortar, plaster, bricks, and tiles. Some of these materials show textural characters similar to those of natural rocks and in some cases, it is necessary to carry out detailed chemical, mineralogical and petrographic analyses to identify their nature (Di Maggio and Nuccetelli 2013).

1.3.3 Precious Stones and Gems

Gems and precious stones are geological materials frequently involved in crimes; their high economic value, small size, and their non-traceability have made them also extremely attractive to organized crime. Criminal organizations use precious

[17] Pollens present in the soil are useful for circumscribing the area of origin of a sample in which the species of plants referable to the pollen samples are well represented, and may provide an effective method of investigation when it is necessary to establish the timing of a deposition of a soil trace on a surface. In fact, the identification and quantity of the pollen species may indicate the season of inflorescence and vegetative propagation.

[18] Phytoliths are biogenetic silica particles formed by the progressive silicification of plant cells. Since the phytoliths take the form of plant cells, each species produces a peculiar form of phytolith.

stones as means of exchange for traffic in arms, drugs, and for all those crimes which require a monetary transaction. Besides the crimes listed above, there are also those relating to the fraudulent falsification and imitation of gems. Even in ancient times, it was customary to falsify gems. The earliest evidence of changing the appearance of gemological material dates back to the Minoan era. Over the centuries, with the new knowledge of materials and development of chemical and physical techniques, artificial alternatives based on lower value materials have evolved as replacements of gems (Di Maggio 2019).

For estimating the value of the gems and/or to determine if they are false or not, stereomicroscopy in a darkfield setting allows an accurate observation of cuts, geometries of the faces, symmetry and polish of the cut, the extent of the inclusions, and structural distortions that determine their degree of purity. The gems have distinctive signs, which can be superficial, called surface signs, or internal, called inclusions, that are formed during the crystallization process of the mineral. The purity of a gem refers to its degree of internal cleanliness, which depends on the nature, number, arrangement, and size of the inclusions, solid and liquid, and on the structural distortions due to the crystal growth process.[19] Stereomicroscopy observation is also useful for the detection of distinctive characteristics of gems falsified with synthesizing techniques. There are different synthesizing processes, however, the most common one consists of melting material with a composition equal to that of the mineral to be imitated, to which metal oxides are added for giving the desired color. Subsequently, the mass of molten material crystallizes as a function of slow cooling. Synthetic stones are quite easily recognizable under the microscope as they have typical curvilinear growth striae and sometimes gas bubbles (Fig. 1.18). In recent times, however, the methods of synthesis have reached such advanced techniques that result in products almost perfectly identical to their natural counterparts to the point of being indistinguishable. In these cases, spectroscopic techniques are used to achieve a confident identification of synthesis.

A frequent precious gems counterfeit is the creation of a gem doublet. This is a very thin layer of natural gem, positioned in the upper part of the doublet, glued to a cheaper or common stone (such as quartz), a synthetic product, or even glass, which makes the lower and larger part of the doublet. This is why gemstone doublets can be difficult to detect when they are already set in jewelry. When a doublet is created, glue is usually used to stick the two parts together. When glue sets, it traps tiny gas bubbles which may seem like natural inclusions to the untrained eye. However, under the stereoscopic microscope, it is quite easy to identify these gas bubbles and to observe their distribution on a single plane which represents the connection between the upper and lower part of the doublet.

[19] The degree of purity is based on what is visible at 10x magnification. Usually, higher the purity, higher the value of the gem, especially in diamonds. However, there are cases in which the inclusions that do not interfere with the hardness of the gems can make them even more beautiful and more valuable.

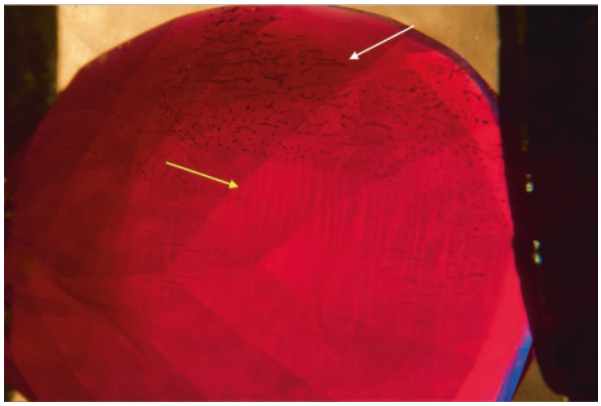

Fig. 1.18 Growth lines (yellow arrow) and flux bubbles in micro-cracks (white arrow) in a synthetic ruby (darkfield – 32×). The growth lines, which are not perfectly straight as in natural stones but curved and very close together, represent the main characteristic of Verneuil synthesis process (Malossi 2018). (Courtesy of Dr. Alberto Malossi, Malossi Gemmecreate srl, Milan, Italy)

Tourmalina Paraíba

Tourmalina Paraíba is a gem from Brazil that was discovered in 1987 in the district of São José da Batalha, which is in the territorial domain of the municipality of Salgadinho within the metropolitan region of Patos, Paraíba. It is an extremely rare and expensive variety of tourmaline that is a safe investment for collectors and others. It is considered to be among the rarest and most precious gems in the world; this precious stone is 10,000 times rarer than a diamond. The presence of copper and manganese gives this stone deeply saturated colors ranging from blue to light blue and from turquoise to green. This tourmaline has become a fad and conquered the international market, mainly in Europe, but at the same time, smuggling of this stone has increased.

In 2018, the Federal Public Ministry (MPF) denounced 11 people involved in the illegal exploitation of tourmaline in Paraíba (Fig. 1.19a). The accusation involved money laundering by criminal organization, clandestine trade in precious stones, bank accounts used for money laundering, and under-billing in the export of goods, and other serious crimes. The criminal scheme was disrupted by Operation Sete Chaves, which began in May 2015.

It was up to the geologists of the Brazilian Federal Police to characterize and evaluate these gems while trying to identify their national origin and distinguish them from the similar African pieces. The first stage of analysis involved observation through the stereomicroscope that allowed to describe these gems in terms of cut and finish, the presence of structural distortions and typology of inclusions, as well as the color namely is the most important characteristic of the Tourmalina Paraíba (Fig. 1.19b). This observation helped to infer whether there were gems of very high quality in a large-sized lot. The subsequent spectroscopic analysis and microprobe examinations enabled to confirm the Brazilian origin of the tourmaline gems, as opposed to African Liddicoatites.

(continued)

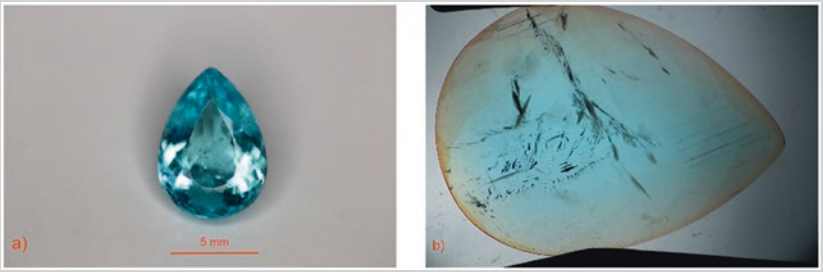

Fig. 1.19 (**a**) Tourmalina Paraíba pear cut (1 carat); (**b**) Tourmalina Paraíba under the stereoscopic microscope (darkfield – 20×). The specimen is featured by solid inclusion of iron and manganese oxides in microfractures. The quality of each stone is directly associated with abundance in fractures

1.3.4 Precious Metals

Precious metals are part of the noble metals group and comprise the native element class of the chemical-structural classification proposed by Hugo Strunz in 1941. These noble metals are particularly resistant to the chemical processes (they resist oxidation and corrosion in moist air and are not easily attacked by acids) and possess some important physical characters such as ductility, which is the ability to withstand plastic deformation without rupture. In the commercial field, the precious metals are gold, silver, platinum, and palladium.

Objects produced with precious metals, or alloys of these metals that have a legal title, have become a new form of investment and money laundering. It has dramatically increased illegal trade and smuggling of precious metals. Besides the crimes listed above, falsification and imitation of precious metals and their alloys in jewelry production, ingots, coins, and other objects involving criminal intent also occur (Di Maggio and Barone 2017).

Pure precious metals are combined with other metals to improve the object's resistance capacity and workability. Since a superficial examination cannot verify the content of precious metal in an alloy, the legislations of a significant number of states recommend that objects made with precious metals and their alloys should be compulsorily engraved with at least two signs as a so-called hallmark: the indication of the purity (title) and the trademark (or manufacturer mark).[20]

[20] The purity is expressed in millesimal fineness. It highlights the relationship between the mass of the metal alloy base and the pure or fine precious metal. For example, a 750‰ alloy will contain 750 fine metal parts and the remaining 250 parts are other metals. The manufacturer mark must be unique and registered at dedicated offices; in fact, only through this mark the manufacturer can be traced and, therefore, be legally responsible for the purity compliance status of the item. The manufacturer mark can be single or a group of letters, monograms, or words; it may also be images of various objects or heraldries.

Generally, counterfeiting of precious metals occurs by substituting precious metals with less precious ones and subsequently plating with the metal to be imitated and also by employing different alloy proportions than the title. Moreover, the trademark and the purity mark are also tempered for counterfeiting.

Although the detailed study of precious metals requires spectroscopic analysis, observations through optical microscopy can also help gain an understanding of their counterfeits as well as their geological origin.

Gold Smuggling

After the seizures of irregular gold by the Brazilian Federal Police, criminal experts have to answer the origin of the metal, among other questions. If it is found to be of alluvial origin, forensic investigation is directed to the mines that use mercury for processing; on the other hand, if it is of primary origin, the research will involve uncontrolled cyanidation.

Stereomicroscopy is useful for identifying resistant minerals that indicate a clear discriminating trace, which actually are mineralogical indicators that are preserved after the physical and chemical extraction of gold.

Figure 1.20 shows the presence of rounded and well-sorted quartz grains that are associated with a partially molten gold mass that indicates the alluvial origin of the samples found in a seizure in the Tapajós Gold Province of the State of Pará.

One of the tasks of the Brazilian Federal Police is to examine and evaluate jewelry seized in police operations related to embezzlement or fraud. Money laundering is increasingly commonly associated with these actions mainly due to the criminals' attempt to illicitly get illegal gold out of the country through ports and airports. One of the main tricks used is the coating of the gold pieces with a silver films to hide the finest materials (Fig. 1.21).

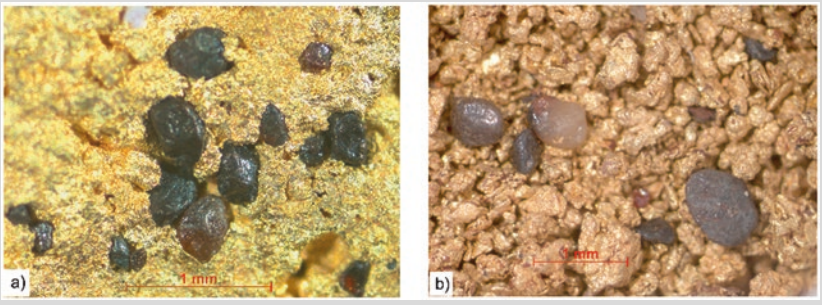

Fig. 1.20 (**a**) and (**b**) Rounded and well-sorted quartz grains associated with a partially molten gold mass

(continued)

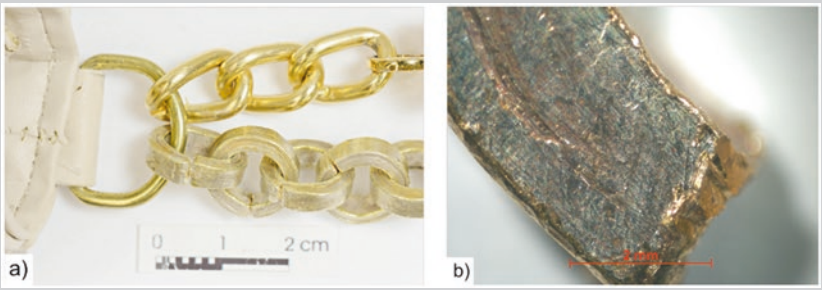

Fig. 1.21 Microscopic identification of a counterfeit jewel seized at Guarulhos airport, in the State of São Paulo; (**a**) Seized counterfeit jewel; (**b**) Detail of the jewel under a stereoscopic microscope where the non-continuous silver coating reveals the golden metal underneath

1.3.5 Building Materials

Building materials are frequently object of study in forensic application. Often, small fragments of building materials, such as bricks, tiles, or concrete, are present in soil and their identification and characterization by optical microscopy can help to localize a micro area of origin of a soil sample when compared with control samples (see Sect. 1.3.2.2).

In the field of forensic engineering, building materials are studied by optical microscopy to understand their behaviour and to determine the causes of deterioration by identifying the relationships between potentially reactive components (Fernandes et al. 2009). Furthermore, through comparative analysis, it is possible to identify the origin and provenance of the materials used as aggregates, such as fluvial and marine sand, pozzolan, gravel, and crushed stone. These studies are of relevant importance as they help in understanding any deficiencies in the quality of the materials used in cases of structural collapse.

Broekmans (2009) reports several cases of degradation of concrete artefacts. One of these cases concerned some concrete foundation pillars which, during the installation phase, underwent fracturing phenomena. The preliminary geotechnical investigations, conducted to identify the causes of the phenomenon, evidenced for the pillars compressive strength values in line with those required for these artefacts but were characterized by insufficient resistance to shear stresses. The polarizing microscope study of some representative samples of the fractured pillars revealed that the composition of the concrete was substantially compliant with what was declared by the supplier (with an aggregate formed by arenite, siltstone, quartz crystals, and rare flint in the coarse fraction, and quartz crystals, alkaline feldspar, amphibole and micas in the finer-grained one) and without evidence of alteration or deterioration phenomena of the concrete component. In any case, the microscopic investigation

revealed a substantial poor cohesion between the particles of the aggregate (in some cases, it was particularly evident due to the formation of interconnected channels), reasonably attributable to the liquefaction of the concrete mixture used. The phenomenon would have been caused by excessive stress on the concrete that is not fully consolidated, resulting in localized expulsions of water from the mix during the concrete processing phase. The compressive strength of the pillars would not have been significantly affected by this phenomenon, substantially counterbalanced by the vertical load during the compaction phase. Conversely, the resistance to shear stresses was required to be significantly reduced, since the cohesion between the aggregate and the cement was lost.

Acknowledgements The authors would like to thank Dr. Pier Matteo Barone for his support and assistance in reviewing the English version of the chapter, and Prof. Carmine Guarino for his help at analyzing the plant fragments of the case "Graminaceae".

References

Angelucci A (1989) Guida allo studio della sedimentologia. Edizioni Nuova Cultura, Rome

Broekmans MATM (2009) Petrography as an essential complementary method in forensic assessment of concrete deterioration: two case studies. Mater Charact 60:644–654

Cucciniello C, Fedele L, Morra V (2019) Microscopia ottica. In: Mercurio M, Langella A, Di Maggio RM, Cappelletti P (eds) Analisi Mineralogiche in Ambito Forense. Aracne Editrice, Latina, pp 43–82

Di Maggio RM (2019) Stereomicroscopia. In: Mercurio M, Langella A, Di Maggio RM, Cappelletti P (eds) Analisi Mineralogiche in Ambito Forense. Aracne Editrice, Latina, pp 23–42

Di Maggio RM, Barone PM (eds) (2017) Geoscientists at crime scene, a companion to forensic geoscience. Springer, Heidelberg

Di Maggio RM, Nuccetelli L (2013) Analysis of geological trace evidence in a case of criminal damage to graves. In: Pirrie D, Ruffell A, Dawson LA (eds) Environmental and criminal geoforensics, SP 384. Geological Society, London, pp 75–79

Di Maggio RM, Barone PM, Pettinelli E, Mattei E, Lauro SE, Banchelli A (2013) Geologia forense. Introduzione alle geoscienze applicate alle indagini giudiziarie. Dario Flaccovio Editore, Palermo

Fernandes I, Broekmans MATM, Noronha F (2009) Petrography and geochemical analysis for the forensic assesment of concrete damage. In: Ritz K, Dawson L, Miller D (eds) . Criminal and environmental soil forensics, Springer, Heidelberg, pp 163–180

Garuba T, Abdulrahaman AA, Olahan GS, Abdulkareem KA, Amadi JE (2014) Effects of fungal filtrates on seed germination and leaf anatomy of maize seedlings (Zea mays L., Poaceae). JASEM 18(4)

Gray A, Liu L, Facette M (2020) Flanking support: how subsidiary cells contribute to stomatal form and function. Front Plant Sci 11:881

Houck M (1992) Microscopy in forensic science. Microscopy Today 5:3–3

Krumbein WC (1941) Measurement and geologic significance of shape and roundness of sedimentary particles. J Sediment Petrol 11:64–72

Malossi A (2018) La storia mai raccontata dei rubini sintetici Douros. IGR Italian Gemological Review 4. https://www.rivistaitalianadigemmologia.com/2021/02/17/la-storia-mai-raccontata-dei-rubini-sintetici-douros/

Powers MC (1953) A new roundness scale for sedimentary particles. J Sediment Res 23(2):117–119
Pye K, Croft DJ (eds) (2004) Forensic geoscience: principles, techniques and applications, SP 232. Geological Society, London
Ruffell A (2009) Forensic pedology, forensic geology, forensic geoscience, geoforensics and soil forensics. Forensic Sci Int 202:9–12
Sini G (2006) Introduzione alla Microscopia in Radiazione Polarizzata. Istituto Nazionale di Fisica Nucleare (INFN), Università degli Studi di Bologna, Bologna
Valli VO (2013) Le indagini scientifiche nel procedimento penale. Giuffrè Editore, Milano
Wheeler B, Wilson LJ (2011) Practical forensic microscopy: a laboratory manual. Wiley, Hoboken
Wilson LJ, Wheeler B (2009) Optical microscopy in forensic science. In: Encyclopedia of analytical chemistry. Forensic Sci Sect https://doi.org/10.1002/9780470027318.a9101

Chapter 2
X-ray Diffractometry in Forensic Science

Piergiulio Cappelletti, Sossio Fabio Graziano, and David L. Bish

Abstract X-ray Diffractometry is a very useful analytical technique to achieve detailed information about the crystal structure and mineralogical composition, qualitative and quantitative, of matter. It is a technique that exploits the interaction between solid matter and X-rays that, converged on a substance, are diffracted. The outgoing X-rays, on the basis of the wavelength of the incident beam and according to the path within the analyzed sample provide information on fundamental parameters of the crystalline state as the distance of the lattice planes and the parameters of the elementary cell. The analytical result is called diffraction pattern containing a series of peaks that show the intensity and angular position of the diffracted X-rays. Typically, a diffraction pattern represents, for individual minerals, a kind of distinct fingerprint and can be used to easily identify the material or distinguish it from others, especially with the use of modern databases. X-Ray Diffractometry can be successfully used in a variety of fields: building materials, geological samples, environmental pollutants and increasingly by forensic sciences as a scientific aid for the analysis of evidence from crime scenes.

Keywords X-ray diffractometry · Diffraction · Diffractometer · Diffractometry in forensic sciences

P. Cappelletti (✉)
Dipartimento di Scienze della Terra, dell'Ambiente e delle Risorse (DiSTAR), Università Federico II di Napoli, Napoli, Italy
e-mail: piergiulio.cappelletti@unina.it

S. F. Graziano
Dipartimento di Farmacia, Università Federico II di Napoli, Napoli, Italy
e-mail: sossiofabio.graziano@unina.it

D. L. Bish
Molecular Structure Center, Indiana University, Bloomington, IN, USA
e-mail: bish@indiana.edu

M. Mercurio et al. (eds.), *Mineralogical Analysis Applied to Forensics*, Soil Forensics, https://doi.org/10.1007/978-3-031-08834-6_2

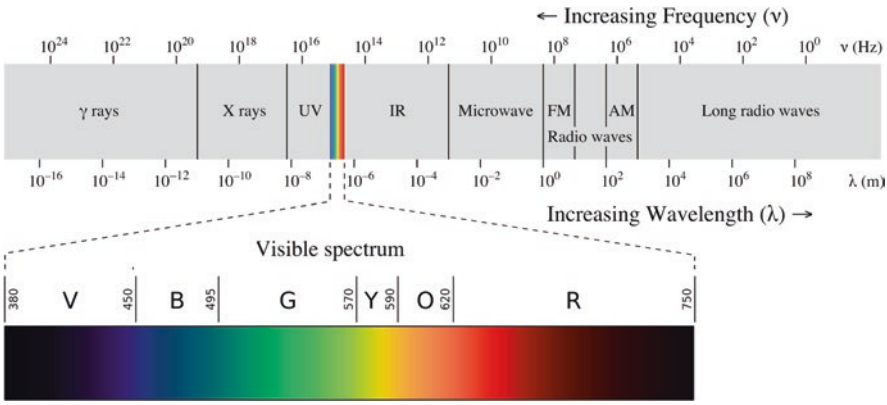

Fig. 2.1 Electromagnetic spectrum

X-ray diffractometry is a very useful technique for materials investigation based on the physics of X-rays and their interaction with solid matter. Two fundamental moments marked the use of this radiation in multiple fields: the discovery of X-rays by Röentgen in 1895 and the discovery of X-ray diffraction by the group of Laue in 1912 (Cullity and Stock 2001; Klug and Alexander 1974; Moore and Reynolds 1997). These two events marked the beginning of X-ray diffractometry as a tool for studying solid materials.

X-rays are electromagnetic radiations with a short wavelength depicted in Fig. 2.1. They originate via electronic (i.e., involving electrons) processes and can have energies/wavelengths overlapping with gamma rays (which originate via nuclear processes).

2.1 X-Rays: Characteristics, Production, Analytical Procedures

X-rays are generally produced by two different processes: involving ejection of an electron from atoms or via the acceleration of electrons. The physics of these processes are described in any text dealing with elements of X-ray production and, for this reason, this chapter discusses only the concepts directly related to the application of X-ray diffraction in forensic science. Whenever any electrically charged particle with sufficient kinetic energy accelerates (or decelerates) rapidly, X-rays are produced.

The radiation emitted by a struck atom includes a wide range of wavelengths. Part of these wavelengths depends on the energy of the electron beam that hits the atom but beyond a certain threshold of excitation the emitted radiation becomes independent from the incident one and assume values that depend only on the type of hit atom, which became emitter of a characteristic radiation.

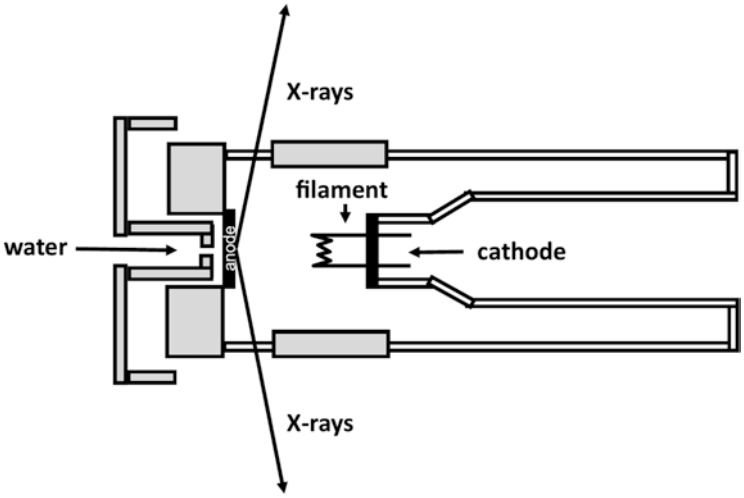

Fig. 2.2 X-ray tube schematic cross section

Traditional laboratory X-ray diffraction instruments use electrons from a filament (usually W) that impinge on a metal anode, all contained within a vacuum container (Fig. 2.2). The filament is surrounded by a metal cup, kept at the same high negative potential as the filament, which has the function of directing electrons towards a narrow region of the target, the so-called focal point, which generally reflects the shape of the filament. The high potential (tens of thousands of V) imposed between the cathode and the anode generates a flow of electrons towards the anode (target), which is hit by the beam of electrons at very high velocity. As most of the electrons' kinetic energy is converted to heat, the anode is almost always water cooled to prevent its fusion. X-rays are produced at the anode and are emitted in all directions, exiting the tube through two or more windows that are highly transparent to X-rays, usually Be.

2.2 X-Ray Diffraction

Well-ordered crystalline solids contain atoms that are typically arranged in three-dimensional space with a fundamental unit repeating by translation; this unit can be defined by three different axial lengths, *a, b, c*, and three different interaxial angles, α, β, γ.

If a X-ray beam hits a row of identical atoms in phase, they all emit a characteristic radiation with a spherical wave consistent with the incident radiation. The different spherical waves will interfere each other in a constructive way (with a resulting increased intensity) only under certain angles depending on the path made

by each spherical wave. The constructive interference condition for a row of atoms is given by Laue's equation developed in 1912.

Extending the concept of constructive interference in three dimensions, it is sufficient to consider three non-coplanar rows, the tangent line to the simultaneous intersection of the three emission fields represents the path of constructive interference. Constructive interference conditions can be derived using a geometrical procedure evaluating diffraction from a plane of atoms. This interpretation was intuited by Bragg in 1913 and considers not atoms or rows but parallel planes of atoms equally separated by a value *d*. Considering an X-ray beam striking the reticular plane at an angle θ and the corresponding diffracted beam (Fig. 2.3), constructive interference will occur when the path difference between the two incident and the scattered waves, which is 2dsinθ, is a multiple of the wavelength λ.

Thus, the equation:

$$2\text{dsin}\theta = n\lambda$$

where:

λ = the X-ray wavelength;
θ = the angle between S_0 and the parallel planes;
the vector S_0 represents the direction of the incident X-rays;
the vector S represents the direction of the diffracted X-rays;
d represents the distance between two parallel planes that scatter X-rays.

Bragg's equation summarizes the application of X-ray diffraction interacting with solid matter and can be found in several texts. The distance between parallel planes is defined as the "interplanar distance" *d* and is directly obtainable from Bragg's equation. Through decades of study, it has been discovered that any crystalline solid has a given set of interplanar distances, determined by the crystal structure of the solid. Thus, measurement of interplanar spacings facilitates identification of the investigated material, given an appropriate set of standard data.

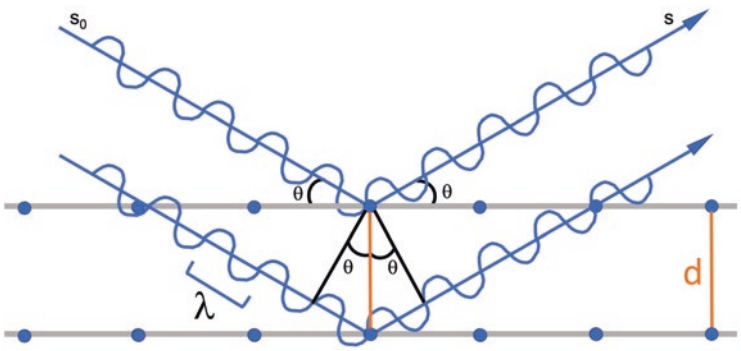

Fig. 2.3 X-ray diffraction path

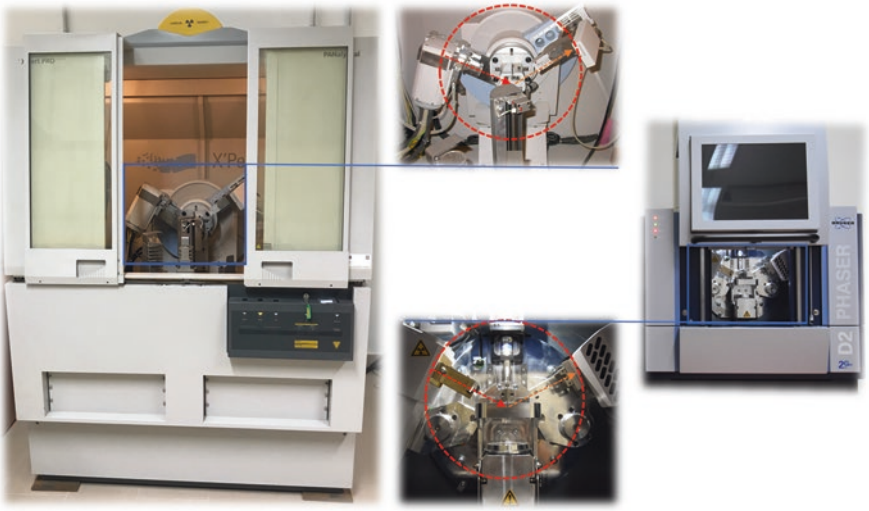

Fig. 2.4 Two examples of modern diffractometers currently used at the DiSTAR – University of Naples Federico II – Italy

2.3 Collecting and Analyzing Data

The X-ray diffractometer is the primary instrument for the study of crystalline solids.

Depending on power configurations and accessories, modern diffractometer very generally, consist of an X-ray source (tube), a support to accommodate the sample holder and an X-ray detection device. A variety of physical slits are added to this configuration to limit X-ray beam divergence and scattering (Fig. 2.4).

The sample is in the center of a goniometric circle while the x-ray source and receiver simultaneously rotate to measure at which angles the Bragg equation is satisfied (Fig. 2.5 – left). The result of a diffractometric analysis is a set of pairs of values, 2θ angle vs intensity of diffraction, which is called a diffraction pattern (Fig. 2.5 – right). The diffraction pattern is not a spectrum, as the wavelength of the radiation is constant.

Thus, each crystalline solid has its own X-ray diffraction pattern which can be used for identification, much like a fingerprint.

2.4 Phase Identification

Every crystalline solid produces a diffraction pattern characterized by a set of *d* values and relative intensities. The study of a diffraction pattern, based on the previous assumption, therefore allows a qualitative and quantitative interpretation, the

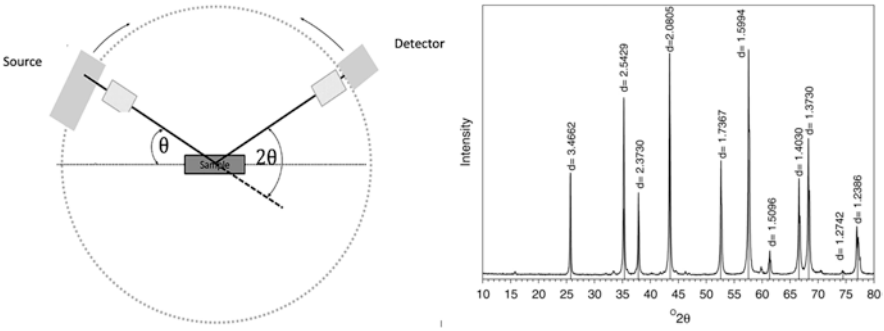

Fig. 2.5 Schematic geometry of a diffractometer along with a representative diffraction pattern. *d* values are directly computed from the X-ray wavelength and the 2-theta value, using the Bragg equation

9- 432 JCPDS-ICDD Copyright (c) 1999 Radiation: 1.54050 Quality: i

Ca (PO) (OH)
5 4 3

Calcium Phosphate Hydroxide

Hydroxylapatite, syn

Rad: CuKal Lambda: 1.54056 Filter: d-sp: Guin. -114.6
Cutoff: Int: I/Icor:
Ref: de Wolff, P., Technisch Physische Dienst, Delft, The Netherlands, ICDD Grant-in-Aid

Sys: Hexagonal S.G.: P63/m (176)
a: 9.418 b: c: 6.884 A: C: 0.7309
A: B: C: Z: 2 mp:
Ref: Ibid.

Dx: 3.15 Dm: 3.08 SS/FOM: F(30)=54.3(.0158,35)

ea: nwB: 1.651 ey: 1.644 Sign: - 2V:
Ref: Dana's System of Mineralogy, 7th Ed., II 879

Color: Green, bluish green, yellow-green, grayish green, violet, violet-blue, violet, colorless, light greenish white, gray, brown, pinkish red, pinkish-red, blue
Sample obtained following the procedure indicated by Hodge et al., Ind. Eng. Chem. Anal. Ed., 10 156 (1938). CAS no.: 1306-06-5. I/I1 are peak values from a pattern which shows slight broadening of prism reflections. Validated by calculated data 24-33. Apatite group, apatite subgroup. PSC: hP44. To replace 34-10. See ICSD 22059, 22060, 24240, 26204, 26205 and 34457 (PDF 73-293, 73-294, 73-1731, 74-565, 74-566 and 76-694). Mwt: 502.32.
Volume[CD]: 528.80.

d A	Int.	h k l
8.17	12	1 0 0
5.26	6	1 0 1
4.72	4	1 1 0
4.07	10	2 0 0
3.88	10	1 1 1
3.51	2	2 0 1
3.44	40	0 0 2
3.17	12	1 0 2
3.08	18	2 1 0
2.814	100	2 1 1
2.778	60	1 1 2
2.720	60	3 0 0
2.631	25	2 0 2
2.528	6	3 0 1
2.296	8	2 1 2
2.262	20	3 1 0
2.228	2	2 2 1
2.148	10	3 1 1
2.134	4	3 0 2
2.065	8	1 1 3
2.040	2	4 0 0
2.000	6	2 0 3
1.943	30	2 2 2
1.890	16	3 1 2
1.871	6	3 2 0

d A	Int.	h k l	d A	Int.	h k l	d A	Int.	h k l
1.841	40	2 1 3	1.530	6	3 3 1	1.280	7	4 2 3
1.806	20	3 2 1	1.503	10	2 1 4	1.265	3	3 2 4, 6 0 2
1.780	12	4 1 0	1.474	12	5 0 2	1.257	9	2 1 5
1.754	16	4 0 2	1.465	4	5 1 0	1.249	1	4 3 2
1.722	20	0 0 4	1.452	13	3 0 4, 3 2 3	1.235	11	5 1 3
1.684	4	1 0 4	1.433	9	5 1 1	1.221	9	5 2 2
1.644	10	3 2 2	1.407	4	4 2 2, 4 1 3			
1.611	8	3 1 3	1.348	3	5 1 2			
1.587	4	5 0 1	1.316	5	4 3 1, 4 0 4			
1.542	6	4 2 0	1.306	4	5 2 0, 2 0 5			

Strong lines: 2.81/X 2.78/6 2.72/6 3.44/4 1.84/4 1.94/3 2.63/3 2.26/2

Fig. 2.6 ICDD card example

latter directly linked to the intensity of the peaks of a given phase which, in the pattern, are proportional to the amount of the specific phase in a mixture (Cullity and Stock 2001).

J. D. Hanawalt, a chemist who worked for Dow Chemical in 1930, was the first to understand the need to create a database of diffraction patterns for materials useful for identification by comparison (Hanawalt search manual, ICDD 1999 – Fig. 2.6).

Today, this database is represented by the Powder Diffraction File (PDF) of the International Center for Diffraction Data (ICDD). Data in the PDF today include a variety of information on the material, in addition to a catalog of the *d* values and intensities of the materials diffraction peaks. This database interfaces with a wide range of globally distributed diffraction analysis software and contains numerous subfolders, such as minerals, metals and alloys, pharmaceuticals, excipients, superconductors, semiconductors, etc.

Identifying Constituents of Matter to Support Provenance Hypotheses

There are numerous applications and scientific research regarding X-ray diffractometry applied in the forensic field (Curry et al. 1982; Foner and Adan 1983; Rendle 2003; Kugler 2003; Ruffell and Wiltshire 2004; Kotrlý 2006; Abraham et al. 2007 and references therein) and certainly, among these, the first application is related to obtain information on geological and non-geological findings from crime scenes.

In May 1978 the body of Italian Prime Minister, Aldo Moro, was found in a car parked in the center of Rome (Fig. 2.7 – Lombardi 1999). On March 1978, Prime Minister was kidnapped by Red Brigades that also killed Moro's bodyguards. After almost 2 months an anonymous telephone call indicated

Fig. 2.7 Mr. Moro's body found inside the trunk. (Modified after Lombardi 1999)

(continued)

	Coat Pocket	Trousers cuffs	Shoes	Car floor	Car fenders	Car tires
Beach sand		0.75 g	minor adhesion	mixed with other items	mixed with volcanic rock soil	in the grooves
Volcanic soil			minor adhesion	mixed with other items	thick encrustation	
Bitumen			smears and pellets	smears and pellets	pellets	pellets
Road asphalt					small aggregates	small aggregates
Vegetal *Fragmenta*	few spikes	a capitulum of *Centaurea*		a varied assortment	minor fragments	
Building material			tiny bricks (?) fragments	a large assortment	small bricks (?) fragments	small bricks (?) fragments
Thermosetting polyesters					many fragments	many fragments
Paint			a tiny red flake	a varied assortment	several flakes	a few flakes
Fibers			just a few	a varied assortment		

Fig. 2.8 Evidence found on crime scene. (Modified after Lombardi 1999)

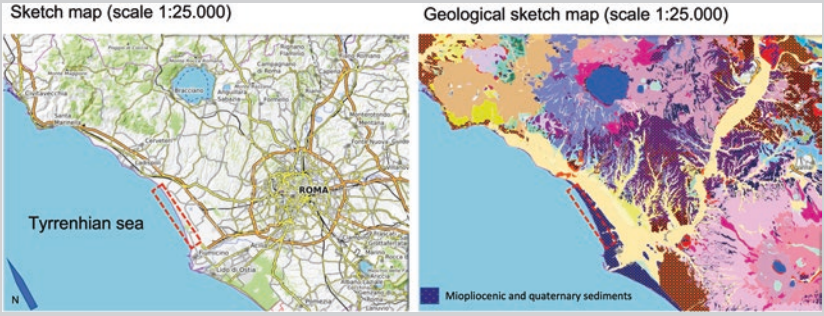

Fig. 2.9 Investigation area suggested by experimental evidence. (Area from Lombardi 1999 – Maps source: www.geoportale.regione.lazio.it)

the presence of a message from Red Brigades in a car parked in a street in the center of Rome. In that car there was Mr. Moro's body, killed few hours before.

During forensics investigation, sand, soil and other evidence were found on Mr. Moro's body and studied by means of optical microscopy and X-ray diffractometry (Fig. 2.8).

The latter, combined with other instrumental analyses, was very useful to assess sand composition, allowing investigators to draw some main inferences:

(a) The metamorphic rock fragments, and their minerals (microcline, part of the quartz, albite, orthoclase and chlorite) derived from the alteration of Cretaceous-Oligocene flyschoid formations outcropping along the coast in northern Latium.
(b) The volcanic fragments and their minerals (pyroxenes, amphibole, olivine, biotite and garnet) had textural and compositional characteristics which were easily ascribable to the alkaline-potassic Quaternary volcanics outcropping extensively in central-northern Latium (Fig. 2.9).

Due to the lack of specific provenance studies on sand composition along the coast near Rome, a systematic inspection of all accesses to the beach was carried out, sampling a 150 km long shore (Fig. 2.12).

(continued)

Fig. 2.10 Schematic map of the places concerning suspect's activities (left); crime scene photos: trunk of the vehicle and some findings (right). (Modified from Fitzpatrick and Raven 2012)

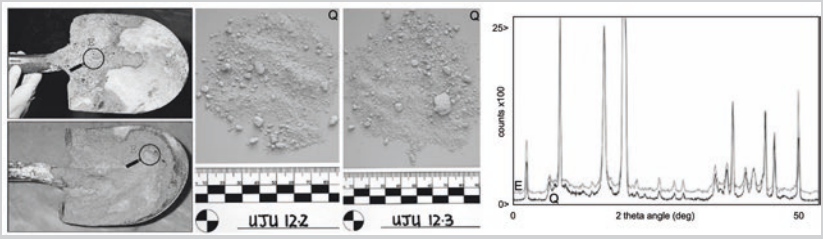

Fig. 2.11 Soil samples found on crime scene evidence (E – gray diffraction pattern) compared with bulk control sample from a quarry within the area under investigation (Q – black diffraction pattern). (Modified from Fitzpatrick and Raven 2012)

This scientific approach and the use of geological instrumental investigations permitted to compare and find similarities between sand collected on Mr. Moro's body and selected areas helping in narrowing investigation area.

Another example on the application of X-ray diffractometry, can be found in Fitzpatrick and Raven (2012). On September 2000, neighbors reported to police a disturbance at the home of two women living in the Adelaide suburb of Oakbank (Fig. 2.10 – left). That same evening, the husband of one of the women called the police referring that both his wife and mother-in-law were missing. He found blood stains and broken glass on the lounge room floor, while towels were missing, along with the quilt and pillow from his son's bedroom. His wife's car and his 22-year-old son were also missing. The following day, the car was found more than 200 km away by police near Moonta (Fig. 2.10 – left) on Yorke Peninsula. Inside the trunk, crime scene investigators found a pine post and a faintly bloodstained shovel, both sides of which were caked with pinkish powdery soil (Fig. 2.11). In the vehicle, investigators

(continued)

also located a green jade bracelet and boots, which were thinly coated with fine pinkish soil (Fig. 2.10 – right), as well as a blood-stained knife, blood-stained towels, bedding, and a pile of sticks, the kind suitable for starting a fire. Shortly afterward, police arrested the 22-year-old son in Moonta, where he had been attempting to get help for his broken-down car. Later in the day he was charged with the murder of his mother and grandmother.

The deposited layers of soil adhering to the shovel, jade bracelet, and boots (Fig. 2.10 – right) were examined and characterized. The mineralogical composition indicated dominant quartz, subordinate well crystalline kaolinite, minor muscovite, with traces of feldspar and talc (Fig. 2.11). The nature of this mineralogical composition suggested the soil materials originate from subsurface kaolinite-rich weathered zones, such as a mining area or quarry.

Sufficient descriptive, mineralogical, and chemical data were acquired on the questioned soil materials from the back and front of the shovel to compare properties, classify the soil materials, and attempt to build a conceptual soil model of their likely origin and mode of formation on the shovel. On the experimental results basis a control site from which collect control soils was identified in a quarry near Oakbank whose soil samples were analyzed by X-ray diffractometry with a *"conclusive"* degree of comparability and were virtually *"indistinguishable"*.

Despite there being no evidence of soil disturbance, some weeks after the event, women's bodies were (uncovered by wild animals) found a couple of meters away from the sampling site.

2.5 Sample Preparation: Good and Bad Practices

A correct preparation of sample is the mandatory basis for obtaining good and reliable analyses; diffraction data must be reproducible and the sample must be compositionally representative. The goodness of the results, in terms of a precise drawing, positioning and intensity calculation of the peaks, strictly depends on a correct preparation of the sample, especially in the presence of complex polyphasic materials (Bish and Reynolds 1989). These materials can be composed of minerals with a different hardness value (Mohs scale), for this reason one of the most common errors is to have a too coarse grain sized powder which will result in an inaccurate and imprecise representation of the intensities or in unusually intense and sharp peaks. Similarly, materials subjected to excessive grinding can generate erroneously widened peaks as well as producing small amounts of amorphous substance (Nakamura et al. 1989).

Fig. 2.12 Modern micronizer (left) currently used at the DiSTAR – University of Naples Federico II – Italy. Schematic section of the micronizer jar (right)

An automatic instrument that allows to obtain particles with a uniform size <10 μm is the automatic micronizer (Fig. 2.12 – left), which therefore is an ideal instrument to obtain the requirements for an optimal analysis (Bish and Reynolds 1989). The sample placed inside a specific jar (Fig. 2.12 – right) is ground in wet conditions by the mechanical action of agate cylinders, vibrated by the instrument. The result is a suspension of deionized water or alcohol and sample, which is subsequently dried, containing all particles with grain size statistically <10 μm.

Samples to be analyzed need to be placed on a specific sample holder to be analyzed. Even this operation, if not carried out correctly, can produce representation errors in the final diffraction pattern. The most common errors, directly related to a non-optimal deposition of the sample concern position and intensity of the peaks and are a direct function of the size of the area that houses the sample itself (Parrish et al. 1966).

Since the area irradiated by the incident X-ray beam increases as the 2θ diffraction angle decreases, it is very important to ensure that the beam falls fully on the sample down to the lowest angle of interest to avoid having low intensity peaks where the incident X-ray beam is not completely on the sample (Parrish et al. 1966).

X-ray diffraction on powders assumes an infinitely thick sample or a sample thick enough to be irradiated but not passed through (Cullity 1978). Once again, the ideality of this condition is extremely difficult to obtain, especially regarding samples made up of very small quantities (as is often the case with "forensic" samples).

Ideally, a correctly prepared sample, placed on a sample holder should have a flat surface with no roughness, curvature or inclinations whatsoever that can modify, in the geometry of the diffractometer, the 2:1 angular relationship between the incident beam and the sample surface, resulting in consequently systematic deviations in the position and widths of the peaks (Klug and Alexander 1974).

Displacement of the height of the sample is one of the most common errors in diffractometry on powders, and the inaccurate height of the sample on the support usually manifests itself with a systematic error on the position of the phase peaks (Bish and Reynolds 1989).

The result (Fig. 2.13) of this error, in visual and practical terms, is manifested by a shift of the corresponding peak towards low angles in the case of a sample lower than the support, vice versa, the opposite.

Another very common error in diffractometry, depending on deposition technique on the sample holder, is represented by the phenomenon of the preferential orientation of the crystalline particles.

In this way, particles do not appear to be statistically oriented with respect to the incident X-ray beam, thus generating an increase in intensity of reflections corresponding to the cleavage planes.

To mitigate preferential orientation of powder samples, different techniques have been proposed, by different authors, over the years (just to cite a few: Klug and Alexander 1974; Smith and Barrett 1979; Bish and Reynolds 1989) such as preparation of samples with random orientation or using side- or back-loading of the sample, into a hollow holder. Alongside these techniques, others involve mixing sample with amorphous materials, defined as "fillers".

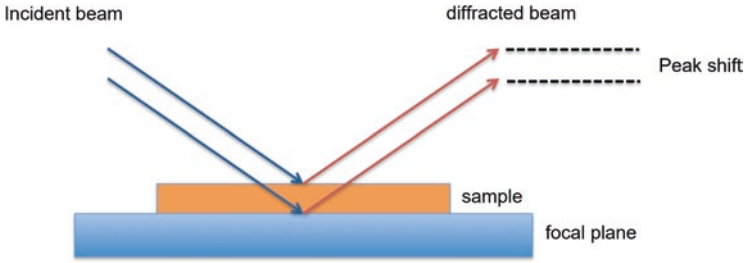

Fig. 2.13 Incorrect sample presentation

Identification of Counterfeit Substances

In 2015 the Food and Drug Administration's Forensic Chemistry Center described the development of a method for analyzing pharmaceutical solid dosage forms, active pharmaceutical ingredients (API) and excipients using X-ray diffractometry (XRD) (DeWitt 2015). The suggested method was validated by measuring the XRD patterns of known counterfeit pharmaceutical products and comparing them with the XRD patterns of authentic products (Fig. 2.14).

Counterfeit pharmaceuticals are illegally manufactured and widely distributed throughout the world. These mixtures are unapproved and unregulated products that may contain dangerous or harmful ingredients, or an insufficient amount of the active pharmaceutical ingredient (API).

(continued)

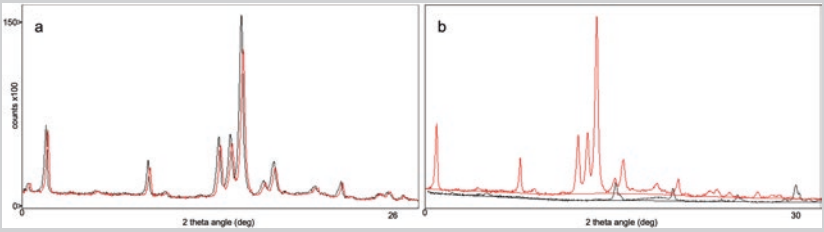

Fig. 2.14 X-ray diffractometry used in: (**a**) variability studies between authentic dosage forms and (**b**) for comparing authentic (red diffraction pattern) and counterfeit dosage forms (black diffraction pattern). (Modified after DeWitt 2015)

First of all, was checked the variability among produced lots (Fig. 2.14a) and then, acquired patterns were compared with those from counterfeit dosage forms (Fig. 2.14b). It was found that, assuming the tolerance of peak shifts less than 0.2°, authentic dosage form was evident for all investigated lots.

Higher peak shifting or missing/additional peaks were, instead, the criteria for the identification of a counterfeit product.

2.6 Preferred Orientation in Clay Minerals

Identification of clay minerals, unlike what has been explained in the previous paragraph, takes advantage of the preferred orientation of this class of minerals, to emphasize their basal reflections and thus allow accurate recognition. These minerals have very similar structures in the X and Y directions, diagnostic parameters are therefore to be found on the Z axis. The relatively small size of the Z axis in clay minerals results in low and wide peaks that are difficult to distinguish from the background of the diffraction pattern (Bish and Reynolds 1989). This condition, to favor the recognition of these minerals, paradoxically, requires maximizing the preferential orientation and to have the largest possible number of crystallites oriented parallel to the surface of the sample. The conditions for having such a high degree of preferential orientation are the following:

(a) the crystallites must have a good planar morphology,
(b) must be separated from each other in aqueous suspension,
(c) the sample must exclusively contain minerals with a planar structure,
(d) the sample support must be very smooth so as not to create an irregular surface, after the deposition of the first level of the sample, previously dispersed in solution.

While the morphology of crystallites is not a controllable variable and sometimes generates very different diffraction intensities even within the same sample, separation of crystallites in aqueous suspension is a very useful and easily implemented

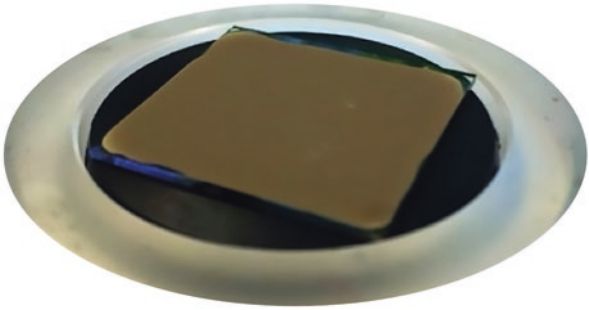

Fig. 2.15 Oriented aggregate of clay sample prepared on a glass support

technique. The analytical procedures were developed by Jackson (1969) and essentially consist in a first coarse grinding of the sample, followed by a mechanical separation of the particles in aqueous suspension by means of ultrasonic instruments (Moore and Reynolds 1997). Subsequently, at precise intervals regulated by Stokes' law (1851), the suspension is decanted and the sedimented fractions are removed. The result at the end of the sedimentations is a sample, always in suspension but ideally containing single crystals of clay minerals. This resulting suspension is centrifuged (Moore and Reynolds 1997) to allow separation of the particles according to size and, at the end of several centrifuge cycles, recovered. In the above-mentioned suspension, there are therefore single crystals of clay minerals which are concentrated either by partial drying or by means of an ultracentrifuge to be then redispersed in a smaller volume of water. The concentrated suspension, by means of pipettes, is then deposited on glass supports (Fig. 2.15) and dried at a room temperature, to avoid damage to non-crystalline fraction, eventually present. The crystals deposited on the support, in this way, will settle according to their elongated habitus, thus offering the diagnostic direction Z to the X-ray beam (Moore and Reynolds 1997).

Oriented aggregates, prepared according to the above-described techniques, are then analyzed (a) under normal conditions, (b) after heat treatments at different temperatures to ensure the collapse of each eventually present expanding layer and (c) under conditions of glycol-ethylene solvation (Bradley 1945). This triple analysis is directly functional to the recognition of clay minerals since it will produce three different diffraction patterns which will show, in comparison with the "normal" acquisition, a displacement and/or a change in morphology of the characteristic peaks of a specific clay mineral.

2.7 Quantitative Analysis

Quantitative analysis dates back to 1925, when Navias determined the amount of mullite in a baked pottery, and to 1936 when Clark and Reynolds suggested the internal standard method later perfected by Alexander and Klug in 1974 (Snyder and Bish 1989).

Today, there are several methods useful for the quantitative reconstruction of an unknown sample, for example:

Internal standard method/RIR method (Reference Intensity Ratio): considers the intensity ratios between peaks belonging to different phases within the sample. The method applies only to powders, to which a known quantity of a standard substance has been added and mixed. Visser and De Wolff in 1964 used and then proposed corundum (Al_2O_3) as a common reference internal standard (Chung 1974a, b).

External standard method for subsequent additions: a known quantity of another phase is added to the sample.

Full-pattern fitting/Rietveld method: fits and models the entire diffraction profile, refining possible percentage values for the different phases present.

The latter method provides numerous advantages over conventional quantitative analysis techniques: the fit of the whole pattern, in fact, minimizes the negative effect of any overlapping of peaks, considers more accurately the contribution of the background (Wiles and Young 1981) and also allows to correct any preferred orientation using a refinement algorithm that uses the March-Dollase formula (Dollase 1986).

Quantification of Sample Constituents

The precise determination of the quantities of the constituents of matter, whether soil, sand, or human remains, can be of great help in supporting the work of investigators with experimental information.

In 2002, during the investigation of an alleged homicide several exhibits were submitted for soil comparisons between recovered samples from crime scene, and two geographical locations; the location where the deceased was discovered, and another site. Soil collected from the driver's footwell was consistent with originating from the roadside near the deceased (Pitts and Clark 2020).

Soil analysis was an important aspect for forensic investigations. It was used to link vehicles, tools or persons to crime scene locations or secondary sites. The problem in reported investigation was to correctly evaluate quantitative mineralogy in quartz sands.

Data for quartz, feldspar, and mica percentage intensities from the <20 mm fraction was not included in the interpretation process because these minerals can be present as anthropogenic sources (for example road surfaces using common types of rock aggregate).

Further evaluation of potential matches was performed by comparing the original diffraction patterns (Fig. 2.16).

The soil samples were first examined distinguishing physical characteristics. A sub-sample of quartz grains from each sample was hand-picked and the quartz fine fraction recovered, examined using XRD and compared using

(continued)

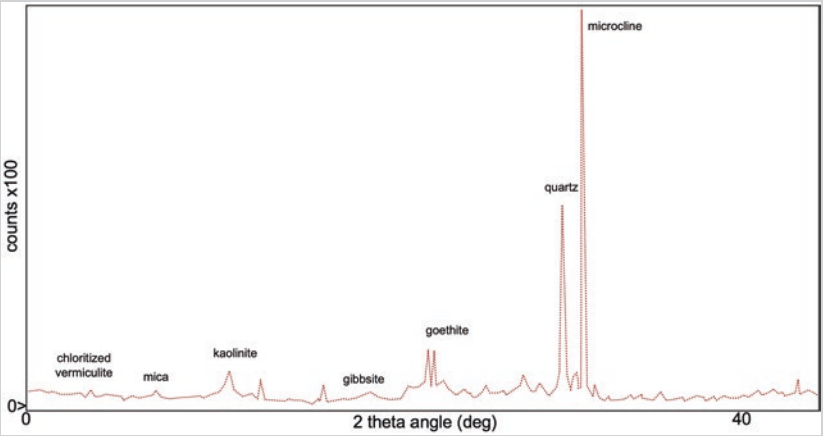

Fig. 2.16 X-ray diffraction pattern obtained from a reference sample in the Spearwood Dunes. (Modified from Pitts and Clark 2020)

a search-match process between crime scene samples and nearby geologic locations known to have similar features.

In this case mineralogical characterization of quartz grains belonging to the <20 mm fraction helped in discriminating the quartz-dominated sandy soils of the Swan Coastal Plain in the Perth region.

2.7.1 Full-Pattern Fitting/Rietveld Method

The digital acquisition of a diffraction pattern provides the possibility to perform a quantitative analysis of a sample using all the data of a given pattern instead of considering only the intensities of the major reflections. The full-pattern fitting method, therefore, works on the whole pattern, also including the background, comparing it with one or more patterns of synthetic minerals or obtained from data of crystalline structures (Bish and Howard 1986; Hill and Howard 1987; O'Connor and Raven 1988) or by the combination of standards diffraction patterns. An example of such methods is certainly represented by the FULLPAT program (Chipera and Bish 2002, downloadable at http://www.ccp14.ac.uk/ccp/web-mirrors/fullpat/), which combines the advantages of full-pattern fitting with traditional methods that employ RIR. FULLPAT can quantize all phases of a sample, including partially ordered or amorphous ones such as clay minerals and volcanic glasses. The use of an internal standard allows to conduct unconstrained analyzes by directly comparing the reference standards for each phase of the sample.

In any case, however, the method currently most used and which refers to the full pattern fitting technique, is the Rietveld method.

The Rietveld method (Rietveld 1969) was initially conceived for the refinement of crystal structures using neutron diffraction data. Basically, it consists in adapting the whole experimental diffraction pattern to calculated profiles allowing to obtain quantitative information on the phases present from the scale ratios for each phase in a mixture (Bish and Post 1993). The refinement is performed by minimizing the weighted sum of the square differences between the intensities, observed, and calculated, at each step, in a digitally acquired powder diffraction pattern.

This technique requires prior recognition and knowledge of the crystalline structure of the minerals (although not necessarily of all) present in a sample. In a typical Rietveld refinement strategy for a quantitative analysis, the following are varied: (a) the individual scale factors of the phases (relative to the weight content of each phase); (b) the peak-shape parameters for each phase, together with the background calculation and the cell parameters. In some cases, the atomic positions and the occupations of the sites for the most abundant phases can also be refined, if it is of interest to determine these characteristics; in particular for some phases (e.g., zeolites) to vary the occupancy of some sites (extra-framework cations, water molecules) may be necessary to obtain more accurate scale factors (and therefore weight percentages) (Bish and Post 1993).

Minerals in Human Remains

Investigation by X-ray diffractometry can be very useful for studying human remains. Skeleton, teeth, kidney stones, gallstones, just to name a few anatomical parts, are made up of minerals.

The study of burned human remains is of considerable importance in forensic science, forensic anthropology, and crime scene investigation. An understanding of the changes that the body has undergone as a result of burning can provide significant information regarding the context and conditions of the burning event itself. Such crime scene information can include the temperature of the fire, the position of the fire, and the presence of accelerants (Piga et al. 2009).

A visual inspection of the remains is the basis of this kind of investigation, but it has also been shown both experimentally and statistically that changes within the skeletal microstructure involve changes in bone that can predict burning context.

In Piga et al. (2009), a particular focus on the hydroxylapatite (HA) mineral phase was carried out; HA is the main inorganic component of bones. A reference samples was fired at different temperatures and for different soaking times evidencing modifications in crystallite size (A value increases) (Fig. 2.17 – left).

The burning of the experimental specimens at different temperatures also caused the disappearance of the calcite and the simultaneous appearance of calcium oxide peak ($2\theta = 37.5$) at 775 °C, becoming more evident at 800 °C

(continued)

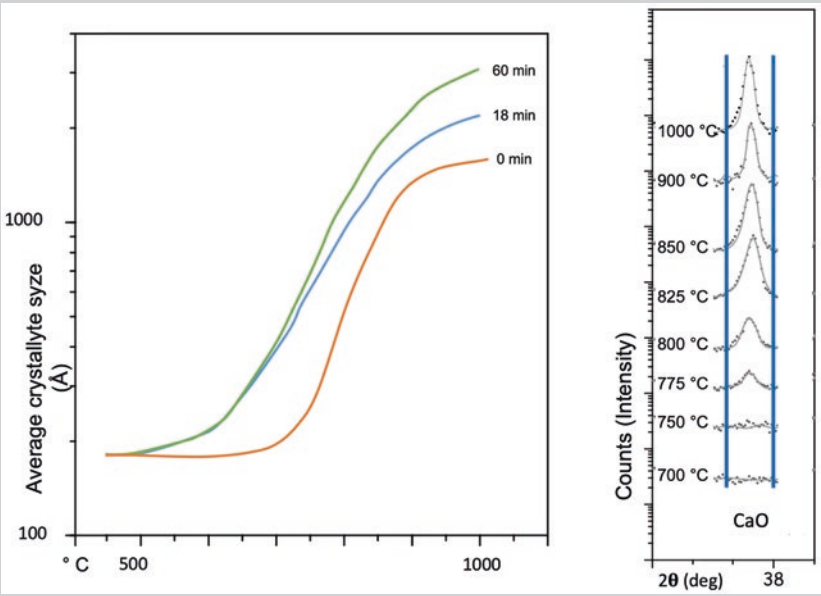

Fig. 2.17 Crystal size (left) and x-ray diffraction pattern from reference samples at different temperatures/soaking times (right). (Modified from Piga et al. 2009)

and increasing with temperature until 1000 °C where this phase reached its maximum amount (Fig. 2.17 – right).

Knowledge of the characteristics of minerals can provide useful information about the state of the remains (unburned or burned and at what temperature) that may be effective in forensic investigations.

2.8 Environmental Crimes: Evaluation of the Presence of Asbestos Minerals in Massive Samples

In recent years the X-ray diffractometric methods continuously evolved and improved in such a way as to overcome drawbacks related both to the technique itself and to its application to asbestos (De Stefano et al. 2004). The possibility of using XRPD for the determination of the possible presence of asbestiform phases in massive samples, is officially recognized by Italian laws (D.M. 6 September 1994) along with infrared spectroscopy with Fourier transform (FT-IR) and scanning electron microscopy (SEM). XRPD provides, as widely recalled in this chapter, mineralogical information on crystalline phases present in polimineralic mixtures (rocks or synthetic geomaterials), therefore also asbestos minerals can be easily identified even if present in negligible percentages (lower than 1% by weight). It is also

necessary to remember, however, that the mineralogical information may not be sufficient to discriminate between the different fibrous varieties: for example, the X-ray patterns of the serpentine polymorphs – $Mg_3Si_2O_5$ $(OH)_4$, are hardly distinguishable if the experimental conditions are not particularly accurate; only an in-depth and targeted data collection strategy enables to discriminate between non-fibrous (lizardite and antigorite) and fibrous varieties (ortho- and clino-chrysotile, "disordered" chrysotile). Quantitative analysis methodology with the Rietveld approach has proved to be particularly useful and effective for the assessment of the asbestiform component in asbestos-cements (Gualtieri and Artioli 1995; Gualtieri 1999, 2007), extensively used during the 70s and 80s (pre-Ronchi decree, dated 1992), or in polyvinyl linoleum flooring of public buildings (schools, hospitals), currently still present in many buildings. The characterization of these latter materials requires a specific heat treatment (at about 460 °C, Verkouteren et al. 2002) before the diffractometric investigation, in order to correctly discriminate the different inorganic phases combined with polymeric materials (rubber), such as kaolin often used as a filler, which has diffraction peaks that can be easily confused with those of chrysotile asbestos.

2.9 Cultural Heritage Crimes: Identification of the Geological Provenance of Geoarchaeological Materials

X-ray diffraction is particularly relevant in the characterization of materials used in the field of Cultural Heritage. In recent years there have been numerous uses of this very versatile analytical technique on rocks used as building stones and other geomaterials such as plasters, mortars, ceramics to correctly identify their origin, composition, nature, and products of degradation (very often crystalline compounds themselves) due to atmospheric agents that could compromise the survival of cultural heritage.

The concept of mineral as a marker can be very important for an accurate characterization of the origin of geomaterials used in historical monuments, also to provide indications on possible restoration interventions (of materials damaged by time or criminal acts) or to identify the origin/belonging of stolen pieces.

In Banchelli et al. (1997), sandstone samples (*Pietra Serena*, *Pietraforte*) coming from important historical monuments (e.g., *Loggia dei Lanzi*, *Palazzo Strozzi*, etc.) of the city of Florence were carefully characterized in terms of amount and type of clay minerals (XRPD on <4 μm fraction according to the method described in Sect. 2.6). This investigation allowed to establish with high precision the exploitation areas of these geological materials and, in some cases, even identify the exact excavation horizons within historical mining sites. A further validation of this methodology was given by the historical and archival data concerning the architectural evolution (construction, remakes, restorations) of these historical monuments which *de facto* confirmed what was proved by the mineralogical analysis.

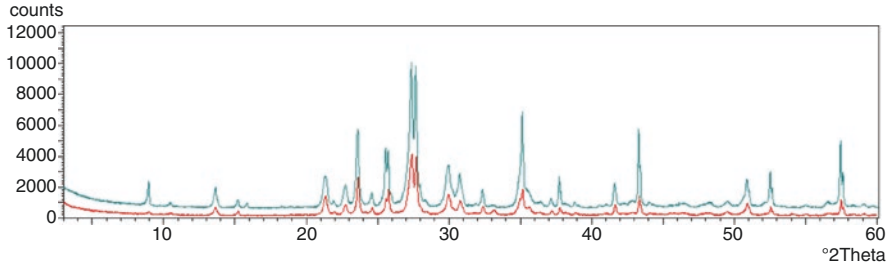

Fig. 2.18 Comparison between the diffraction patterns of a lava sample coming from M. Olibano (green) and of the RT 14_lava sample coming from a wall system of the Rione Terra in Pozzuoli (red). (Modified from de Gennaro et al. 2008)

Geomaterials of *Insula* 14 of the *Rione Terra* di Pozzuoli, were studied combining XRPD techniques with a physical-mechanical characterization (in particular a porosimetric investigations). This analytical approach allowed to identify the different lithofacies of Neapolitan Yellow Tuff and lavas (de Gennaro et al. 2008) occurring in several outcrops of the province of Naples (Quarto, Licola, Marano for the Yellow Tuff and M. Olibano for the Phlegraean lavas) (Fig. 2.18) and widely used over the centuries.

Another experimental work allowed to distinguish Piperno from the piperno-like Ignimbrite Campana facies (both important volcanoclastic building stones from Campi Flegrei volcanic district, very similar macroscopically, and used in historical construction and monuments in the Campania region and in particular in the provinces of Naples and Caserta) (Calcaterra et al. 2013). Sodalite – $Na_8Al_6Si_6O_{24}Cl_2$, a feldspathoid of the cancrinite-sodalite family – was the mineral-marker since it is present only and exclusively in the Piperno formation, while completely absent in the Ignimbrite Campana.

2.10 Concluding Remarks

The applications, the examples and the case studies reported in this chapter can and must be considered only as the tip of the iceberg considering the enormous scalability and the great versatility of X-ray diffractometry applied to forensic investigations.

Summarizing, this technique can be used to:

– investigate and study even very small samples. One of the fundamental (and in some cases, most critical) aspects in forensic applications is often represented by the small amount of available sample for analysis. However, choosing properly the sample preparation techniques, it is possible to obtain very reliable and significant findings even starting from very small samples. As a matter of fact, it is possible to obtain reliable mineralogical information even from only 0.08 mg of

sample (Vaniman and Bish 1990) and to obtain quantitative analyses with LLD (Lower Limit of Detection) of crystalline phases between 100 and 500 ppm (Bish and Chipera 1991).
– Identification and delimitation of the area to be investigated. Qualitative/quantitative mineralogical information, properly evaluated together with the geological context, although not conclusive, can be very important in defining the area to be investigated.
– The investigation of the compositional characteristics of stolen artifacts or the identification of potential replacements for damaged materials (in monumental and civil buildings) can represent other major fields of application of X-ray diffractometry, with reference to the field of Cultural Heritage.

The case studies reported here and the many methodological applications of X-ray diffractometry, demonstrate how this analytical technique is finding more and more opportunities to be used in important forensic investigations.

The data that can be obtained both in qualitative and quantitative terms, turn out to be more and more a valid and sometimes essential support to the investigation and analysis of samples from crime scenes.

References

Abraham JT, Shukla SK, Singh AK (2007) Application of X-ray diffraction techniques. Forensic Sci Commun 9(2):1–6

Banchelli A, Fratini F, Germani M, Malesani P, Manganelli del Fà C (1997) The sandstone of Florentine historic buildings: individuation of the marker and determination of the supply quarries of the rocks used in some Florentine monuments. Sci Technol Cult Herit 6(1):13–22

Bish DL, Chipera SJ (1991) Detection of trace amounts of erionite using X-ray powder diffraction: erionite in tuffs of Yucca Mountain, Nevada, and Central Turkey. Clay Clay Miner 4:437–445

Bish DL, Howard SA (1986) Quantitative analysis via the Rietveld method. Workshop on quantitative X-ray diffraction analysis. Nat'l Bur Stds 6:23–24

Bish DL, Post JE (1993) Quantitative mineralogical analysis using the Rietveld full-pattern fitting method. Am Mineral 78:932–940

Bish DL, Reynolds RC Jr (1989) Sample preparation for X-ray diffraction. Rev Mineral 20:73–99

Bradley WF (1945) Molecular association between montmorillonite and some polyfunctional organic liquids. J Am Chem Soc 67:975–981

Calcaterra D, Langella A, Morra V, Cappelletti P, Colella A, de Gennaro R, de Gennaro M (2013) Il Piperno. In: de Gennaro M, Calcaterra D, Langella A (eds) Le Pietre storiche della Campania: dall'oblio alla riscoperta. Luciano Editore, Napoli, pp 179–198

Chipera SJ, Bish DL (2002) FULLPAT: a full-pattern quantitative analysis program for X-ray powder diffraction using measured and calculated patterns. J Appl Crystallogr 35:744–749

Chung FH (1974a) Quantitative interpretation of X-ray diffraction patterns I. Matrix flushing method of quantitative multicomponent analysis. J Appl Crystallogr 7:519–525

Chung FH (1974b) Quantitative interpretation of X-ray diffraction patterns II. Adiabatic principle of X-ray diffraction of mixtures. J Appl Crystallogr 7:526–531

Cullity BD (1978) Elements of X-ray diffraction, 2nd edn. Addison-Wesley Publishing Company Inc, p 555

Cullity BD, Stock SR (2001) Elements of X-ray diffraction, 3rd edn. Prentice Hall, Upper Saddler River

Curry CJ, Rendle DF, Rogers A (1982) Pigment analysis in the Forensics examination of paints I. Pigment analysis by X-ray diffraction. J Forensic Sci Soc 22(2):173–177
D.M. September 6, 1994, Ministry of Health (G.U. n.288, ordinary supplement of December 10, 1994) Regulations and technical methodologies for the risk assessment, remediation, control and maintenance of materials containing asbestos in buildings
de Gennaro M, Langella A, Cappelletti P, Colella A, Buccheri G, D'Amore M (2008) I geomateriali dell'Insula 14. In: Edizioni Scientifiche Italiane, a cura di Aveta A. Diagnostica e conservazione l'insula 14 del Rione Terra, vol 4, pp 183–205
De Stefano L, Palumbo M, Cioffi R (2004) L'amianto campionamento ed analisi, Franco Angeli ed, 160 pp
DeWitt KM (2015) X-ray powder diffraction method development and validation for the identification of counterfeit pharmaceuticals. Mater Sci:1–28
Dollase WA (1986) Correction of intensities for preferred orientation in powder diffractometry: application of March model. J Appl Crystallogr 19:267–272
Fitzpatrick RW, Raven M (2012) How pedology and mineralogy helped solve a double murder case: using forensics to inspire future generations of soil scientists. Soil Horizons 53:14–29. https://doi.org/10.2136/sh12-05-0016
Foner HA, Adan N (1983) The characterization of papers by X-ray diffraction (XRD): measurements of cellulose crystallinity and determination of mineral composition. J Forensic Sci Soc 23(4):313–321
Gualtieri AF (1999) The aid of X-ray powder diffraction to the characterisation and treatment of asbestos containing materials. Period Mineral 68(1):1–11
Gualtieri AF (2007) Un nuovo futuro per l'amianto. HI-Tech Ambiente 9:66–67
Gualtieri A, Artioli G (1995) Quantitative determination of chrysotile asbestos in bulk materials by combined Rietveld and RIR methods. Powder Diffract 10(4):269–277
Hill RJ, Howard CJ (1987) Quantitative phase analysis from neutron powder diffraction data using the Rietveld method. J Appl Crystallogr 20:467–474
Jackson ML (1969) Soil chemical analysis-advanced course. Published by the author, Madison, 895 pp
Klug HP, Alexander LE (1974) X-ray diffraction procedures for polycristalline and amorphous materials. Oxford University Press, Oxford, p 332
Kotrlý M (2006) Application of X-ray diffraction in forensics science. Z Kristallogr Suppl 23:35–40
Kugler W (2003) X-ray diffraction analysis in the forensics science: the last resort in many criminal cases. Adv X-ray Anal 46:1–16
Lombardi G (1999) The contribution of forensic geology and other trace evidence analysis to the investigation of the killing of Italian Prime Minister Aldo Moro. J Forensic Sci 44(3):634–642
Moore DM, Reynolds RC Jr (1997) X-ray diffraction and identification and analysis of clay minerals, 2nd edn. Oxford University Press, New York
Nakamura T, Sameshima K, Okunaga K, Sugiura Y, Sato J (1989) Determination of amorphous phase in quartz powder by x-ray powder diffractometry. Powder Diffract 4:9–13
O'Connor BH, Raven MD (1988) Application of the Rietveld method refinement procedure in assaying powdered mixtures. Powder Diffract 3:2–6
Parrish W, Mack M, Taylor J (1966) Determination of apertures in the focusing plane of X-ray powder diffractometers. J Sci Instrum 43:623–628
Piga G, Thompson TJU, Malgosa A, Enzo S (2009) The potential of X-ray diffraction in the analysis of burned remains from forensic contexts. J Forensic Sci 54(3):534–539. https://doi.org/10.1111/j.1556-4029.2009.01037.x
Pitts KM, Clarke RM (2020) The forensic discrimination of quartz sands from the Swan Coastal Plain, Western Australia. Forensic Sci Int Rep 2:Art. no. 100130. https://doi.org/10.1016/j.fsir.2020.100130
Rendle DF (2003) X-ray diffraction in forensics science. Rigaku J 19(2):11–22
Rietveld HM (1969) A profile refinement method for nuclear and magnetic structures. J Appl Crystallogr 2:65–71

Ruffell A, Wiltshire P (2004) Conjunctive use of quantitative and qualitative X-ray diffraction analysis of soil and rocks for forensics analysis. Forensic Sci Int 145:13–23
Smith DK, Barret CS (1979) Special handling problems in X-ray diffractometry. Adv X-ray Anal 22:1–12
Snyder RL, Bish DL (1989) Quantitative analysis. Rev Mineral 20:101–142
Vaniman DT, Bish DL (1990) Yoshiokaite, a new Ca, Al-silicate mineral from the Moon. Am Mineral 75:676–686
Verkouteren J, Windsor E, Conny J, Perkins R, Ennis (2002) Analysis of kaolinite/chrysotile mixtures by ashing and x-ray diffraction. Powder Diffract 17(3):196–201
Visser JW, De Wolff PM (1964) Absolute intensities. Report 641.109. Technisch Physische Dienst, Delft
Wiles DB, Young RA (1981) A new computer program for Rietveld analysis of X-ray powder diffraction patterns. J Appl Crystallogr 14:149–151
www.geoportale.lazio.it

Chapter 3
Scanning Electron Microscopy (SEM) in Forensic Geoscience

Paola Petrosino, Duncan Pirrie, Licia Santoro, and Roberto de Gennaro

Abstract This chapter offers an overview of Scanning Electron Microscopy (SEM) and Electron Microanalysis fundamentals using Energy Dispersive Spectroscopy (EDS) and Wavelength Dispersive Spectroscopy (WDS). The main technical features and steps necessary to acquire high-resolution images and obtain reliable chemical analytical results are here briefly summarized. The chapter also describes the main advantages of using this non-destructive technique for forensic geosciences applications, with a particular focus on Automated Mineralogy (AM). This analytical technique expands the potentiality of modern SEM systems, allowing a rapid achievement of mineral classification and modal composition of grain mixtures. Finally, we present real case studies on applying SEM-EDS, WDS, and AM techniques to several fields of forensic geology. Significant examples will include studies on prediction of soil provenance, fingerprinting of airborne asbestos, and comparison between soils and sediment samples to test an association between a soil residue found at a crime scene and relevant items for investigation.

Keywords Electron microanalysis · Non-destructive techniques · Automated mineralogy · Airborne asbestos · Soil provenancing

P. Petrosino (✉) · R. de Gennaro
Dipartimento di Scienze della Terra, dell'Ambiente e delle Risorse (DiSTAR), Università Federico II, Napoli, Italy
e-mail: paola.petrosino@unina.it; robdegen@unina.it

D. Pirrie
School of Applied Science, Faculty of Computing, Engineering and Science, University of South Wales, Pontypridd, UK

IUGS Initiative on Forensic Geology, Pontypridd, UK
e-mail: duncan.pirrie@southwales.ac.uk

L. Santoro
Dipartimento di Scienze della Terra, Università di Torino, Torino, Italy
e-mail: licia.santoro@unito.it

M. Mercurio et al. (eds.), *Mineralogical Analysis Applied to Forensics*, Soil Forensics, https://doi.org/10.1007/978-3-031-08834-6_3

Fig. 3.1 Field Emission Scanning Electron Microscope (SEM) at DiSTAR – Dipartimento di Scienze della Terra, dell'Ambiente e delle Risorse – University of Napoli Federico II

Scanning electron microscope (SEM – Fig. 3.1) allows both the acquisition of detailed images of the surface morphology of solid fragments and, coupled with Energy Dispersive Spectroscopy (EDS), provides information on their chemical composition. As such it is a powerful and widely used tool in forensic applications.

Both manual scanning electron microscopy and automated mineralogy systems based on SEM-EDS have considerable application in forensic geoscience and are also widely used in other forensic science disciplines, such that the methodology is widely accepted in court. SEM and microanalysis are widely used in traditional geoscience research. To date, automated mineralogy systems have been most widely used in the fields of economic geology, metallurgy and mineral processing as a result of the ability to characterize the ore and gangue mineralogy, texture, chemistry, mineral associations and quantify recovery and mineral liberation. Another application area of automated mineralogy is in petroleum geoscience, as this technique allows the petrology, mineralogy and porosity in drill cuttings to be determined (Pirrie and Rollinson 2011). Increasingly the automated systems are being adopted as standard geoscience research tools in petrology, environmental geology and archaeological geoscience. Depending on the nature of the forensic investigation, both manual SEM and/or automated mineralogy can provide significant datasets.

Traffic accidents or crimes such as burglaries, assaults and shootings may leave traces such as pieces of glass, paint, textiles or gunshot residues which, if found on

clothing or shoes, can testify to someone's presence at the crime scene. The way in which experts tackle this issue is twofold: they can identify the object from which the small fragment originates (for example, they can determine whether the pieces of glass on a suspect's clothing came either from a car window or a drinking glass), or they can compare the fragment with a series of potential sources, most of which are present at the crime scene, to infer its origin (Zadora and Brozek-Mucha 2003). SEM combined with microanalysis is a technique used in forensic science for the analysis of gunshot residues, paint, glass fragments and soils. In general, it directly follows optical microscope observation, which is the routine technique for defining the morphological characteristics of unknown fragments and is critical when the size or the quantity of the recovered material is very small. Furthermore, unlike optical observation, SEM-EDS methodology allows data to be collected on both the morphology and chemical composition of unknown fragments. In comparison with polarised light microscopy, which needs thin section preparation, SEM does not necessarily require any specific pre-treatment to analyse geological materials. This technique has all the advantages of a non-destructive technique, which is very important in the forensic field, because the materials that constitute potential evidence can be stored in the court files and preserved for further investigations or trials. Large specimen chambers and various stages to accommodate diverse specimen types, chamber pressure adjustable to a level which prevents an uncoated specimen from charging, possibility to cut and paste the images onto each other and align so as to support comparison, are only some of the recent achievements of the technique, which make it more and more suitable for forensic geosciences. In as much, automated mineralogy based on SEM-EDS provides a fully integrated mineral and rock analysis system that is rapid, accurate, repeatable and statistically valid, and hence its application in forensic soil analysis is increasingly gaining ground.

3.1 Scanning Electron Microscopy

The naked eye, at a visual angle of about 1/60°, can distinguish objects with a resolution of about 0.1 mm at an optimum distance of 25 cm. In optical microscopy, on which is based the functioning of electron microscopy as well, the aid of optical lenses allows a resolution of about 2.000 Å (Murphy and Davidson 2013). This microscopy, which uses a light source, is still a basic tool in scientific research in many fields (biology, chemistry, earth sciences, etc.). Around the end of the nineteenth century, however, the discovery that electrons could be deflected by a magnetic field marked a turning point for microscopy. The idea of using an electron beam instead of a light source opened the way to a technique that has evolved over time, becoming increasingly sophisticated, and in just over a century has reached new milestones in terms of resolution, magnification and analysis of specific characteristics of the sample under investigation.

The resolution limit is defined as the minimum distance at which two different structures can be focused and still appear as two separate objects. A physical law,

Abbe's law, proves that the resolution limit depends on the wavelength of the illumination source. The blurring of image is the consequence of excess of magnification with a source of a given wavelength.

Abbe's equation is

$$d = 0{,}612\,\lambda / n\,sen\,\alpha$$

where

d = resolution
λ = wavelength of imaging radiation
n = index of refraction of medium between point source and lens, relative to free space
α = half the angle of the cone of light from specimen plane accepted by the objective (half aperture angle in radians)
n sin α is often expressed as NA (numerical aperture)

Using a source at a shorter wavelength can greatly increase the resolution, which allows for sharp images at very high magnifications. The possibility of accelerating the electrons at high energies (between 2 and 1000 keV) results in extremely short wavelengths of the incident beam of (between 0.027 and 0.0009 nm), thus achieving very high-resolution values. The interactions between the incident electron beam and the atoms of the sample become very important. If the specimen is ultra-thin, electrons can pass through it without being absorbed and form the image using a Transmission Electron Microscope (TEM). Electrons cannot be transmitted through a thicker sample for which it is only possible to get information from the signals that are re-emitted from the surface (electrons, X-rays and photons), which are used in a conventional SEM (Amelinckx et al. 1997). The SEM, in fact, uses a focused electron beam to scan the surface of the specimen, producing various types of signals. Hence, we can say that in SEM an electronic signal is converted into a visual signal to return a very detailed image.

3.2 The Signals of an SEM

As already mentioned, the formation of an SEM image depends on the acquisition of the signal produced by the electron beam and by interactions with the specimen, which can be elastic or inelastic. Elastic interactions are the result of the deflection of the incident electron by the nuclei of atoms or their external electrons of comparable energy. This interaction involves a weak loss of energy due to the collision and a significant deflection of the electrons. Those that are elastically deflected at an angle greater than 90° are called backscattered electrons (BSE) and provide a good image of the sample. Inelastic interaction, on the other hand, is characterised by the transfer of a significant portion of the energy from the incident electrons to the atoms that make up the surface of the specimen. The loss of energy depends on

whether its electrons are excited individually or collectively, and on the amount of energy that binds the specific electron to the atom. In the first instance, the excitation of the sample's electrons due to the ionisation of its atoms leads to the emission of secondary electrons (SE), which are conventionally assigned an energy of less than 50 eV and are used to create an image of the sample and analyse it. In addition to these electrons, however, several other signals are emitted, such as characteristic X-rays, Auger electrons, or cathodoluminescence, each of which, when properly collected, can be used to provide specific information about an unknown sample. Figure 3.2 shows the various areas of the sample from which specific signals can be extracted. The electrons of the incident beam are not immediately repelled from the surface of the sample, but have a certain penetration capacity, which defines a region of primary excitation, where the signals are produced (Vernon-Parry 2000). The extent and shape of this area is conditioned by the energy of the incident beam, but also by the atomic number of the elements involved and, therefore, by the density of the sample. The excitation region will resemble a teardrop if this region of the specimen consists of elements with a low atomic number and a hemisphere if it is made up of elements with high atomic number.

The secondary electron (SE) signal, which is the most used, is a consequence of the ionisation of the atoms when they are hit by the incident electron beam, which leads to the emission of the electrons weakly bound to the nucleus of the atom. These are very low-energy electrons (3-5 eV) that can only be emitted from the first few nanometers of the sample: this characteristic makes them the most suitable for

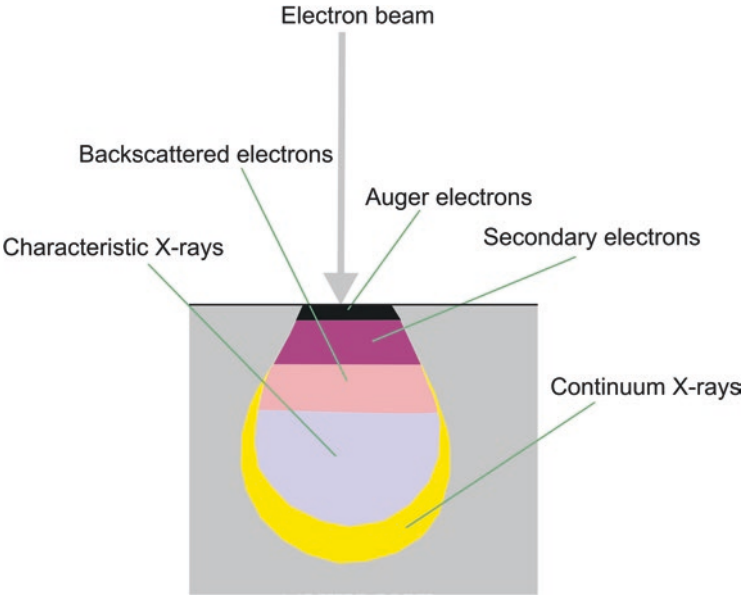

Fig. 3.2 Interactions of the electron beam and the specimen with the zones producing the different signals

reconstructing the morphology of the specimen surface with an excellent resolution. Their low energy, on the other hand, makes them easily attracted by a detector with suitable features, and the quality of the topographical image is linked to the quantity of secondary electrons that are able to reach the detector, which in turn depends on the position of the sample's surface with respect to the incident electron beam: when they are perpendicular, in fact, the zone that emits secondary electrons is narrower than when the specimen is tilted (Zhou et al. 2007).

Backscattered electrons (BSE) are widely used for getting both topographical and compositional information. Backscattered electrons are re-emitted at an energy greater than 50 keV. The elastic collision between the electron and the nucleus of a specimen's atom causes it to be bounced-back with a large deflection angle. In general, between 10 and 50% of the electrons in the incident beam undergo backscattering, losing about a quarter of their energy. The nuclei of elements with a higher atomic number have more positive charges and are therefore more likely to produce backscattering and emit a more intense signal. This is the main reason why backscattered electrons can provide information on the distribution of the various chemical elements within the sample (Fig. 3.3). Their ability to supply information on deep areas of the sample is certainly greater with respect to SE, since backscattered electrons have high energy and are therefore less likely absorbed, which, however, results in a definite loss of lateral resolution (1 micron compared to 10 nm for SEs). Recently, a technique that combines diffraction with backscattering (EBSD – Electron Backscattered Diffraction) has been developed, which is very useful for defining the crystal structure of nanometer-sized samples.

Characteristic X-rays is the signal most widely used to obtain information about the specimen chemical composition using an SEM (electron microanalysis). When an electron from the innermost shell is hit by one from the incident beam it is knocked out and an electron from the outer shell drops down to take its place and restore the charge balance following ionization. In this way, after X-ray photon emission, the element returns to its original state.

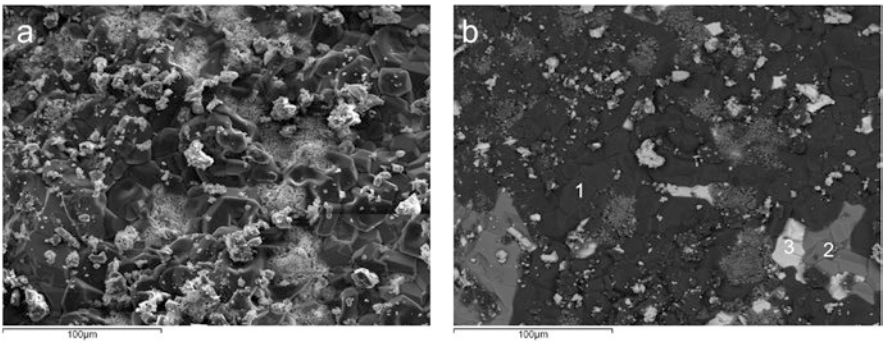

Fig. 3.3 Microphotograph of an oxidized crust embedding an iron coin obtained with SE (**a**) and *backscattering* (**b**). In the latter Cu oxides appear dark grey (1), Sb oxides intermediate grey (2), Pb oxides (3) pale gray. (From Petrosino et al. 2019)

There are several minor signals that can supply useful specific information as well.

Auger electrons are generated to remove the excess energy produced when, after ionisation, an electron from an outer electron shell replaces one from an inner shell. The energy values are typical for individual chemical elements, so even Auger electrons give information about the chemistry of the sample but, for the low associated energies, only provide information on the very external portion of the sample.

Cathodoluminescence is another stabilisation mechanism that follows the interaction between the beam and the sample. Some materials, when electrons move to the innermost orbits to replace the vacancies resulting from ionisation, release excess energy as photons with wavelengths in the infrared, visible or ultraviolet range. These photons can be appropriately analysed and provide images with a resolution of approximately 50 nm.

Thanks to the ***transmitted electrons***, an SEM image can be obtained if the sample is thin enough for the electrons of the incident beam to pass through (1 micron). In this case, the detector is positioned behind the unknown sample: this technique explores the internal structure of ultra-thin samples. The integration of a scanning electron beam with a suitably positioned detector for transmitted electrons is the basis of modern STEM (Scanning Transmission Electron Microscopy) techniques.

Finally, the ***specimen current*** represents the difference between the primary electron beam current and the total re-emission current (secondary, backscattered, Auger electrons): the weaker the total emission current, the higher the specimen current. Specimen current can be conducted away to give an image with a reverse contrast to SE and BSE images, but it requires long scan times for imaging purposes and can only be successfully employed with conducting specimens. In as much, for its low bandwidth it is rarely used.

3.3 The Structure of an SEM

The simplest configuration of an SEM comprises a column with an emission source (gun) at the top, which emits electrons and accelerates them to an energy comprised between 0.1 and 30 keV (Fig. 3.4).

The simplest source is a tungsten filament, which, however, produces an electron beam too large to acquire a high-resolution image. To prevent this, several electromagnetic lenses and apertures are placed along the beam path to focus it and allow the electrons to strike only a narrow portion of the sample (1–100 nm). A high vacuum is required in the column, which prevents the deflection of electrons by any obstacles encountered on their path. The sample chamber, beam coils, signal detectors and appropriate image processing systems complete the equipment.

A source must produce an extremely stable, highly focused electron beam working at variable energies with a small dispersal. The first, and probably still the most widely used SEMs have a tungsten or LaB_6 (Lanthanum hexaboride) filament, but in the latest generations there is a tendency to replace the filament with a type of

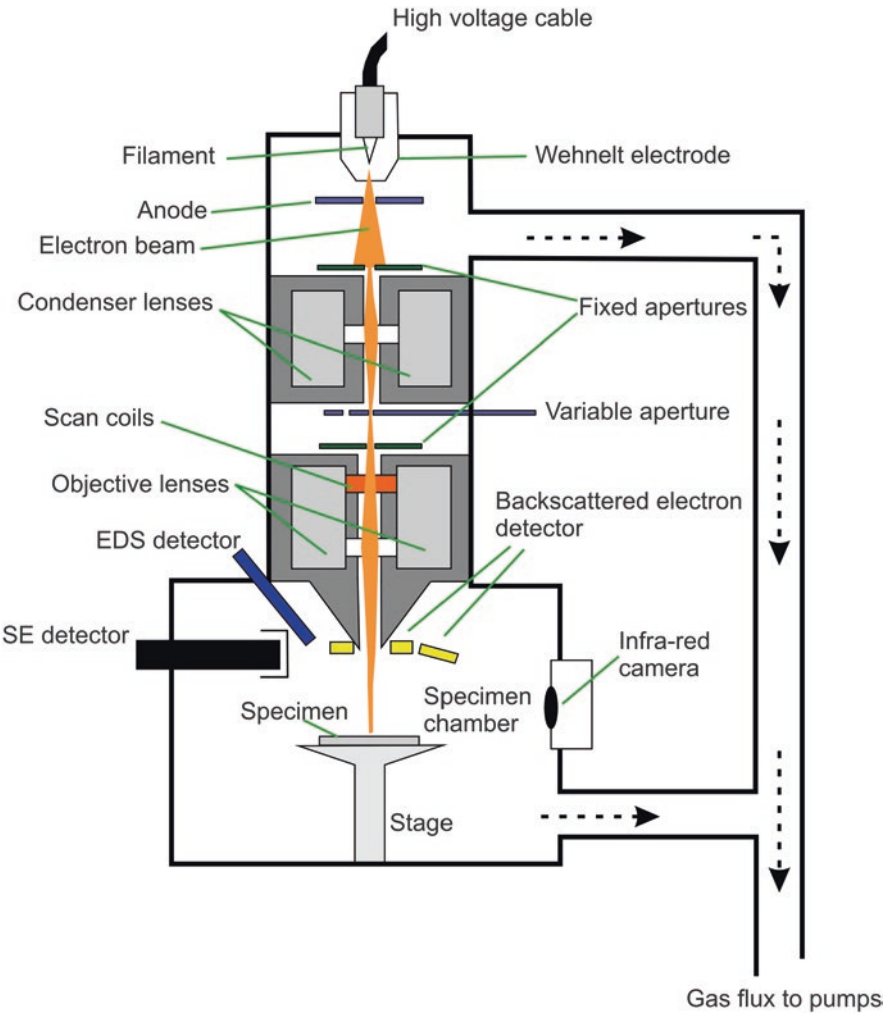

Fig. 3.4 Sketch of the main parts of an SEM-EDS apparatus

emission known as "field" emission, which allows increasing the current minimizing the risk of dispersion. Another important guide to the choice of the source is its average life, that is the hours of activity before it 'strikes'.

The most common electronic source is represented by a V-shaped tungsten filament, which acts as the cathode, a Wehnelt cylinder and a hollow anode (Fig. 3.5). The filament is heated to temperatures exceeding 2800 °K and begins to emit electrons. When the anode is activated, the electric field created between the anode and cathode extracts the electrons and accelerates them towards the anode, but a weak negative potential is applied to the Wehnelt cylinder to make them converge towards the anode and prevent scattering. The emission of electrons increases as the current

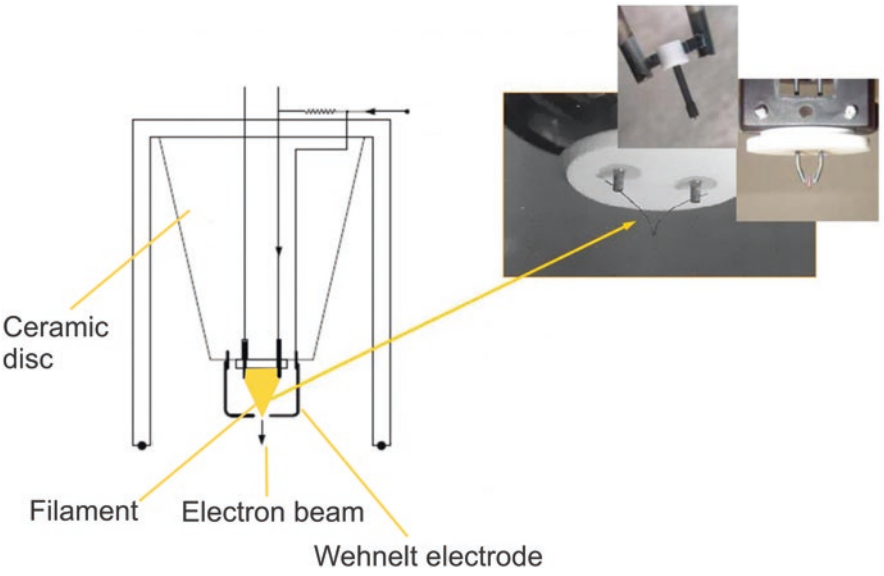

Fig. 3.5 Schematic representation of the functioning of a thermoionic emission filament (tungsten, LaB_6)

supplied to the filament increases, but there is a point, known as saturation, at which the emission no longer increases when more current is supplied. At the saturation point the current is emitted only at the very tip of the filament arc, and scattering is minimized.

At the same heating temperature, and therefore the same current, the LaB_6 filament allows a greater emission of electrons, so it can produce sharper images and has a longer average life than the common tungsten filament. In addition, it allows the electron beam to be focused much more sharply and dissipates less energy, thus enabling very high-resolution images to be achieved. Unlike the tungsten filament, however, the LaB_6 filament oxidises easily at high temperatures, so a column-vacuum much higher than that achieved by routinely used SEMs is required to avoid contamination. Both sources, however, need high temperatures to emit electrons thanks to the thermionic effect, so although they are fairly cheap, they suffer wear and tear, and high-resolution images lose their brightness. For this reason, the latest generation of SEMs uses a field emission source (FEG – Field Emission Gun), represented by a single tungsten crystal, usually very sharp (Fig. 3.6), around which a strong electric field is formed (first anode). Electrons are extracted by the tunnel effect and attracted to a second anode instead of being generated by strongly heating the filament.

The electron beam can be focused by magnetic or electrostatic fields, but the huge aberration effects prevent the normal use of the latter. The magnetic field is produced by coils (electromagnets) to which currents are applied to control the path of the electrons and, above all, to reduce the size of the beam, which results in

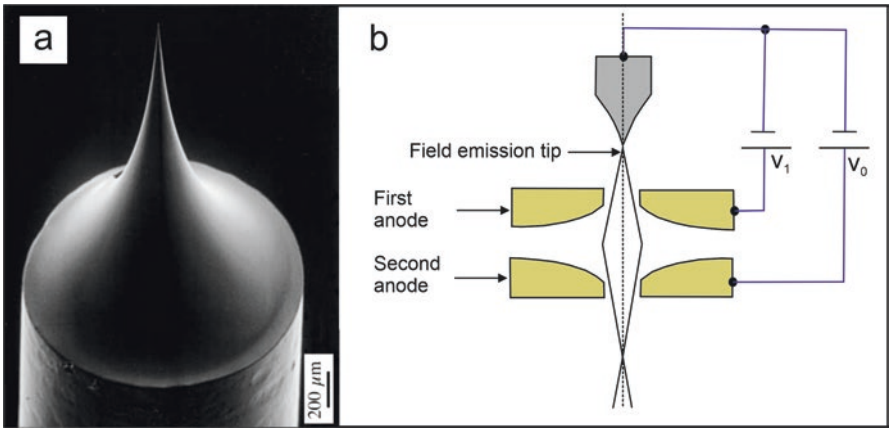

Fig. 3.6 Field emission gun (**a**) and schematic representation of its functioning (**b**)

allowing the investigation of a very small specimen area. In fact, the electron beam exits the anode and tends to diverge, hence the condenser electromagnetic lens is placed here to contain its size. An aperture is associated with this lens to exclude the passage of many of the electrons inhomogeneous and not perfectly contained in the beam. Below the aperture the beam tends to diverge again, so objective lenses are needed to make it converge on the specimen, further reducing its diameter. The size and focus of the beam are directly related to the image resolution we can achieve, but several other parameters can affect image quality, such as working voltage, aperture size, working distance (WD) and electronic lens aberration. From the complex balance of all these parameters, which an experienced user can manage according to the type of instrument and the expected result, a better quality image can be obtained.

Contamination of the column or apertures and/or defects in the lenses deform the beam to an elliptical final section instead of a perfectly round one. This imperfection is called astigmatism, and results in some areas of the sample being under focused. Astigmatism is corrected by a series of small coils that are placed around the beam and allow good resolution images to be obtained even in worse situations. Depth of field refers to the part of the sample that appears "in focus" under certain instrumental conditions. It is intuitable that it depends on the amplitude of the angle α and, above all, on the working distance, the increase of which increases the depth of field, but at the expense of the resolution. In general, reduced working distances are preferable when the sample is flat, while for rather irregular samples it is better to work at greater distances to have a larger focused area (Fig. 3.7).

The image formation, which represents an important function of an SEM, is linked to the type of signal recorded, i.e., BSE, SE, Auger or transmitted electrons or even specimen current. The appropriate detectors are able to quantify the amplitude of these signals coming from a single point of the specimen, but to obtain an image, a real "scan" is needed, i.e., move a spot of electrons over an entire area of the unknown sample, and receive the re-emitted signal. Coils intervene again to direct the beam in

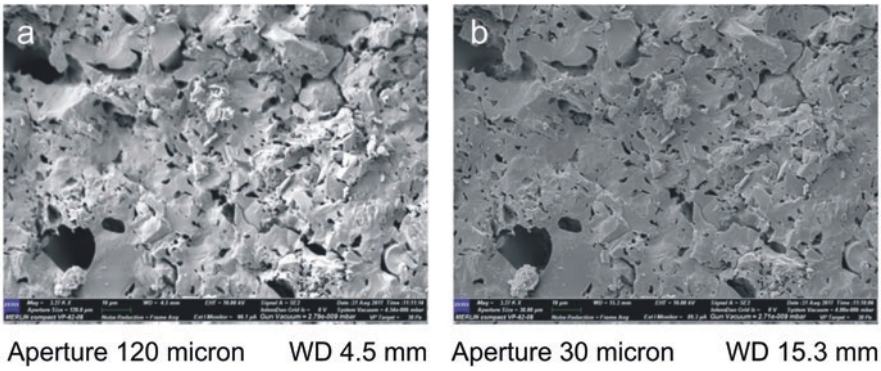

Fig. 3.7 SE image of a ceramic material under different apertures of the objective lens (3300×)

such a way that it can scan the selected area by moving in both a horizontal or vertical direction. The signal recovered from the active detector (e.g., that of the SE secondary electrons) is suitably processed and projected onto a screen, taking care to keep the output signal synchronized with the electron beam by means of a signal generator, so that the image can be viewed as it is acquired. In order to form an image using the SEs, which have low energy and therefore are able to provide excellent information regarding the surface of the sample, an electronic multiplier is necessary, since the low energy is associated with such a low current that the SE signal becomes almost comparable to noise. Generally, the detector for the SE is placed laterally with respect to the sample and recovers less than 30% of the SE signal that, however, is sufficient to form an acceptable image, since the asymmetrical position of the detector, especially for a non-smooth sample, allows the operator to enhance or mask certain areas of the sample itself, in order to obtain a more aesthetically pleasing image. In some cases it is also possible to tilt the specimen, so as to vary the angle of incidence of the beam on its surface, which increases the area from which SEs are emitted.

In normal SEMs, at high magnifications, the SEs work at a distance of 10–20 mm, and the detector can be positioned close enough to the sample so that its top is well exposed. More modern SEMs, increase resolution by working at much shorter distances, in which case the positioning of the detector for the SEs becomes more delicate, and additional lenses are used to produce a strong magnetic field on the surface of the sample and direct the SEs back into the column. The BSE detector, on the other hand, provides information on the distribution of atoms within the sample, as heavier elements give a stronger BSE signal. The image results in a series of chiaroscuros, where the darker materials are those made up of the lighter elements.

To complete the description of the equipment, it is necessary to mention the vacuum system, which is very important in preventing the beam from anomalous deviations or contamination of the electron source. The desired vacuum is obtained thanks to the action of either low-vacuum or high-vacuum pumps. The formers have a mechanical pumping system made up of a rotor that compresses a gas by increasing its pressure and, when it reaches a certain value, expels it through a one-way

valve. A vacuum of approximately 5×10^{-5} Torr is achievable with this pump, but normally, to avoid excessively long pumping times, a 1×10^{-2} Torr vacuum value gives way to high-vacuum pumps. There are different types (oil circulation diffusion pump, ion pump, turbomolecular pump) but their common purpose is to reach the operating vacuum conditions, up to 10^{-6}–10^{-7} Torr, required by the LaB_6 filaments or for field emission.

3.4 Electron Microanalysis

Electron microanalysis is a modern technique commonly used to quantify the content of individual chemical elements in solid materials or to map the distribution of these elements at the micrometer or nanometer scale. Microanalytical techniques are based on the analysis of certain characteristics of the re-emission X-ray spectrum (characteristic X-rays). There are two main types of electron microanalysis used in mineralogy: Energy Dispersive Spectroscopy (EDS), which resolves re-emission X-ray spectra in terms of the energies associated with individual chemical elements, and Wavelength Dispersive Spectroscopy (WDS), in which these spectra are resolved in terms of the different wavelengths that characterise the X-rays re-emitted by different chemical elements. The latter technique allows the quantification of most chemical elements with a spatial resolution at the micrometer scale and a detection limit of a few ppm. EDS is a more routine technique, which is frequently used in conjunction with SEMs. Although it has lower analytical capacity and precision than WDS, it has the advantage of rapid acquisition and can work synchronously with the electron microscope, making it the instrument of choice for elemental mapping.

According to the Rutherford-Bohr atomic model, in a neutral atom the number of positively charged protons (Z) occupying the nucleus is equal to the number of electrons orbiting the nucleus on specific energy levels defined by a quantum number. As Z increases, further and further away from the nucleus new orbits are occupied, whose electrons are less attracted to it. The main quantum number defines the energy of the orbit: the one closest to the nucleus is called K, followed by L and M.

Characteristic X-rays are generated as a result of the excitation of electrons in an atom by an electron beam, which causes one, or a few, electrons from an innermost level to be removed, creating a kind of ‘vacancy’ that is occupied by electrons from an outermost orbit. When the transfer of an electron from an outermost to an innermost orbit takes place, X-rays are produced, which are actually photons with an energy equal to the difference in energy between the source and target levels.

These energies are generally measured in eV, where 1 eV is the energy corresponding to a 1 V change in the electronic potential of an electron (= 1.602 × 10–19 J). The energy range for working with EDS is between 1 and 10 keV. The “critical excitation energy” (Ec) is the minimum energy that incident electrons must have to remove an electron from its orbit. For microanalysis, the energy of the incident electrons (E_0) must be at least twice that of Ec to make excitation effective. For

elements with Z > 35, a switch from the analysis of the K to that of the L lines is needed to minimize the values of energy required for the electron beam. In fact, the beam current necessary to excite the K lines of elements with Z higher than 35, would exceed the maximum voltages allowed for the instrumentation.

The energy of X-rays is related to their wavelength by the relation

$$E\lambda = 12.396$$

where E is expressed in eV and λ in angstroms.

The bombardment by electrons not only produces characteristic lines of X-rays related to the transition between different energy levels but a continuous spectrum (the so-called "continuous", also known as white or polychromatic radiation) of X-rays as well, covering all energy values between 0 and E_0 (the energy of the incident electrons), produced by the interaction between the latter and the nuclei of the atoms. The intensity of the 'continuum' decreases monotonically as the energy of the X-ray increases and is approximately proportional to Z. For microanalysis, it helps to define the background from which the energy peaks characteristic of the levels of the individual elements stands out.

The EDS spectrometer uses the pulse height principle: in practice, a detector, which delivers pulses proportional in height to the energy of the X-ray photons, is used in conjunction with a multi-channel analyser. The detector is a crystal, the incident X-rays of which cause ionisation, producing an electrical charge that is amplified and reaches the analyser, where it is processed. Commonly used detectors are lithium compensated silicon crystals (Lithium Drifted Silicon Detectors), currently often replaced by SDDs (Silicon Drift Detectors) which allow greater accuracy and much shorter counting times and have the advantage of not needing to be cooled with liquid nitrogen. The EDS spectrum (Fig. 3.8a, b) in digital form is represented with the X-ray energies on the x-axis (generally divided into channels

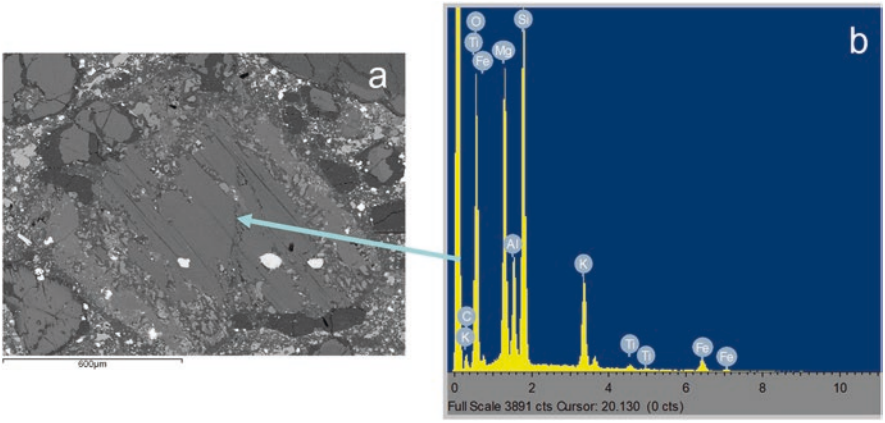

Fig. 3.8 Backscattered image of a rock in thin section containing a brown mica crystal (**a**) with the respective EDS spectrum (**b**). (From Petrosino et al. 2019)

corresponding to 10 or 20 eV) and the number of counts for the individual channel on the y-axis. Resolution is defined as the full width of the Gaussian profile at half maximum height (FWHM). By convention, it is set on the Kα line of Mn (5.89 keV) and for SiLi and SDD detectors the optimal FWHM values are 130–150 eV. Before acquiring the values of the energies of the individual photons corresponding to the X-rays emitted by a given element, a certain time interval is necessary to minimise noise. For this reason, the system has a specific dead time, which is the time after the arrival of a photon during which the detector does not register the effect of the signal of any other photons. As a rule, for SDDs, the best signal is obtained for values of 100.000 counts sec^{-1} or higher, a good balance between the need to lower the dead time in order to use most of the received signal, which means shortening the analysis time, and the need to obtain a high resolution, which means minimising noise with rather high dead times.

A brief mention of WDS (Wavelength Dispersive Spectroscopy) microanalysis systems, which also uses the X-rays originating from a sample hit by an electron beam, seems appropriate here. These microanalysis systems, which are based on wavelength dispersion rather than energy dispersion, are only recently beginning to be linked to SEMs; WDS is normally used in Electron Microprobe Analysis (EMPA). The X-rays generated by the sample are selected using a crystal (or, in microprobes, crystals) with cell-specific characteristics. The geometry of the X-ray-generating sample and the analysing crystal is such that they always maintain the same take-off angle. When X-rays meet the crystal at a specific angle Θ, only those that satisfy Bragg's law are reflected in such a way that only one wavelength is transmitted to the detector (Reimer 1998). The wavelength under investigation can be varied by varying the relative position of the sample with respect to the analysing crystal, since the distance between the X-ray source and the crystal is a linear function of the wavelength. Thus, only the X-rays emitted by an element can be recorded by the spectrometer and transmitted to the detector, and the position of a given analysing crystal must be changed to measure another element. In the most common configuration, known as Johann's, the crystal rotates around a circle of radius R, the radius of the focusing circle, known as Rowland's circle (Fig. 3.9). The specimen, analyser crystal and detector must be on Rowland's circle and remain there for all wavelengths of interest to allow efficient focusing of the X-rays. Since the sample position and take-off angle are fixed, the analyser crystal and detector must move but remain on Rowland's circle; in addition, the analyser crystal rotates as the distance between the X-ray source and the crystal changes, so it goes without saying that very sophisticated techniques of precision engineering are involved in WDS systems.

In single spectrometers, which are normally mounted on SEMs, there are four to six analyser crystals, that can be changed to capture wavelengths of X-rays emitted by different elements. Classical microprobes, on the other hand, have several spectrometers (usually five, mounted vertically around the sample chamber) and different sets of analyser crystals, with very different cell characteristics, suitable for the acquisition of signals from specific chemical elements. The signal thus filtered by the analyser crystal reaches a gas counter-type detector and, passing through a

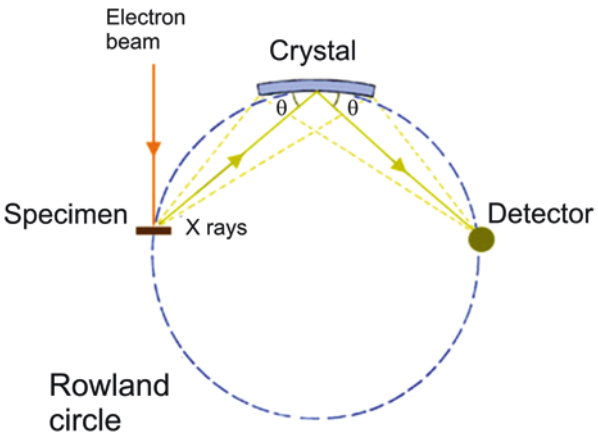

Fig. 3.9 Configuration of specimen, analyser crystal and detector in a WDS spectrometer

collimator, is absorbed and re-emitted in terms of photons, which on a central coil cause an ionisation that in turn produces an electrical impulse with an amplitude proportional to that of the original X-rays.

The signal emitted in terms of energy dispersion or wavelength of the X-rays associated with the individual chemical element can be used for qualitative and quantitative determination. The main focus here is on how to acquire qualitative and quantitative data in energy dispersive microanalysis techniques, as EDS detectors are commonplace in modern SEMs. In principle, all elements between atomic number 4 (Be) and atomic number 92 (U) can be detected with this technique, although older detectors allowed analysis of elements starting from Z = 11 (Na).

Qualitative microanalysis is based on the identification of lines in the spectrum of re-emitted energies, which are typical of the individual chemical elements. As the analysis output is an energy spectrum (see Fig. 3.8a,b), it is fairly easy to identify the presence/absence of a particular chemical element in the specimen area under investigation. The greatest advantage of qualitative EDS is that it allows the acquisition of the entire spectrum of energies of interest (from 0.1 keV up to the energy of the beam – 15 or 20 keV) in a very short time (between 10 and 100 sec). The operation of identifying the peaks is, however, not easy since, especially at low energies (<3 keV), the energies connected to the individual sub-levels present considerable overlaps.

Modern EDS techniques allow for a number of outputs, such as obtaining the distribution of a particular chemical element along a linear path traced by the user on a specimen. By using the beam in a TV-like scanning mode, it is also possible to construct so-called elemental maps for individual elements, from which it is possible to identify the portions of the specimen where a specific element is present and gain an indication of its relative concentration. If a colour tone mode is chosen for the representation, the areas in which the tone is more intense are those in which the unknown element is more abundant (Fig. 3.10). For elemental mapping, EDS

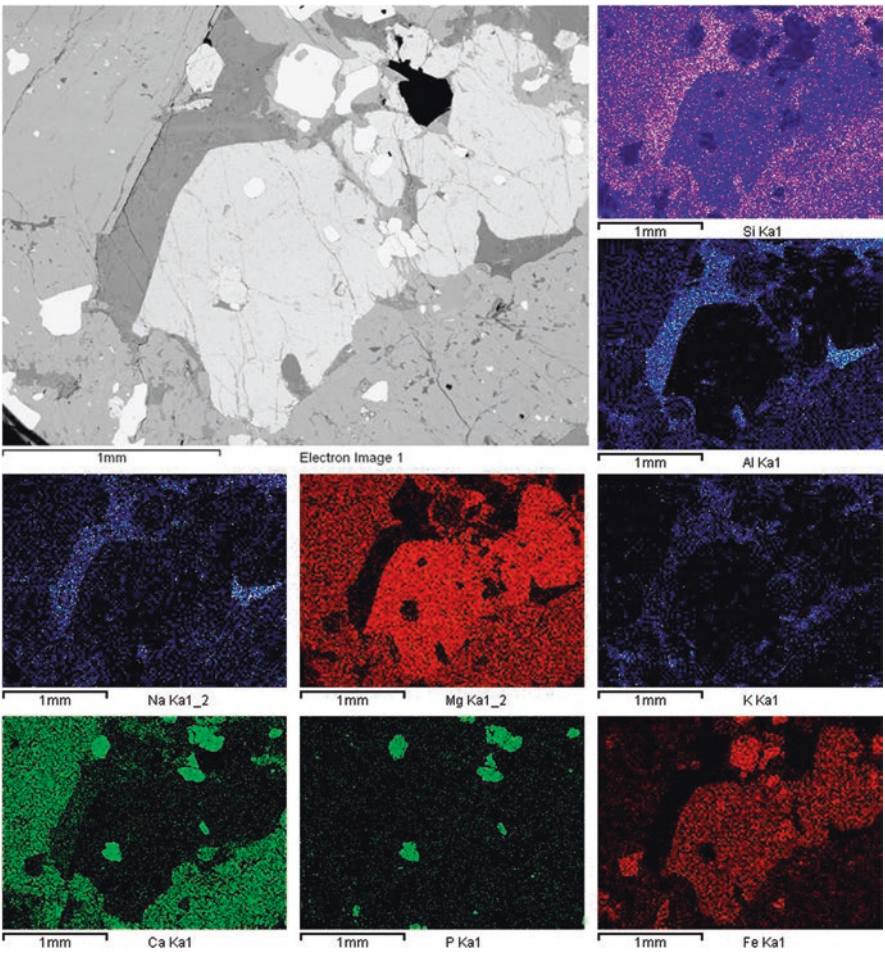

Fig. 3.10 2D elemental maps produced through Oxford Instruments X-Stream Inca EDS system linked to a JEOL JSM 5310 SEM. It is possible to carry out a semiquantitative estimate of the distribution of the single element in the investigated area and a preliminary evaluation of its concentration (a higher colour intensity means a higher concentration). The comparison of the distribution of various elements in the same area allows a qualitative evaluation of the crystalline or amorphous phases present in that zone of the specimen.

systems are preferred because of the speed of data acquisition and the extreme versatility of modern image analysis software associated.

Quantitative analysis, aimed at determining the amount of a chemical element present at a spot in the unknown sample, is certainly more difficult. It is based on a comparison between the intensities of the energies of the same element in a sample and in a standard of known concentration, acquired under the same conditions as the unknown. The technique used to process the data acquired for quantitative analysis

is due to Raimond Castaing (1921–1999) who, in 1951, under the supervision of André Guinier, discussed in Paris a PhD thesis on the fundamentals of quantitative microanalysis; in fact, in the course of his research, he had built the first WDS-type electron microprobe with a quartz analyser crystal, which earned him the nickname 'the father of microanalysis'. According to Castaing's principle (1951), the relative intensity of a given X-ray line for an element is proportional to its concentration in the sample, on the assumption that the penetration capacity is independent of the composition of the sample. Given this assumption, the apparent concentration (C′) of a given element will be

$$C' = \left(I_{camp} / I_{std}\right) C_{std}$$

where I_{camp} and I_{std} are the intensities measured in the sample and standard, respectively. The system must necessarily make corrections, the most important of which is to eliminate the background signal, which cannot be associated with any element in particular, but always accompanies the re-emission X-ray spectrum. It is intuitive that the problem is more complicated in multi-element spectra (such as those of silicates) in which there is also a certain overlap of the energy peaks of the individual elements. Background compensation, by subtraction or another method, is basic for EDS analyses. Other corrections applied are those related to the so-called matrix effects, which depend on the elements coexisting in the spectrum with the unknown element of interest. The most common correction methodology for matrix effects in quantitative microanalysis, whether WDS or EDS, is called ZAF, an acronym that stands for correction for atomic number (Z), absorption (A) and fluorescence (F) effects.

X-ray intensities are measured from photon counts, so the accuracy of the method is limited by statistical error. Instrumental instabilities should be less than 1% and, above all, uncertainties in the compositions of the standards should be minimal, which is not always guaranteed with silicates that are frequently zoned. For major elements, it is not difficult to obtain a degree of precision (2σ) of ±1%, although it is perhaps more realistic to say that the precision of the method is ±2%, due to the error introduced by peculiar characteristics of the sample or by the recalculations that the system performs for corrections. Theoretically, the system can resolve element percentages in the order of 1000 ppm, although by lengthening the acquisition time a better sensitivity can be achieved, fully comparable with that of WDS (Newbury and Ritchie 2015). Spatial resolution, on the other hand, is related to the penetration capacity of the electron beam which, being constant with respect to mass, depends on the density, and therefore the chemical nature of the substance under examination. Typical spatial resolution for silicates is 2 microns, but a homogeneous sample of fairly coarse particle size is required for quantitative analysis to be reliable.

3.5 Specimen Preparation

The SEM examination of non-biological samples does not need any major requirements with regards to the observation and imaging of the sample: in general, on the contrary, the "rougher" the surface of the sample, the better the acquired images. It is necessary to glue the samples with a conductive glue (based on Ag or graphite) to a sample holder ("stub" – Fig. 3.11). The possibility of application is limited by the size of the sample, which for the old generation SEMs did not exceed 3–4 cm, a problem now overcome by the large chambers of modern FEG-SEMs which allow the introduction of specimens up to 10–15 cm within the chamber. It is also possible to work on loose sediments or powders, taking care to make them adhere to the stub, which is generally done with the aid of a double-sided graphite tape. To make the sample surface conductive, minimising the effects of poor SE and BSE emission, it is covered with a thin layer of gold or a film of graphite whenever possible. Clearly, this is a permanent modification of the sample: the new SEMs, which work at low emissions, for example with the additional in lens detector, or with tricks such as inserting a jet of nitrogen in the chamber to eliminate the electrons that tend to concentrate on the surface of a non-conductive sample, allow good observations to be made even on non-metallic samples. If one intends to work at high magnifications, it is in fact necessary to avoid coating the sample, as the gold particles become evident and mask the characteristics of the sample even at magnifications above 100.000x. This technique is also preferred for forensic analysis, as it does not involve any modification to the original sample to be analysed, although when carrying out automated SEM-EDS the sample must be coated prior to analysis. Semi-quantitative and, above all, quantitative microanalysis requires the sample to expose

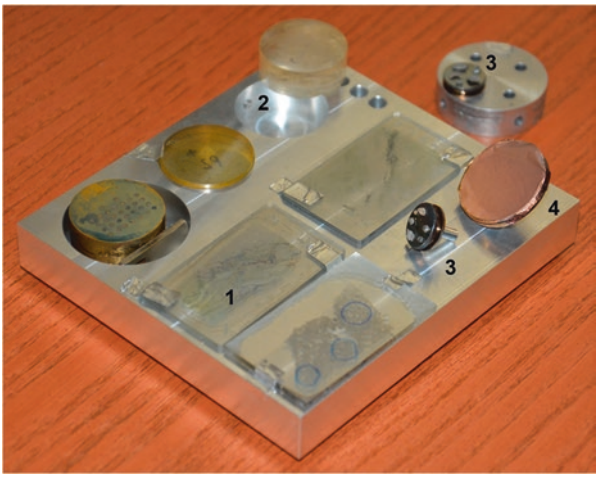

Fig. 3.11 Specimens for SEM-EDS analysis: thin section of a rock (**1**) and polished resin-embedded fragments (**2**) for microanalysis, *stubs* with rock fragments (**3**) for SEM observation and polycarbonate filter (**4**) for the analysis of asbestos airborne fibers. (From Petrosino et al. 2019)

perfectly smooth surfaces to incident electrons. For this reason, rock samples are prepared as thin sections, slightly thicker than those normally used for observation under polarised light, while the loose fragments are usually embedded in thermosetting resin and polished with abrasive diamond pastes gradually decreasing in grain-size (from 30 to 1 micron), which makes it impossible to keep the sample in its original form.

Unless you have an ESEM (Environmental Scanning Electron Microscope), whose sample chamber is maintained at ambient pressure, SEMs cannot accommodate biological samples as they are, since they are 80% water, and when a vacuum is created the aqueous fraction vaporises and contaminates the chamber, compromising the quality of the image. SEM observation of biological samples, therefore, requires a dehydration pre-treatment which, however, must not significantly modify their structure, as even simple air-drying of biological substances can produce significant variations.

3.6 Automated Mineralogy

Automated Mineralogy (AM) analytical systems combine the use of a SEM-EDS with a sophisticated software package for data processing and automation. Samples for analysis can be prepared as: (a) polished thin sections, (b) embedded in epoxy resin and polished, or (c) for very fine-grained particles they can be measured directly on carbon stubs without sectioning and polishing. The system design consists of a hardware platform and a specific software module controlling the SEM during the collection of raw data, processing the data and the construction of the digital images. In detail, the automation software scans or rasters a focused beam of electrons over the sample surface on a grid across the sample, measuring a variety of signals generated by electron sample interactions (secondary electrons, backscattered electrons, X-rays, cathodoluminescence and transmitted electrons) and mapping the data with the construction of a high-resolution image. Measurements must be collected in high vacuum mode (ca. 10^{-5} to 10^{-7} Pa). Some AM solutions on the market are integrated with the SEM hardware platforms (e.g., QEMSCAN, MLA, Mineralogic Mining, TIMA-X), while other consist of only a processing software package (AMICS and AZtecMineral, INCAmineral) to be installed on existing SEM hardware. A summary image of the AM analysis workflow is showed in Fig. 3.12.

Measurements begin with the collection of backscattered electrons (BSE). A long-term stable electron beam and a powerful BSE detector are required in order to obtain a good quality initial BSE image. Typical gun sources are tungsten cathode, LaB_6 or field emission gun, but the latter equipment is strongly advised as it provides the higher stability required for automated analysis. Prior to the analyses, a fixed working distance must be set to ensure that the analysed minerals always have the same BSE image grey levels, as long as the image calibration is constant. The BSE image grey level can be calibrated with reference materials with different BSE

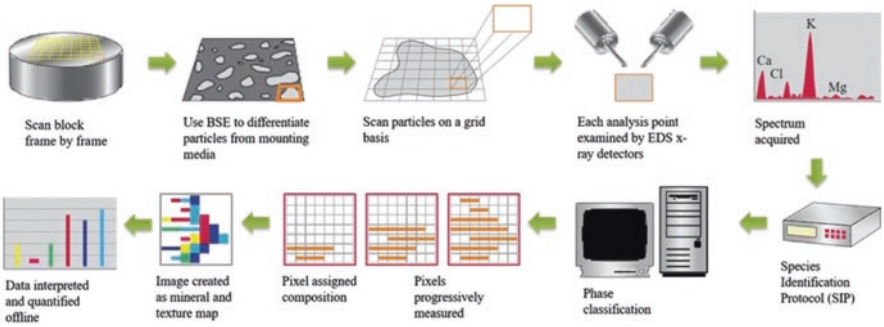

Fig. 3.12 Starting at the left, the sample is mounted in epoxy and sectioned, creating a smooth, flat surface. The electron beam scans across the sample surface and identifies particles based on the contrast between minerals and the mounting media. The system then scans each particle on a grid basis, and collects and interprets an X-ray spectrum for each pixel in the grid to determine its mineral phase. The results for all pixels are combined in a digital image that represents the mineralogy in the scanned particle. Digital mineral maps provide visual representation of the mineralogy and how minerals relate to each other (QEMSCAN analysis workflow modified from FEI's AM and petrography brochure)

grey levels, such as gold (very bright), copper (intermediate), quartz or aluminum (dark grey). After the collection of a BSE image for a given frame or area, several steps of image processing are performed, to facilitate the measurement on a specific target depending on the analytical target. Different AM systems use different image filters prior to the measurements acquisition. As examples, background removal, selection of a grey level threshold, removal of the undersized or oversized particles, removal of touching particles or particles touching the frame boundary, segmentation of the particle structure, etc. The user can customize the analytical procedure by choosing the frame size of the grid across the sample, depending on the image resolution required, and the step size for measurements acquisition. After BSE acquisition and image processing, the measurements continue with the acquisition of dispersive X-ray spectra (EDS) at selected points according to the BSE image adjustments. SEMs used for AM analyses are commonly equipped with either two or up to four EDS spectrometers to increase the speed of the analyses by increasing the X-ray count rate. The classification of the minerals, phases and mineral compounds in the samples is obtained by the comparison of the acquired EDS spectra for each point analysis with an extensive mineral list of approved reference EDS spectra: if the EDS spectrum of an analysed point matches with one spectrum of a mineral in the reference list, for example pyrite, the measured point will be automatically classified, and the label pyrite will be assigned to the analysed point. In contrast, if there is no match between the acquired spectrum and the reference EDS spectra list, the point will be labelled as "unclassified".

The system combines these data points to generate digital false colour mineral maps, from which it then extracts modal mineralogy, elemental deportment, textural and particles/grains size and geometry, particle liberation and other statistical

outputs to be used for downstream applications. In order to optimize the results, after data acquisition, the mineral classification can be re-processed in off-line mode. After user checks, the "unclassified" minerals can be checked and assigned after further investigations and output data can be validated and adjusted. Different AM solutions use different algorithms to gain and process data.

QEMSCAN, for instance, (Quantitative Evaluation of Minerals by SCANning Electron Microscopy. FEI Company, Hillsboro, OR, USA) and MLA (Mineral Liberation Analysis software, FEI Company) acquire X-Ray spectra and BSE grey values for each analysis point on the basis of a measurement grid. EDS spectra acquired and saved for each analysis point are compared against a reference list known as the Species Identification Protocol (SIP) and the minerals, phases and mineral compounds are classified on the basis of the first match, meaning that after a matching entry in the SIP list is found, the following entries are not considered (Gottlieb et al. 2000; Pirrie et al. 2004; Butcher and Botha 2010; Pirrie and Rollinson 2011; Haberlah et al. 2010, 2011).

MINERALOGIC MINING (Carl Zeiss Microscopy Ltd., Cambridge, UK) utilises a high-count EDS analysis solution and the minerals are classified by their stoichiometry based on the normalized weight per cent (wt.%) of each element quantified in the mineral phases. This means that the mineral classification is sensitive to elemental variations. Moreover, the system measures the physical parameters such as area, elongation, diameter, porosity etc., using high resolution BSE images of the particles rather than derived digital mineral maps, leading to an improved accuracy of any physical measurement of the particles (Graham et al. 2015; Simons and Graham 2016; https://www.zeiss.com/microscopy/int/products/scanning-electron-microscopes/mineralogic-systems0/mineralogic-mining.html).

TIMA-X (TESCAN Integrated Mineral Analyzer TIMA, TESCAN ORSAY HOLDING, a.s., Brno, Czech Republic) data acquisition starts with a BSE image, then the software provides a segmentation of the particles, which enables the creation of high-count spectra suitable for EDS quantitative analysis; the software creates a gradient image using the BSE image and the elemental X-ray intensities. The gradient image is then processed by a watershed transformation that detects continuous edges and the minimum gradient that is regarded as an edge; two segments in contact and with a similar composition and low gradient, are merged into a single segment rather than remaining separated (Hrsta et al. 2018; TESCAN).

AMICS (Advanced Mineral Identification and Characterization System, Bruker 2017), INCAMineral software and AZtecMineral (Oxford Instruments plc, HighWycombe, UK) acquire a BSE image, which is then processed by image processing analysis and EDS spectra acquisition. The mineral identification is made online during analysis based on measured chemical composition. The results of analysis can be explored and extracted after analysis.

In addition, all the AM solutions, offer several data acquisition modes designed to customize the measurement process and optimize the time taken for sample measurement vs the data resolution and imaged area. The user can decide to collect the modal mineralogy or the textural parameters (grain/particle size, liberation, etc.), or both, for the whole sample, for selected particles or for a specific mineral phase.

3.7 Applications of SEM in Forensic Geoscience

In forensic geoscience, one of the most common applications in trace evidence analysis is the comparison of soil samples collected from an item of interest in the investigation (e.g., footwear, clothing, digging implements or a vehicle) and a known crime scene such as the location of an assault or a body deposition site. Soil is complex, and comprises both natural inorganic compounds (minerals), man-made anthropogenic particles, some of which will be inorganic, and organic constituents including macro and microscopic plant debris, spores and pollen, natural organic chemical compounds, invertebrate and occasionally vertebrate debris. The forensic soil analysis will commonly be focused on one or more of these constituents within the overall soil sample. General guidance is available relating to the collection of soil samples from crime scenes (e.g., Pirrie et al. 2021a), sample recovery from exhibits (e.g., Pirrie et al. 2021b) and then the wide range of analytical tools available in forensic soil analysis (e.g., Ruffell et al. 2021). Whilst some soil types will be dominated by the organic components, other soils are dominated by minerals derived from the underlying bedrock geology and overlying superficial deposits. In such samples, mineralogical analysis to allow soil comparisons is a very powerful tool. Soil mineralogy can be quantified using traditional polarising light microscopy, X-Ray diffraction, or automated scanning electron microscopy. The different methods acquire mineralogical datasets in different ways and ideally can be combined in the analysis of a single sample, as each methodology has slightly different advantages and disadvantages. Polarising light microscopy cannot be used in the analysis of samples with a significant clay fraction and is instead best suited in the analysis of coarse silt, sand, or indeed coarser grained geological materials. It provides mineralogical data in textural context, and allows optical features (e.g., microfossils, quartz grain types, etc.) to be determined which cannot be achieved using the other commonly used methods. X-Ray diffraction is widely used, particularly in the analysis of soils with a significant clay fraction, however, the quantification of the analysis can be affected by the presence of strongly crystalline phases. Minerals present at an abundance of less than about 2% may not be identified (whilst potentially being of forensic significance). In addition, for full mineral characterisation samples need to be powdered, and analysed air dried, glycolated, and then heated in a step-wise manner, such that by the end of the analysis the sample has been fundamentally changed and cannot be re-analysed. A final constraint in XRD is that the mineralogical data are not in textural context; an X-Ray diffraction analysis may report quartz, plagioclase, feldspar, yet texturally this could be an unconsolidated sand, with individual grains of the different minerals, a granitic rock fragment or a cemented sandstone – hence the forensic significance may be limited and open to challenge. Automated mineralogy based on SEM-EDS has four main advantages in terms of forensic soil analysis: (1) large populations of particles can be measured at a high resolution in a single sample,

providing statistically robust data; for example in forensic soil analysis, if the sample size is great enough, we would routinely characterise soil mineralogy through the analysis of >4000 grains based on the acquisition of >200,000 individual EDS analyses. (2) The analysis is both quantitative and in textural context; data outputs include both the modal mineralogical data but also the false colour mineral maps, which are effectively comparable with a traditional thin section polarising light photomicrograph. (3) All inorganic phases present within the sample are measured, whether they are opaque or translucent, man-made in origin or natural. (4) The sample measurement is operator independent and automated, although it should be noted that data processing is not and is a function of the skill set of the individual carrying out the analysis.

3.7.1 Applications of Manual Scanning Electron Microscopy and Microanalysis

In some forensic scenarios, manual scanning electron microscopy and microanalysis can provide valuable data which may aid interpretation and/or provide evidential data. During the examination of forensic geoscience trace evidence, it can be significant to image the evidential material in context with the surface on which it is present. For example, items of clothing may be submitted for analysis which have soil either on the surface of, or embedded into, the fabric. Areas of the clothing can be cut from the item and mounted onto a stub for direct SEM examination. If an environmental SEM is available then no further preparation will be required (clothing will have been dried prior to submission for analysis), whist if using a high vacuum system gold or carbon coating will be required. The direct SEM examination can provide information regarding the directionality of the soil traces – for example has the item of clothing simply come into contact with a surface vertically, or has the item been dragged across a surface? Recent work by Murray et al. (2016, 2017) provides a good case study. Such information can be valuable as an independent test of a sequence of events described by individuals within the forensic enquiry.

Combined imaging and microanalysis is widely used in the identification of unknown materials recovered during forensic investigations. For example, at autopsy trace materials may be recovered from a victim's body and may be submitted for SEM-EDS/WDS analysis to identify the nature of those unknown materials (see Gentile et al. 2020 for a review of SEM-EDS in a medical context). Geological scenarios include the transfer of trace evidence from, for example, a rock or concrete fragment used as a weapon to a wound on a victim's body. Other case work we have carried out using manual SEM imaging has included the characterisation of sediment recovered from the trachea of a victim and debris

recovered by washing a victim's skin and/or hair. Trace evidence recovered from drowning victims can aid the understanding of where the individual entered the water.

Less commonly in forensic geoscience investigations there is a need to describe in detail mineral concentrates, rocks, and materials constructed from geological commodities (e.g., bricks, concrete, etc.). Rock samples may be encountered in forensic investigations where for example they have been used as weapons, or to assist in the disposal of items in water. Commonly the provenance of the rock may need to be determined (e.g., was it derived from the crime scene or brought to that

Predictive Geolocation

In some case work, a soil, sediment or dust sample may be collected from an item of relevance to the investigation and submitted for analysis to try to determine the geographical location of the unknown location. This type of investigative analysis is known as predictive geolocation (Pirrie et al. 2017) or predictive soil provenancing (de Caritat et al. 2019, 2021); see also Stern et al. (2019) for an excellent case study. In such investigations, it is critical to collect as many layers of data from the unknown sample as possible, and manual SEM imaging is a significant step within this process. The imaging of a soil subsample may allow the identification of biogenic and man-made components which are present within that soil and may provide additional data regarding its potential geographical source location and/or human activity occurring within that location. This type of analysis may also be used to identify microfossils "inherited" within the soil profile and derived from either the underlying bedrock geology, or in some cases, from geological commodities introduced to an area (e.g., from solid fuels such as coal, construction stone, aggregates, etc.). Within this type of analysis, grain surface textures and the presence/absence of coating materials can be significant in terms of the processes involved in the transport of the soil/sediment/dust. Several authors have published extensively on the imaging of quartz grain surface textures, and their classification and interpretation in terms of the origin and transport processes involved in the history of the grains (e.g., Bull and Morgan 2006; Morgan et al. 2010). Work has focused on quartz grains, which may have distinctive micro-textures on the grain surfaces, resulting from the mechanisms of grain transport and automated texture recognition has been developed (Newell et al. 2012). In addition, quartz grains present within soil profiles, may have inherited textural features indicative of the underlying bedrock geology – for example grains may have distinctive quartz overgrowth cement textures resulting from the diagenesis of a bedrock sandstone source, which may increase the distinctiveness of the soil sample (Fig. 3.13).

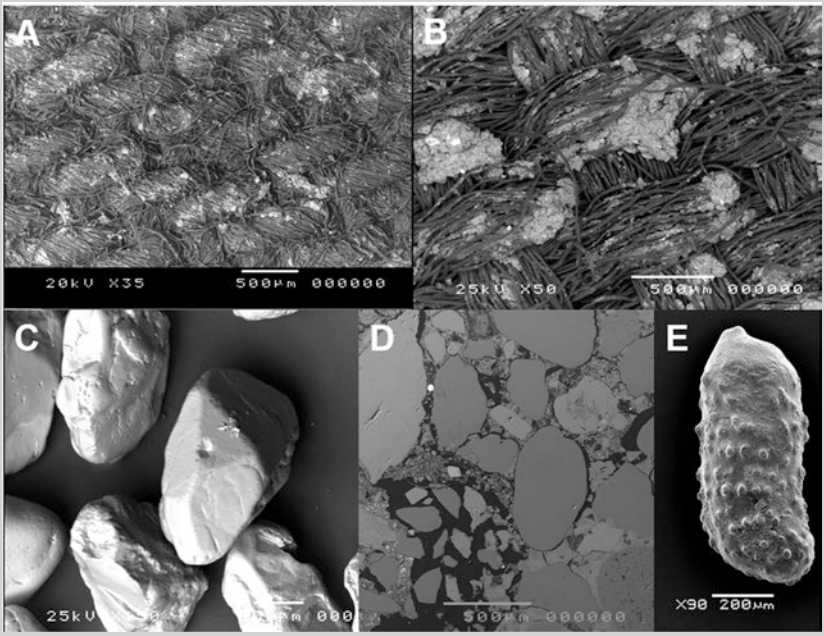

Fig. 3.13 Examples of the use of scanning electron microscopy in forensic geoscience. (**a**, **b**) Imaging soil in context with the surface it is on can allow an interpretation of the nature of the contact between the item and the soil; in B the soil distribution suggests that the item has been dragged over a surface. (**c**) Quartz grain textures have been widely used to determine the transport history but can also be used to infer the nature of the source. (**d**) Polished thin section of a poorly consolidated concrete. (**e**) Foraminifera recovered from a surface soil at the scene of a drive-by fatal shooting

scene by the offender, which suggests a degree of premeditation prior to the offence), and manual SEM may form part of the overall geological characterisation allowing provenance determination. Man-made geological materials such as concrete and brick may also be encountered in forensic investigations of both crimes, but also in cases of civil litigation where for example there is deterioration of the construction material. At the other end of the particle size scale, there is increasing interest in the forensic application of environmentally acquired "very small particles" in which their analysis is based on SEM-EDS characterisation (e.g., Stoney et al. 2015).

Fingerprinting Airborne Asbestos

There is a direct cause and effect relationship between mesothelioma lung cancer insurgence and asbestos inhalation. The inhalation of asbestos particles occurs when asbestos-containing materials decompose or are physically disturbed, and SEM-EDS is the best technique to identify the dispersal of these materials as fine dust in the open air or indoors, through the analysis of a polycarbonate filter exposed to suction of fixed volumes of air at constant flows. During demolition of materials containing asbestos from a disused factory, natural winds were supposed to favour the exposure of a wider group of people, other than those directly working at the demolition. A court judgement was required to prove if the inhabitants of a building located ca. 500 m away from the demolition worksite could have been exposed to airborne asbestos. Airborne dust was recovered according to the requirements of local laws on the terraces of the building, on different days with different weather conditions and local wind directions, both during demolition phases and when there was no work in the disused site. SEM-EDS analyses of suitably prepared filters proved to the court that some asbestos airborne fibers were always recovered, but they increased in number during the demolition phases and in relation to specific local wind conditions (Fig. 3.14).

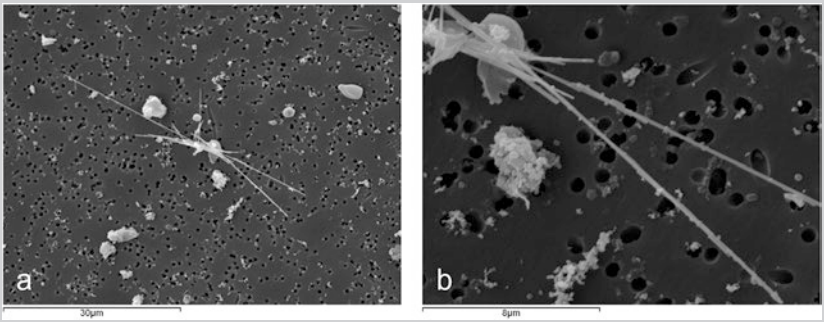

Fig. 3.14 SE microphotograph of airborne asbestos particles (crocidolite) on polycarbonate filter 2.000x (**a**) and 7.500x (**b**)

3.7.2 Applications of Automated Mineralogy

In the UK, automated mineralogy based on SEM-EDS systems has been used in the investigation of serious crimes. The methodology has been adopted and accepted in numerous criminal trials. Its application in other regions has been limited to date based on the availability of automated SEM-EDS systems in laboratories where staff are willing or have the skill set to be involved in forensic investigations. With the wider range of such systems becoming available and their much broader

adoption across the Earth Sciences, then it is likely that automated mineralogy will be adopted more widely as a forensic tool. As discussed above the main advantage of the automated mineralogy approach is that a large population of particles can be measured and quantified, and the resultant data set is in textural context. Usually prior to analysis samples must be embedded in resin, cut and polished and carbon coated. Although such sample preparation is in part destructive, the remaining sectioned grains are still available for examination within the prepared block. This approach is not however, appropriate where there may be highly soluble mineral phases present, as most polishing systems use water, albeit for a limited part of the polishing process. If the material for analysis is very fine grained, then particles can be mounted directly onto double sided carbon tags, attached to SEM stubs and then measured directly following carbon coating, but the impact of the 3D topography on analysis limits this approach to very fine particle sizes only. The other main limitation of automated SEM-EDS is that phases with a very similar chemistry cannot be distinguished, and in very fine particles there may be mixed spectra as a result of the beam excitation volume being greater than the discrete mineral phases.

Most commonly, automated mineralogy systems have been used to characterise soil and sediment samples to test a potential association between "questioned" soil samples collected from an item of relevance to the investigation (e.g., footwear) and a known sample collected from either the known crime scene and/or an alibi location (a location identified as being a potential "innocent" source for the soil trace evidence). Even within the typically small size of a questioned forensic sample, it is usually possible to measure a large population of particles, such that the resultant dataset is statistically significant. The quantitative mineral data produced can be used for sample comparison, but the false colour particle images automatically generated are of considerable value in the interpretation and comparison of the datasets and for demonstrating the data visually in a court of law.

Soil Comparison

As an example of this approach, a victim's body was discovered in an alleyway. The investigation identified that the young victim had been assaulted in an adjacent area where there were exposed soils and her body then dragged into the alleyway. An individual known to the victim was interviewed and footwear linked to this individual (via DNA evidence) was recovered following an attempt to dispose of it. This item of footwear along with the clothing and footwear from the victim were submitted for examination. Because of the sensitivity of the analysis, items submitted for analysis need to be carefully examined, so that discrete areas of soil, which will relate to a single location need to be collected, rather than bulk samples which will be sourced from multiple locations. Both the quantitative modal mineralogy and the particle textures in soil samples recovered from the victim's footwear and the suspects footwear were directly comparable in terms of the main mineral phases

(continued)

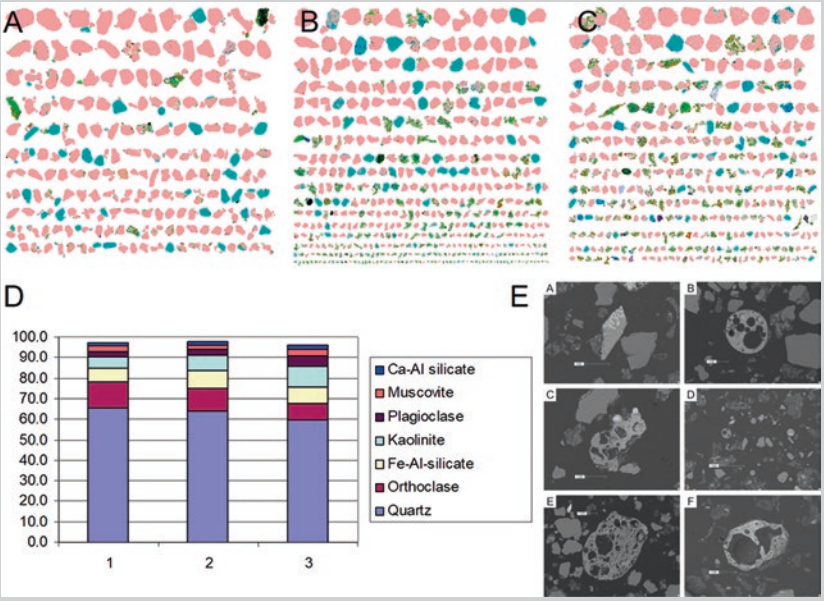

Fig. 3.15 Automated mineralogy in serious criminal investigations. Automated mineralogy particle images arranged by size from (**A**) crime scene, (**B**) victim's footwear and (**C**) suspect's footwear. (**D**) Comparison of the average modal abundance of the dominant mineral phases present in (1) soil samples from the crime scene (n = 9), (2) soil samples from the victim's footwear (n = 11) and (3) soil samples from the suspect's footwear (n = 2). (**E**) Scanning electron microscope images of slag particles present in the soil sample from the crime scene (a, b), victim's footwear (c, d) and the suspects footwear (e, f)

present with known control samples collected from the crime scene (Fig. 3.15). Man-made particles of slag and fly ash were also present in all three samples; whilst these particle types may be relatively common in the environment, their presence in all three sample groups is supporting evidence for an association (Fig. 3.15). The only significant difference in the data was that CaAl silicates, interpreted to be small fragments derived from concrete, were more common in the soil samples from the suspects footwear. Surfaces leading away from the body deposition site were constructed from concrete; the potential inference is that the offender walked away from the scene; the victim didn't. At trial the suspect was found guilty of murder.

Automated mineralogy also has significant potential in predictive geolocation investigations providing fully quantitative data to enhance location description. For predictive geolocation to work, there needs to be a clear correlation between the bedrock geology and the inherited soil mineralogy. To test this Pirrie et al. (2019a)

analysed the composition of soil samples from profiles developed on different geological units throughout SW England and were able to clearly demonstrate that the mineralogical profile of the soil was indicative of the underlying bedrock geology. In addition, Pirrie et al. (2019b) utilised automated mineralogy to identify small fragments of construction materials present within soil samples to aid the description of the built environment based on particles present in soil samples of unknown origin. Automated mineralogy can also be used to provide quantitative data at the thin section scale; this approach has been used in the provenancing of archaeological materials (e.g., Bevins et al. 2021; Nash et al. 2021) but can also be applied to different forensic contexts.

A potential future application of both manual SEM and also automated mineralogy is in the investigation of both the provenance of mineral concentrates and potential criminal substitution of ore concentrates during their transport from mineral processing plant to final end user. Increasing concern regarding the sourcing of raw materials from legal and ethical sources is requiring end users to be able to prove the original source of that raw material. A range of mined mineral commodities are strongly associated with both unregulated artisanal and illegal mining and mining activity which supports criminal cartels. This is most widely reported for the so-called conflict minerals (ores for tin, tungsten and tantalum along with gold), but with increasing demand, and restricted geological sources; other commodities such as cobalt are also of concern. In addition, it is recognised that as these bulk cargos are shipped from the producing mineral processing plant to the end user, they can be intercepted and part of the cargo substituted with low value materials. As such there is a strong need for quantitative mineral analysis methods to be developed for the provenancing, tracing and investigation of bulk ore concentrates and associated metallurgical materials.

References

Amelinckx S, Van Dyck D, Van Landuyt J, Van Tendeloo G (1997) Electron microscopy, principles and fundamentals. Wiley-VCH, Weinheim, 527 pp

Bevins RE, Ixer RA, Pirrie D, Power MR, Cotterell T, Tindle A (2021) Alteration fabrics and mineralogy as provenance indicators; the Stonehenge dolerite Bluestones and their enigmatic "spots". J Archaeol Sci Rep 36:102826

Bull PA, Morgan RM (2006) Sediment fingerprints: a forensic technique using quartz sand grains. Sci Justice 46:107–124

Bruker (2017) AMICS Software—Advanced Mineral Identification and Characterization System; Brochure DOC-H82-EXS018, Rev.1. Bruker: Berlin, Germany, p. 2. Available online: https://web.archive.org/web/20200810115608/, https://www.bruker.com/de/products/x-ray-diffraction-and-elementalanalysis/eds-wds-ebsd-sem-micro-xrf-and-sem-micro-ct/quantax-eds-for-sem/amics-software.html

Butcher AR, Botha PWSK (2010) Automated mineralogy derives key characteristics directly from reservoir rock. The American Oil & Gas Reporter, January 2010, 4 pp

Castaing R (1951) Application of electron probes to metallographic analysis. Ph.D. Dissertation, University of Paris 1951

de Caritat P, Simpson T, Woods B (2019) Predictive soil Provenancing (PSP): an innovative forensic soil provenance analysis tool. J Forensic Sci 64:1359–1369

de Caritat P, Woods B, Simpson T, Nichols C, Hoogenboom L, Ilhea A, Aberle MG, Hoogewerff J (2021) Forensic soil provenancing in an urban/suburban setting: a sequential multivariate approach. J Forensic Sci: 66(5):1679–1696

Gentile G, Andreola S, Bailo P, Battistini A, Boracchi M, Tambuzzi S, Zoja R (2020) A brief review of scanning electron microscopy with energy-dispersive X-ray use in forensic medicine. Am J Forensic Med Pathol 41(4):280–286

Gottlieb P, Wilkie G, Sutherland D, Ho-Tun E, Suthers S, Pereira K, Jenkins B, Spencer S, Butcher A, Rayner J (2000) Using quantitative electron microscopy for process mineralogy applications. J Miner Met Mater Soc 52(4):24–25

Graham SD, Brough C, Cropp A (2015) An Introduction to ZEISS Mineralogic Mining and the correlation of light microscopy with automated mineralogy: a case study using BMS and PGM analysis of samples from a PGE-bearing chromitite prospect. In: Proceedings of the Precious Metals '15, Falmouth, UK, 11 May 2015; Minerals Engineering International (MEI): p 11

Haberlah D, Williams MAJ, Halverson G, McTainsh GH, Hill SM, Hrstka T, Jaime P, Butcher AR, Glasby P (2010) Loess and floods: high-resolution multi-proxy data of Last Glacial Maximum (LGM) slackwater deposition in the Flinders Ranges, semi-arid South Australia. Quat Sci Rev 29:2673–2693

Haberlah D, Owen M, Botha PWSK, Gottlieb P (2011) SEM-EDS based protocol for subsurface drilling mineral identification and petrological classification. In: Broekmans MATM (ed) Proceedings of the 10th International Congress for Applied Mineralogy (ICAM), 01-05 August 2011, Trondheim, Norway, pp 265–273

Hrstka T, Gottlieb P, Skála R, Breiter K, David Motl D (2018) Automated mineralogy and petrology—applications of TESCAN Integrated Mineral Analyzer (TIMA). J Geosci 63:47–63

Morgan RM, Robertson J, Lennard C, Hubbard K, Bull PA (2010) Quartz grain surface textures of soils and sediments from Canberra Australia: a forensic reconstruction tool. Aust J Forensic Sci 42:169–179

Murphy DB, Davidson MW (2013) Fundamentals of light microscopy and electronic imaging. 2, Wiley-Blackwell, 538 pp

Murray KR, Fitzpatrick RW, Bottrill RS, Berry R, Kobus H (2016) Soil transference patterns on bras: image processing and laboratory dragging. Forensic Sci Int 258:88–100

Murray KR, Fitzpatrick RW, Bottrill RS, Berry R, Kobus H (2017) Patterns produced when soil is transferred to bras by placing and dragging actions: the application of digital photography and image processing to support visible observations. Forensic Sci Int 276:24–40

Nash DJ, Ciborowski TJRR, Darvill T, Parker Pearson M, Ullyott JS, Damaschke M, Evans JA, Goderis S, Greaney S, Huggett JM, Ixer RA, Pirrie D, Power MR, Salge T, Wilkinson N (2021) Petrological and geochemical characterisation of the sarsen stones at Stonehenge. PLoS One 16(8):e0254760

Newell AJ, Morgan RM, Griffin DL, Bull PA, Marshall JR, Graham G (2012) Automated texture recognition of quartz sand grains for forensic applications. J Forensic Sci 57:1285–1289

Newbury DE, Ritchie NWM (2015) Performing elemental microanalysis with high accuracy and high precision by scanning electron microscopy/silicon drift detector energy-dispersive X-ray spectrometry (SEM/SDD-EDS). J Mater Sci 50:493–518

Oxford Instruments INCAMineral. Available online: https://web.archive.org/web/20200810110842/. Accessed on 10 Aug 2020

Oxford Instruments—AztecMineral: Dedicated Mineralogy on Multi-Purpose SEM. Available online: https://web.archive.org/web/20200810111028/. Accessed on 10 Aug 2020

Oxford Instruments (2012) INCAFeature. High Performance Feature Detection, Analysis and Classification; Brochure OINA/075/E/0412. Oxford Instruments: High Wycombe, UK, 2012; 4pp

Petrosino P, de Gennaro R, Mondillo N (2019) Microscopia Elettronica a scansione. In: Mercurio M, Cappelletti P, Di Maggio RM, Langella A (eds) Analisi mineralogiche in ambito forense, Aracne:169–217

Pirrie D, Rollinson GK (2011) Unlocking the applications of automated mineral analysis. Geol Today 27(6):226–235

Pirrie D, Butcher AR, Power MR, Gottlieb P, Miller GL (2004) Rapid quantitative mineral and phase analysis using automated scanning electron microscopy (QemSCAN); potential applications in forensic geoscience. Geol Soc Lond, Spec Publ 232:123–136

Pirrie D, Dawson LA, Graham G (2017) Predictive geolocation; forensic soil analysis for provenance determination. Episodes 40:141–147

Pirrie D, Crean DE, Pidduck AJ, Nicholls TM, Shail RK (2019a) Automated mineralogical analysis of soils as an indicator of local bedrock lithology: a tool for rapid forensic geolocation. Geol Soc London, Spec Publ 492. https://doi.org/10.1144/SP492-2019-42

Pirrie D, Pidduck A, Crean DE, Nicholls TM (2019b) Identification and analysis of man-made geological product particles to aid forensic investigation of provenance in the built environment. Forensic Sci Int 305:1–15

Pirrie D, Ruffell A, Dawson L, McKinley J (2021a) Crime scenes: Geoforensic assessment sampling and examination. In: Donnelly L, Pirrie D, Harrison M, Ruffell A, Dawson L (eds). A guide to forensic geology. Geological Society, London Chapter 4:88–110

Pirrie D, Ruffell A, Dawson L (2021b) Geological evidence recovery from exhibits. In: Donnelly L, Pirrie D, Harrison M, Ruffell A, Dawson L (eds) A guide to forensic geology. Geological Society, London Chapter 5:111–128

Reimer L (1998) Scanning electron microscopy: physics of image formation and microanalysis. Springer Verlag, Berlin Heidelberg, 527 pp

Ruffell A, Pirrie D, Dawson (2021) Geological evidence analysis. In: Donnelly L, Pirrie D, Harrison M, Ruffell A, Dawson L (eds). A guide to forensic geology. Geological Society, London Chapter 6:129–156

Simons B, Graham S (2016) Iron oxide analyses by Automated Mineralogy. http://www.petrolab.co.uk/

Stern LA, Webb JB, Willard DA, Bernhardt CE, Korejwo DA, Bottrell MC, McMahon GB, McMillan NJ, Schuetter JM, Hietpas J (2019) Geographic attribution of soils using probabilistic modeling of GIS data for forensic search efforts. Geochem Geophys Geosyst 20:1–20

Stoney DA, Bowen AM, Stoney PL (2015) Utilization of environmentally acquired very small particles as a means of association. Forensic Sci Int 254:26–50

TESCAN (2017) TIMA-X—TESCANIntegratedMineralAnalyser; Brochure 2017.04.10; TESCAN: Brno, Czech Republic, 16p

Vernon-Parry AD (2000) Scanning electron microscopy: an introduction. Ill-Vs Review 13(4):3–4

Zadora G, Brozek-Mucha Z (2003) SEM–EDX—a useful tool for forensic examinations. Mater Chem Phys 81:345–348

Zeiss—Microscopes for Automated Mineral Analysis. Available online: https://web.archive.org/web/20200724134840/https://www.zeiss.com/microscopy/int/products/scanning-electron-microscopes/mineralogic-systems.html. Accessed on 17 Oct 2021

Zhou W, Apkarian RP, Lin Wang Z, Joy D (2007) Fundamentals of scanning electron microscopy. In: Zhou W, Lin Wang Z (eds) Scanning microscopy for nanotechnology. Springer, New York, 1–40

Chapter 4
Infrared Spectroscopy and Application to Forensics

Giuseppina Balassone, Dominik Talla, Anton Beran, and Fabio Bellatreccia

Abstract Infrared spectroscopy is applied to many research topics, spanning across the fields of chemistry, geology, soil and materials science, biology, medicine and even cultural heritage. Since the 1950s, IR spectroscopy has been recognized as a fundamental analytical technique in mineralogy and earth sciences, along with X-ray diffraction, for phase identification and structural investigation of pure and/or mixed solid samples, as well as liquids and gases. Applications of FTIR spectroscopy to forensic sciences concern many geological and non-geological materials, such as rocks, stems and powders, soils, minerals, gemstones, asbestos, glasses and other amorphous materials, pigments and natural dyes, inorganic contaminants, or plastic. In this chapter, various case studies are reported for different natural and artificial substances, by considering some approaches such as fingerprinting, qualitative analysis of discrete features in the spectral signal, quantitative analysis, and spatial analysis (imaging).

Keywords Infrared spectroscopy · Forensic science · Geological materials · Artificial substances · Fingerprinting · Qualitative analyses · Quantitative analyses · Imaging

G. Balassone (✉)
Dipartimento di Scienze della Terra, dell'Ambiente e delle Risorse (DiSTAR), Università Federico II, Napoli, Italy
e-mail: balasson@unina.it

D. Talla · A. Beran
Institut für Mineralogie und Kristallographie, Universität Wien, Wien, Austria
e-mail: dominik.talla@univie.ac.at; anton.beran@univie.ac.at

F. Bellatreccia
Dipartimento di Scienze, Sez. Scienze Geologiche, Università Roma Tre, Rome, Italy
e-mail: fabio.bellatreccia@uniroma3.it

M. Mercurio et al. (eds.), *Mineralogical Analysis Applied to Forensics*, Soil Forensics, https://doi.org/10.1007/978-3-031-08834-6_4

Infrared (IR) absorption spectroscopy is an analytical method, developed in the early twentieth century, based on the interaction between electromagnetic radiation in the infrared spectral range (wavelengths between 0.8 and 1000 μm) and matter (Beran and Libowitzky 2004). Being a vibrational spectroscopy technique, it is based on the partial conversion of the energy of the incident photons to mechanical oscillation of molecules, atomic groups, and even to the crystal lattice of a particular solid substance as a whole. The specific wavelengths at which these absorptions occur are dictated by the mass of the oscillating species and the strength of the chemical bonds joining it to the rest of the given structure, resulting in their resonance when exposed to the appropriate wavelength. This explains the uniqueness of the shape of the spectral envelope for each chemical compound. Thus, through the study of the infrared spectrum, essential information can be obtained about the composition, structure of the analysed compound as well as on the presence of particular structural defects or impurities.

From an applied point of view, this technique brings the benefit of simplicity and versatility; organic and inorganic crystalline and glassy solids can be analysed, while specific configurations/techniques and accessories allow the measurement of gases, liquids, solutions, and suspensions as well.

Given its mentioned versatility, IR spectroscopy is applied to many research topics, spanning across the fields of chemistry, geology, soil and materials science, biology, medicine, cultural heritage, etc. (e.g., Derrick et al. 1999; Amalfitano and Balassone 2005; Balassone and Beran 2005; Nakamoto 2009; Artioli 2010; Madeiovà et al. 2011; Nicolić 2011; Årnes 2017; Della Ventura et al. 2014; Della Ventura 2017; Balassone and Bellatreccia 2019). Moreover, the cost of the necessary equipment is usually reasonable. Since the 1950s, IR spectroscopy has been recognized as a fundamental analytical technique in mineralogy and earth sciences, along with X-ray diffraction, for phase identification and for structural investigation of pure and/or mixed solid samples, as well as of liquids and gases. The first database collection of IR mineral spectra was done by Farmer (1974) that still nowadays represents an important reference IR spectroscopy textbook (Della Ventura et al. 2014, and references therein). In the late 1960s and early 1970s, a new IR technique was developed – Fourier Transform InfraRed spectroscopy (FTIR) – which led to the commercialization of a new class of spectrometers based on computerized processing of an FFT (Fast Fourier Transform) algorithm.

In the FTIR spectrometer, the IR radiation is emitted by a source converting electricity into thermal radiation (i.e., Globar, Nernst bar, ceramic light sources). The emitted thermal (infrared) radiation is led through a Michelson interferometer, after which it is focused on the sample. This has the advantage of being able to collect the spectral data in the entire spectral range simultaneously, with great improvement in both speed and signal-to-noise ratio (Della Ventura et al. 2014). Since the 1980s, the IR microscopy (Humecki 1995) became widespread. Currently, FTIR microscopy is a well-established method for characterizing variously complex samples, including its application in forensics (Chalmers et al. 2012). In recent years,

the use of focal-plane-array (FPA) area detectors has revolutionized FTIR spectroscopy in the mid-IR (MIR) spectral region. These devices are composed of small IR detectors (pixels) with dimensions of only a few tens of microns or less, which allow the acquisition of thousands of spatially resolved IR spectra simultaneously, generating mid-IR spectral pixel maps with a high lateral resolution. The optical system of an IR microscope equipped with FPA is an apertureless imaging system. With this type of state-of-the-art apparatus, it is possible to obtain various imaging modes at a resolution of a few microns, as well as to acquire large amounts of data in just a few minutes with remarkable sensitivity (Della Ventura et al. 2014, and references therein). The imaging systems for FTIR microscopes currently on the market offer unmatched performance, thanks to their high spatial resolution and remarkable sensitivity. Nano-FTIR also recently came into use, a technique that can be considered as a combination of an FTIR instrument with an atomic force microscope (AFM) and which allows investigations with a resolution down to the nanoscale of extremely limited amounts of material (Amarie et al. 2009).

In addition to these methods, synchrotron radiation (SR) is currently used in FTIR microscopy and FTIR imaging studies (Della Ventura et al. 2014, and references therein; Della Ventura 2017, and references therein). This method is particularly suitable for studies on extremely small samples (down to a few tens of microns) or those requiring considerable spatial and temporal resolution. Over the past twenty years, several synchrotron beamlines dedicated to FTIR (SR-IR) spectroscopy and microscopy have been built. In Italy, SR-IR lines are active at INFN Laboratories in Frascati (https://web.infn.it/Dafne_Light/index.php/beamlines/sinbad-ir) and ELETTRA in Trieste (https://www.elettra.trieste.it/it/lightsources/elettra/elettra-beamlines/sissi/sissi.html).

Applications of FTIR spectroscopy to forensic sciences concern many geological and non-geological materials, such as rocks, stems and powders, soils, minerals, gemstones, asbestos, glasses and other amorphous materials, pigments and natural dyes, inorganic contaminants, as testified by the wide literature exiting on this topic (e.g., Fitzpatrick 2008, 2009; Fitzpatrick et al. 2006; Lanzarotta 2016; Muro et al. 2016; Murray and Tedrow 1992; Pye and Croft 2004; Ruffel and McKinley 2005; Keaney et al. 2009; Saferstein and Hall 2020).

4.1 Theoretical Background

In the scientific literature, the theoretical and technical aspects of IR spectroscopy are widely treated in numerous specialized texts (*e.g.,* Schrader 1995; Smith 1996; Stuart 2004; Chalmers and Griffiths 2002; Griffiths and de Haseth 2007; Nakamoto 2009; Atkins and de Paula 2012; Henderson et al. 2014). Some basic notions useful to understand the theoretical basis of the method will be presented below.

4.1.1 The Infrared (IR) Radiation

On the wavelength scale, IR radiation lies between the visible and microwave regions of the electromagnetic spectrum (Fig. 4.1). As each type of electromagnetic radiation, it is a transverse sine wave consisting of an electric (*E*) and a magnetic (*H*) component, each oscillating in one of two perpendicular planes. It is important to note that for our purposes, interactions with matter involve mainly the electrical component.

The parameters allowing to characterize any electromagnetic wave are:

- *wavelength* (λ): distance between two equivalent points of a sine wave; μm is the usually used unit (1 μm = 10^{-4} cm);
- *amplitude* (*A*): is proportional to the wave intensity, which equals its square root;
- *frequency* (ν in Hz or sec^{-1}): number of oscillations per second;
- *propagation rate* (c = 2998 x 10^8 m/sec in vacuum), the velocity of light;
- *wavenumber* ($\bar{\nu}$ in cm^{-1}): number of wavelengths per unit of distance (for IR wavelengths per cm); ($\bar{\nu}$ = 10,000/μm);
- *time period of the vibration* (*T*).

The relationship between these parameters is:

starting with classical mechanics $\lambda = c \cdot T$, instead of *T*, ν is used, where $\nu = 1/T$

$$\lambda = \frac{c}{\nu}$$

The wavenumber unit is most widely used in IR spectroscopy. The infrared spectral region, located between 14,000 and 10 cm^{-1}, is conventionally subdivided into three sections (Table 4.1 and Fig. 4.1) and the IR region of interest for most geological materials is MIR (Medium InfraRed).

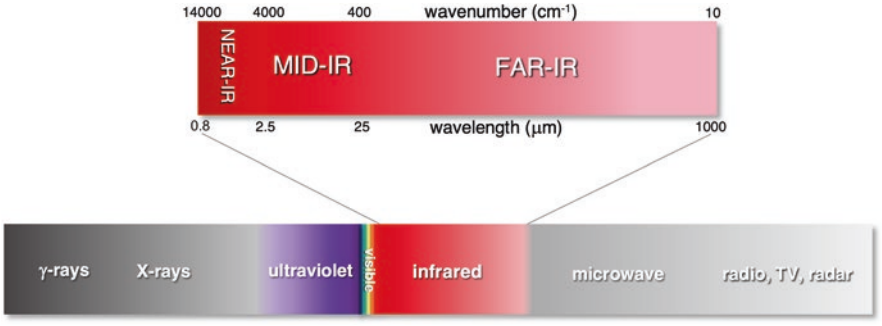

Fig. 4.1 The electromagnetic spectrum

Table 4.1 Subdivision of infrared fields

	$\bar{\nu}$ (cm^{-1})	λ (μm)	ν (THz)
Near (NIR)	14,000–4000	0.8–2.5	374.7–119.9
Medium (MIR)	4000–400	2.5–25	119.9–12.0
Far (FIR)	400–10	25–1000	12.0–0.3

4.1.2 The Absorption of IR Radiation

When IR radiation hits a molecule, it can be absorbed, reflected, or diffused; absorption IR spectroscopy is based on the first process. If a photon of a particular *frequency* (ν) enters a material whose molecular structure allows mechanical resonance at that particular frequency, it is absorbed and part of its energy converted into atomic vibrations. In this sense, since the energy of electromagnetic radiation is directly related to its frequency ($E = h\nu$), the kinetic energy of the structure or its constituent parts is raised from the ground state (E_i) to a higher-energetic state (E_f) according to the relation:

$$\Delta E = E_f - E_i = h\nu = hc\bar{\nu}$$

with h being the *Planck constant* (6.63×10^{-34} Js)

As already mentioned, the energy transferred to the substance by the radiation is converted into vibrational energy. Quantum mechanics has shown that the difference between two *vibrational energy levels* (ΔE) is quantized, *i.e.* it can only take on discrete values.

Since the intervals between vibrational levels are of the order of 10^2–10^3 cm^{-1}, it is evident that these can be excited by IR radiation. Actually, this also applies to rotation and translation of entire molecules; however, in solids, these types of motion are generally inhibited, so they will not be considered in this brief treatment.

4.1.3 The Harmonic Oscillator Model

The nature of the interaction between IR radiation and molecules can be represented by the model of the harmonic oscillator, which allows to show some very useful information (Beran et al. 2004). A diatomic molecule is characterized by (i) two atoms, with masses m_1 and m_2, joined by a chemical bond and (ii) the chemical bond, for our purposes represented identically to a mechanical spring, whose elastic constant is k, and correlates with the bond strength (Fig. 4.2a).

The situation can be expressed via classical mechanics, relating the vibrational frequency of such a system to the above-mentioned parameters by the equation:

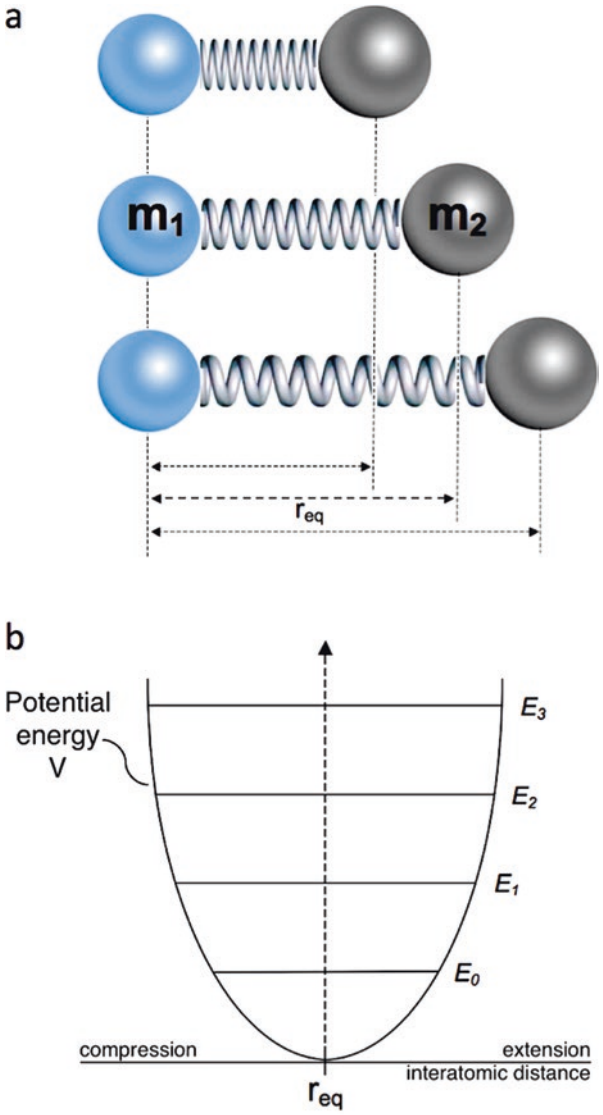

Fig. 4.2 (**a**) Diatomic molecule in the harmonic oscillator model (r_{eq} equilibrium distance between atoms of mass m_1 and m_2) and (**b**) simplified graph of potential energy for the harmonic oscillator

$$\nu = \frac{1}{2\pi}\sqrt{\frac{k}{\mu}}$$

where $\mu = \frac{m_1 m_2}{m_1 + m_2}$ is the reduced mass.

Although most molecules are much more complex systems, this simple equation demonstrates that (i) the *vibrational frequency* (ν) increases with higher values of the *elastic constant* (k), *i.e.*, the *bond strength*, and (ii) the *frequency* (ν) decreases as the mass of the atoms involved increases.

Using this model and applying the principles of quantum mechanics, it is possible to establish the specific vibrational selection rules, *i.e.* the jumps permitted between the energy levels (Fig. 4.2b).

The permitted transitions are only those that involve jumping but one level at a time. Then, it is possible to demonstrate, by applying the principles of statistical mechanics, that the most likely transition is from the *ground state* (E_0) to the first *excited vibrational level* (E_1). Real molecules, however, are not harmonic oscillators, which modifies the selection rules by allowing jumps of two or more levels at a time as well. This results in the possibility of having absorptions due to combinations between different vibrational and/or harmonic modes of the same vibration (combination modes and overtones): *e.g.*, by considering the stretching vibration of an H_2O molecule at 3600 cm^{-1} and the bending vibration at 1600 cm^{-1}, a combination mode at 5200 cm^{-1} can be observed. A single OH group at 3600 cm^{-1} having a Me-OH bending mode at 900 cm^{-1}, results in a combination mode at 4500 cm^{-1}. H_2O molecules or OH groups with stretching vibrations occurring around 3600 cm^{-1} show their first overtones at 7200 cm^{-1} (2×3600 cm^{-1}). In general, overtone bands are of great practical importance in NIR spectroscopy.

4.1.4 Transition Moment and General Selection Rule in IR Spectroscopy

Depending on the distribution of atoms within the molecule, it may or may not have a dipole moment, resulting from the distribution of atomic charges associated with each constituent atom. In some cases, it can be permanent, as in polar molecules in which the positive and negative charges are asymmetrically distributed. One such example is the H_2O molecule, in which the negative oxygen atom is exposed on one side, with both positive hydrogen cations concentrated close together on the opposite side of the molecule (Fig. 4.3a).

However, there are also non-polar symmetric molecules, in which it is the atomic vibration, induced by the absorption of IR radiation, which leads to a temporary asymmetric distribution of charges; for instance, in CO_2, some vibrational modes generate a temporary oscillating dipole (Fig. 4.3b).

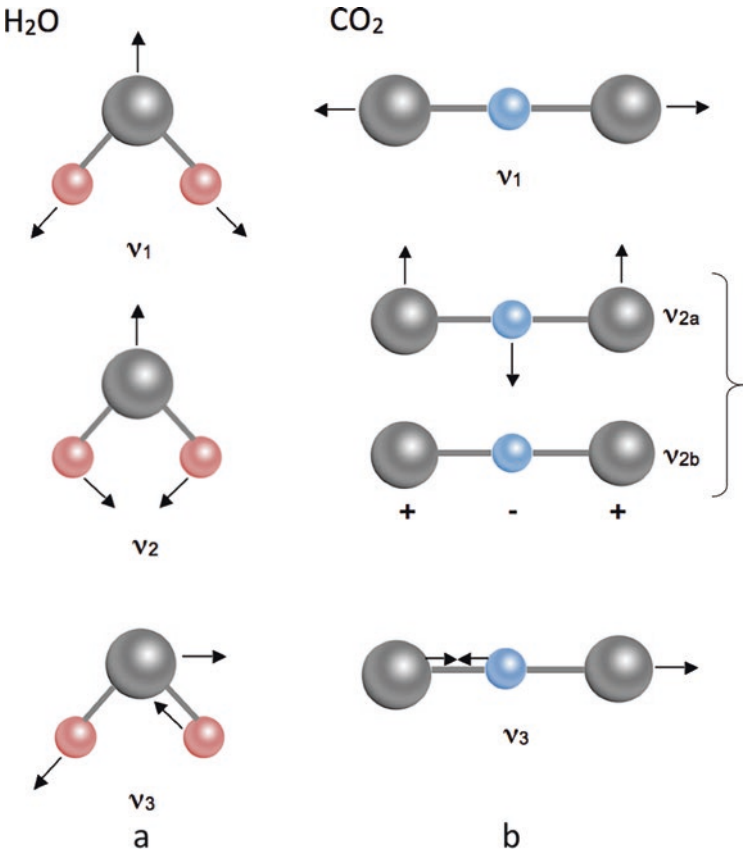

Fig. 4.3 Normal vibrational modes in the molecules of H_2O (**a**) and CO_2 (**b**), with ν_1 and ν_3 corresponding to the *symmetric* and *anti-symmetric stretching vibrations*, respectively, and ν_2 to the *bending vibration*; ν_{2a} and ν_{2b} are *doubly degenerated bending vibrations* of CO_2. (Redrawn from Beran et al. 2004)

Thus, the shape of the molecules determines their capability to interact with IR radiation, as it dictates the distribution of electrical charges, determining the character of allowed vibrational modes.

A vibration is called IR-active when it is excited by IR radiation of a specific frequency. This occurs when the vibration of the molecule can give rise to a variation of the dipole moment, generating a transition dipole moment. The general selection rule can be defined as follows: a vibrational transition will be active in the IR only if the dipole moment of the molecule varies during the vibration, or rather if the transition moment is different from zero (Atkins and de Paula 2012).

4.1.5 The Normal Vibration Modes of Molecules

Even the most complex molecule composed of N atoms can vibrate only in 3 N – 6 (3 N – 5 for linear molecules) vibrational modes, called normal modes. In the case of a diatomic molecule (N = 2), there will be only one mode of vibration (3×2–5 = 1), in which the bond between the two atoms periodically lengthens and shortens. In the case of polyatomic molecules, there will be many different modes of vibration since the lengths of the bonds and the angles between them can vary in complex ways. For example, the H_2O molecule (N = 3) has 3×3–6 = 3 normal modes (Fig. 4.3a), while the linear CO_2 molecule (also with N = 3), has 3×3–5 = 4 normal modes (Fig. 4.3b). Depending on the type of deformation affecting the molecule during vibration, vibrational modes can be classified into several types (Fig. 4.4 and Table 4.2).

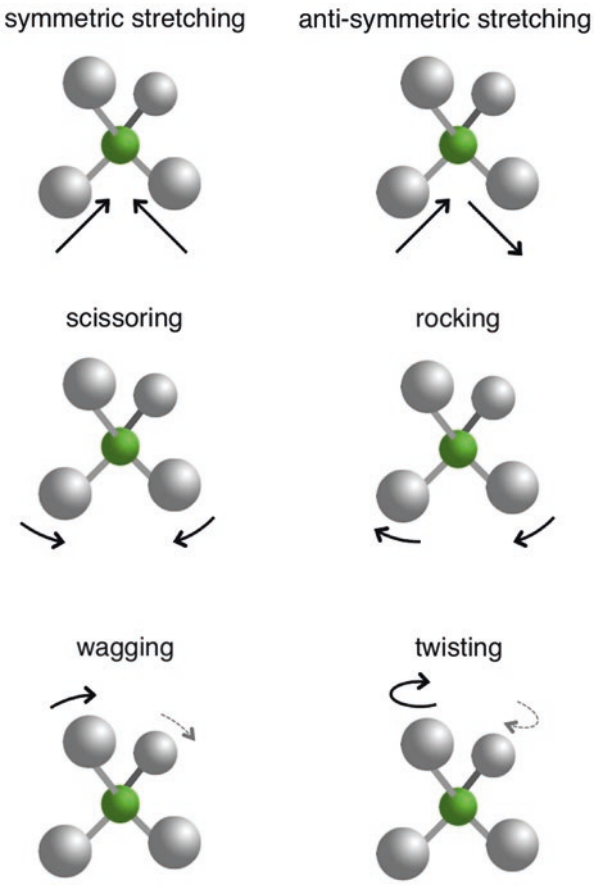

Fig. 4.4 Stretching (symmetric and anti-symmetric) and bending vibrational modes of a tetrahedral molecule both in-the-plane (scissoring and rocking) and off-the-plane (wagging and twisting)

Table 4.2 Symbols of different ways of molecular vibration

Symbol	Description	Symmetric	Anti-symmetric
ν	Stretching	ν_s	ν_a *or* ν_{as}
δ	Bending/scissoring	δ_s	δ_a *or* δ_{as}
ρ	Rocking		
π, ω	Wagging		
τ	Twisting		

– stretching – lengthening and shortening of the interatomic distance along the chemical bond;
– bending – variation of the angle between chemical bonds.

These vibrational modes can be also distinguished into symmetric or anti-symmetric with respect to the global symmetry of the molecule; therefore, with respect to the geometric plane that contains the bonds involved, the angle between which varies, it is possible to define:

– scissoring and rocking – symmetric and anti-symmetric deformations within the plane;
– wagging and twisting – symmetric and anti-symmetric deformation outside the plane.

Despite this complexity, it is possible to determine which vibrational modes are IR active or not from the analysis of the molecule's symmetry. For example, the number of different energy levels decreases as the symmetry of the atomic group increases; the number of vibrational states with the same energy (degenerate levels) increases as symmetry increases.

This type of analysis is trivial for simple molecules, but in the case of more complex structures or crystals, it can be very challenging, as it requires the application of the principles of group theory, widely treated in specific texts (Turrell 1972; Rousseau et al. 1981; Nakamoto 2009; Atkins and de Paula 2012).

Homonuclear diatomic molecules, such as H_2, O_2, N_2, etc., being perfectly symmetrical, have no permanent or temporary dipole, so their stretching mode is not IR active.

In the case of CO_2, which has no permanent dipole moment, only three of four normal modes are IR active. The anti-symmetric stretching of carbonyl bonds and the two bending vibrational motions (in and out of the plane) cause the appearance of a temporary non-zero dipole moment, variable over time (Fig. 4.3b). Conversely, symmetric stretching of CO_2 does not lead to IR absorption, since it does not change the symmetry centre of the molecule. At all times, the change of one C=O bond length is nullified by the same change of the other one, resulting in a permanent symmetric charge distribution and thus no non-zero dipole moment.

In the H_2O molecule, which has a permanent dipole, all normal modes are IR active (Fig. 4.3a). In more complex systems, the total theoretical number of fundamental vibrations will rarely be observed in the IR spectrum, as various additional factors can increase or decrease the number of absorption bands. For discrete or

organic molecules, vibrational spectra are more easily interpretable, as organic molecules are weakly interacting, and their functional groups and peripheral bonds vibrate independently from the rest of the molecule.

4.1.6 Transmittance, Absorbance and Beer-Lambert's Law

An IR spectrum in transmission mode is obtained when IR radiation passes through the sample, causing it to lose part of its original intensity. This loss is much more pronounced at certain specific energies (wavenumbers), which correspond to values at which a molecular vibration is excited within the sample (Della Ventura 2017).

An infrared spectrum generally consists of a graph showing the percentage of *transmittance* (*T*) or the *absorbance value* (*A*) on the y-axis, preferentially plotted vs the wavenumber, less commonly vs wavelength or frequency (x-axis). *Transmittance* (*T*) is the fraction of IR radiation at a given wavenumber passing through the sample:

$$T\left(\bar{\nu}\right) = I / I_0$$

where I_0 and I are the intensity of the incident beam and of the beam exiting the sample, respectively (Fig. 4.5a). The *transmittance* is normally expressed as a percentage:

$$\%T\left(\bar{\nu}\right) = I / I_0 \cdot 100$$

The *transmittance* (*T*) relates to another feature, the *absorbance* (*A*), by the following equation:

$$A\left(\bar{\nu}\right) = \log\left[1 / T\left(\bar{\nu}\right)\right] = -\log T\left(\bar{\nu}\right)$$

The Beer-Lambert law shows that the *absorbance* (*A*) is directly proportional to the optical path or *thickness of the sample* (*t*) expressed in centimetres, the *molar concentration* of the absorber (*c*), and the *molar absorption coefficient* ($\varepsilon_{\bar{\nu}}$), according to the relation:

$$A\left(\bar{\nu}\right) = \varepsilon_{\bar{\nu}}\, c\, t$$

Absorbance (A) is dimensionless if measured as a linear quantity (peak height) and it has the unit cm^{-1} if measured as an *integrated quantity* (peak area) A_i.

The *linear absorption coefficient* (α) is obtained by normalizing the dimensionless *linear absorbance* (*A*) to the *thickness* of the sample (t), resulting in the unit cm^{-1}. If *integrated absorbance* (A_i) values in cm^{-1} are employed by normalizing to the thickness, the unit for the *integrated absorption coefficient* (α_i) is cm^{-2}.

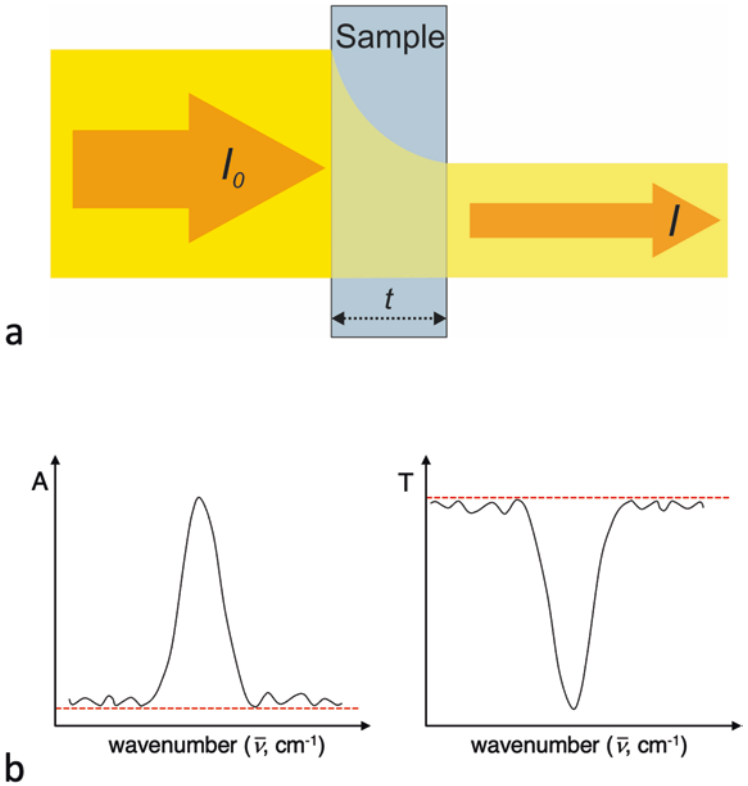

Fig. 4.5 (**a**) Transmission of IR radiation through a sample, I_0 and I are the intensities of the incident and transmitted beam, respectively, through a sample plate of thickness *t*. (**b**) IR spectral envelope showing an absorption band with *absorbance* units, A = −log T (dimensionless *Absorbance*), in use and the corresponding pattern with *transmittance* units, T = I/I_0 (multiplied by 100 defines the *transmittance* in %), on the y-axis. In both cases, the spectrum is plotted as a function of the *wavenumber* $\bar{\nu}$. The dashed red line corresponds to the baseline

$$\alpha\left(\bar{\nu}\right) = A\left(\bar{\nu}\right) / t$$

From the *Beer-Lambert law*, it derives that the linear and the integrated absorption coefficients also depend linearly on the molar concentration of the absorber:

$$\alpha\left(\bar{\nu}\right) = \varepsilon_{\bar{\nu}}\, c$$

The scaling factor $\varepsilon_{\bar{\nu}}$ is the *linear molar absorption coefficient*. As stated above, this coefficient is a constant for a given substance/matrix at a given ($\bar{\nu}$) and must be determined by other analytical methods or calibration curves. However, its invariability applies only for a given range of concentrations, above which the linearity between *absorbance* (*A*) and *concentration* (*c*) can be influenced by other chemical-physical phenomena. In the case of *linear absorbance measurements* (judging peak height), ($\varepsilon_{\bar{\nu}}$) is expressed as [L·cm^{-1}·mol^{-1}]. In the case of integrated

measurements with i*ntegrated absorbance* A_i [cm^{-1}] or with the *integrated absorption coefficient* α_i [cm^{-2}] in use, the integrated molar absorption coefficient is expressed in [$L \cdot cm^{-2} \cdot mol^{-1}$] units (Libowitzky and Beran 2004).

A useful version of the Beer-Lambert law, that allows to calculate the concentration of the absorber (c) in weight % instead of the less preferred $mol \bullet L^{-1}$ units, is:

$$c_{\%} = \frac{A\left(\bar{\nu}\right) f_c}{\varepsilon_{\bar{\nu}} t D}$$

where (D) is the density of the sample (in g/cm^3) and (f_c) corresponds to the molecular weight of the absorber divided by a factor of 10.

4.1.7 The IR Spectrum: Position, Intensity and Shape of Absorption Bands

An IR spectrum is given by a sequence of maxima of absorption (bands or peaks with absorbance units in use) recorded most as a function of the wavenumber, less commonly using frequency or wavelength units (Fig. 4.5b). The overall position and type of absorption bands indicate the combination of the molecular groups present in the sample. The parameters that characterize an absorption band are: position, intensity and shape.

The position of a band is indicated by the *wavenumber* $\left(\bar{\nu}\right)$ in cm^{-1} or, especially in older literature, by the *wavelength* λ in μm. As stated above, the position of absorption bands is mainly influenced by the structural characteristics of the absorbers (molecular mass, sample character and local bond topology). The intensity of a band is given either by its *linear absorbance* (*A*), which can be determined by measuring the peak height from an appropriately defined baseline, or more precisely, by the *integral absorbance* (A_i), considering the area below the curve.

From a qualitative point of view, absorption bands can be classified as strong (s), medium (m) and weak (w), based on a purely empirical estimate. The shape of the absorption peaks can vary significantly, depending on the characteristics of the samples analysed. Theoretically, the shape is mostly related to Gaussian or Lorentzian functions, which have a symmetrical profile. In the case of substances with isolated functional groups such as OH, CH, CN, which have weak or zero interactions with their structural surroundings, or those with a high *molar absorption coefficient* ($\varepsilon_{\bar{\nu}}$ *),* the absorption bands will generally be sharp and well resolved.

More commonly, especially in solid materials, the bands are broad, asymmetric and frequently have shoulders, due to overlaps of several more or less-resolved components. This is also true for samples consisting of a mixture of various compounds, or with multiple functional groups of the same type, but bound in different structural sites. In such a case, the interactions with the surrounding structure will be different for the identical functional groups, resulting in the change of the bond strength and therefore the absorption wavenumbers for each individual site. A

typical example are the OH groups in amphiboles (tremolite-ferroactinolite series, minerals also forming asbestos), in which the donor oxygen is bound to three sites with metal cations. When these are all the same, *i.e.* Mg, only one well-resolved absorption band at around 3670 cm^{-1} is present, but when some of these atoms are replaced by Fe, a set of split bands at slightly different wavenumbers (3670–3625 cm^{-1}) can be observed (*e.g.*, Libowitzky and Beran 2004).

Finally, it should be noted, that especially in ionic crystals, the bands are normally very wide, since they are the result of absorptions of the numerous vibrations of the entire crystal lattice. However, if we are dealing with crystals which are characterised by structural atomic groups, such as CO_3^{2-}, SO_4^{2-}, PO_4^{3-}, SiO_4^{4-}, etc., or H_2O and CO_2 molecules, the absorption spectra are clearly dominated by the significant stretching and bending vibrations of the respective atomic groups.

Consequently, it can be tricky to obtain a realistic measure of the absorption area (A_i); for this reason, the estimation of linear absorbance (A) is used most, by simply measuring the height of the peak from the baseline, although this does not best represent the real absorption intensity. To solve this problem, modelling spectra through curve fitting (Hawthorne and Waychunas 1988) can be used instead, by fitting the experimental curve with mathematical functions (Gaussian, Lorentzian, Voigt, etc.) The goodness of such a fit is then corroborated by the values of statistical parameters such as R^2, χ^2, etc. However, this approach gives realistic results only with a reliable experimental model to constrain the characteristic elements of the functions such as the full width at the half-height (at half-maximum) of the individual peaks (FWHM) as well as the total number of peaks.

4.1.8 Features of the IR Spectrum and Their Interpretation

IR spectra of solid materials are typically divided into two main regions: (1) the functional group region from 4000 to 1500 cm^{-1} and (2) the fingerprint region, between 1500 and 400 cm^{-1}.

In the first region, the assignment of a band to specific functional groups is relatively simple, since absorptions generally occur as well-resolved and intense bands. Contrary, the fingerprint region is much more complex, as the absorptions due to vibrations related to the oscillations of the entire structure (lattice modes) are combined and superimposed in many ways. However, this series of overlapping bands represents the fingerprint of the given substance.

Characteristic absorptions due to specific functional groups occur in comparable wavenumber ranges in the spectra of all compounds containing them and can be used for their identification. The individual types of these functional groups have absorptions in a relatively narrow field of $(\bar{\nu})$, making it possible to summarize them in tables, useful for the correct assignment of a particular absorption band (Table 4.3). A similar situation occurs in the case of atomic groups such as CO_3^{2-}, SO_4^{2-}, etc., occurring in crystalline inorganic solids and minerals (Table 4.4).

Table 4.3 Characteristic frequencies (cm^{-1}) of organic functional groups

Bond	Compound	Frequency range	Intensity*
C-H	Alkanes	2970–2850	s
C-H	Alkenes	3095–3010 995–675	m s
C-H	Alkynes	3300	s
C-H	Aromatic rings	3100–3010 900–690	m s
O-H	Monomeric alcohols, phenols H-bonded alcohols, phenols Monomeric carboxylic acids H-bonded carboxylic acids	3650–3590 3600–3200 3650–3500 2700–2500	v v/b m b
N-H	Amines, starches	3500–3300	m
C=C	Alkenes	1680–1610	v
C=C	Aromatic rings	1600–1500	v
C≡C	Alkynes	2260–2100	v
C-N	Amines, starches	1360–1180	s
C≡N	Nitriles	2280–2210	s
C-O	Alcohols, ethers, carboxylic acids, esters	1300–1050	s
C=O	Aldehydes, ketones, carboxylic acids, esters	1760–1690	s
NO_2	Nitro compounds	1570–1500 1370–1300	s

Modified after Balassone and Bellatreccia (2019)
* intensity: s = strong, m = mean, b = broad, v = variable

Table 4.4 Characteristic frequencies (cm^{-1}) of atomic groups present in minerals and natural solid materials

Group	Stretching vibrations	Bending vibrations
MOH^-	3700–2900	1300–400
H_2O	3700–2900	1650–1600
CO_3^{2-}	1600–1300	950–650
NO_3^-	1500–1250	900–700
BO_3^{2-}	1300–1200	800–600
SO_4^{2-}	1200–1050	700–600
PO_4^{3-}	1100–950	600–550
SiO_4^{4-}	1000–800	550–400
$Si_xO_y^{z-}$	1200–900	800–400
AsO_4^{3-}	900–750	400
VO_4^{3-}	900–750	400
WO_4^{2-}	850–750	350–300
Formiates, acetates, oxalates	1700–1300	1050–700
Cyanates, cyanides, thiocyanates	2200–2000	–

Modified after Derrick et al. (1999) and Beran et al. (2004)

IR spectra are interpreted by using both the tables above and by comparison with reference spectra collected in databases, often provided by instrument manufacturers (i.e., Bio-Rad, Bruker, Thermo Fisher™-Nicolet™). With regard to inorganic crystalline materials, there is extensive scientific bibliography (i.e., van der Marel and Beutelspacher 1976; Nakamoto 2009), while for geological materials such as minerals and glasses, literature is not as abundant (with some exceptions – Farmer 1974; Hawthorne and Waychunas 1988; Beran and Libowitzky 2004; Henderson et al. 2014; Della Ventura 2017). Many data are presented only in specialized papers.

4.2 Instruments and Methodologies

Infrared spectrometers are of two types: dispersive instruments and the Fourier Transform IR spectrometers (FTIR).

The dispersive technique, almost entirely replaced by FTIR instruments, is based on a 'double-beam spectrometer', where a sequence of wavelengths is made by a monochromator. The radiation emitted from the light source is split by a rotating mirror (chopper) into two equivalent beams, *i.e.*, the sample beam and the reference beam. The sample beam is absorbed partially by the sample and hits the detector with attenuated intensity; the reference beam is not attenuated. An aperture adjusts its intensity to the sample beam, in such a way that the detector receives a continuous signal. The aperture is connected with a chart writer and records the absorption bands. The splitting of light in the monochromator is achieved by scattering at an optical grid. As mentioned before, dispersion systems have been largely supplanted by interferometer instruments, but some studies in the NIR are still carried out with these instruments even in the last decade (Chalmers et al. 2012).

FTIR spectrometers with a 'single-beam technique' have been developed and commercialized since 1970 thanks to computerization (using the Cooley-Tookey algorithm) and microelectronics (Griffiths and de Haseth 2007). The basic principle is that all wavenumbers of the IR spectrum are measured simultaneously thanks to an interferometer, which transforms the polychromatic IR radiation, emitted by the source and modified by interactions with the sample, into an interferogram. The core of the instrument, the interferometer, was invented in 1880 by Albert A. Michelson. With the development of computers and the "Fast Fourier Transform" algorithm (Cooley and Tukey 1965) the conversion of the interferogram into a spectrum was successfully performed, leading to the spread of the FTIR spectrometers. The interferometer allows the simultaneous scanning of all frequencies present in the IR radiation generated by the source. This implies some considerable advantages over the classic dispersion spectrophotometers, *i.e.*, a better signal-to-noise ratio (SNR), drastically reduced analysis times, high energy throughput at constant resolution, high accuracy, no significant sample warming during measurement, absence of diffuse radiation, which can generate noise and/or unresolved signals. The main components of an FTIR spectrophotometer are the IR radiation source, the interferometer and the detector.

IR Radiation Source In MIR, the most used conventional sources are black-body sources, such as Globar®, a sintered silicon carbide filament heated to 1400 K. It emits broadband IR radiation, which approximately corresponds to that of a black body, over a wide range of wavelengths varying from NIR to FIR. The best performance as to the radiant intensity with this type of source is observed in the MIR field. Therefore, the NIR and FIR regions are not investigated by default, since they require alternative IR sources, such as the quartz-W halogen lamp for NIR or high-pressure Hg vapour lamps for FIR (Chalmers et al. 2012). Other conventional sources may be the Nernst bar, a Y-Th-doped ZrO_2, and ceramic light sources, where a ceramic bar wound by a heating wire, *e.g.,* Pt or Pt-alloy, is coated with an additional sintered layer. In addition, unconventional expensive sources such as synchrotron light are extremely advantageous for high-resolution FTIR microscopic studies of very small samples (SR-FTIR – Della Ventura et al. 2014, and references therein).

Interferometer It consists of a fixed mirror, a moving mirror and a semi-reflective beam-splitter element. The collimated polychromatic IR beam, produced by the source, reaches the beam splitter, which divides it into two components, directed along perpendicular paths, one towards a fixed mirror and the other towards a moving mirror. The beam splitter consists of a thin Ge film interposed between two plates of IR-transparent material, such as KBr, more rarely ZnSe or CsI (MIR) or CaF_2 (NIR).

The two beams reflected by the mirrors are sent back to the beam splitter, where they are recombined giving rise to constructive ($n\lambda$, n = 0, 1, 2, etc.) or destructive ($1/2\lambda$, n = 1, 3, 5, etc.) interference (having covered optical paths of different length). The shift of the moving mirror allows to vary the optical path of one of the two beams, to obtain the entire selection of frequencies through the phenomenon of constructive or destructive interference of the components of both beams. The null position of the moving mirror corresponds to identical paths of the two beams, which are therefore in phase for all frequencies, producing a maximum intensity of the polychromatic radiation reaching the detector. For positions $\neq 0$, there will be a sinusoidal variable intensity (cosine function), with the maxima corresponding to constructive interference of radiation wavelengths. A signal proportional to the offset between the two beams (therefore to the position of the moving mirror at the given time) reaches the detector. The interferogram, originally produced by the FTIR, is a graph in which the intensity is a function of the position of the mirror or optical path (in cm). After digital processing with the Fourier transform (FFT) algorithm, the interferogram is converted to an FTIR spectrum, with absorbance (A) or transmittance (%T) plotted against wavenumber $\left(\bar{\nu}\right)$ [cm^{-1}] or wavelength [μm]. The moving mirror must have a constant and well-calibrated speed, and it must also maintain a constant angle throughout its movement. FTIR instruments have high resolution and minimum scanning times. Basically, fast computers are needed, as transformation must be done simultaneously.

Detector The detector converts the incident IR radiation into an electrical signal, and subsequently to digital form. FTIR instruments generally have high-sensitivity photoconductive detectors, as is the MCT type (Hg-Cd telluride), requiring a liquid-nitrogen cooling system. MCT detectors are commonly sensitive for areas of 1–2 mm width, whereas in FTIR microscopes they have smaller sizes (50–250 μm). For imaging applications, FTIR spectrometers use multi-element focal plane array (FPA) MCT detectors. In instruments with pyroelectric bolometers, these can consist of deuterated triglycine sulfate (DTGS or DLaTGS) or lithium tantalate, $LiTaO_3$ (LITA). A DLaTGS detector with a polyethylene window can be used for the investigation of the FIR region. For high-sensitivity applications, a liquid helium-refrigerated Si bolometer is used. NIR instruments have detectors made of PbS, InGaAs and InSb, while for shorter wavelengths in the NIR region, Si detectors are employed (Chalmers et al. 2012).

In addition to FTIR table-top instruments, portable FTIR spectrometers are also available, with low weight and sturdy Michelson interferometers, allowing non-invasive in-situ analyses on different samples/surfaces.

4.2.1 Analysis in Reflectance

Reflectance analysis can be carried out on opaque or massive samples, which are too thick to allow the transmission of IR radiation (Fig. 4.6a, b). One type of reflectance analysis is in 'Attenuated Total Reflectance' mode (ATR), which necessitates the use of a particular accessory, which is a crystal of IR-transparent material with a high refractive index (Fig. 4.6c). This accessory can be KRS-5 (mixed thallium bromides and iodides), Ge or ZnSe crystals, today mostly diamond is used. The crystal is in direct contact with the sample. Despite total reflection of the IR beam within the refractive crystal, some of the IR photons penetrate the sample some fractions of a micron deep, being partly absorbed or attenuated. After n reflections, the decrease in radiant intensity can be detected by the instrument, providing the ATR spectrum. The ATR technique can also be used for powders, frequently replacing the classical KBr pellet method. In addition, the spectra of a given substance are comparable only if acquired at the same incidence angle. A variant of the ATR analysis is multiple internal reflection, where the sample is placed on both sides of the ATR crystal, leaving small portions free, to allow the entry and exit of the radiation from the crystal (Fig. 4.6d).

For fibrous or laminar samples, the diamond anvil cell (DAC) technique can be used (Fig. 4.6e), which allows the flattening of fibres with moderate pressure (Fredericks 2012; Ceppatelli et al. 2016) and subsequent observation by micro-FTIR. The fiber is flattened down to ~10 μm thick, and then observed in mid-IR. Actually, this technique can be considered destructive, since it modifies the morphology, crystallinity and orientation of the original sample. However, the consumption of material is minimal, since even but a single fiber of ~1 mm in length is required (Fredericks 2012).

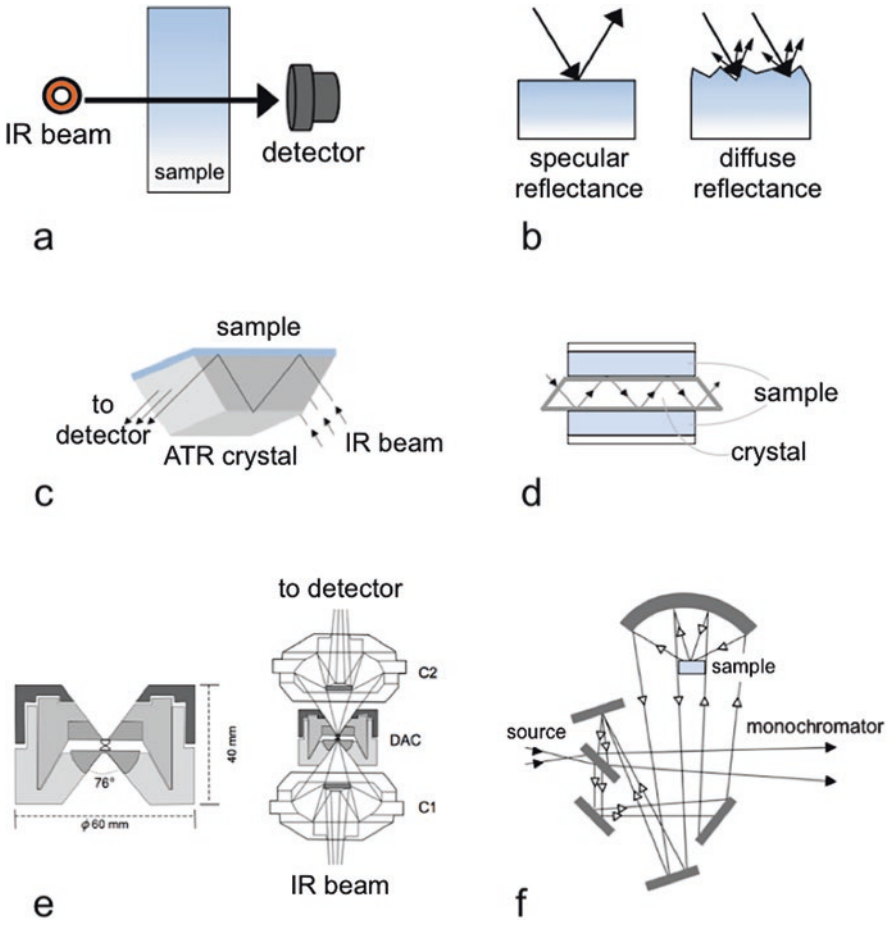

Fig. 4.6 Schematic representation of the FTIR acquisition in (**a**) transmission and (**b**) in specular and diffuse reflectance (Redrawn from Della Ventura 2017). (**c**) Principle of ATR methodology (Redrawn from https://www.azom.com/article.aspx?ArticleID=5958). (**d**) Variant of ATR, multiple internal reflection (Redrawn from http://www.uniroma2.it/didattica/MA2/deposito/spettroscopia_infrarossa.pdf). (**e**) Instrumental diagram of the DAC, with the device positioned in the Cassegrain optics system (C1, C2) of an FTIR microscope (Redrawn from Chalmers et al. 2012). (**f**) Diagram of the beampath within the DRIFT accessory. (Redrawn from http://www.uniroma2.it/didattica/MA2/deposito/spettroscopia_infrarossa.pdf)

Diffuse reflectance analysis (DRIFT) uses a complex system of plane mirrors and a spherical or ellipsoidal (focusing) mirror, causing multiple reflections of the primary beam (Fig. 4.6b,f). Thereafter, the powder sample interacts with the radiation and partly absorbs it. As a result, the radiation is diffused in all directions, with the intensity of the reflected and diffused radiation being proportional to the sample reflectance ($\%R = I_0/I_{rad\ diff\ refl}\ 100$). One of the advantages of this technique is that no preparation of powder sample pellets is required (see Sect. 4.3).

Specular reflectance (SR) analysis can be performed on reflective solid samples. It is a non-destructive analytical technique but requires highly polished surfaces. The reflectance spectrum is transformed into a "transmittance-equivalent" spectrum through the *Kramers–Kronig transformation*, which takes into account the refractive indices and absorption parameters of the sample. Reflectance-absorption spectra (RAS) are obtained after recording the background signal on a metal mirror (gold, aluminium, etc.), using the same opening window that will be used for the analysis of the transparent polished sample plate, placed on the mirror.

4.2.2 Quantitative Analysis

In case of moderate species concentrations, the *absorbance* (*A*) is linearly proportional to the concentration of the absorbing species. Quantitative measurements first require the conversion of the spectra to absorbance (using additional transformations for ATR spectra), an operation performed automatically by modern spectrometers. MIR and NIR spectra measured in DRIFT mode are converted to "equivalent absorbance" units by the $log_{10}(1/R)$ relation or the *Kubelka–Munk algorithm* (Chalmers et al. 2012). From the resulting IR absorbance- or "absorbance-equivalent" spectra, the intensities of relative peaks (height or area ratio) can be interpreted. The starting point of any spectral processing is the definition of an algorithm for modelling the instrumental background and peak parameters, such as peak shape and width at half height, better known as *Full Width at Half Maximum*, *FWHM* (Hawthorne and Della Ventura 2007). These calculations are normally performed by the software supplied with the spectrometers, or by specific data-processing programs, such as Omnic™, PeakFit™, GRAMS™, etc. (Della Ventura 2017). Processed data can be used for quantitative analysis, of the entire spectra, or selected areas can be processed mathematically across large batches, using chemometric analysis techniques, such as multivariate analysis including PCA (Principal Component Analysis). Furthermore, data processing serves to develop quantitative calibrations (conducted, where necessary, even with polarized light), to produce classifications or to discriminate particular types of samples (Chalmers et al. 2012).

In the field of quantitative FTIR spectroscopy applied to minerals, there is extensive scientific literature concerning quantitative measurements of particular chemical species. Calibrations for the assessment of the molar absorption coefficient (ε) in anisotropic minerals were performed by Libowitzky and Rossman (1996, 1997), while in Della Ventura (2017), quantitative studies of fibrous silicates (*asbestos*, amphiboles) are reported. The quantitative analysis of crystalline materials requires careful monitoring of experimental conditions and parameters, such as sample thickness, homogeneity of the material, determination of the optical properties of the material and mainly an accurate determination of the molar absorption coefficient specifically related to the given material (see Sect. 5.2). In addition, as demonstrated by Libowitzky and Rossman (1996), for optically anisotropic crystalline

substances, the *value of total absorbance* (A_{tot}), using the values of absorbances measured with polarized IR radiation along all three principal optical directions, must be determined to obtain reliable quantitative estimations. Polarized IR radiation is usually provided using a KRS-5 wire grid polarizer.

4.2.3 FTIR Microscopy and Imaging

FTIR spectrometers can be routinely equipped with an optical microscope. Micro-FTIR has made the infrared technique much more effective and particularly useful for the study of small particles and/or for specific areas of complex samples. At the end of the twentieth century, EK Abbe demonstrated that the maximum lateral resolution of an optical instrument is subject to the physical limit of diffraction, *i.e.*, ~2λ/NA, where NA is the numerical aperture of the lens. With microscopes having NA ~0.6, the lateral resolution is 3–4 times the wavelength (~1.7 μm at 4000 cm^{-1}) (Della Ventura et al. 2014). In confocal microscopes, spatial resolution goes as low as 3 μm (Minsky 1988).

The micro-FTIR aims to achieve the best lateral spatial resolution within the sample, *i.e.*, to allow imaging at the diffraction limit. For sample focusing, FTIR microscopes are equipped with two Schwarzschild or Cassegrain reflection lenses, housed on two spherical mirrors centred on the same optical axis. The use of these optical systems is forced by the necessity of limiting chromatic aberration and minimizing the overall absorption of IR radiation. For FTIR microscopy studies in MIR, a conventional source such as Globar is used for samples with a linear size or diameter ≥ 10 μm, while better spatial resolutions are obtained by means of synchrotron radiation (Chalmers et al. 2012; Della Ventura et al. 2014). Many FTIR microscopy systems can be adapted for FT-NIR microspectroscopy; spatial resolution is limited by the NIR wavelength to about 2–5 μm. Since band absorbance is much lower in this region, significantly thicker samples are needed compared to microspectroscopic studies in MIR.

Most FTIR microscopes are equipped with single-element MCT detectors (see Sect. 4.2); with this type of single-array devices, a spectral sample map can also be produced, provided that the option of automated movement of the sample stage, managed by the computer, is available. Focal-plane-array (FPA) detectors have revolutionized the field of mapping and imaging in the mid-IR spectral region. Using FPA detectors, devices originally conceived by the military, it is possible to divide the image of the sample under the microscope into a series of pixels with a size of 5.5 μm, with each pixel recording a specific infrared spectrum. The dimensions of the focal plane arrays range from 16x16 pixels to 128x128 pixels. More than 16,000 spectra can be obtained simultaneously. In real time, the map of an area the size of 1×1 mm can be obtained, with the resolution limit decreasing to about 5 microns (wavelength limit). In ATR microscopy imaging, a resolution close to 2 microns can be achieved by means of a Ge crystal with a refractive index of 4.

It should be mentioned, that besides FTIR microscopy the use of beam condensers, based on mirror systems or CsI lenses, inserted along the optical path of the IR beam in the optical bench, offers a very simple and cheap method for a first characterisation of small samples.

4.3 Sample Preparation

Depending on the type of sample, *i.e.,* rocks, stems, crystals, dust, fibers, etc., and the information required, different sample preparation techniques, destructive or non-destructive, can be used (Table 4.5).

4.3.1 Powders

Pellet Method, Transmission Analysis A very small amount of powdered material is required with this user-friendly and fast method. Depending on the characteristics of the sample, any quantity from 7 mg down to 0.5 mg or less can be used for making pellets. Micropellets are frequently used in combination with beam condensers. This aspect is very important for forensic analysis, where often very small quantities of material are available. The powder must be very fine-grained (size of grains at best <2 μm, possibly tested by sieving), to ensure a good resolution of the absorption spectra. To obtain homogeneous and representative samples, grinding may be done by means of an agate mortar or mills, at best using isopropyl alcohol, acetone or similar liquids to limit any possible alteration of the material during the process (*e.g.*, oxidation or crystal structure modifications). The pulverized sample is dispersed in an IR-transparent material in the MIR range (~4000–250 cm^{-1}), typically potassium bromide, KBr (a strongly hygroscopic salt, to be stored in a drying oven), more rarely polyethylene. Even *nujol* oil can be used for preparing a sample paste. In order to obtain good-quality spectra of pellets, the right amount of sample powder is mixed with 150–200 mg of KBr in a mortar or mill, until a homogeneous and fine mixture is obtained. The mixture is transferred to a pellet press, which produces a glass-like disc by compression under vacuum. The pellets are then placed into the sample holder of the spectrometer and measured after having acquired the instrumental ref-

Table 4.5 FTIR analysis and usable sample types

Technique	Signal	Sample
Trasmission	Transmittance/absorbance	Powders, crystals, thin sections, liquids
Reflection	Attenuated total reflectance (ATR)	Thick samples, non-opaque surfaces, powders, crystals
	Diffuse reflectance (DRIFT)	Powders
	Specular reflectance (SR)	Crystals, thin sections
	Reflection-absorption (RAS)	

erence spectrum (background) using a blank (sample-free) pellet. Micropellets with a sample/KBr ratio of 0.0025 are also suitable for use in the mid-IR range. Polyethylene pellets with a sample/polyethylene ratio of 0.1 are used for measurements in the Far-IR region (Beran et al. 2004). Before the spectra collection, it is recommended to store the pellets in an oven at 110 °C to eliminate any trace of moisture absorbed by the KBr during preparation. Furthermore, to avoid the contamination of the pellets with skin fat, it is essential to handle the tablets carefully. Quantitative measurements of pellets (for instance to quantify the amount of a mineral in the sample) can be carried out by using calibration curves related to reference materials with a known content of the substance of interest. A careful monitoring of instrumental parameters, *i.e.*, dispersion, weight ratio of sample to IR-transparent host material, pellet thickness, clean work, etc., are needed for accurate measurements. This type of preparation is suitable for the analysis of rocks and minerals, sands, clays, soils, etc. It is a destructive technique, therefore not suitable in the case of unique samples. Fortunately, the pellets, if properly stored, can be re-analysed. However, today the ATR method is frequently and successfully used for the measurement of powder spectra, where the powder is slightly pressed on the ATR crystal.

DRIFT Reflective Analysis For the study of specific materials, such as samples containing asbestos, diffuse IR reflection spectroscopy (DRIFT) is an interesting measurement mode. In this case, the powdered sample is placed into the sample carrier as it is, the IR radiation is diffusely reflected from the sample surface, collected by a mirror, and sent to the detector. This technique is particularly interesting for the study of asbestos cement or similar materials, because little material is required that can be simply obtained by scratching walls, bricks, tiles, etc. with an abrasive paper and placing the powder on the DRIFT sample carrier without further preparation (Woods et al. 2014; Della Ventura 2017).

4.3.2 Single Crystals, Doubly Polished Slabs

Single crystals, gemstones or any other polishable materials can be analysed by transmission FTIR spectroscopy, typically by micro-FTIR (Sect. 4.2.3). Very detailed spectroscopic data (i.e., imaging) can be collected from areas up to a few tens of μm^2 in size with a conventional IR source down to a few μm^2 using a synchrotron source (Della Ventura et al. 2014). Doubly polished slabs are typically prepared, by mounting a single crystal or crude sample fragment on a glass plate by means of a heat-sensitive and acetone-soluble resin (e.g., Crystalbond™ 509 Aremco). Then, the sample is polished by increasingly fine abrasive cloths/papers and pastes. The operation is repeated identically for the other side of the sample after having glued it to the carrier plate by its first polished surface, thus obtaining a double-polished plane-parallel slab of defined thickness, suitable for IR transmission measurements.

In the case of quantitative measurements (see Sect. 4.2.2) of particular chemical species in crystals, which require polarized IR radiation, the crystallographic

orientation (in the case of optically anisotropic crystals) and precise knowledge of sample thickness are parameters of fundamental importance for meaningful evaluations. The analysis of this type of samples is to be considered almost completely non-destructive, since the material removed by the polishing procedure is minimal and, as in the case of pellets, the slabs can be stored and re-analysed. Samples with a polished surface can also be observed in specular reflectance (SR) or in RAS mode, if appropriately mounted on reflective metal holders (see Sect. 4.2.1).

4.4 Applications in Forensics

FTIR spectroscopy in forensic sciences is applied effectively for the identification of largely varied materials such as pigments, paints, fibers, adhesive tapes, explosives, drugs, plant hair, chemicals, minerals, etc. (Chalmers et al., 2012; Muro et al. 2016).

In particular, FTIR technique is an important tool for the examination of the evidence when a fast chemical-physical characterization is required on limited amounts of sample material, with little sample preparation needed. Those are the most important prerogatives of FTIR spectroscopy, also applicable in totally non-destructive mode in some setups. Therefore, as already mentioned, vast scientific literature exists, describing the investigation of diverse organic and inorganic materials, both natural and artificial, using infrared spectroscopy.

A classic use of infrared spectroscopy for forensic purposes is characterization of soils (i.e., Thornton 1986; Chalmers et al. 2012; Fitzpatrick 2008, 2009; Murray and Tedrow 1992; Pye and Croft 2004; Ruffel and McKinley 2005). Materials from the ground and useful as forensic evidence can be found in many crime scenes, such as footwear, clothing, objects for burial in land, vehicles, etc.; soil samples can then be used to exclude or associate a suspect with a particular scene (Woods et al. 2014, 2016). From a mineralogical point of view, soils consist mostly of clay minerals and other phyllosilicates (micas and serpentine group minerals), Fe, Mn and Al oxides and hydroxides, carbonates, sulfates, quartz, feldspars, sulfides and halogenides; amorphous phases can occur as well. Especially amphiboles and mica-group minerals can be easily identified by their IR spectra in the OH stretching vibrational region from 3750–3500 cm^{-1} (Beran, 2002).

Among other geological materials that can be analysed by FTIR in the forensic field there are *asbestos* (Della Ventura 2017) and precious stones and gems. The latter, due to their high economic value, small size and relative non-traceability, are of extreme interest for illicit activities (Di Maggio 2019). Falsification of gemstones is carried out essentially by: (a) exaltation (artificial transformation of a poor specimen into a more valuable one, or obliteration of clearly visible defects, such as fractures or cracks); (b) synthesis (artificial reproduction of specimens possessing the same chemical, physical and optical properties as natural analogues); (c) replacement (exchange of more valuable gems with less valuable natural stones or artificial materials) (Di Maggio 2019).

After having described in the previous section the general principles, techniques and equipment used in FTIR spectroscopy, some forensic case studies requiring

FTIR spectral evaluation applied to both geological and non-geological materials in the context of specific crime scenes will be provided.

4.4.1 Fingerprinting

In the most basic configuration, two spectra are measured, first a reference spectrum and then that of a sample obtained from the crime scene. Both measurements take place at best subsequently to one another, using the same instrument setup, sample configuration and the identical background spectrum, measured beforehand. The extent of similarity between both spectral envelopes determines a potential match; in the ideal case, the shape of the spectral curve of the reference sample is near-to-identical to that of the sample from the crime scene. When noticeable discrepancies occur, it must be assumed that both sample materials – the reference sample and that from the crime scene – are different. Several examples of the use of fingerprinting in the scope of judiciary cases are described below. The fingerprinting technique is the most used in forensic applications due to its straightforwardness, which aids in swiftly yielding the comparison between two samples.

Comparison of Car Paint

Ongoing cooperation with the Vienna traffic police necessitates frequent application of IR fingerprinting for the comparison between samples of car paint taken from crime scenes or accidents and that of the suspected vehicle.

Alternatively, as in the case discussed below, attempts at insurance fraud are often made, claiming that a given car was involved in a particular accident and insurance payment is requested. Fortunately, these claims are mostly short-lived. An extensive European Police database containing IR reference spectra of paints and coatings of all types of cars allows easy comparison of the IR reflection spectrum of the unknown sample with a standard IR spectrum of that given color of the specific car type.

Varnishes, paints as well as plastic (as will be discussed below) are quite malleable; therefore, their pulverization by milling and subsequent dilution with KBr is not a good option. Instead, the paint sample is rolled onto a gold-coated polished surface, which itself serves to obtain the initial background spectrum. Then, the sample is measured in reflection mode using a standard IR microscope. The spectral comparison depicted below in Fig. 4.7 clearly shows that, in difference to the claims of the plaintiff, no traces of any foreign car paint could be obtained from the damaged section of the rear damper. Contrary, the numerous traces of white powdery pigment could unambiguously be identified as calcium carbonate (calcite). It therefore became apparent that the damage to the given car was not the result of a collision with another vehicle, but with a piece of masonry due to careless driving in reverse. Instead of the expected remuneration, the car owner found himself sued for an attempt at insurance fraud.

(continued)

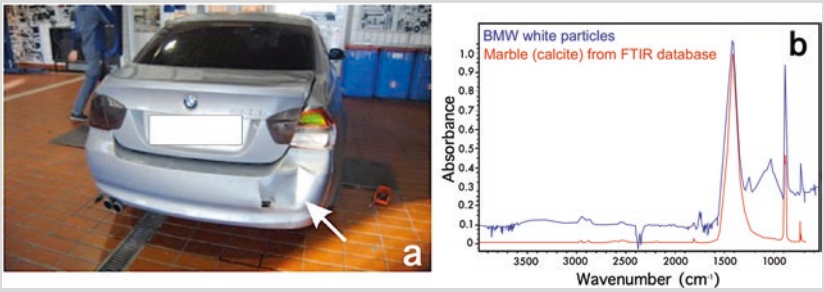

Fig. 4.7 The damaged portion of the rear bumper of the car claimed to have been involved in an accident (**a**). Comparison of the FTIR reflectance spectrum of white powdery residue from the damaged section (blue curve) with the spectrum of calcite (red curve) showing an unambiguous match for all major bands (**b**). Extra bands in the spectrum of the sample from the damaged car section are due to contamination with the gray paint scratched off the vehicle during collision. (Courtesy of the Land Office of Criminal Investigation Vienna)

Foreign Object in Bread

A somewhat peculiar case was the presence of a foreign object in a bread loaf from a major Austrian bakery (Fig. 4.8). After finding the unusual object, the buyer, suspecting infringement against food quality standards, reported the find to the Inspectorate of Commerce. In order to process the complaint, use was made of Police forensic assets to determine what exactly the object is. Among others, a transmission IR spectrum of a KBr pellet containing powder from a fragment of the sample was acquired (Fig. 4.8). Comparison with the forensic spectral database yielded an unambiguous match with hydroxylapatite, $Ca_5(PO_4)_3(OH)$, the major component of tooth enamel.

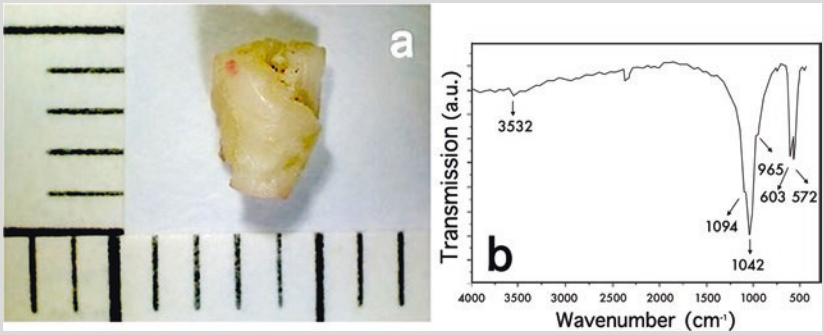

Fig. 4.8 (**a**) The tooth fragment contained within a baked bread loaf. (**b**) The material could be clearly identified as hydroxylapatite (tooth enamel) by FTIR spectroscopy. (Courtesy of the Land Office of Criminal Investigation Vienna)

(continued)

More worryingly, the dimensions and shape of the tooth fragment suggested it to be a human one, invoking the question about how it got into the bread loaf. The tooth was archived by the Police to assist as potential evidence in the investigation of a crime of injury or even murder. Fortunately, the enigmatic object did not have to fulfill this role.

Murder in Car

Murder, being one of the most serious crimes, demands thorough investigation of any evidence present. Often, the suspect underestimates the potential of modern techniques in utilizing even the smallest amount of material available. A few fibers, as in this example, were sufficient to precisely determine that the victim, dressed in a mantle consisting of a fabric containing one type of synthetic fibers, was indeed murdered in the car found on the crime scene, the seats of which were composed of a different fabric.

As depicted in Fig. 4.9, a mixture of fibers, identified as polyamide (of which the victim's clothing was composed) and polyester, which in contrast constituted the fabric of the car seat, was found on the seat where the victim lay dead. Reciprocally, the polyester fibers were present on the victim's polyamide clothing.

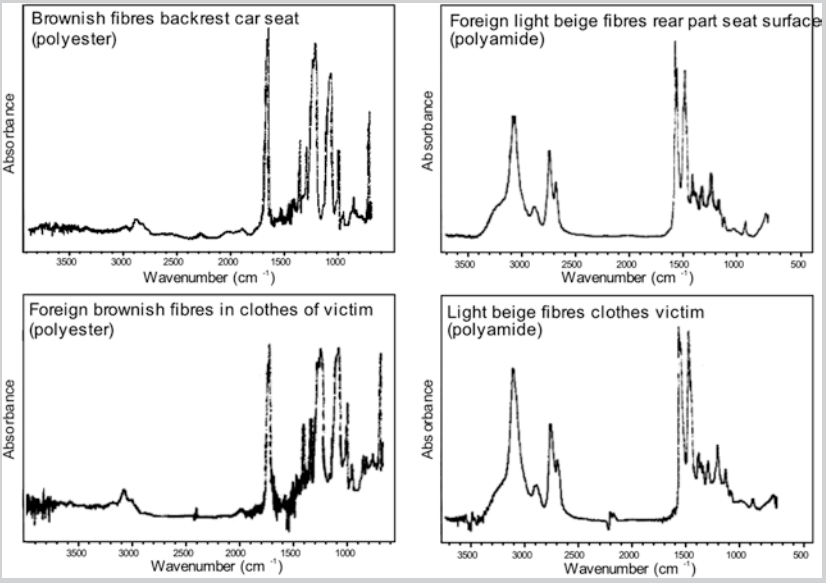

Fig. 4.9 The victim was dressed in light beige clothing consisting of polyamide. The dark brown car seat consisted of brown polyester. Since both types of fibers were found on the car seat and in the respective regions of the victim's clothing, it is apparent that the murder indeed took place in the given car collision. (Courtesy of the Land Office of Criminal Investigation Vienna)

Identifying Amber

The principle of fingerprinting in itself remains nearly the same, regardless of the investigated sample type. What differs is the type of sample preparation and measuring technique (reflection versus ATR or transmission mode). This third example involves the inspection of an object that has been claimed as an amber. As one can imagine, the high price of genuine amber leads to countless attempts at imitations and scams.

Since the unknown sample was a polished elephant sculpture (Fig. 4.10a) and therefore a work of art, destructive procedures (such as scratching the

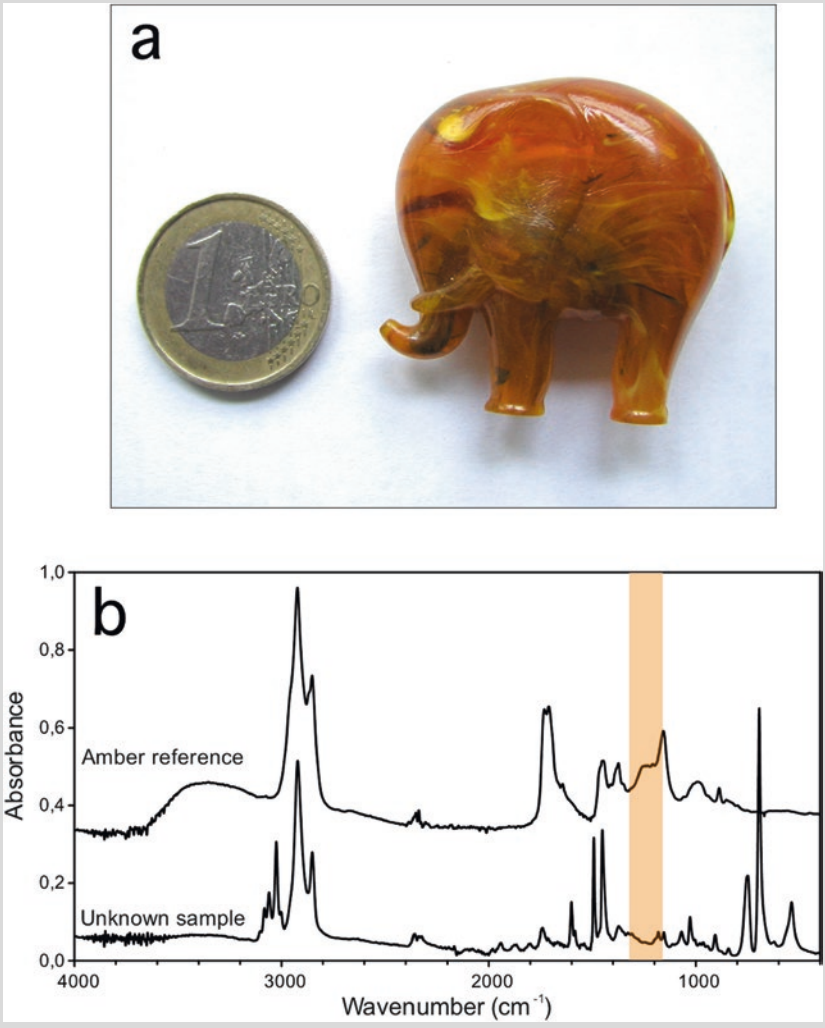

Fig. 4.10 (**a**) The analysed elephant sculpture (photo by D. Talla). (**b**) The comparison between the FTIR spectrum of genuine Baltic amber and the unknown sample. The position of the succinite shoulder visible in the amber reference sample is emphasized by an orange stripe. The feature does not occur in the unknown sample. (Image by D. Talla)

(continued)

sample to remove material for milling) were not an option. Therefore, the ATR measurement was used, with the quality of the results significantly enhanced by limited 'flexibility' of resinous substances, allowing them to achieve better contact with the surface of the analytical ATR crystal (in this case diamond).

The typical feature aiding reliably at discerning between genuine baltic amber and its imitations is a shoulder of a band at roughly 1160 cm^{-1}. The shoulder itself occurs at ~1240 cm^{-1} and is known as the so-called 'Baltic' or 'succinite shoulder', with the latter name derived from the pine genus *Pinus Succinifera sp.*, the fossilized resin of which represents Baltic amber. Unfortunately, as seen in Fig. 4.10b, the IR spectrum of the unknown sample (the small elephant sculpture) does not show the succinite shoulder, to the great disappointment of the owner (the actual material turns out to be polystyrene).

Discerning Between Different Types of Plastic

Recently, a company sued its supplier for using a different type of plastic than the one covered by the agreement. Instead of stiffer Acetonitrile Butadiene Styrole (ABS), the company claimed that the parts were made of much softer polyethylene (PE). Two reference spectra were recorded, one using material gently scraped off a piece of LEGO® as the ABS reference, and then the same procedure applied to a polyethylene bottle. Despite certain malleability, fine shavings of the plastic could be scraped off the sample and then milled and diluted by an IR-transparent material, such as KBr, in a weight ratio of roughly 1:200. The mixture was pressed under vacuum to obtain a transparent KBr pellet, allowing measurements in transmission mode. To use the least material possible, the KBr micropelleting press was employed, with the mixture added through a tiny round aperture of a metal gasket (Fig. 4.11a).

As can be seen from both reference spectra in Fig. 4.11b, some spectral regions are rather similar, owing to the presence of the same chemical functional groups in many types of plastic. However, ABS typically shows a well-resolved extra band at ~2240 cm^{-1} as well as other characteristic groups of bands, all observed also in the disputed piece, which indeed consists of ABS, not polyethylene. Therefore, the case was won by the supplier, who did not commit the crime of using another material to produce the necessary parts.

It is important to take into account the presence of additional bands in some types of plastic due to the presence of fillers, colorants and softeners (Fig. 4.11b, arrow). Indeed, the actual perception leading to the conclusion that the part is too soft and therefore probably made of PE was caused by too much softener added to the ABS plastic, as was proven by subsequent analyses.

(continued)

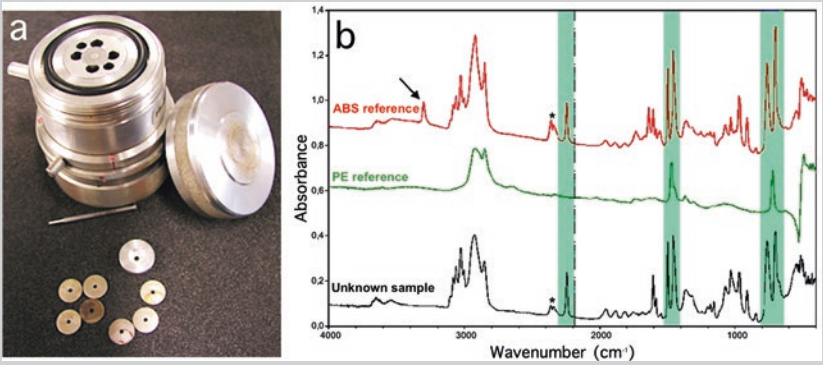

Fig. 4.11 (**a**) The micropelleting press inset, along with the metal gaskets used as sample holders (photo by D. Talla). (**b**) Reference spectra of ABS and PE in comparison with the unknown sample. As can immediately be seen, the same characteristic bandgroups occur in ABS as well as the unknown sample. The bandgroup at ~2350 cm^{-1} marked by an asterisk owes its existence to atmospheric CO_2. (Image by D. Talla)

4.4.2 Qualitative Analysis of Discrete Features in the Spectral Signal

It is a common situation that while the overall IR spectrum of the sample from the crime scene corresponds with that of the reference standard, additional weaker bands are also visible. These are caused by foreign molecules, structural defects and different other loosely bound structural units, which can be incorporated into the fundamental crystal structure. The presence (or absence) of some species such as hydrous inclusions, intrinsic OH or H_2O groups, CO_2 or ammonia may reflect possible tampering with the original sample material. Many cases are known in the field of gemmology such as, for example, heat treatment of gems in order to enhance their color.

These modifications, in addition to representing a fraud, drastically reduce the value of a gem compared to the same untreated stone. The following two boxes of this Section report examples of fraud in gemology.

Identifying Synthetic Quartz

While the fingerprinting technique serves for a general comparison, the presence, absence or shape variation of specific IR absorption features can provide clues about sample provenance, synthetic origin, heat treatment or indicate a match between two samples of the same material. The first example reported in this box refers to the use of an IR technique to distinguish synthetic hydrothermally grown quartz from natural ones. Despite a few exceptions, it has proven to be an effective tool in most cases. The investigated material is a gemstone so the option of destroying part of the sample cannot be considered. In addition, the angles of the facets are such as to induce total reflection of any light entering the stone, forcing it to leave the gem by the table (the upper flat facet). This makes the gem 'shine'. Unfortunately, IR radiation entering the stone behaves much the same way, leading to poor signal during transmission measurements. The gem is placed into a specialized holder (Fig. 4.12a), where it is held by a pair of indented anvils by its edges. Only slight pressure is applied to the anvils by means of soft springs to prevent chipping. It is often necessary to move the stone or rotate it in the anvils to obtain a measurable signal.

Most natural quartz samples contain traces of hydrogen in the form of OH defects. Their concentration is low, leading to discrete weak bands occurring in the transmission spectrum at wavenumbers between 3000–3600 cm^{-1}. An additional bandgroup can be seen in rose quartz at 3650–3700 cm^{-1}, which is believed to be caused by inclusions of a pink phase similar to dumortierite (Goreva et al. 2001). In all cases, most quartz obtained by the hydrothermal technique contains a massive amount of hydrous inclusions. This leads to pronounced absorption of the incident IR radiation in the given spectral region, causing the occurrence of a single broad hump or complete lack of signal. Especially citrine, one of the most expensive natural color varieties of quartz, is prone to be replaced by synthetic material. Indeed, the black spectrum in Fig. 4.12b shows just a strong broad hump, indicating the synthetic origin of the stone. Other qualitative techniques, apart from this basic discrimination, exist such as the inspection of the presence and variations in the shape of the 3595 cm^{-1} peak, also related to OH defects in amethyst (Karampelas et al. 2005).

(continued)

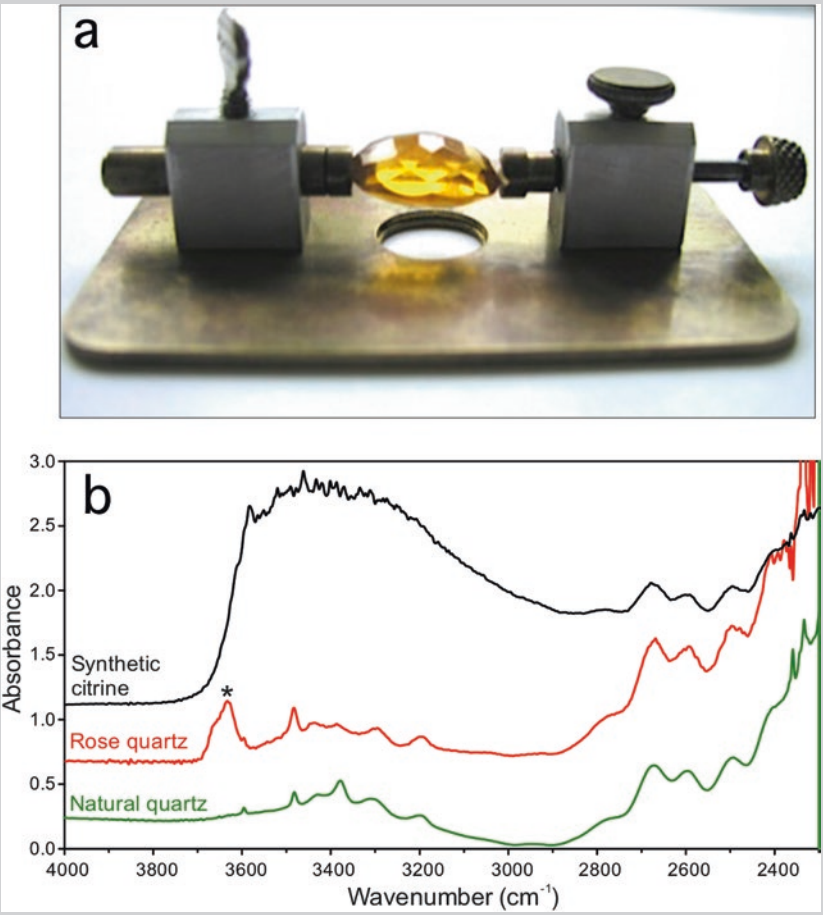

Fig. 4.12 (**a**) The gemstones sample holder for transmission FTIR measurements. The wing screw on the top left enables to adapt the anvil distance to accommodate both small and large samples (photo by D. Talla). (**b**) OH absorption region of the IR spectrum of natural colourless quartz, natural rose quartz showing an additional bandgroup at highest wavenumbers (asterisk) and the measured synthetic citrine sample. The OH absorption of the synthetic sample is so strong as to cause full signal loss in the 3600–3000 cm^{-1} spectral region. (Image by D. Talla)

Identifying Heat-Treated Amber

The synthetic origin of a gemstone is not the only factor reducing its price. Many stones are natural, yet having undergone further treatment to enhance their clarity or colour. Often, the seller does not admit such tampering, in hopes of a bigger profit. The procedure, however, mostly influences the spectra of the substance, either by causing the rearrangement of structural defects, such as nitrogen traces in diamond (Hainschwang et al. 2005), or the partial decomposition of the substance itself.

The heat treatment of amber in order to enhance its color towards shades of darker yellow or even red is a good example of the latter, leading to partial oxidation of the resinous substance (Wang et al. 2017). Some visual characteristics of treated samples already hint that such a process took place, such as discoidal stress fractures around gaseous inclusions, caused by the expanding gas upon heating (Fig. 4.13) or darker-coloured oxidation cracks on the sample surface, in case it had not been repolished afterwards.

The reason for most changes observed in the FTIR spectra of amber after tempering are linked to oxidation; bands caused by C-H bonds, both saturated and unsaturated, lose amplitude, as the bonds are gradually converted into carbonyl groups (Fig. 4.14). As a typical consequence, the amplitude ratio between the 2932 cm^{-1} band and the peak at 1732 cm^{-1} decreases significantly.

Unlike the example involving amber in the fingerprinting section (Sect. 4.4.2), the material in most cases will be finished faceted jewelry. If this is the case, it will not be possible to remove even the tiniest amount of material to

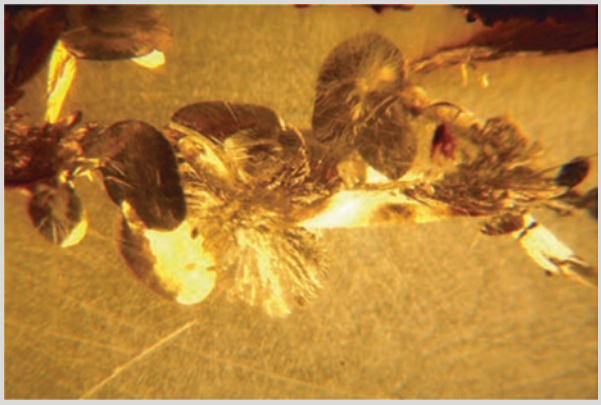

Fig. 4.13 Discoidal decrepitation cracks in heat-treated amber. (Wang et al. 2017. Courtesy of The Gemmological Association of Great Britain UK)

(continued)

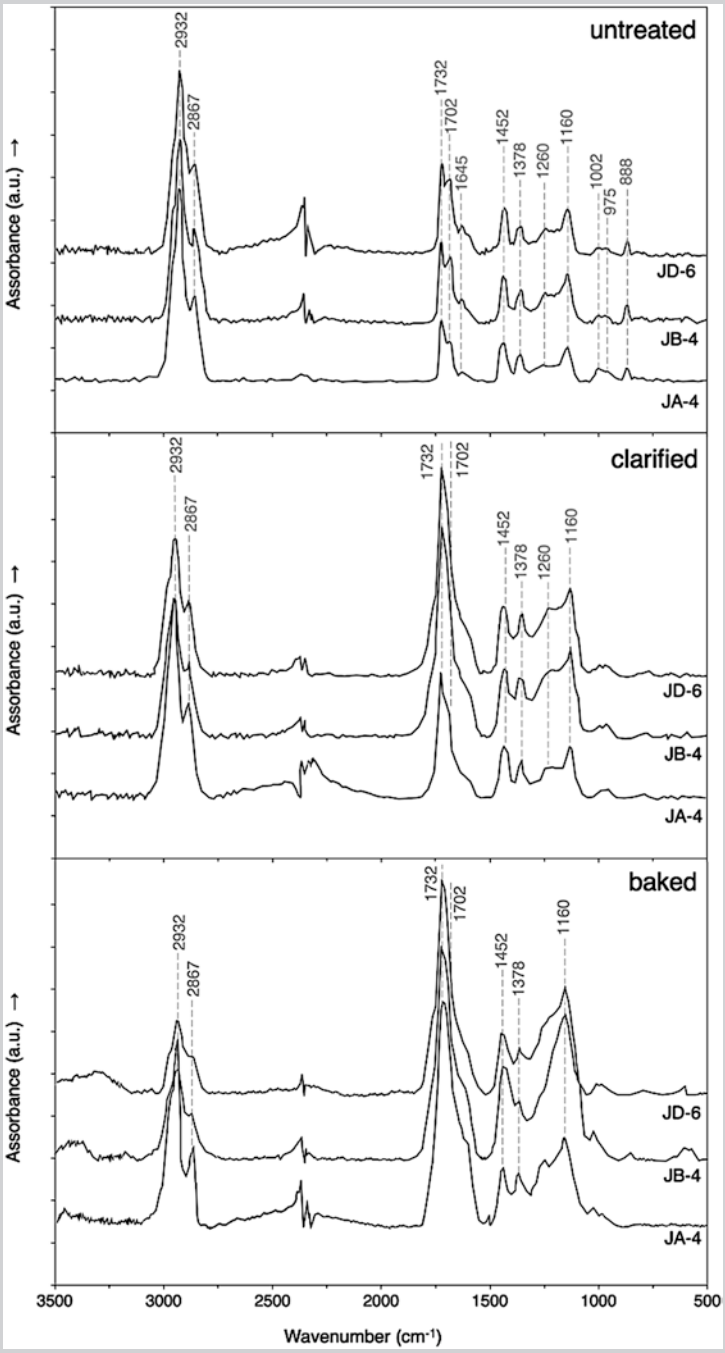

Fig. 4.14 The gradual decrease in amplitude of C-H-related bonds (2932 cm^{-1}) and increase of peaks related to carbonyl groups (1732 cm^{-1}). (Redrawn from Wang et al. (2017), courtesy of The Gemmological Association of Great Britain UK)

(continued)

Fig. 4.15 An amber wristband consisting of separate amber beads on an elastic string (photo by D. Talla)

make a KBr pellet, also considering the hardness of the material. However, as far as amber is concerned, its softness allows to do that although care must be taken to scratch the material off a part of the stone where the damage will not be apparent. In the case of a collar or the wristband depicted below, a good region for sampling is in between the beads, close to the edge of the hole drilled through the bead that accommodates the string (Fig. 4.15).

Identification of Stains on the Crime Scene

A recently emerging field of forensic FTIR application is its use for the fast discrimination of materials from the ground and useful on the crime scene (Mistek and Lednev 2018 and references therein), also using the ATR technique (Orphanou 2015). Unlike the standard time-consuming practice of DNA typing after visual inspection and preemptive tests, the measurement of the stain by ATR is fast, non-destructive and very effective, thanks to modern discriminatory studies between different types of fluids. Table 4.6 summarizes the characteristic bands used to discriminate between some body fluids and their mixtures.

Using more advanced statistical methods, important additional information can be obtained. As an example, Zhang et al. (2017) hinted at a correlation between the age of a blood stain and the absorbance of the band at 3308 cm^{-1}.

(continued)

Table 4.6 Diagnostic bands for some body fluids

Body Fluid	Peak Frequency (cm^{-1})	Peak Assignment	Vibrational Mode
Blood	3292	Amide A	Symmetric N–H stretching
	2956	Methyl stretches of lipids in plasma	CH_3 stretching
	1651	Amide I (α-helix)	C=O stretching
	1540	Amide II	N–H bending coupled to C–N stretching
	1456	Methyl bending of amino acid side chains, lipids, and proteins	Asymmetric CH_3 bending
	1395	Fibrinogen/methyl bending of amino acid side chains, lipids, and proteins	Symmetric CH_3 bending
	1350–1220	Amide III	C–N stretching
	1250–925	Carbohydrates (glucose)	Symmetric C–O stretching
Saliva	3282	Amide A	Symmetric N–H stretching
	2926, 2850	Methylene stretches of lipids in oral mucosa	Asymmetric and symmetric CH_2 stretching
	2059	Thiocyanate anions (SCN^-)	C–N stretching
	1645	Amide I (α-helix)	C=O stretching
	1544	Amide II	N–H bending coupled to C–N stretching
	1452, 1393	Methylene bending of amino acid side chains, lipids, and proteins	Asymmetric and symmetric CH_2 bending
	1239	Amide III/phospholipids	Asymmetric C–N stretching, PO_2^- stretching
	1080–950	Sugar moieties (glycosylat- ed. proteins)	CH_2OH groups, C–O stretching and COH groups bending, symmetric PO_2^- stretching

Modified from Orphanou (2015). Courtesy of Elsevier

An even more complex Positive Least Squares Discrimination Analysis (PLSDA) and subsequent cross-validation even enabled to reliably discern between human blood and that of domestic animals in addition to the age of the stains (Lin et al. 2018) based on the FTIR ATR spectra.

4.4.3 *Quantitative Analysis*

The sample material from the crime scene often consists of more than one substance. As is the case for drug samples often contaminated with remains of the solvents and precursors used for their fabrication, the ratio of these aids not only to confirm the identity between the unknown sample and the standard proving the suspect as guilty, but also to identify a particular fabrication site of the drug. Examples of quantitative FTIR spectral interpretations are described in the following boxes.

Measurement of Cocaine Content in Samples Seized in Trinidad and Tobago

In its most basic form, the procedure of IR spectroscopic quantification involves the determination and refinement of the experimental setup used throughout the entire analytical campaign. In the second step, standards containing varying amounts of the substance of interest must be prepared and measured under the established measurement conditions. A correlation between the *linear* or *integral absorbance* (amplitude or area of absorption bands, respectively) characteristic of the substance of interest and its concentration serves to obtain a calibration curve. In turn, the value of the *integrated molar absorption coefficient* ε, which puts into relation the substance content and the amplitude/area of its peaks in the spectrum can be refined. In a much less crude scenario, at least a least-squares technique is applied to refine the value of the ε coefficient more accurately.

Even with the most rudimentary practice, when nothing more than a two-point background subtraction is often used to determine the band amplitude or area, the results then obtained on the unknown samples can serve, at least in a crude manner (the apparent band amplitude/area may vary according to a different background caused by different diluents), to discern between distinct samples containing the title substance based on its different dilution ratio.

Such was the approach of Maharaj (2008) to quantify the concentration of cocaine in samples from material seized in Trinidad and Tobago in 2005. After the determination of the optimum wavenumber region with most pronounced correlation with the cocaine content at 732 cm^{-1}, the content of the substance in individual samples could roughly be analysed (Fig. 4.16). The good match with contents in weight percent determined by an independent measuring technique (gas chromatography with photoionization detection) is apparent for most samples.

(continued)

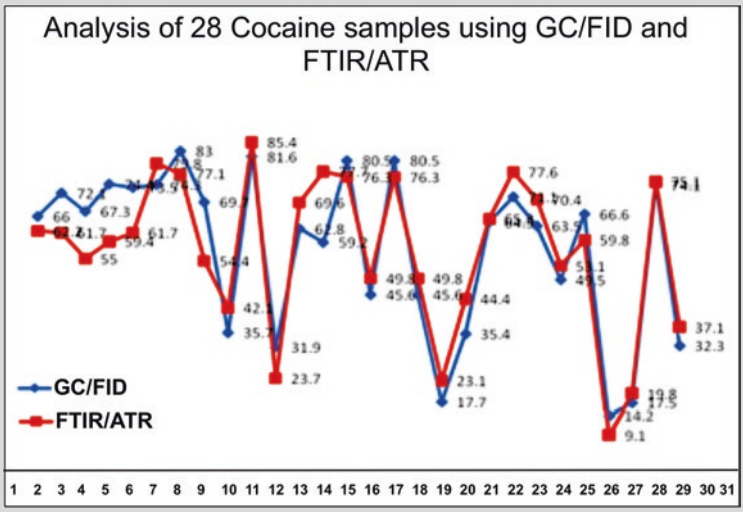

Fig. 4.16 The cocaine content in samples confiscated in Trinidad and Tobago in 2005 expressed as wt% cocaine. The concentration calculated from IR spectra (red) corresponds well to results obtained on the samples using chromatography (blue). (Redrawn from Maharaj 2008, https://www.researchgate.net/publication/320891143_Quantitative_Analysis_Of_Cocaine_Using_Fourier_Transform_Infra-Red_Spectroscopy-attenuated_Total_Reflectance_A_Preliminary_Investigation/figures)

Measurement of Melamine Content in Milk

While many attempts at deception have only financial issues as a consequence, some practices can even become dangerous. Such is often the case of food adulteration. A good example is the adulteration of milk by melamine, a substance rich in nitrogen, added to simulate a higher protein content in the dairy product (Jawaid et al. 2014).

The classic procedures developed for the measurement of melamine content in dairy products (chromatography, ELISA) require laborious sample preparation involving centrifugation and the use of solvents to first remove the proteins, since the measurement does not discriminate between nitrogen associated with the milk protein and melamine. IR spectroscopy represents an effective and swift alternative to these techniques.

In this specific case, milk samples free of melamine needed to be freeze-dried to obtain a powder for the next stage of the procedure, in which several mixtures in defined weight ratios to melamine were prepared. The mixtures were then converted to KBr pellets in a dilution ratio 1:100. In addition, FTIR spectra of pure melamine and pure milk were recorded to enable a qualitative

(continued)

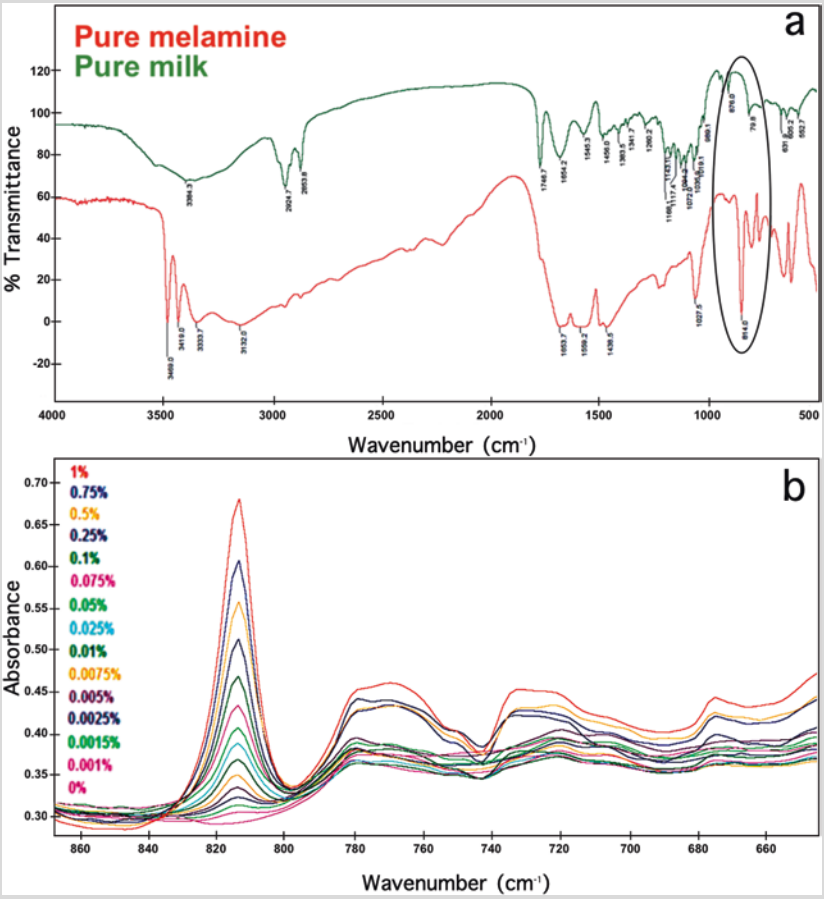

Fig. 4.17 (**a**) The spectra of pure milk (green) and pure melamine (red) plotted in transmittance with emphasis of the 814 cm^{-1} band used for further quantification. (**b**) Spectra of the fourteen synthetic milk standards with variable melamine content. (Redrawn from Jawaid et al. (2014). Courtesy of Royal Society of Chemistry UK)

identification of those spectral regions, where typical bands of the particular adulterant occur, and which are thus suitable for quantification (Fig. 4.17a). Two spectral regions with pronounced melamine bands were determined, the first in the region between 3500 and 3000 cm^{-1}, with the strong bands attributed to the stretching and bending of the amino groups. The characteristic band at 814 cm^{-1}, which was chosen for subsequent quantification, is characteristic of out-of-plane bending of the 1,3,5-s-triazine ring of melamine, which is not present in milk protein.

Having determined the best feature for quantification, the synthetic mixtures of milk and melamine came to use as reference standards, enabling to

(continued)

Table 4.7 Verification of measured and actual melamine content in six spiked samples indicating very good reliability of the outlined measuring method

Milk sample	Original amount	Added (μg mL^{-1} or g^{-1})[a]	Found (μg mL^{-1} or g^{-1})	Recovery (%)	RSD (% $n = 3$)
Infant powder milk	–	10	9.92	99.20	1.90
	–	15	14.97	99.80	1.49
	–	25	25.92	100.20	1.38
Liquid milk	–	10	9.89	98.90	2.07
	–	15	14.93	99.54	1.70
	–	25	25.03	100.12	1.51

Jawaid et al. (2014). Courtesy of Royal Society of Chemistry UK
[a] μg mL^{-1} for raw milk and mg g^{-1} for powder milk sample

assess the correlation between the absorbance of the diagnostic melamine band and melamine content (Fig. 4.17b).

The authors (Jawaid et al. 2014) then assessed a correlation trend and developed a Partial Least Squares model. After the verification of their model by the 'cross-one-out' cross-validation procedure, they made a comparison of calculated results with the known values of melamine content of six samples spiked with variable amounts of the substance (Table 4.7). It can be seen that the procedure performs very well and allows to swiftly determine melamine content in unknown milk samples in a matter of minutes instead of hours, as is the case with the other measurement techniques.

Measurement of Formaldehyde Content in Cheese

It is not always as easy to determine a strong and well-resolved spectral feature, which could be used for further quantification. In many cases, statistical methods must be used to enhance the relatively small differences, such as the mathematical evaluation of a correlation and variance spectrum to precisely determine, which spectral regions react in a linear fashion to changing contents of the adulterant, such as in a study concerning formaldehyde content in soft cheese (Alkhalf and Mirghani 2017).

In this particular case, the comparison between the pure and adulterated product was not so straightforward, as can be seen in Fig. 4.18. Indeed, the spectral background dictated by the dominant cheese matrix itself (the shape of which also varies according to cheese type) did not show any strong-enough spectral features unambiguously assigned to formaldehyde (apart perhaps from the bandgroup at ~990 cm^{-1}).

Thus, to develop a reliable technique for the assessment of the formaldehyde content, a series of 21 standards of the soft cheese spiked with varying amounts of the formaldehyde contaminant (0–100 mg/100 g cheese) was prepared. After the recording of the spectrum of each of the 21 standard samples, all the spectra were summed up and divided by 21 to obtain a mean spectrum.

(continued)

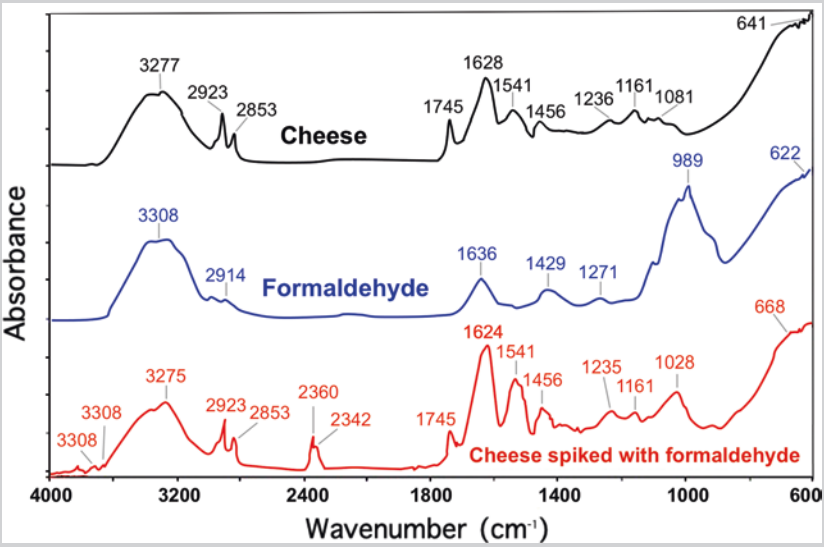

Fig. 4.18 The reference spectra of pure cheese, pure formaldehyde and cheese spiked with formaldehyde. (Redrawn from Alkhalf and Mirghani 2017)

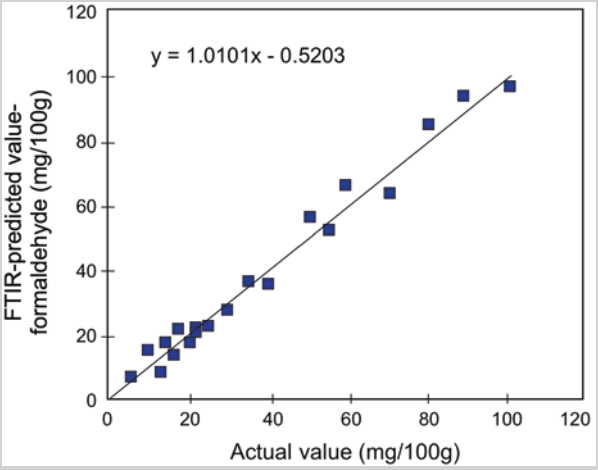

Fig. 4.19 The plot of actual formaldehyde content versus the result calculated from the PLS model using spectral data from the 800–1600 cm^{-1} spectral region. (Redrawn from Alkhalf and Mirghani 2017)

Subsequently, the difference between the absorbance value of each original spectrum and the mean was obtained, enhancing the variance at each individual wavenumber value. This enabled the authors to select the spectral region with the absorbance values showing the most pronounced linear response to changes in formaldehyde content. By means of the Partial Least Squares (PLS) technique, a reliable linear model for the determination of formaldehyde content in unknown samples was obtained, using the chosen part of the IR spectrum. The very good match of actual values and those calculated from the IR spectra can be seen in Fig. 4.19.

Visualization of Latent Evidence by IR radiation

Considering the term "*spatial IR analysis*", one would immediately expect the spatially resolved acquisition of FTIR spectra and their subsequent evaluation. However, the most rudimentary use of IR radiation to document the distribution of a substance or latent evidence on the crime scene is the mere use of an IR light source to illuminate the target and a suitable IR camera, without the need to obtain any specific spectra. Similar to screening often done with UV radiation, some details can occasionally be visualized only with the use of other wavelengths than those of visible light. Several good examples are given by Lin et al. (2007), which used this illumination technique to localize and reliably discover blood stains even after the blood dilution to half its initial concentration, written text, gunpowder residue and even tire prints on textile substrates. Some examples are given in Fig. 4.20 below. As can be seen in many, the use of IR not only reveals hidden traits, but also suppresses those, which mask them when viewing the object in visible light.

Fig. 4.20 A section of underpants viewed in visible light (**a**) and using the infrared portion of the spectrum (**b**); in the latter case, the stripes are suppressed, and a written inscription enhanced. No text is visible in the burnt portion of a document (**c**), yet it is apparent when using IR imaging (**d**). A blue pair of shorts reveals nothing out of the ordinary in visible light (**e**), yet an apparent imprint of a rubber tire is visualized when viewing the object in IR (**f**). (Modified after Lin et al. 2007).

Identifying the Presence of Explosives in Fingerprints

Although the example described above proves effective as an initial tool for the assessment of the situation on the site, most imaging strategies are intended not only for visualization of the distribution of various substances, but also for their identification or confirmation of their presence. This most abundantly used technique, corresponding to hyperspectral imaging, is based on mapping the surface spectra pixel by pixel with an instrument of sufficiently high pixel resolution. In such a case, the particles of compounds adhering to a matrix can be identified by comparison with spectroscopic fingerprint databases, as demonstrated in Sect. 4.4.1. With knowledge of the compounds, either identified or suspected and their spectra, an unambiguous spectral feature can be selected, which assists in the mapping of the distribution of the given substance on the sample. Despite obvious bands clearly discerning the spectrum of RDX explosive (cyclotrimethylenetrinitramine, also called cyclonite) from other constituents of the analysed fingerprint by ATR in this example (Fig. 4.21), the authors (Chen et al. 2009) followed the procedure, which has now become standard practice, using advanced statistical techniques [Principal Component Analysis (PCA)] and Band-Target Entropy Minimization (BTEM) to discern spectral regions reliably differentiated from background noise. For more details on the statistical techniques used, the reader is referred to comprehensible resources such as the description of PCA by Jaadi (2021) and BTEM by Kneale and Brown (2018). However, these computational procedures are already integrated in numerous spectroscopic and statistical software packages.

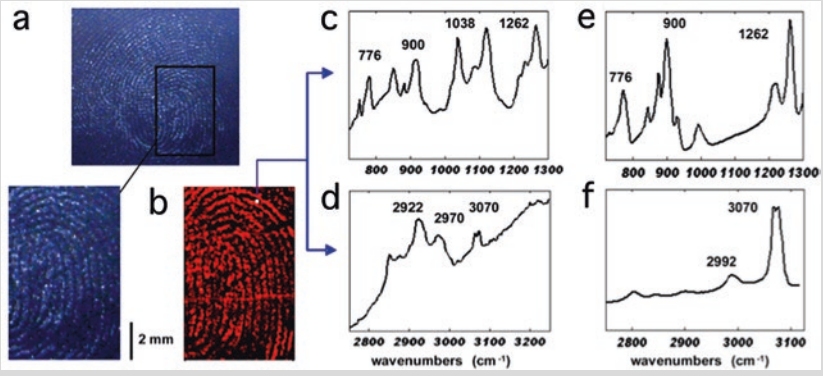

Fig. 4.21 The initial spatially resolved measurements of a region of a fingerprint (**a**), specifically its region depicted in (**b**). A grain showing a strong indication of bands related to the RDX explosive has been identified (**c, d**). A comparison is drawn with the IR spectrum of pure RDX explosive (**e,f**). (Chen et al. 2009. Courtesy of Royal Society of Chemistry UK)

(continued)

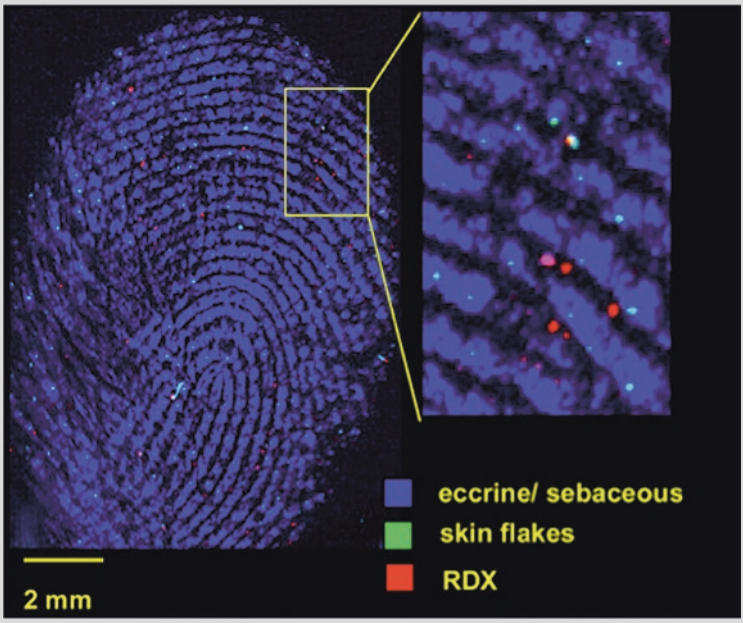

Fig. 4.22 Hyperspectral image of the analysed portion of the fingerprint. An apparent accumulation of the particles of the explosive substance (red) in the troughs between the papillary ridges is evident. (Chen et al. 2009. Courtesy of Royal Society of Chemistry UK)

After repeating the above-mentioned statistical procedure for the discrimination of spectral components for all identified substances, a precise hyperspectral distribution map of the explosive powder particles, sebaceous fluid ('skin oil') and skin flakes in the fingerprint could be obtained (Fig. 4.22).

Dilution of Medicinal Products

A very similar imaging approach finds many other applications not only in forensics, but also in quality control. In the case of peroral medicaments, the active ingredient is often known in advance, confirmed to be contained in the sample and its concentration measured by means of independent techniques, such as HPLC with UV in the following example. However, the presence of the active substance does not mean that a fraud has not been committed. Frequent tendencies of diluting medicaments by inert compounds and fillers to increase profit occur. In this example, the above-mentioned chromatographic measuring technique determined a content of a mere 70.4% of the active ingredient in the pills, well below the minimum content limit dictated

(continued)

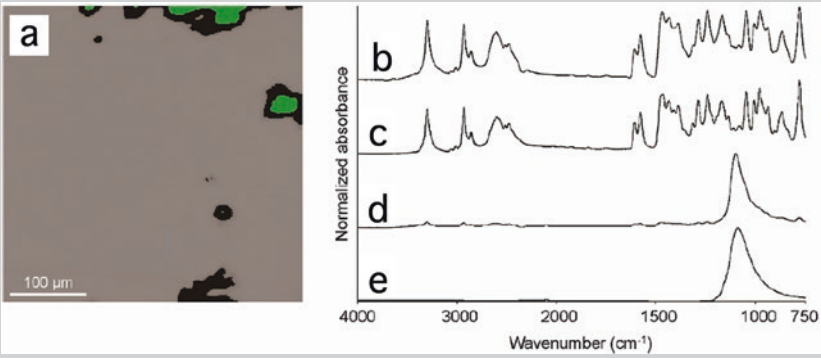

Fig. 4.23 Visualization of the distribution of the active ingredient (gray) and the diluent depicted as green (**a**). While the ATR spectrum of the gray region (**b**) corresponds to the spectral standard of the active ingredient from API (**c**), the green regions prove to consist of sodium sulfate, as results from the comparison between their spectrum and that of pure sodium sulfate (**d, e,** respectively). (Lanzarotta 2016. Courtesy of MDPI)

by the API (American Pharmaceutical Institute). In the subsequent court procedure, it was desirable to obtain information not only regarding how much the active ingredient was diluted, but also with which substance, which could, in this case, not be determined with the HPLC-UV technique. Using a specialized drop-down FTIR-ATR tool of only 100 µm to perform spatial ATR analysis, Lanzarotta (2016) was able not only to provide an image of the spatial distribution of the medicinal substance and the diluent used to decrease its content, but also to recognize the diluent as an inorganic sulfate, with subsequent chemical testing confirming it to be sodium sulfate (Fig. 4.23).

4.4.4 Spatial Analysis (Imaging)

A multicomponent sample is identified not only by its constituent parts, but also by their layout or texture. Inclusions of foreign bodies in the host substance or the aggregates of which the sample consists, may take on characteristic forms, aiding the comparison between the sample from the crime scene and a reference.

Acknowledgements The authors would like to thank Ing. Bettina Bogner, Police Command Vienna, Senior Crime Scene Investigator, sworn and court certified expert, for kindly providing us with necessary photographic and spectral documentation, enabling us to provide the descriptive practical examples, issued directly from forensic field work, for many examples of FTIR fingerprinting. We greatly acknowledge Gerald Giester of the Institute of Mineralogy and Crystallography, University of Vienna, for providing the synthetic as well as genuine gemstone sample material to illustrate the use of FTIR both in fingerprinting techniques as well as in qualitative applications.

References

Alkhalf MI, Mirghani MES (2017) Detection of formaldehyde in cheese using FTIR spectroscopy. Int Food Res J 24(Suppl):S496–S500

Amalfitano C, Balassone G (2005) Spettrometria FT-IR. In: Adamo P (ed) Metodi di Analisi Mineralogica del Suolo. IUSS – SISS Metodi Analitici per l'Agricoltura, Franco Angeli, Roma, pp 1–23

Amarie S, Ganz T, Keilmann F (2009) Mid-infrared near-field spectroscopy. Opt Express 17:21794–21801

Årnes A (2017) Digital forensic. Wiley, Middlesbrough, p 376

Artioli G (2010) Scientific methods and cultural heritage. An introduction to the application of materials science to archaeometry and conservation science. Oxford, New York, p 553

Atkins PW, de Paula J (2012) Chimica fisica, Zanichelli, p 992

Balassone G, Bellatreccia F (2019) Spettroscopia nell'infrarosso. In: Mercurio M, Langella A, Di Maggio RM, Cappelletti P (eds) Analisi Mineralogiche in Ambito Forense. Aracne Editrice, Latina, pp 219–259

Balassone G, Beran A (2005) Microscopia FT-IR. In: Adamo P (ed) Metodi di Analisi Mineralogica del Suolo. IUSS –SISS Metodi Analitici per l'Agricoltura, Franco Angeli, Roma, pp 1–14

Beran A (2002) Infrared spectroscopy of micas. Rev Mineral Geochem 46:351–369

Beran A, Libowitzky E (eds) (2004) Spectroscopic methods in mineralogy, EMU notes in mineralogy, vol 6, p 670

Beran A, Voll D, Schneider H (2004) IR spectroscopy as a tool for the characterization of ceramic precursor phases. In: Beran A, Libowitzky E (eds) EMU notes in mineralogy, vol 6, pp 189–226

Ceppatelli M, Scelta D, Tuci G, Giambastiani G, Hanfland M, Bini R (2016) High pressure chemistry of graphene oxide in the presence of Ar, N_2, and NH_3. J Phys Chem C 120(9):5174–5187

Chalmers JM, Griffiths PR (2002) Handbook of vibrational spectroscopy. Wiley, Chichester, p 3862

Chalmers JM, Edwards HGM, Hargreaves MD (eds) (2012) Infrared and Raman spectroscopy in forensic science. Wiley, Chichester, p 601

Chen T, Schultz ZD, Lewin IW (2009) Infrared spectroscopic imaging of latent fingerprints and associated forensic evidence. Analyst 134:1902–1904

Cooley JW, Tukey JW (1965) An algorithm for the machine calculation of complex Fourier series. Math Comput 19:297–301

Della Ventura G (2017) The analysis of asbestos minerals using vibrational spectroscopies (FTIR, Raman): crystal-chemistry, identification and environmental applications, EMU notes in mineralogy, vol 18, pp 135–169

Della Ventura G, Marcelli A, Bellatreccia F (2014) SR-FTIR microscopy and FTIR imaging in the earth sciences. Rev Mineral Geochem 78:447–479

Derrick MR, Stulik D, Landry JM (1999) Infrared spectroscopy in conservation science. The Getty Conservation Institute, Los Angeles, p 236

Di Maggio RM (2019) Stereomicroscopia. In: Mercurio M, Langella A, Di Maggio RM, Cappelletti P (eds) Analisi Mineralogiche in Ambito Forense. Aracne Editrice, Latina, pp 23–42

Farmer VC (1974) The infrared spectra of minerals, Monograph 4. Miner Soc Great Britain & Ireland, London, p 539

Fitzpatrick RW (2008) Nature, distribution and origin of soil materials in the forensic comparison of soils. In: Tibbett M, Carter DO (eds) Soil analysis in forensic taphonomy – chemical and biological effects of buried human remains. CRC Press, Taylor & Francis Group, Boca Raton, pp 1–28

Fitzpatrick RW (2009) Soil: forensic analysis. In: Jamieson A, Moenssens A (eds) Wiley Encyclopaedia of forensic science. Wiley, Chichester, pp 2377–2388

Fitzpatrick RW, Raven M, McLaughlin MJ (2006) Forensic soil science: an overview with reference to case investigations and challenges. In: Fitzpatrick RW (ed) Proc first intern workshop on criminal and environmental, Perth, Australia, https://www.researchgate.net/publication/315709110_Soil_Forensic_Analysis

Fredericks PM (2012) Forensic analysis of fibres by vibrational spectroscopy. In: Chalmers JM, Edwards HGM, Hargreaves MD (eds) Infrared and Raman spectroscopy in forensic science. Wiley, Chichester, pp 153–170
Goreva YS, Ma C, Rossman GR (2001) Fibrous nanoinclusions in massive rose quartz: the origin of rose coloration. Am Mineral 86:466–472
Griffiths PR, de Haseth JA (2007) Fourier transform infrared spectroscopy, 2nd edn. Wiley, New York, p 560
Hainschwang T, Katrusha A, Vollstaedt E (2005) HPHT treatment of different classes of type I brown diamonds. J Gemmol 29:261–273
Hawthorne FC, Della Ventura G (2007) Short-range order in amphiboles. Rev Mineral Geochem 67:173–222
Hawthorne FC, Waychunas GA (1988) Spectrum-fitting methods. Rev Mineral 18:63–98
Henderson GS, Neuville DR, Downs RT (eds) (2014) Spectroscopic methods in mineralogy and materials sciences, Rev Mineral Geochem 78:800pp
Humecki HJ (1995) Practical guide to infrared microspectroscopy. CRC Press, Boca Raton, p 472
Jaadi Z (2021) A step-by-step explanation of principal component analysis (PCA). https://builtin.com/data-science/step-step-explanation-principal-component-analysis. Accessed 30 Sept 2021
Jawaid S, Talpur FN, Afridi HI, Nizamani SM, Khaskheli AA, Naz S (2014) Quick determination of melamine in infant powder and liquid milk by Fourier transform infrared spectroscopy. Anal Methods 6:5269–5273
Karampelas S, Fritsch E, Zorba T, Paraskevopoulos KM, Sklavounos S (2005) Distinguishing natural from synthetic amethyst: the presence and shape of the 3595 cm^{-1} peak. Mineral Petrol 85:45–52
Keaney A, Ruffell A, McKinley J (2009) Geological trace evidence: forensic and legal perspectives. In: Ritz K, Dawson L, Miller D (eds) Criminal and environmental soil forensics. Springer, Berlin, pp 221–237
Kneale C, Brown SD (2018) Band target entropy minimization and target partial least squares for spectral recovery and quantitation. Anal Chim Acta 1031:38–46
Lanzarotta AC (2016) Analysis of forensic casework utilizing infrared spectroscopic imaging. Sensors 16(3):1–12
Libowitzky E, Beran A (2004) IR spectroscopic characterization of hydrous species in minerals. In: Beran A, Libowitzky E (eds) Spectroscopic methods in mineralogy, EMU notes in mineralogy, vol 6, pp 227–279
Libowitzky E, Rossman GR (1996) Principles of quantitative absorbance measurements in anisotropic crystals. Phys Chem Min 23:319–327
Libowitzky E, Rossman GR (1997) An IR calibration for water in minerals. Am Mineral 82:1111–1115
Lin ACY, Hsieh HM, Tsai LC, Linacre A, Lee JCI (2007) Forensic applications of infrared imaging for the detection and recording of latent evidence. J Forens Sci 52:1148–1149
Lin H, Zhang Y, Wang Q, Li B, Fan S, Wang Z (2018) Species identification of bloodstains by ATR-FTIR spectroscopy: the effects of bloodstain age and the deposition environment. Intern J Legal Med 132:667–664
Madeiovà J, Balan E, Petit S (2011) Application of vibrational spectroscopy to the characterization of phyllosilicates and other industrial minerals, EMU notes in mineralogy, vol 9, pp 171–226
Maharaj R (2008) Quantitative analysis of cocaine using Fourier transform infrared spectroscopy-attenuated total reflectance: a preliminary investigation. Intern J Third World Med 7(2):1–5
Minsky M (1988) Memoir on inventing the confocal scanning microscopy. Scanning 10:128–138
Mistek E, Lednev IK (2018) FT-IR spectroscopy for identification of biological stains for forensic purposes. Spectroscopy 33:8–19
Muro CK, Doty KC, Bueno J, Halámková L, Lednev IK (2016) Vibrational spectroscopy for forensic applications. In: Katz E, Halamek J (eds) Forensic science: a multidisciplinary approach. Wiley VCH, Weinheim, p 446
Murray RC, Tedrow JCF (1992) Forensic geology. Prentice Hall, Englewood Cliffs, p 240

Nakamoto K (2009) Infrared and Raman spectra of inorganic and coordination compounds. A, B, 6th edn. Wiley, New York, p 419
Nicolić GS (ed) (2011) Fourier transforms – new analytical approaches and FTIR strategies. InTech, Rijeka, p 538
Orphanou CM (2015) The detection and discrimination of human body fluids using ATR FT-IR spectroscopy. Forensic Sci Intern 252:e10–e16
Pye K, Croft JD (eds) (2004) Forensic geoscience: principles, techniques and applications, Geological Society. Special Publications, London, p 232
Rousseau DL, Bauman RP, Porto SPS (1981) Normal mode determination in crystals. J Raman Spectr 10:253–290
Ruffel A, McKinley J (2005) Forensic geoscience: applications of geology, geomorphology and geophysics to criminal investigations. Earth Sci Rev 69:235–247
Saferstein R, Hall AB (2020) Forensic science handbook – volume I. CRC Press, Taylor & Francis Group, Boca Raton, p 778
Schrader B (1995) Infrared and Raman spectroscopy, methods and applications. VCH, Weinheim, p 808
Smith BC (1996) Fundamentals of Fourier transform infrared spectroscopy. CRC Press, Taylor & Francis Group, Boca Raton, p 202
Stuart B (2004) Infrared spectroscopy: fundamentals and applications. Wiley, Chichester, p 203
Thornton JI (1986) Forensic science progress 1, forensic soil characterization. Springer, Berlin, pp 1–35
Turrell G (1972) Infrared and Raman spectra of crystals. Academic, London/New York, p 384
Van Der Marel HV, Beutelspacher H (1976) Atlas of infrared spectroscopy of clay minerals and their admixtures. Elsevier Scientific Publ., Co. Univ. California, p 396
Wang M, Mingxing Y, Nie S, Liu F (2017) Gemmological and spectroscopic features of untreated vs. heated amber. J Gemmol 35:530–542
Woods B, Lennard C, Kirkbride KP, Robertson J (2014) Soil examination for a forensic trace evidence laboratory – part 1: spectroscopic techniques. Forensic Sci Intern 245:187–194
Woods B, Lennard C, Kirkbride KP, Robertson J (2016) Soil examination for a forensic trace evidence laboratory – part 3: a proposed protocol for the effective triage and management of soil examinations. Forensic Sci Intern 262:45–55
Zhang Y, Wang Q, Li B, Wang Z, Li C, Yao Y, Huang P, Wang Z (2017) Changes in attenuated total reflection Fourier transform infrared spectra as blood dries out. J Forensic Sci 62:761–767

Chapter 5
Raman Spectroscopy and Forensic Mineralogy

G. Diego Gatta, Luciana Mantovani, and Geoffrey D. Bromiley

Abstract Raman Spectroscopy is a non-destructive technique which provides detailed information about chemical structure, phase and polymorph, crystallinity and molecular interactions. It is a light scattering technique, in which a molecule scatters incident light from a high intensity laser light source. A Raman spectrum features a number of peaks, showing the intensity and wavelength position of the Raman scattered light. Each peak corresponds to a specific molecular bond vibration, including individual and groups of bonds. Typically, a Raman spectrum is a distinct chemical fingerprint for a particular molecule or material, and can be used to readily identify the material, or distinguish it from others, especially with the use of modern spectral libraries. Raman spectroscopy can be used to analyse many different materials, including solids, powders, liquids, gels, slurries and gases, inorganic, organic and biological materials, pure chemicals, mixtures and solutions. For these reasons, Raman techniques are used increasingly in forensic science fields to characterise gemstones, pigments, explosives and some dangerous materials.

Keywords Raman spectroscopy · Raman effect · Raman instruments · Raman in forensic sciences · Raman gemmology

G. D. Gatta (✉)
Dipartimento di Scienze della Terra, Università degli Studi di Milano, Milano, Italy
e-mail: diego.gatta@unimi.it

L. Mantovani
Dipartimento di Scienze Chimiche della Vita e della Sostenibilità Ambientale, Università di Parma, Parma, Italy
e-mail: luciana.mantovani@unipr.it

G. D. Bromiley
School of Geosciences, University of Edinburgh, Grant Institute, Edinburgh, UK
e-mail: geoffrey.bromiley@ed.ac.uk

M. Mercurio et al. (eds.), *Mineralogical Analysis Applied to Forensics*, Soil Forensics, https://doi.org/10.1007/978-3-031-08834-6_5

5.1 Raman Spectroscopy: Basic Notions

The Raman effect was discovered in 1928 by Chandrasekhara Venkata Raman (Fig. 5.1). In recognition of this discovery, he was awarded the Nobel Prize for Physics in 1930. The Indian scientist showed that when light interacts with an optical medium, a small fraction of the emitted radiation has a different energy from the incident radiation, and that the difference in energy is governed by the vibrational characteristics of molecules (or atomic clusters) responsible for scattering the light (Raman and Krishnan 1928). The first theoretical discussion of the Raman effect was provided four years later, in 1934, by George Placzek.

Today, Raman spectroscopy is one of the most widely used vibrational spectroscopic techniques for material characterization. It provides information about both interatomic bonding and chemical environment. Raman spectroscopy can be used to study compounds in different states of aggregation (solid, liquid or gas), and is a non-destructive technique, allowing characterization of samples without any specific preparation. Measurements are also quick and require only a few tens of cubic micrometres of sample.

Fig. 5.1 Sir Chandrasekhara Venkata Raman in 1930. (Source: www.nobelprize.org/prizes/physics/1930/raman/biographical/)

5.1.1 The Raman Effect

Raman spectroscopy is based on the inelastic scattering of light. When a beam of light interacts with a target material, some of the light may be scattered in all directions. Almost all of the scattered radiation has exactly the same energy as the incident radiation, and follows the law of elastic (or Rayleigh) scattering. However, a small fraction of this radiation has a different energy. In quantum terms, this is expressed by saying that some of the scattered photons have a different energy from those of the incident photons.

Different energy means different frequency and wavelength, because energy, wavelength and frequency are mutually governed by the equation:

$$E = h\nu = hc / \lambda$$

where h and c are, respectively, the Planck constant ($6.626 \cdot 10^{-34}$ Js) and the speed of light in vacuum, ν is the frequency and λ the wavelength of the radiation. Inelastically scattered photons, by the Raman effect, have energies that reflect the chemical nature and interactions between atoms in the material (Atkins and de Paula 2014). For a simplistic description of the interatomic phenomena that generate the Raman effect, we can consider a single molecule formed of a few atoms. In a molecule consisting of N atoms, one can predict the existence of 3N independent forms of motion, consisting of translational, rotational, and vibrational modes. There are 3N-6 vibrational modes, and these are particularly important in condensed states of matter. A polyatomic molecule can vibrate in two ways: by *stretching*, when the bond lengths between atoms vary, symmetrically or asymmetrically, and by *bending*, when the bond angles change (Lin-Vien et al. 1991), as shown in Fig. 5.2. When a beam of light interacts with a molecule, energy from the photons is transferred to the molecule, raising it to an excited energy state that has a life-time of about 10^{-14} seconds. After the excitation, it is highly likely that the molecule

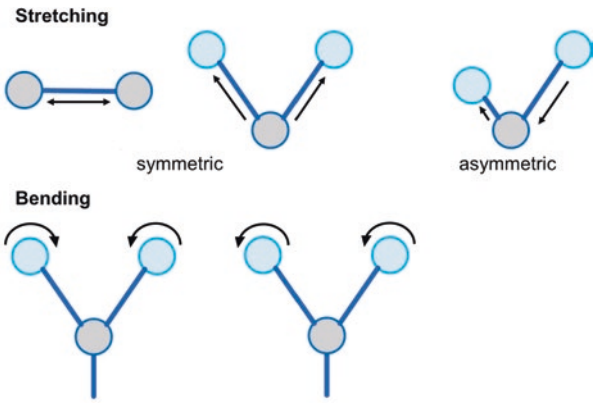

Fig. 5.2 Vibrational modes in molecules. (Modified after Gatta et al. 2019)

returns back to its fundamental (i.e. ground) state, re-emitting photons with exactly the same frequency v0 as the incident radiation (i.e. elastic or Rayleigh scattering, Fig. 5.3). However, the emitted photons may have different energy: this non-elastic phenomenon is considerably less likely and intense (10^{-9} – 10^{-16} times less intense) than Rayleigh scattering.

There are two possible scenarios, as shown in Fig. 5.3:

(a) In response to the excitation, the molecule decays to an excited vibrational state, emitting photons with slightly lower energy with respect to the incident radiation, with: $E_{\text{Stokes-photon}} = h\nu_0 - h\nu_1 < E_0$. This type of scattering, called "Stokes" scattering, is the most common relaxation mechanism, as at room temperature most oscillators are at the fundamental vibrational state.

(b) If the molecule is already in an excited vibrational state $h\nu_1$, in response to excitation by light it may decay from the excited to the ground state, emitting photons with energy $h\nu_0 + h\nu_1$. This is a higher energy than the incident radiation, with: $E_{\text{anti-Stokes photon}} = h\nu_0 + h\nu_1 > E_0$. Thus, the "anti-Stokes" part of the spectrum is also generated, with symmetrical, although much less intense, signals with respect to the Stokes counterpart, separated by the Rayleigh signal.

Stokes and anti-Stokes emissions generate the Raman spectrum: it represents a picture of the characteristic vibrational energies of a given molecular species or, more generally, of a given material. It should be noted that the Raman spectrum includes only some of the possible vibrational modes, the so-called "Raman-active modes". In a Raman-active mode, a change of polarization of the molecule (or group of interconnected atoms) must occur during the vibration itself. This occurs with vibrations in which variation of bond lengths alters the electronic distribution around the atoms (Lewis and Edwards 2001). The implication of this is that the presence (or absence) of Raman modes contrasts that in other vibrational

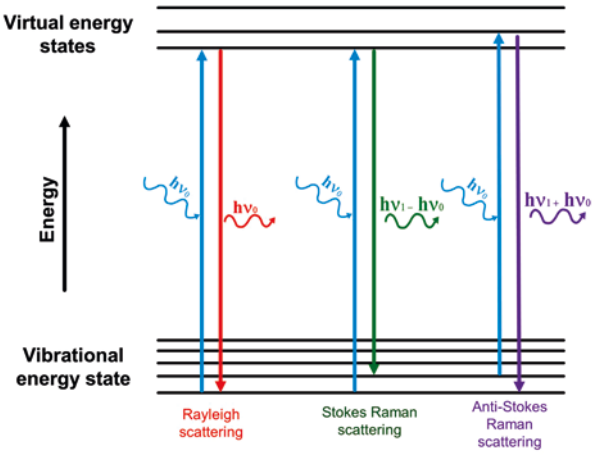

Fig. 5.3 Energy level diagram, showing excitation and relaxation phenomena responsible for Rayleigh, Raman Stokes and Raman anti-Stokes signals. (Modified after Gatta et al. 2019)

spectroscopies, such as infrared spectroscopy (IR): for IR spectroscopy, the absorbed energies cause changes in the dipole moment of a given molecule (or group of interacting atoms), regardless of polarizability. As a result, IR vibrational active modes are generally non-active in Raman spectroscopy.

It is also possible to explain the phenomenon of Raman scattering in terms of classical mechanics, describing the vibrations between interconnected atoms: the atomic nuclei can be represented by dimensionless points, while the various types of atomic interaction as ideal springs following Hooke's law. The vibrational motion of the atoms around their equilibrium positions can be considered as harmonic (as a first approximation), and the vibration frequency (ν) of this harmonic oscillator and its energy (E) vary following the expressions:

$$\nu = (1/2\pi)(K/\mu)^{1/2} \text{ and } E = 1/2 \cdot Kd^2,$$

where K is the force constant, which depends on the bond force between the two vibrating atoms, μ the reduced mass, which depends on the mass (and therefore on the chemical nature) of the two vibrating atoms, and d is the distance between the atoms.

The system can be made more complex by increasing the number of interconnected atoms. Atomic mass, and strength and type of bond make the Raman spectrum of a specific molecular species (or, in general, of a given substance) almost unique. The limitation of this classical mechanical theory is that the energy that governs the vibration phenomena is not quantized.

An isolated molecule is a simple and clear reference model for understanding vibrational phenomena. The scenario becomes more complex from a molecule to a crystal, with its regular and periodic arrangement of atoms: in response to a perturbation, a collective excitation is produced, whose properties are governed by the crystalline structure and, therefore, by the interatomic relations. As a crystal consists of fundamental units represented by the "unit cell", the atomic vibrations of a given cell propagate to adjacent cells. The Raman spectrum of a crystal will be more complex (and difficult to interpret) than that of a molecule, but it is unique for a given material, providing an excellent means of mineral identification.

5.1.2 Raman Spectrum

The Raman spectrum of a given substance is a two-dimensional representation in which, usually, the excitation frequencies (expressed in wavenumbers) are given on the abscissa (horizontal axis) and the relative intensities of the signals on the ordinate (vertical axis). A wavenumber corresponds to the reciprocal of the wavelength, usually expressed in cm, so that the wavenumber is usually given in cm^{-1}. Molecular vibrations have wavelengths ranging between 10^{-3}–10^{-2} cm, corresponding to wavenumbers between 10^2–10^3 cm^{-1} (up to 4000 cm^{-1}). The origin of the horizontal

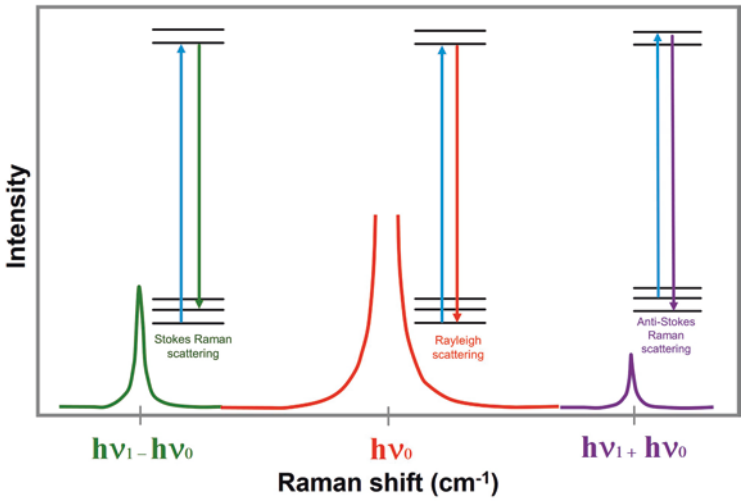

Fig. 5.4 Raman spectrum. The origin of the horizontal axis matches with the Rayleigh radiation, with symmetrically distributed Stokes (positive) and anti-Stokes (negative) signals. (Modified after Gatta et al. 2019)

axis coincides with the Rayleigh radiation wavenumber (*i.e.*, the same wavelength as the incident radiation). Symmetrically, Stokes (positive) and anti-Stokes (negative) signals lie either side of the origin. The difference between the Rayleigh radiation and the position of each band (or signal, or peak) corresponds to the energy acquired or released by the molecule (or group of interconnected atoms) with respect to the initial vibrational state (Fig. 5.4). To avoid the effect of the Rayleigh signal, which is much more intense than the spectroscopic bands of interest, instruments are equipped with special devices that act as filters, removing only the wavelength of Rayleigh emission. As the abscissa of the spectrum represents the "Raman shift", *i.e.* the wavenumber difference between the scattered and incoming photons, and the frequencies of scattered radiations are independent of the excitation wavelength, the same spectrum can be obtained by using different laser emitters.

All the information that a Raman spectrum can provide depends almost exclusively on the Stokes lines. Rayleigh radiation does not provide any information as it has the same energy for any given sample, and anti-Stokes lines are generally too weak in intensity to be detected, and can only be used for particular types of investigations. Figure 5.5 shows a typical Raman spectrum: the *x*-axis gives Raman shifts of the active signals (expressed in cm^{-1}), whereas the *y*-axis gives the Raman intensities of each signal, proportional to the number of Stokes photons collected by the detector. The range of energies reported in a normal Raman spectrum can extend, in wavenumber, from a few tens of cm^{-1} up to about 4000 cm^{-1}, covering almost all of the main interatomic vibrations.

The basic use of a Raman spectrum is the identification of an unknown substance, via comparison with the Raman spectra of substances available in the

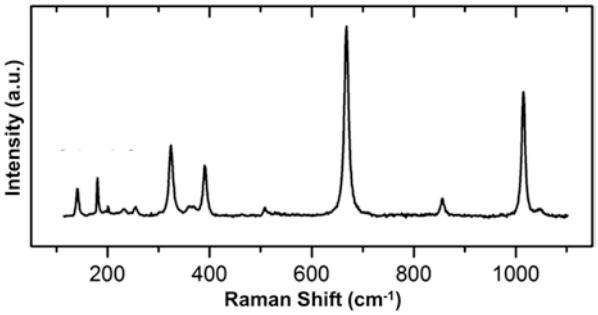

Fig. 5.5 Raman spectrum of a silicate (diopside, CaMgSi2O6). (Modified after Gatta et al. 2019)

literature or, nowadays, in open databases (details in Sect. 5.2.2). However, it is clear that the Raman spectrum brings information regarding not only the chemical nature of a given material, but also how the atoms are arranged within the structure. This leads, for example, to the fact that polymorphs (*i.e.,* substances with identical chemical compositions but different crystalline structures) have significantly different Raman spectra. This technique permits a quick and reliable distinction between materials that differ in terms of the three-dimensional atomic arrangement in crystalline structures (*e.g*., silica polymorphs: quartz, cristobalite, tridymite). Another useful parameter in the structural study of a given sample is peak width (usually represented by the "full-width-at-half-maximum" – FWHM), which reflects the degree of crystallinity of the material: broad peaks correspond to materials with crystalline structures not completely ordered, while a high order of the atomic arrangement usually generates narrow peaks (Lewis and Edwards 2001). It should be added that condensed materials do not need to be crystalline to generate a Raman spectrum: amorphous materials (*i.e*., materials that possess only a short-range order at the atomic scale) also generate Raman spectra.

5.1.3 Raman Spectroscopy: From Past to Present

At the end of the 1930s, Raman spectroscopy had become a non-destructive chemical-structural investigation method for compounds of differing nature, but the technique required experienced operators and dedicated equipment (for example, dark chambers). Since the early 1960s, the introduction of laser sources has circumvented many of the previous limitations in producing intense, monochromatic light for the exciting radiation, expanding the application of Raman spectroscopy to many fields. Subsequently, Fourier transform interferometers (FT) were used for the analysis of scattered light, and by the late 1980s, FT-Raman spectrophotometers were also commercially available for many analytical applications (Weber and Merlin 2013). Modern commercial Raman spectrometers differ significantly from early instruments, often with diverse assemblies depending on use. Most

Fig. 5.6 Example of a bench top microRaman spectrometer. (Source: S&I GmbH)

manufacturers (*e.g.*, Renishaw, Horiba, Bruker, etc.) nowadays supply benchtop instruments equipped with a "microRaman" assembly, that is, a Raman spectrometer coupled with an optical microscope (Fig. 5.6).

The most common configuration for current Raman spectrometers includes five main components: a monochromatic laser source, a microscope (in microRaman assembly), a spectrometer, a detector for converting photons into electrical signals, and a control unit for data acquisition. To complete this system, a series of filters are placed along the optical path of the laser. In order, there are: *a)* an interference filter to avoid spurious emission lines (plasma); *b)* a series of different optical density filters for power regulation; *c)* a notch filter with a dual function: promoting convergence of the beam on the sample, through the objective of the microscope (in the case of the microRaman assembly), while also eliminating the Rayleigh component, leaving only the Stokes and anti-Stokes signals after the incident beam-sample interaction. Stokes and anti-Stokes components are dispersed (by a crystal lattice) and collected by a detector (usually a charge coupled device, CCD), which produces the Raman spectrum (Fig. 5.7). The monochromatic source usually consists of a laser whose wavelength, in commercial instruments, can range from near infrared (NIR ≈ 1064 nm) to ultraviolet (UV ≈ 180 nm). The most widely used laser sources are: UV (244 or 325 nm), argon (Ar: 488.0 nm or 514.5 nm), helium-neon, (He-Ne: 632.8 nm), ruby (694.3 nm), and neodymium-YAG (Nd-YAG: 1064 nm). As already mentioned, Raman active modes are independent of the excitation wavelength (and therefore of the laser type), because they depend exclusively on the difference between two vibrational levels. For a given substance, the Raman spectra are theoretically identical whatever laser is used. However, it is necessary to take into account that: *(a)* the intensity of the Raman signal is proportional to the fourth power of the frequency; in other words, the signal obtainable with a 244 nm UV laser (40,984 cm^{-1}) is much more intense compared to its counterpart obtained with a 1064 nm (9399 cm^{-1}) NIR laser; *(b)* lasers with higher frequency energy (*e.g.*, UV,

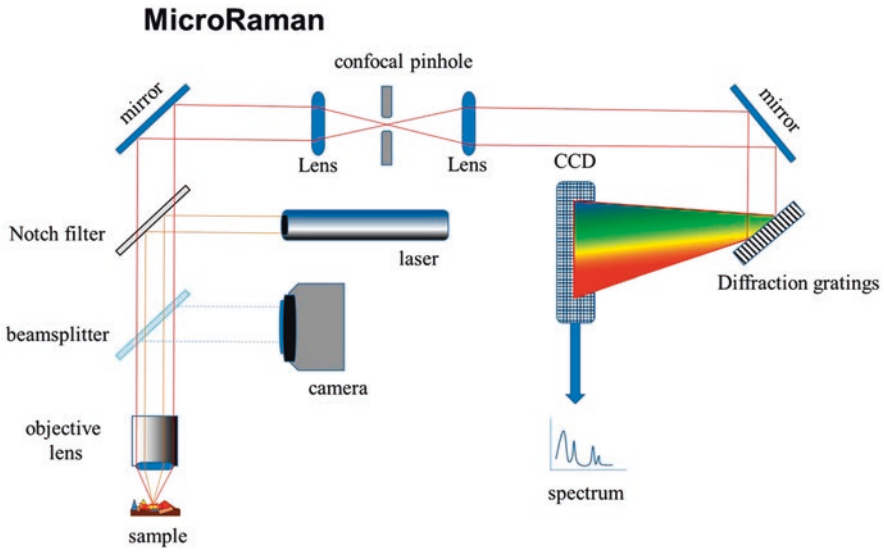

Fig. 5.7 Schematic representation of a microRaman spectrometer, with the main components. (Courtesy of D. Bersani)

visible) are able to activate, in the sample, undesirable electronic transitions, generating intense fluorescence emissions that overlap the weak Raman signals (an effect due to the emission of bright radiation at a wavelength longer than that of the incident radiation -which does not necessarily fall into the visible spectrum- in response to electronic transitions; see Sect. 5.2.3); *(c)* high frequency lasers can cause sample damage during irradiation, such as photodecomposition, resulting in the emission of anomalous Raman spectra.

Modern microRaman instruments allow selection of a micro-region (diameter of the laser beam is usually a few μm), providing characterization at the micrometric level. In terms of the depth of sample-beam interaction, experiments carried out with a microRaman assembly generate only superficial effects (*i.e.,* a few micrometres below the surface). Modern instruments are designed in order to vary the sampling depth by means of a device known as a confocal lens. The spatial resolution depends mainly on the laser and the objective used (usually 10×, 20×, 50×, 100×) and can vary from a few up to a hundred μm^2. Usually, microRaman devices are equipped with a co-axial camera.

In addition to bench top Raman instruments, nowadays there are portable instruments which, using optical fibres, permit non-destructive investigation without any manipulation of the sample (Fig. 5.8). These devices are widely used in cultural heritage, for analyses of immovable objects or for field investigations (*e.g.*, a crime scene). The potential of these devices is promising, although their performance is not comparable to those of bench-top instruments. In lab instruments, to obtain an optimal Raman spectrum the sample is placed at the correct focal distance, thanks to a sample holder that allows micrometric movements in three mutually orthogonal

Fig. 5.8 Example of a portable Raman spectrometer. (Source: www.enspectr.com)

directions; in addition, the sample holder is firmly assembled to the instrument and does not suffer from unwanted vibrations. In portable Raman devices, it is possible to move the probe to obtain the correct focusing; however, as the sample is not clamped to the instrument, it is highly likely that external vibrations affect the measurement, causing loss of focus and producing artefacts in the spectrum.

Recently, complex and highly performing instruments have started taking hold, such as the combined scanning electron microscope (usually equipped with energy-dispersive system EDS for microchemical analysis) coupled with microRaman spectrometer (SEM-EDS – Raman). All the advantages derived from a combined morphological, chemical, and spectroscopic investigation can be obtained from this kind of hybrid instrument.

5.1.4 Unconventional Techniques Based on Raman Spectroscopy

Over the last few decades, there has been a significant evolution of Raman spectroscopy, driven by new technological achievements along with the discovery of new phenomena. In the following text there is a brief description of two "unconventional" Raman techniques.

The Raman Resonance Spectroscopy (RR) uses an incident radiation of energy equal (or at least very similar) to that required to promote an electronic transition in the material studied. In this technique, the resonance process is coupled to the

process of electronic transition, with a resultant intensification of the Raman signal, which can be up to orders of magnitude higher (10^2–10^6) than that of a conventional Raman spectrometer. This has considerable advantages in the interpretation of spectra and identification of substances even at low concentrations. This technique is mainly used in the study of complex molecular systems such as proteins: by exciting them with a specific frequency, it is possible to select the Raman effects related to a particular segment of the macromolecule, or isolate a particular chromophore element (Carey 2012).

Surface-enhanced Raman spectroscopy (SERS) is based on the effect where the intensity of the Raman signals increases when the target substance is adsorbed on a metal surface. The nature of this amplification effect, accidentally discovered in the 1970s, is still a matter of discussion in the scientific community. In general, two theories can explain this phenomenon, known as the "electromagnetic theory" and the "chemical theory". The first refers to the excitation phenomena arising due to the weak interaction of a molecule (or a compound) placed on the metal surface. The second explains the amplification effect by the formation of charge-transfer complexes. The increased intensity is several orders of magnitude higher than the corresponding signal collected in the absence of the metal support, and the effect is much more pronounced when molecular species lie on a wrinkled metal surface or in contact with nanometric film of metallic particles. SERS spectroscopy can have a signal amplification equal to 10^4–10^8 times higher if compared to a conventional Raman signal, and reach even an increase of 10^{14} times when coupled with resonant Raman spectroscopy. This latter application is termed "SERRS". With these values of amplification, SERRS can reach a level of sensitivity allowing the detection of even a single molecule on a metal support (Chang 2013).

5.2 Applications of Raman Spectroscopy: Gemmological Materials

5.2.1 Raman Spectroscopy in Gemmology: Advantages and Disadvantages

The identification of gemstones, whether synthetic or natural, treated or un-treated, is a key point in the study of gemmological materials and is the basis for their commercial evaluation. For this purpose, diverse analytical techniques are usually used for a preliminary characterization of the stone, and for advanced characterization. The primary task for a gemmologist is to define, unambiguously, the nature of the gemmological material. An overview of the different techniques used in gemmology is given in Anderson (1996).

There is an endless series of case studies, pertaining to gemmology, which intersect the interests of a forensic expert. We can mention, for example, the analysis of a reliquary, which is basically unmovable, or the analysis of a stolen historical

object for which diagnosis is aimed at assessing criminal acts, *i.e.* whether material is authentic or a (even ancient) copy. The aim is, therefore, characterization of the material, which cannot exclude historical and artistic value, without necessarily focusing on the aesthetic aspects of the gem. Raman analysis in gemmology has great potential:

1. it is not destructive;
2. it is quick, allowing the analysis of several samples in a short time;
3. it is informative at different levels: not only for a mere identification, but also to unveil, in some cases, complex treatments of the gem;
4. it can be performed on site with a portable spectrometer, without the need to unmount a gem from the bezel setting.

However, some limitations also occur:

1. fluorescence can overlap the main Raman-active vibrational modes, making spectral interpretation difficult or impossible; however, fluorescence may also be helpful, revealing the presence of trace elements or of structural defects, potentially diagnostic for gem identification or to unveil a treatment;
2. Raman analysis is not possible on metal artefacts; however, gems, which are in almost all cases silicates or oxides, usually have good Raman signals;
3. the cost of a portable Raman spectrometer (currently 20–30 kEuros) is higher than that of other standard gemmological instruments, and for this reason it is not usually used in diagnostics; the cost is, however, balanced by the remarkable rapidity of data acquisition;
4. aspects such as cut quality cannot normally be assessed; on the other hand, structural defects or inclusions, whether fluid or solid, can provide useful data for identification and, in some cases, even to give clues on the origin of the gem (occurrence) or its manipulation (treatments to change transparency, colour, etc.).

5.2.2 Identification of Gems Through Raman Spectroscopy

The main question for a forensic mineralogist, when dealing with gems, is "true or false"? From a forensic point of view, the concept of "true" or "false" must be reconsidered: any material is "true", and becomes "false" when, willingly or not, it is marketed as something else. A correct protocol for gem characterization contains different levels of analysis, in which Raman spectroscopy has an enormous predictive power.

A first degree of characterization is to define whether the gem corresponds to the presumed mineral, or not. Usually, a Raman spectrum is diagnostic of a mineral species (Figs. 5.9 and 5.10), even after a few seconds of data acquisition. Identification is possible by simple comparison of Raman bands with those characteristic of the minerals (or their synthetic counterparts), starting from data available in the literature and, nowadays, also in open databases (for example RRUFF,

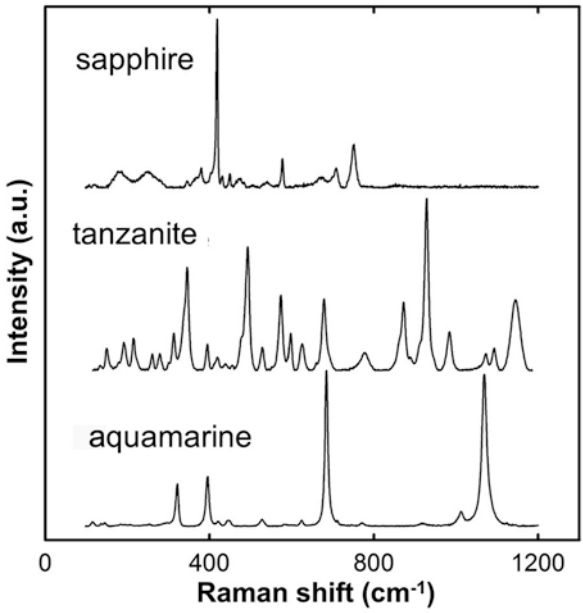

Fig. 5.9 Raman spectra of blue gems, corresponding to different mineral groups. Source: RRUFF database, data from samples X800006 (sapphire), X060001 (tanzanite), R040002 (aquamarine)

Lafuente et al. 2015). Comparison can be done manually or using commercial programs ("phase matching"). A surprising number of incorrect identifications in catalogued material are found using this method, especially in museum collections. An interesting case study is that of a collection of seventeenth–eighteenth century jewels of the Regional Museum of Messina, Italy, in which only 14 samples out of 25 confirmed previous identification (Barone et al. 2015). In this case, the concept of "true" or "false" refers to the incorrect identification of stones, of which the mineralogical nature could not be known centuries ago. In a different context, such as a commercial one, incorrect identification could highlight criminal intent. For the forensic mineralogist, the investigation protocol will be the same, but in this second context, it will assume a different relevance.

Comparative analysis of gemstones with similar colour, cut and transparency validates the method as shown, for example, by Bersani et al. (2014) for a series of potential "emeralds". The comparative microRaman investigation identified glass, quartz and almandine garnet among the green gems. Similar studies have been carried out on alleged rubies and diamond analogues (Bersani and Lottici 2010; Barone et al. 2016).

A complex case is that of the so-called doublets (or triplets): assembled gemstones constructed from two or more combined materials, in which the most valuable one is usually placed at the top. The Raman signal is generated from the surface of the stone (with a penetration of a few micrometres). If there is the suspicion of a doublet, it will be necessary to unmount the stone (from the bezel setting, for

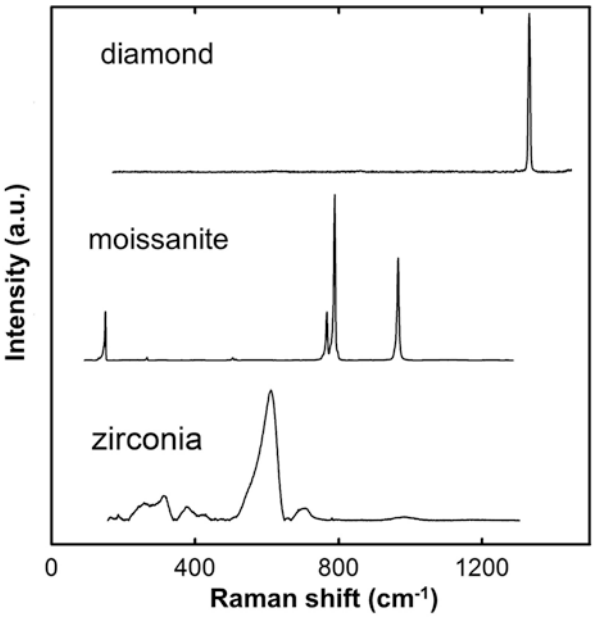

Fig. 5.10 Raman spectrum of diamond and of two simulants: moissanite (SiC) and cubic zirconia (ZrO_2). The peak at 1380 cm^{-1} is distinctive of diamond. (Source: RRUFF database, data from samples R050204 (diamond), R110106 (moissanite), X080012 (zirconia))

example) and collect Raman spectra from different segments of the gem. Examples of Raman identification of doublets are described in Giarola et al. (2012) and Barone et al. (2016).

Determining the history of investigated samples is an additional aim of gemmological investigations. This requires identification of a gem as natural or synthetic, unveiling any treatment that the gem has undergone. The synthesis of gem-quality crystals, with analogous crystallographic features to natural counterparts, developed in the nineteenth century, with significant evolution and refinement of method in recent decades. Synthesis methods are summarised in Shigley (2000). Determining whether a given gemstone is synthetic or natural is not as an easy task: Raman spectra between a natural sample and its synthetic counterpart are generally very similar, excluding some relatively minor details (*e.g.*, the width of the Raman peaks in the case of synthetic rubies (Zu et al. 2010)).

Inclusions and structural defects provide excellent markers of the natural origin of the gem. The laboratory synthesis of a gem takes place over a different time period and route compared to geological processes, leaving evidence in the final product (Dele-Dubois et al. 1986; Shigley 2000). For example, Dele et al. (1997) report the presence of inclusions of compounds such as cryolite or tungstate (added during the synthesis process to speed up crystal growth) within synthetic rubies. Such inclusions, never present in natural rubies, can be easily identified by Raman spectroscopy.

Even structural defects, recognised by observations in photoluminescence (fluorescence, in particular), can be used as additional evidence to distinguish between natural and synthetic materials. For example, photoluminescence provides one of the few tools to define whether a diamond is synthetic or natural. There are two types of synthesis protocols of diamonds: vapour deposition (chemical vapour deposition, CVD) and high pressure/temperature synthesis (high pressure – high temperature, H*P*H*T*). H*P*H*T* synthesis products are distinguishable by morphology (the crystals are usually found as interpenetrating cube-octahedra, while natural crystals are simple octahedra), by the presence of growth sectors (clearly visible through UV fluorescence), or defects due to the presence of metals (Fe or Ni used for the synthesis route) that generate specific signals in photoluminescence.

Vapour deposition syntheses are more complex to identify; identification may be possible, for example, using a photoluminescence peak due to a defect related to Si inclusions (at 737 nm) not present in natural diamonds (Fig. 5.11).

A complex problem to be addressed pertains to treated gemstones. A gem may have undergone several treatments to satisfy marketing requirements (for example, a particular colour). Treatments can be divided into two different types: those aimed at changing transparency, and those aimed at modifying colour. The main treatment to improve the transparency of a gem is impregnation. This kind of treatment can be tolerated by the market if it is carried out with non-polymerizing materials, such as oils, or, conversely, not well accepted if it is carried out with materials such as epoxy resins, which polymerize and are extremely difficult to remove. Identification of

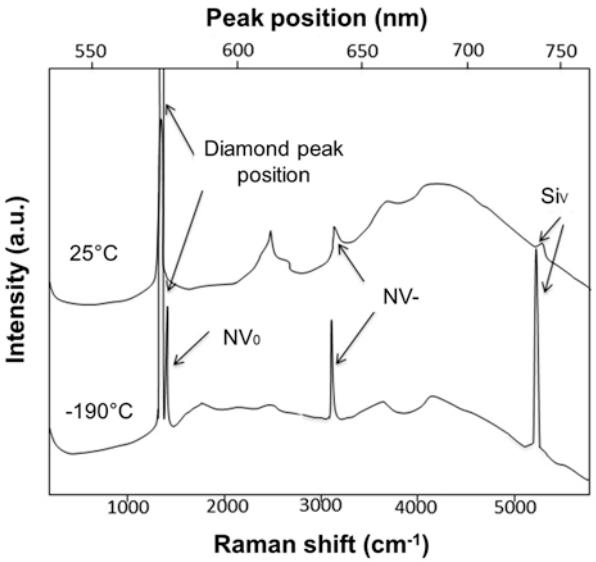

Fig. 5.11 Raman fluorescence spectra of synthetic CVD diamond, identified on the basis of the Si vacancy peak. The NV^0 and NV^- sites refer to vacancies occupied, respectively, by neutral or negatively charged N. (Source: redrafted from Åström et al. 2014)

impregnators by Raman spectroscopy can be relatively straightforward, with peaks ranging between 1200 and 1800 cm^{-1} related to the active Raman modes of C-C and C-O stretching, absent in almost all natural gems (Bersani and Lottici 2010). Coating and dyeing are the most common colour treatments: coating is achieved by applying a thin film to the surface of the stone, and dyeing involves the introduction of a colouring agent into the gemstone. Presence and nature of dyes can usually be unveiled by Raman spectroscopy. However, colour change can also be achieved through the creation/removal of structural defects. Defects can act as light absorption centres, and therefore colour centres, improving the appearance of the gem. For example, yellow-straw shades in diamond are due to structural defects in which nitrogen atoms are present (the so-called "N3 sites"), and usually decrease the value of a gem, but if the number of defects is high enough to generate an unusually marked colour, they make the gem precious. Suppression or creation of defects, obtained through heating or irradiation treatments, leaves evidence detectable in photoluminescence spectra (HORIBA 2015).

A further level of characterization is determination of the origin of a gem, with different levels of approximation (*e.g.,* geological environment, specific deposit). From an operational point of view, this is feasible if a gemstone possesses particular features ascribable to a given geological environment or a specific deposit (*e.g.,* chemical markers, inclusions, etc.). The observation of subtle changes in Raman spectral features, governed by compositional variations, allows identification, for example, of various families of garnet and beryl, used as gemstones. In garnets, the exact positions of the main Raman peaks change with composition (Andò et al. 2009). In beryl, however, the active Raman signals pertaining to H_2O stretching regions are particularly useful: the presence of alkaline elements, interacting with H_2O molecules within structural channels running along the *c*-axis, leads to a significant shift of the peaks (ranging between 3597 and 3594 cm^{-1} for peaks associated with alkalis, and between 3609 and 3606 cm^{-1} for peaks not associated with alkalis). This made it possible to classify beryls according to alkaline element content, with a comparative analysis of gems from the main deposits worldwide (Łodziński et al. 2005). Inclusions, fluid or solid, provide an additional tool for characterization. Inclusions provide information about the geological origin of the gem, and in particular about pressure, temperature, and fluid fugacities of the genetic environment. Observations in confocal light with a microRaman instrument permit direct investigation of inclusions within crystals. Bersani and Lottici (2010) reported an interesting case study of an inclusion of rutile within a garnet crystal. The nature of the inclusion was unknown, and that of the host crystal was only presumed. From the positions of Raman bands of the matrix, it was possible to describe the garnet type, and from the difference between the sum (spectra of the matrix + inclusion) and of the matrix only, the characteristic spectrum of the (included) rutile was obtained.

Of particular interest are the inclusions in corundum, sapphire and ruby. In sapphires, Palanza et al. (2008) identified inclusions which allowed not only determination of the genetic environment of the stones, but also of specific deposits. For example, zircon inclusions with metamictic halos are typical of sapphires from

alkaline basalts, whereas those from marbles are characterized by the presence of inclusions of calcite, jasper and fluids (*e.g.*, CO_2).

Inclusions are also used to distinguish between synthetic and natural gems. In rubies, for example, pyroxene and nepheline inclusions are commonly present in stones from volcanic veins (typical of rubies from Vietnam); calcite, amphibole and spinel inclusions in stones from metamorphic carbonates (*e.g.,* rubies from Burma); quartz and apatite inclusions in stones from metasomatic rocks (*e.g.*, rubies from Vietnam). In diamonds, Raman peaks of inclusions such as garnets, clinopyroxenes and melilites allow formation pressures of stones to be bracketed.

Fluid inclusions, usually consisting of water, nitrogen or carbon dioxide, are easily detectable by Raman spectroscopy as their main signals have wavenumber higher than 1000 cm^{-1}, and thus significantly different from bands of the host stone (*e.g.*, of oxides or silicates). Even fluorescence bands generated by rare-earth elements, if present, can be used as an additional tool for gem characterization.

Gems Provenance

A total number of 14 non-certified faceted emeralds have been studied using a standard micro-Raman spectrometer. Among the samples, six simulants and eight emeralds have been recognized. The simulants have been identified mostly as glass, but a quartz triplet and a couple of garnets are also present. Among the emeralds, two have been identified as synthetic and hydrothermally grown, on the basis of the –OH stretching vibration and of the position and width of the 1070 cm^{-1} band (Fig. 5.12a). In addition, solid (with graphite) and fluid (with CO_2 or CH_4) inclusions have been identified and used to formulate a hypothesis about the provenance of the mineral, along with the Cr^{3+} laser-induced luminescence band. In fact, a comparative analysis of the photoluminescence spectra of the studied emeralds, with those published in previous studies (*e.g.*, Moroz et al. 2000), show similar patterns to emeralds from Afghanistan or to synthetic products (Fig. 5.12b).

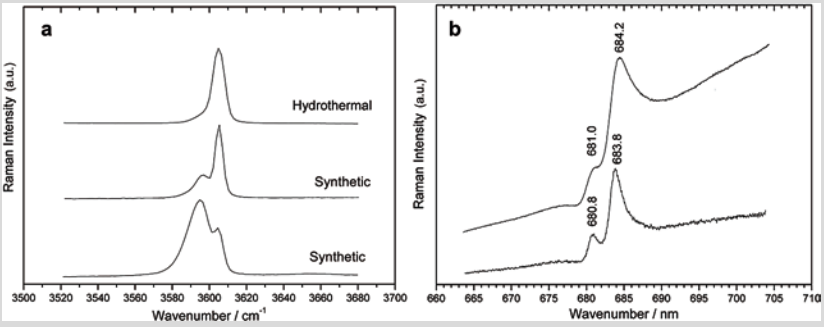

Fig. 5.12 (**a**) Raman spectra, in the OH stretching region, of three emeralds with different origins; (**b**) Photoluminescence emissions of Cr^{3+} ions present in two emeralds of different origin. (Modified after Bersani et al. 2014)

(continued)

Furthermore, enhancement treatments have been discovered in all the samples investigated, revealing the presence of almond oil. Raman spectra collected with the stone in different orientations also revealed the relationship between the gem cut and its optical axes.

In this case study, all Raman spectra were collected from loose gems; however, similar results may be expected on mounted gems. Even though a micro-Raman apparatus is able to provide superior results, especially about inclusions, we can presume that even a portable Raman equipment can be used to characterise mounted gems in immovable collections.

5.2.3 Analytical Issues

From an operational point of view, the investigation of gems does not require any specific preparation, and there are no particular differences from the operating protocols used in other forensic areas. There are, however, two experimental aspects that are particularly relevant in Raman investigations of gems: orientation of the stones and fluorescence. Usually, gems are single crystals, often faceted and polished consistently with the principal crystallographic directions. Raman spectra collected with different crystal orientations can be very different and it is necessary to pay attention to the analysis of peak intensities. Intensities of Raman modes depend on the orientation of the crystal, which generates a different polarization of the radiation. As shown in the Raman spectrum of the zircon gemstone ($ZrSiO_4$), displayed in Fig. 5.13, crystal orientation can have a significant effect on the profile, making identification of the stone rather tricky. For polycrystalline materials, such as jades or onyx, an experimental spectrum is the combination of a series of spectra generated by different orientations of the coexisting crystallites; some diagnostic peaks could be very weak or even absent, preventing rapid mineral identification. On the other hand, the positions of the peaks do not vary with orientation, as positions are dictated by the energy of the vibrational frequencies. Therefore, peak positions remain particularly indicative for stone identification (Bersani and Lottici 2010).

Fluorescence originates because the laser source, in addition to the Raman active modes, is able to excite free electrons of structural defects or of transition metals, with consequent leaps to different energy levels and subsequent re-emission by fluorescence. A fluorescence signal is generated even at concentrations below 1% of the emitting element or defect, and if it falls within the visible field. The fluorescence signal is usually much more intense than the Raman peaks (Fig. 5.14), and produces a background that can completely obscure Raman signals. Therefore, fluorescence can cause considerable problems during identification, for which diagnosis is based mainly on the most intense Raman peaks. On the other hand, fluorescence

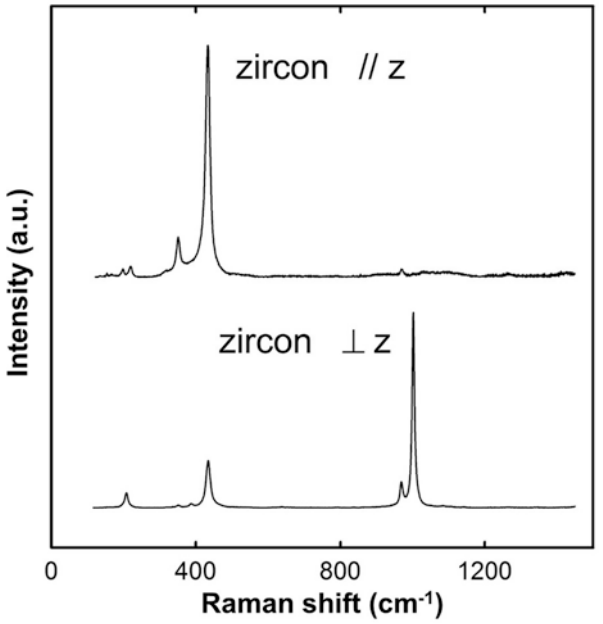

Fig. 5.13 Effect of orientation on the Raman spectrum of a zircon crystal, collected parallel and perpendicular to the crystallographic axis *z*. (Source: RRUFF database, data from sample R050034)

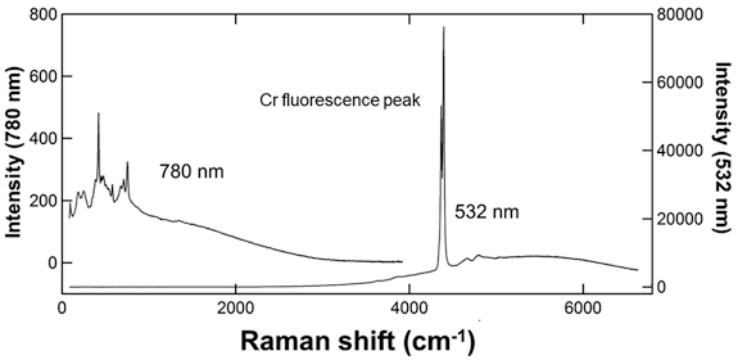

Fig. 5.14 Raman spectrum of a ruby crystal with a strong fluorescence line due to chromium. Fluorescence is activated by a source at a shorter wavelength than the element's characteristic fluorescence. More specifically, a 532 nm source activates the 694 nm fluorescence of Cr (spectrum on the right side). Using a higher wavelength source, there is no fluorescence, as shown by the spectrum on the left side, collected on the same crystal but with a 780 nm source. Data collected with the same exposure time. Note, from the comparison of *y*-scales, that the fluorescence peak has intensities two orders of magnitude higher than the Raman peaks. Source: RRUFF database, data from sample X080006

effects are indications of structural defects, inclusions, and trace elements, and sometimes are useful for characterizing and validating a gem. As seen in the previous section, fluorescence effects can be useful in many cases for identifying the origin or potential treatments of a gemstone. It is, therefore, necessary to understand how to reduce or, in other cases, optimise fluorescence phenomena. Fluorescence occurs when the energy of the laser radiation source is higher than that required for the energy leap with the consequent emission, and it is reduced when the Raman spectrum has signals that are far, in wavenumber, from the peak of fluorescence. As the energy is inversely related to wavelength, only radiation sources with wavelengths lower than the fluorescence wavelength will be able to cause the phenomenon. In a Raman spectrum, the position of a fluorescence peak is the difference between the frequency of the source and that of the photoluminescent element, expressed in wavenumbers (cm^{-1}). A shift of the fluorescence peak changes as a function of the radiation, according to:

$$\lambda_{ph} = 10^7 / \left[\left(1/\lambda_s \right) - RS \right]$$

where λ_{ph} is the wavelength of the fluorescence peak in nm, λ_s that of the emitting laser beam, and RS the shift of the Raman line in cm^{-1}.

The wavelength of the source has a significant effect on the quality of Raman spectra. In Fig. 5.14, Raman spectra collected from a ruby crystal, obtained with two different wavelengths (780 and 532 nm, respectively), are reported. The gem has a low concentration of Cr (a few thousand ppm by weight), sufficient to give fluorescence effects with peaks at 692–694 nm. While 532 nm radiation causes a strong fluorescence emission, and a spectrum dominated by the fluorescence band of chromium (and its background), 780 nm radiation has insufficient energy to generate Cr fluorescence. A multi-laser device can, therefore, reduce (or break down) fluorescence, using an energy radiation much higher or much lower than that of the peak emission. However, as Raman signals weaken in intensity with a decrease in source energy, the use of sources with wavelengths higher than 1000 nm, usually obtained with a Nd:YAG laser at 1064 nm, requires a Fourier Transform Filtration System (FTIR Raman) to improve the quality of the signal (Bersani and Lottici 2010). If fluorescence effects are desirable for gem identification, the combination of source type and spectral range should be carefully evaluated. The example in Fig. 5.13 is very indicative in this respect: if the collected spectral range was confined only up to 4000 cm^{-1}, the fluorescence peak of Cr at 694 nm would not have been observed. In general, fluorescence peaks are best defined by *in situ* observations at liquid nitrogen temperature (−193 °C).

5.2.4 Portable or Bench Top Spectrometer?

Given the simplicity of utilization, a portable Raman spectrometer is a device within reach of a forensic mineralogist. However, a portable spectrometer has many limitations:

1. The inevitably mechanical vibrations prevent a portable spectrometer from carrying out investigations at a micrometric spatial resolution. The spatial resolution is that of the beam, which is not focused by a microscope. The Raman investigation should be restricted to visible (to the naked eye) and handy samples;
2. The portable spectrometer is generally equipped with a single laser source. Therefore, the collected spectra can be severely affected by fluorescence (not solvable without a change of source radiation);
3. The actual spectral resolution of the spectrometer ranges between 4 and 10 cm^{-1}, significantly worse than the resolution of 1–2 cm^{-1} of lab instruments.

A portable Raman spectrometer is, however, an indispensable device in case of unmovable objects or to operate in the field (Bersani and Lottici 2010). On the basis of all these considerations, it is clear that the choice of instrument depends on the level of investigation. For simple identification, in most cases a portable Raman spectrometer is sufficient. For more detailed identification and characterization, a microRaman apparatus is necessary.

5.3 Other Applications of Raman Spectroscopy: Inks and Pigments, Explosives, Dangerous Minerals

5.3.1 Inks and Pigments

In some forensic investigations it may be necessary, for example, to determine the nature of an ink used on paper, parchment or other such support, or to determine the order of application of inks (of different nature) on the same substrate. The aims of such study may be different: defining whether the ink under investigation is historical or modern (given the diverse chemical nature of inks used in different historical periods), or whether an ink has been superimposed by a more recent one. The answer to these questions can result in the identification of fraud, falsification or damage to artworks.

Ink can be prepared through: *(a)* a dispersion of fine insoluble and coloured powders (pigments) or *(b)* a solution of soluble dyes, in an aqueous or organic medium (known as the "vehicle") to which diverse functional additives are incorporated (*e.g.*, polymers, adhesives, surfactants). Usually, pigments represent the lowest weight fraction of an ink (less than 20–25 wt.%). Conversely, the fluid, which promotes dispersion of the pigments and governs their fixation onto substrates, represents the dominant fraction (usually 70–75 wt.%). In some cases, additives are added in order to modify, for example, the viscosity of the ink or to facilitate the dispersion, penetration or fixing of pigments onto the support. The chemical nature of pigments and dyes can be very different: they can be organic or inorganic. The use of minerals, as substantial components of inks, has marked the history of these materials.

Since a few centuries B.C., a recipe to prepare a bluish black ink has been known: the ferrogallic ink. This type of ink is obtained by mixing gallotannic acid (usually extracted from oak galls or galls of other trees, hence the name), green vitriol (iron sulfate), gum arabic, and water. Due to its simple preparation protocol and modest cost, ferrogallic ink was used until the early decades of the twentieth century (Barrow 1955; Rouchon-Quillet et al. 2004; Leach 2012). Different variations of this ink were prepared in different periods and geographical areas. However, in some compositions this type of ink can dissolve the substrate, as it is substantially acidic. Furthermore, many writings found today with brown colouration were originally black, and the colour change involves a degenerative process that damages supports. The main components of inks usually produce good Raman signals, despite the micrometric thickness left on substrates, which facilitates forensically-oriented studies using characterization, differentiation, and comparison of inks. In addition, focusing the incident beam to different depths, using the optical assembly of microRaman devices, allows stratigraphic reconstruction of overlapping traces of inks with different natures. Severe fluorescence phenomena have been reported in some case studies on modern inks, successfully addressed by applying the SERRS technique, along with a strong dependence of data quality on excitation wavelength (Andermann 2001; Janhäll et al. 2006; Braz et al. 2013; Buzzini and Suzuki 2016). The use of Raman spectroscopy has been highly effective in the study of medieval (or Renaissance) miniatures on different substrates, whose pigments have been unambiguously recognized: azurite ($Cu_3(CO_3)_2(OH)_2$), lazurite ($Na_6Ca_2(Al_6Si_6O_{24})(SO_4,S,S_2,S_3,Cl,OH)_2$) and indigo ($C_{16}H_{10}N_2O_2$) for blue; hematite ($Fe_2O_3$), goethite (FeO(OH)), realgar (α-As_4S_4), cinnabar (HgS), minium ($Pb_2^{2+}Pb^{4+}O_4$) for red and orange; “lead yellow” (or “yellowish”, Pb_2SnO_4), orpiment (As_2S_3), stannic sulphide (SnS_2, “mosaic gold”) for yellow; malachite ($Cu_2CO_3(OH)_2$) and brochantite ($Cu_4SO_4(OH)_6$) for green; lead white ($2PbCO_3{\cdot}Pb(OH)_2$, the synthetic counterpart of hydrocerussite) for white; carbon (C) and ferrogallic ink for black. These pigments have sometimes been found mixed with calcite ($CaCO_3$), gypsum ($CaSO_4{\cdot}H_2O$) or quartz (SiO_2). Three interesting case studies, which describe the potential use of Raman spectroscopy in this field, are reported in Burgio et al. (2010) pertaining to the characterization of works ascribable to Gerolamo da Cremona (1451–1483), Franco de’ Russi (1430–?), and Bartolomeo Sanvito (1433–1511).

Miniature Pigments

Burgio et al. (2010) investigated a series of Italian medieval and Renaissance manuscript cuttings and miniatures, from the Victoria and Albert Museum, by Raman microscopy in order to reveal the nature of pigments used in different periods and different regions. In most manuscripts and cuttings, a series of compounds were identified, mainly minerals: lead white, gypsum, azurite, lazurite, indigo, malachite, vermilion, red lead, lead tin yellow (I), goethite, carbon, and ferrogallic ink. Some miniatures, e.g. the historiated capital “M”

(continued)

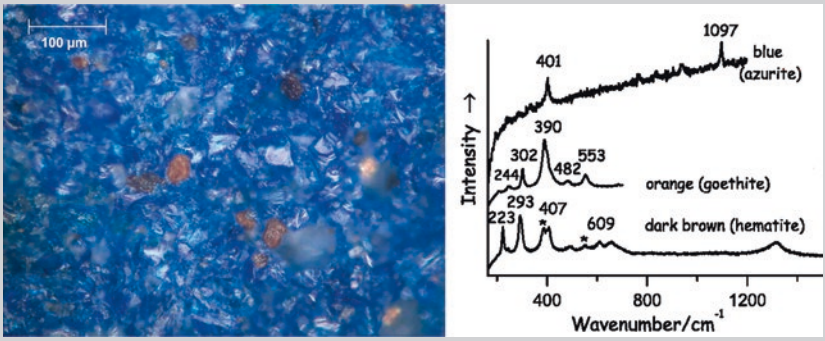

Fig. 5.15 microphotograph (× 200) of the blue area on a manuscript and Raman spectra from the blue, the orange and the dark brown crystals. (Modified after Burgio et al. 2010)

painted by Gerolamo da Cremona or the Petrarca manuscript by Bartolomeo Sanvito, show exceptional quality and provided excellent subjects for the investigation. Unusual materials were found. In medieval manuscripts, all the blue areas were usually painted with azurite. However, in this study, crystals of azurite were always found mixed with a minor fraction of green, orange, reddish and dark brown, or black crystals (see Fig. 5.15). The green crystals were malachite. It was usually assumed that the orange to black crystals were particles of the two most common copper oxides, the orange-red cuprite Cu_2O and the dark brown (or black) tenorite CuO, which occur as weathering or degradation products of azurite (Smith and Clark 2002). However, Raman spectra fit those of hematite (Fe_2O_3) and/or goethite (FeO(OH)) (see Fig. 5.15). No evidence of cuprite or tenorite was found. The authors emphasised how, to the best of their knowledge, there were no medieval recipes in which the use of iron oxides, in admixture with azurite, was reported for painting miniatures. Surprisingly, the experimental findings of their study show how the presence of iron oxides seems to be a regular occurrence on medieval manuscripts, regardless of the period and provenance of the miniatures under investigation. This revealed how the combination of these compounds (i.e., azurite along with iron oxides) was a regular and diffused practice in scriptoria and workshops, in order to obtain the best possible appearance for blue surfaces, in which azurite was the dominant pigment.

5.3.2 Explosives

A further field of forensic application of Raman spectroscopy is that of explosive materials. These materials may be composed of a single or a mixture of substances. Their peculiar feature consists of a very rapid exothermic decomposition, followed

by a violent emission of gas. The emission of gas generates a pressure wave, which governs the macroscopic effects of the explosion. During detonation (*i.e.*, instantaneous decomposition) and deflagration phases, explosives do not generate flames but only shock waves. An explosive is, therefore, made of highly unstable (*i.e.*, energetically metastable) chemical compounds under environmental conditions, which tend to decompose generating more stable reaction products (*i.e.,* with an energetically-favourable configuration). The explosive power of a material can be evaluated by determining its enthalpy of explosion, defined as the difference between the enthalpy of formation of the explosive products and the enthalpy of formation of the explosive. Generally, explosions are governed by REDOX reactions, with a peculiarity: reducing and oxidizing elements are simultaneously present in the explosive molecule. Usually, explosive substances contain nitrogen, the reason being that bonds between N and O have a lower bonding energy than, for example, bonds between C and O.

Some examples may be useful in understanding the behaviour of the most common explosive materials. Common gunpowder, for example, consists of a mixture of saltpetre (potassium nitrate), carbon and sulphur; all the chemical species that compose the powder are solid under environmental conditions. In the explosive reaction, nitrogen is reduced, and carbon and sulphur are oxidized, with a solid-to-gas mass transfer according to the reaction:

$$10KNO_3(\mathrm{s}) + 3\mathrm{S}(\mathrm{s}) + 8\mathrm{C}(\mathrm{s}) \rightarrow 2\mathrm{K}_2CO_3(\mathrm{s}) + 3\mathrm{K}_2\mathrm{SO}_4(\mathrm{s}) + 6CO_2(\mathrm{g}) + 5\mathrm{N}_2(\mathrm{g})$$

But explosive substances may also occur in a different state of matter. One of the best-known explosives is nitroglycerin ($C_3H_5N_3O_9$), which occurs, under environmental conditions, as an oily liquid. This compound is highly unstable and decomposes easily: the intra-molecular bonds are very weak and tend to split in response to modest physical shock, leading to the formation of more stable compounds:

$$4\mathrm{C}_3\mathrm{H}_5\mathrm{N}_3\mathrm{O}_9(\mathrm{l}) \rightarrow 6\mathrm{N}_2(\mathrm{g}) + 12CO(\mathrm{g}) + 10\mathrm{H}_2\mathrm{O}(\mathrm{g}) + 7\mathrm{O}_2(\mathrm{g})$$

It is worth noting that the detonation of four nitroglycerin molecules generates as many as thirty-five gas molecules (at high temperature). The instability of nitroglycerin made its use very difficult. It was Alfred Nobel (1833–1896) who made it usable through a stabilization process mixing first nitroglycerin and diatomite (to which he gave the name "dynamite"), then with other stabilizing materials (such as "explosive gelatine", obtained by mixing cotton-collodion with nitroglycerin). A further explosive substance is trinitrotoluene (TNT, $C_7H_5N_3O_6$). TNT is a yellow crystalline solid; it is insoluble in water, but highly soluble in common organic solvents. It is a stable compound under environmental conditions and is insensitive to physical shock or friction. To detonate, TNT must be triggered by a pressure wave from an explosive booster, with the following decomposition reaction:

$$2\mathrm{C}_7\mathrm{H}_5\mathrm{N}_3\mathrm{O}_6(\mathrm{s}) \rightarrow 3\mathrm{N}_2(\mathrm{g}) + 7CO(\mathrm{g}) + 5\mathrm{H}_2\mathrm{O}(\mathrm{g}) + 7\mathrm{C}(\mathrm{s})$$

In all the aforementioned explosives, nitrogen has oxidation number + 5, which is then converted to molecular nitrogen (with oxidation number: 0). Raman spectroscopy has proven to be very effective in detecting traces of explosives and/or their "precursors". Explosive precursors are common and easily available substances, making the synthesis of this class of highly dangerous materials relatively simple. Some interesting experiments, aimed at verifying the effectiveness of Raman spectroscopy in identifying explosive materials of various nature (solid or liquid), have been described by Botti and Ciardi (2008). The authors described the successful identification of: (1) dinitrotoluene (2,4-DNT), contained as powder (250 mg) in a glass bottle (emulating a scenario of particular concern in air transport), (2) nitroglycerin diluted in methanol (in concentrations of 1 mg/1 ml), and (3) nitroglycerin and TNT films deposited on substrate after solvent evaporation. This last case proved to be especially effective when the concentration of the explosive molecule in the solvent was too low to obtain a good Raman signal directly from the solution. In all the cases described in their study, Botti and Ciardi (2008) demonstrated how active Raman vibrational modes of the $–NO_2$ groups (bending modes – 750–920 cm^{-1}; symmetric stretching – 1200–1360 cm^{-1}; asymmetric stretching – 1540–1620 cm^{-1}) have proven to be effective for rapid identification of explosive substances.

5.3.3 *Dangerous Minerals for Human Health: Asbestos and Crystalline Silica*

Medical mineralogy represents a further field of potential utilization of Raman spectroscopy. There are several connections between mineralogy and medicine, including, *e.g.*, the study of bone tissues or the characterization of crystalline materials generated by organ dysfunction, such as kidney or bile stones. Focusing on forensic applications, a common area is that of occupational diseases, more specifically the respiratory diseases caused by fibrous materials (asbestosis) or crystalline polymorphs of silica (quartz, cristobalite, tridymite). The majority of European countries have identified some asbestiform minerals as dangerous for human health. Therefore, their extraction, processing and marketing (import/export) have been prohibited. In Italy, for example, the mineralogical species identified as dangerous are: chrysotile $Mg_3Si_2O_5(OH)_4$ (CAS 12001–29-5), actinolite $Ca_2(Mg,Fe^{2+})_5Si_8O_{22}(OH)_2$ (CAS 12172–67-7), tremolite $Ca_2Mg_5Si_8O_{22}(OH)_2$ (CAS 14567–73-8), anthophyllite $Mg_7Si_8O_{22}(OH)_2$ (CAS 77536–67-5), amosite (mineralogical name: grunerite, $Fe_7^{2+}Si_8O_{22}(OH)_2$, CAS 12172–73-5), and crocidolite (mineralogical name: riebeckite, $Na_2Fe_2^{3+}Fe_3^{2+}Si_8O_{22}(OH)_2$, CAS 12001–28-4). Chrysotile is a phyllosilicate, whereas all other aforementioned fibrous minerals are amphiboles. Since the beginning of the twentieth century, there was extensive utilization of asbestiform minerals, promoted by their (almost unique) features (*e.g.*, flexibility of fibres and consequent spinning, chemical inertia, high thermal and acoustic insulation capacity, high fire resistance, low density) for various industrial applications. Specifically,

asbestos minerals have often been used as fillers in concretes, bricks, pipes and fireplace cement, thermal-acoustic insulation panels used in buildings and in trains, aircrafts, ships, etc. In this class of materials, the weight fraction of asbestos minerals, used as fillers, is significant (up to 15–20 wt.%). In addition, a series of objects made almost entirely of chrysotile were produced, due to its high workability (*e.g.,* garments, fire-retardant blankets, felt, carpets, ropes, cords, ribbons, cartons, bituminous products, vinyl tiles, reinforced plastics). However, it is worth remembering that the source of fibres in a given setting can also be natural, due to alteration and/or degradation of asbestos-bearing rocks, and the resulting dispersion of these naturally-occurring fibres.

A detailed description of the pathogenic effects of asbestos is beyond the scope of this paper. We merely recall that micrometric or sub-micrometric mineral fibres effectively penetrate through the respiratory tract, primarily causing inflammatory reactions. The main pathologies associated with the inhalation of asbestos fibres are: asbestosis (interstitial pulmonary fibrosis); pleura, pericardium and peritoneum mesothelioma (particular form of carcinoma); lung cancer; pleural plaques; benign lung tumours. The long latency period of the aforementioned diseases is also noteworthy: for asbestosis, it can extend to twenty-five years, and for mesothelioma even sixty years. In some cases, such long latency makes it difficult to trace back the source of the fibres, especially for individuals who have lived in different places and were not exposed workers. From a forensic point of view, the role of mineralogical investigations is expressed, for example, by the analysis of the sputum or of the biopsy of lung tissue from patients suffering from respiratory diseases, such as those mentioned above. In particular, investigations involve characterizing asbestos fibres dispersed within biological material. It should be said that the amount of fibres present in sputum or in samples of biological tissue is often very low, rendering other investigative techniques (*e.g*., X-ray diffraction, X-ray fluorescence, etc.) ineffective. In addition, in this case, micro-Raman spectroscopy permits collection of spectra from single fibrils (which are of micrometric size) and identification of mineralogical species through comparison with spectra of asbestos minerals available in the literature. Furthermore, it should be considered that the aforementioned diseases are not all equally related to any particular type of asbestos, but tend to be specifically related to the mineralogical nature of the material.

The Raman spectrum of chrysotile, which is a phyllosilicate, is very different from those of the other asbestos minerals, which are amphiboles. In addition, the spectra of the aforementioned asbestiform amphiboles are, in turn, mutually different, although they contain some active Raman bands with similar frequencies, due to structural similarities between minerals belonging to the same mineralogical group. A series of studies reporting Raman data of various asbestos species have been published by Rinaudo et al. (2003, 2004), Belluso et al. (2007), Fornero et al. (2008) and Dichicco et al. (2017). The crystalline polymorphs of silica, and specifically quartz, cristobalite and tridymite, are also considered carcinogens for humans, under certain working conditions, by the International Agency for Research on Cancer (International Agency for Research on Cancer – IARC 1997). Silicosis and lung cancer are respiratory diseases caused by inhalation of silica-containing

powders. In general, these are occupational diseases: workers among those most at risk are those employed in mining, foundries, or those involved in the production of glass and ceramic materials. The development of silicosis seems to depend on the intensity and duration of exposure to crystalline silica particles, and on the capacity of the crystallites to reach the alveoli (a condition governed by particle size). The relationship between silicosis and the subsequent development of lung cancer has not been unambiguously demonstrated, even though evidence of correlation between these two pathologies is reported in the literature.

Investigations by micro-Raman spectroscopy connected to occupational diseases, due to asbestos fibres or crystalline silica exposition, can be required in disputes in which a worker, or his/her family members, claim for recognition of an occupational disease. Civil or criminal consequences can be significant, especially for the employer and/or the bodies responsible for health surveillance or social security. The non-destructivity of Raman spectroscopy, and the ability to produce information from samples of micrometric size, has increased utilization of this survey technique, often as a complement to scanning electron microscopy. Raman spectroscopy can also be used for environmental monitoring and identification of airborne fibres (usually captured and deposited on polycarbonate filters for investigations).

5.4 Concluding Remarks

Case studies and examples described in previous sections of this manuscript represent only a segment of the broad range of applications of Raman spectroscopy, selected in order to demonstrate the potential of this technique in mineralogical investigations applied to the forensic sciences. It is possible, therefore, to extend the collection of examples to other scenarios common in forensic investigations, for example to other types of materials often involved in crimes, *e.g.*, antique pottery, metal or ceramic artefacts, small sculptures, or traces of soil, or of wall paintings left on clothing, or even drugs.

Considering this, for Raman spectroscopic investigations:

- samples are not destroyed, and therefore, measurements can always be repeated (an important aspect for almost all Criminal Law worldwide),
- it is possible to provide results even from samples of a few tens of cubic micrometres, without any specific sample preparation,
- spectra from solid (crystalline or amorphous), liquid or gaseous samples can be collected,
- data acquisition, and relative identification of materials under investigation, is usually quick,
- identification is carried out by comparison between experimental spectra and those reported in open international databases (without additional costs),
- with a portable spectrometer, it is also possible to investigate immovable samples.

As such, the technique is increasingly used in forensic diagnostics, with a marked positive trend in the number of equipped laboratories and qualified operators.

Acknowledgements The authors warmly thank Prof. Mario Tribaudino and Prof. Danilo Bersani, for their fruitful support.

References

Andermann T (2001) Raman spectroscopy of ink on paper. Prob Forensic Sci 46:335–344
Anderson BW (1996) Gemmologia Pratica, 3rd edn. Istituto Gemmologico Italiano, Milano
Andò S, Bersani D, Vignola P, Garzanti E (2009) Raman spectroscopy as an effective tool for high-resolution heavy-mineral analysis: examples from major Himalayan and Alpine fluvio-deltaic systems. Spectrochim Acta A Mol Biomol Spectrosc 73:450–455
Åström M, Scarani A, Torelli M (2014) Detecting synthetic CVD-diamond with GemmoRaman-532SG™. In: MAGI Application Note – RA15
Atkins P, de Paula J (2014) Atkins' physical chemistry. OUP, Oxford
Barone G, Bersani D, Jehlička J et al (2015) Nondestructive investigation on the 17-18th centuries Sicilian jewelry collection at the Messina regional museum using mobile Raman equipment. J Raman Spectrosc 46:989–995
Barone G, Bersani D, Lottici PP et al (2016) Red gemstone characterization by micro-Raman spectroscopy: the case of rubies and their imitations. J Raman Spectrosc 47:1534–1539
Barrow WJ (1955) Manuscripts and documents: their deterioration and restoration. University of Virginia Press
Belluso E, Fornero E, Cairo S et al (2007) The application of micro-Raman spectroscopy to distinguish carlosturanite from serpentine-group minerals. Can Mineral 45:1495–1500
Bersani D, Lottici PP (2010) Applications of Raman spectroscopy to gemology. Anal Bioanal Chem 397:2631–2646
Bersani D, Azzi G, Lambruschi E et al (2014) Characterization of emeralds by micro-Raman spectroscopy. J Raman Spectrosc 45:1293–1300
Botti S, Ciardi R (2008) Preliminary detection of explosive standard components with laser Raman technique. ENEA, Frascati, Roma
Braz A, López-López M, García-Ruiz C (2013) Raman spectroscopy for forensic analysis of inks in questioned documents. Forensic Sci Int 232:206–212
Burgio L, Clark RJH, Hark RR (2010) Raman microscopy and x-ray fluorescence analysis of pigments on medieval and renaissance Italian manuscript cuttings. Proc Natl Acad Sci 107:5726–5731
Buzzini P, Suzuki E (2016) Forensic applications of Raman spectroscopy for the in situ analyses of pigments and dyes in ink and paint evidence. J Raman Spectrosc 47:16–27
Carey P (2012) Biochemical applications of Raman and resonance Raman spectroscopes. Elsevier Academic Press, Amsterdam
Chang R (2013) Surface enhanced Raman scattering. Springer, New York
Dele ML, Dhamelincourt P, Poirot JP et al (1997) Use of spectroscopic techniques for the study of natural and synthetic gems: application to rubies. J Raman Spectrosc 28:673–676
Dele-Dubois ML, Dhamelincourt P, Poirot JP, Schubnel HJ (1986) Differentiation between gems and synthetic minerals by laser Raman microspectroscopy. J Mol Struct 143:135–138
Dichicco MC, de Bonis A, Mongelli G et al (2017) μ-Raman spectroscopy and X-ray diffraction of asbestos' minerals for geo-environmental monitoring: the case of the southern Apennines natural sources. Appl Clay Sci 141:292–299
Fornero E, Allegrina M, Rinaudo C et al (2008) Micro-Raman spectroscopy applied on oriented crystals of fluoro-edenite amphibole. Periodico di Mineralogia 77:5–14

Gatta GD, Mantovani L, Tribaudino M (2019) Spettroscopia Raman. In: Analisi mineralogiche in ambito forense. Aracne Editrice, Latina
Giarola M, Mariotto G, Barberio M, Ajò D (2012) Raman spectroscopy in gemmology as seen from a 'jeweller's' point of view. J Raman Spectrosc 43:1828–1832
HORIBA (2015) Coloured diamond defect identification by Raman diffusion and photoluminescence application. In: Mineralogy geology RA15
International Agency for Research on Cancer – IARC (1997) IARC monographs on the evaluation of carcinogenic risk to humans: silica, some silicates, coal dust and para-aramid fibrils. Lyon
Janhäll S, Olofson KFG, Andersson PU et al (2006) Evolution of the urban aerosol during winter temperature inversion episodes. Atmos Environ 40:5355–5366
Lafuente B, Downs RT, Yang H, Stone N (2015) 1. The power of databases: the RRUFF project. In: Highlights in mineralogical crystallography. De Gruyter (O), Berlin, pp 1–30
Leach R (2012) The printing ink manual. Springer, Switzerland
Lewis IR, Edwards H (2001) Handbook of Raman spectroscopy: from the research laboratory to the process line. CRC Press, Boca Raton, FL
Lin-Vien D, Colthup NB, Fateley WG, Grasselli JG (1991) The handbook of infrared and Raman characteristic frequencies of organic molecules. Elsevier, Amsterdam
Łodziński M, Sitarz M, Stec K et al (2005) ICP, IR, Raman, NMR investigations of beryls from pegmatites of the Sudety Mts. J Mol Struct 744:1005–1015
Moroz I, Roth M, Boudeulle M, Panczer G (2000) Raman microspectroscopy and fluorescence of emeralds from various deposits. J Raman Spectrosc 31:485–490
Palanza V, di Martino D, Paleari A et al (2008) Micro-Raman spectroscopy applied to the study of inclusions within sapphire. J Raman Spectrosc 39:1007–1011
Raman CV, Krishnan KS (1928) A new type of secondary radiation. Nature 121:501–502
Rinaudo C, Gastaldi D, Belluso E (2003) Characterization of chrysotile, antigorite and lizardite by FT-Raman spectroscopy. Can Mineral 41:883–890
Rinaudo C, Belluso E, Gastaldi D (2004) Assessment of the use of Raman spectroscopy for the determination of amphibole asbestos. Mineral Mag 68:455–465
Rouchon-Quillet V, Remazeilles C, Bernard J et al (2004) The impact of gallic acid on iron gall ink corrosion. Appl Phys A 79:389–392
Shigley JE (2000) Treated and synthetic gem materials. Curr Sci 1566–1571
Smith GD, Clark RJH (2002) The role of H_2S in pigment blackening. J Cult Herit 3:101–105
Weber WH, Merlin R (2013) Raman scattering in materials science. Springer, Switzerland
Zu E, Sun Y, Zhang P (2010) The analysis of natural and synthetic ruby by Raman spectra. Spectrosc Spectr Anal 30:2164–2166

Chapter 6
ICP-MS – Fundamentals and Application to Forensic Science

Silvestro Antonio Ruffolo, Donatella Barca, Monica Alvarez de Buergo, and Mauro Francesco La Russa

Abstract Inductively coupled plasma mass spectrometry (ICP-MS) represents a powerful technique to measure the concentration of elements in a sample. Its great sensitivity allows to determine concentrations up to ppm, or even ppb. Samples can be analyzed as solutions, or as solids. The latter case involves the use of the laser ablation coupled with ICP-MS (LA-ICP-MS), which made it possible to perform analysis on a very small spot (from 25 to 100 square microns). Principles of this technique are described in this chapter, followed by some applications to forensic science, such as glasses, soils, bullets and biological tissues.

Keywords Trace elements · ICP-MS · Laser ablation · Forensic science

An in-depth petrographic and geochemical study cannot disregard the knowledge of the elemental composition of rock samples. More and more sophisticated instruments allow to analyze major and trace elements, rare earth elements (REE) and isotopic ratios, with a very low detection limit. In the field of novel instrumentations which appeared in the last 30 years, a decisive role is played by inductively coupled plasma mass spectrometry, commonly known as ICP-MS. It is a highly sensitive technique that allows to determine the elemental composition of samples, even when only small amounts are available. Currently, the field of application has extended to the analysis of many chemical elements in different types of matrices such as water, rocks, soils, stone materials and organic materials (Nelms 2005). ICP-MS technique can provide data on the concentrations of trace elements in

S. A. Ruffolo (✉) · D. Barca · M. F. La Russa
Dipartimento di Biologia, Ecologia e Scienze della Terra,
Università della Calabria, Cosenza, Italy
e-mail: silvestro.ruffolo@unical.it; donatella.barca@unical.it; Mauro.larussa@unical.it

M. Alvarez de Buergo
Instituto de Geociencias IGEO Consejo Superior de Investigaciones Científicas
(CSIC) and Universidad Complutense de Madrid (UCM), Madrid, Spain
e-mail: alvarezm@geo.ucm.es

M. Mercurio et al. (eds.), *Mineralogical Analysis Applied to Forensics*, Soil Forensics, https://doi.org/10.1007/978-3-031-08834-6_6

samples, under different chemical and mineralogical forms; its proven versatility has allowed application in several scientific disciplines (environmental sciences, geology, hydrology, biology, chemistry, materials sciences, archeology, food sciences, medicine, pharmacology and forensic sciences). It provides high precision and sensitivity, with quantification limit up to ppm – parts per million – (mg/kg) and even ppb – parts per billion – (μg/kg).

In the multi-elemental analysis of trace elements (1–1000 ppm) and ultra-trace (1–1000 ppb) the ICP-MS, thanks to its potential, offers a number of advantages, such as:

- Determination of many chemical elements, including rare earth elements, in different matrices;
- Short time for the analysis, data collection of many elements at the same time;
- Determination of isotopic ratios.

However, some disadvantages cannot be overlooked, for example, the high costs of the instrumentation and its management. In addition, operational phases of both sample preparation and data processing show some critical issues. As will be seen later, the preparation phase of the ICP-MS analysis involves the destruction (digestion) of the sample. It is a relatively complex procedure characterized by a series of steps which, if not properly carried out, can compromise the quality of the analytical data. Finally, as commonly occurring in most spectrometric techniques, the potential presence of interferences could affect the reliability of results.

To overcome the problems associated with sample preparation, LA-ICP-MS (Laser Ablation Inductively Coupled Plasma Mass Spectrometry) can be used; such a configuration requires a plasma mass spectrometer coupled with a laser-based sampler (Russo 1994). The LA-ICP-MS technique, although being slightly less sensitive than ICP-MS, allows to determine the concentration of trace elements directly on micrometric portions of any solid sample (size of a few cubic centimeters) without any preliminary sample preparation. Unlike ICP-MS analysis of solutions, which allows to determine the total average composition of a bulk sample, LA-ICP-MS provides detailed information on the composition of the investigated spot.

6.1 ICP-MS – Principles

The fundamental principle on which the instrument is based, is the transformation of the sample atoms into positive ions, as a consequence of their transit through a plasma (ionized gas) at a high temperature. The ions are then detected on the basis of their mass/charge ratio (m/z) by a mass spectrometer (Fig. 6.1).

To obtain a mass spectrum, the ions must be accelerated by an electric field, channeled into an analyzer that separates them according to the different mass, and finally detected through a detector capable of recognizing each element based on its m/z ratio.

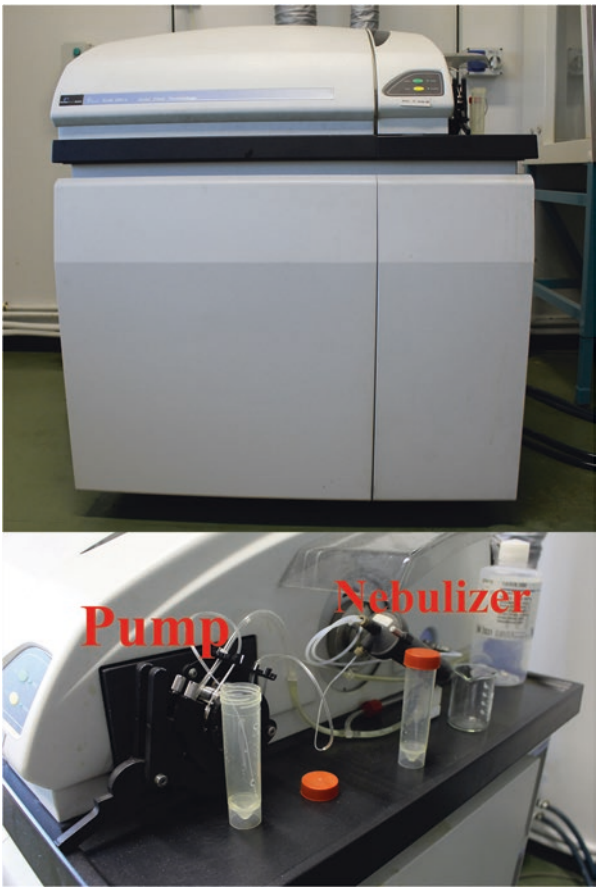

Fig. 6.1 ICP-MS equipment

The tool consists of the following elements (Fig. 6.2):

- Sample introduction system, consisting of a peristaltic pump and a nebulizer;
- ICP torch that generates the plasma and converts the sample into ions;
- Interface that connects the ion source to atmospheric pressure to the high vacuum mass spectrometer;
- Lens system;
- Analyzer that separates ions based on their mass/charge ratio (m/z);
- Detector that counts the amount of each ion;
- Software that provides final concentrations.

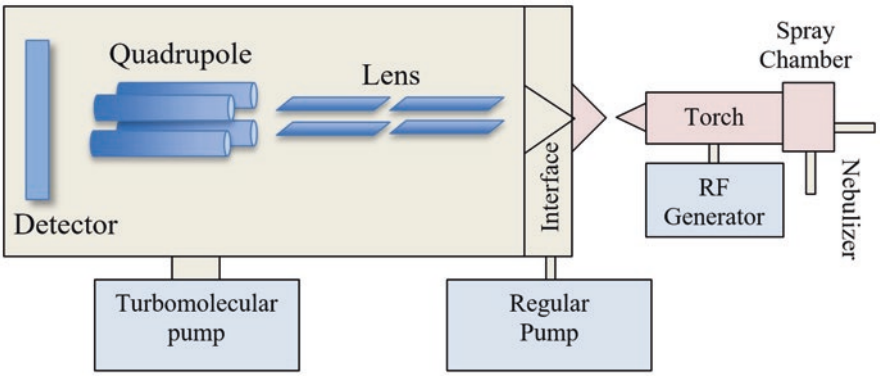

Fig. 6.2 Components of ICP-MS

6.1.1 Analytical Steps

The sample introduced into the injector tube of the torch has to be a gas, a vapor or an aerosol. Regardless of how the sample is introduced (obtained by nebulization of solutions or by laser ablation of solid samples), the goal is always to produce ions that can be analyzed by the mass spectrometer.

If a nebulization process is required, all solid samples must undergo to a pre-treatment and be transformed into an aqueous solution. Indeed, sample preparation is a crucial step of the analysis and may differ according to the nature of the samples. The next paragraph will be specifically devoted to these aspects.

Samples are introduced into the ICP-MS through a peristaltic pump and transformed in aerosols by means of a nebulizer. The nebulization system used in the ICP-MS is called cross flow, and consists of two pumps: one emits the sample and the other releases the argon, which transforms the liquid into an aerosol. Drops with a diameter greater than 810 μm do not remain in suspension; they hit the walls of the spray chamber and are removed by draining through the purge tubes connected to the peristaltic pump. About 1% of the investigated sample will reach the plasma, transported by the gas flow, and ionized.

The inductively coupled plasma (ICP) generation process is structured as follows: a flow of argon is directed into the torch, usually made of quartz. A copper spiral (coil) surrounds the terminal part of the torch and is connected to a radio frequency (RF) generator (Fig. 6.3). An alternating current oscillates in the coil at a speed corresponding to the frequency of the RF generator (27 or 40 MHz). As the argon fluxes in the torch, a spark is applied to the gas causing the ionization of argon atoms. The removed electrons are captured by the magnetic field and accelerated. The process of providing energy to electrons, through the use of a coil, is known as inductive coupling. The highly energetic electrons collide with other argon atoms extracting additional electrons and creating a chain reaction. The gas turns into inductively coupled plasma, which is made up of argon atoms, e^-, and Ar^+ ions. The

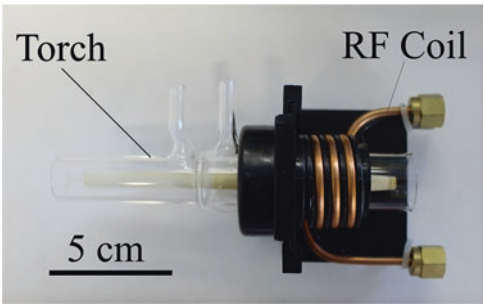

Fig. 6.3 The torch

plasma is stratified in areas with different temperatures; the area involved in the analysis has a temperature range between 6,000 and 7,000 °C.

Ions are then transported across the interface, from atmospheric pressure to an extremely low pressure inside the mass spectrometer. This must be done efficiently and without losing their electrical charge. The interface is formed by two metal cones. Once the plasma has escaped from the torch, it passes through the orifice of a nickel cone (sampler cone) reaching a mechanically cooled vacuum system. Then the flow reaches another orifice (cone skimmer).

The lens system is used to focus the ion beam exiting the skimmer cone towards the detection system. This has the purpose of focusing the ion beam on the region of the analyzer. Upon exiting the interface, the flow of ions undergoes a rapid expansion because of the vacuum, which generated by a turbomolecular pump. Since electrons spread much more easily than ions, an ion beam with a positive charge will be generated. Therefore, repulsion forces will be triggered inside the ion beam and the ions with a higher mass/charge ratio will tend to arrange themselves towards the center of the beam, forcing the lighter ones outwards. This causes a loss of some ions arriving at the detection system, and such a loss will be greater for lighter elements. The task of the lens system is to convey these ions inside the beam.

Then the analyzer separates the ions with different m/z ratio. The quadrupole is one of the most commonly used analyzers and consists of four metal cylinders (rods) arranged parallel and symmetrically with respect to a central axis, two positives and two negatives. The two opposite rods are connected to each other. A direct current is applied to one pair, while a radio frequency on the other. For each pair of direct current and radiofrequency values, only the ions with a certain range of m/z values will reach the detector whereas the others will be deflected out of the quadrupole, passing into the spaces between the tubes.

The detector of the spectrometer consists of a cascade of dynodes (electron multipliers). The ions passing through the quadrupole hit the active surface of the dynode and generate a measurable increase of the electrical signal.

The active surface of the detector releases an electron every time an ion hits it. More precisely, the ions hit the first dynode which, releasing an electron, triggers the signal amplification process. The electrons released by the first dynode hit the second dynode, which in turn releases a greater number of electrons and so on, generating the signal amplification. This cascade of electrons, proportional to the

number of incident ions, will eventually form a measurable electrical signal. By counting the pulses generated by the detector, the system is able to trace how many ions hit the first dynode.

6.1.2 Interference Issue

By using ICP-MS it is possible to simultaneously determine the concentration of elements in different matrices, although it is necessary to investigate possible interferences that can affect the analysis of the examined isotopes.

Such interferences can be divided into two groups:

- Spectroscopic (or isobaric) interferences, due to the superposition of the peaks relative to different ionic species, but having the same m/z ratio;
- Non-spectroscopic, physical, and chemical interferences, linked to the intrinsic characteristics of the sample (Sèbastien et al. 2000).

The isotope-isotope isobaric interferences are due to isotopes having the same characteristic mass but belonging to different elements (for example ^{204}Hg and ^{204}Pb). These interferences are found for m/z values >36 and among the spectroscopic interferences they are the most predictable and easy to resolve.

The software usually carries out automatic corrections by subtracting any interfering peak from the peaks of the isotopes of interest.

Using an argon plasma, the only isotope-isotope isobaric interference impossible to correct is that due to ^{40}Ar, since saturating the detector makes it impossible to determine isotopes having m/z = 40 (such as ^{40}Ca).

Polyatomic interferences, on the other hand, are more difficult to predict and correct than the previous ones. These interferences are due to the formation of polyatomic ions whose characteristic mass coincides with that of the isotope to be analyzed (for example, the ArO^+ ion overlaps the ^{56}Fe isotope).

These ions result from the combination of two or more atomic species present in the plasma gas (Ar) and in the solvents and acids used for the preparation of the samples (H, N, Cl, F, B, O).

Polyatomic interferences affect the entire mass spectrum, the most severe of which are those that occur during the scanning of masses <82, mainly due to $ArCl^+$, ArO^+, ClO^+.

In general, to mitigate this effect, it is a good practice to keep the temperature of the spray chamber at 3 °C in order to allow the condensation of a large part of the solvent, which is mainly responsible for the formation of polyatomic species in the plasma.

Another cause of spectroscopic interference is represented by refractory oxides (MO^+, MO_2^+, MO_3^+), which are formed by incomplete dissociation of the sample matrix or by recombination processes that take place in the plasma.

The elements that are most affected are those that tend to form particularly strong bonds with oxygen, such as Ti, Zr, Ce, Si. The ratios (MO/M) are generally minimized by choosing a low speed of the nebulizer gas flow (≤ 0.8 L/min).

Most of the ions produced in plasma are single-charged. Only the elements that have a second ionization energy lower than that of the first ionization of Ar (16 eV) contribute significantly to the production of 2^+ ions. The problems related to the formation of double charges are of two different types: (i) an underestimation of the concentration of the analyte of interest, which is calculated at the peak m/z with z = 1; (ii) an additive interference on the isotope having mass n = m/z with z = 2.

To limit the interference due to double charges it is important to do not apply high potentials to the plasma, and do not use low velocities for the gas flow nebulizer, because in both cases there would be an increase in the ionization capacity of the plasma. By introducing a tune solution containing barium, characterized by low ionization energy, it is possible to ensure that the conditions of the plasma are such as to minimize the incidence of double charges, verifying that the Ba^{++}/Ba^{+} ratio is less than 3%.

Non-spectroscopic interferences are due to the chemical and physical characteristics of the matrices and of the samples to be analyzed. For example, if precipitates are formed in the analytical phase at the orifice of the cones, they will cause a change in their geometry or even their occlusion, then a loss of precision, sensitivity and reproducibility of the instrument will occur.

Differences in physical characteristics (i.e., viscosity and density) between samples and calibration standards result in a different response in the aspiration, transport, and nebulization phases.

The chemical differences, on the other hand, determine changes in the composition and flow of the ion beam that crosses the interface. In particular, the ions with a lower mass and degree of ionization are more significantly affected by the matrix effect, which is greater for greater masses and for higher degree of ionization of the elements making up the matrix.

To reduce these effects, it is important that standards and samples are very similar both in the chemical composition of the matrix and in the percentage of acids present. When this is not possible, an internal standard can be used to assess the extent of the interference.

6.2 Laser Ablation Coupled with ICP-MS (LA-ICP-MS)

LASER is the acronym for: Light Amplification by the Stimulated Emission of Radiation. Theoretically, lasers can emit at any optical frequency belonging to the electromagnetic spectrum.

The system consisting of the coupling of a laser scaler with a LA-ICP-MS plasma mass spectrometer allows to perform microdestructive multi-element analyses of solid samples, even with very small amounts (Fig. 6.4).

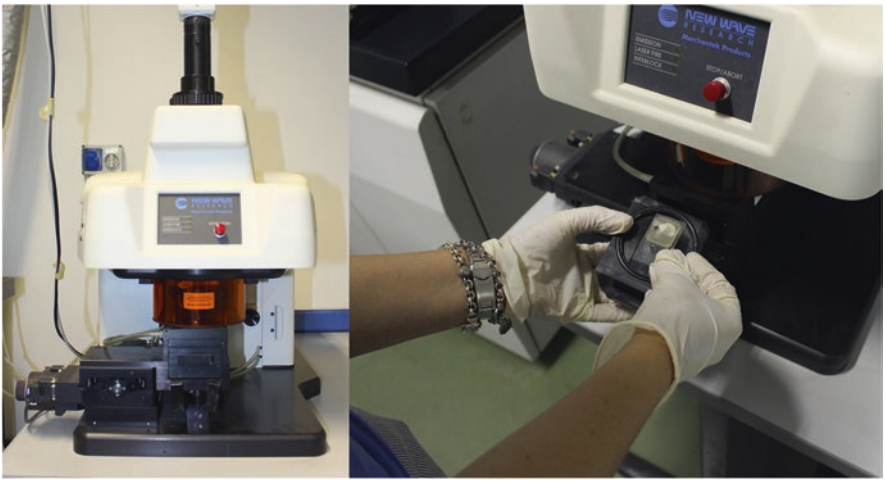

Fig. 6.4 Laser ablation equipment

Analysis performed with LA-ICP-MS requires no pre-treatment, although it can be useful to prepare glossy sections at least 100 microns thick to have a better view of the sample and to select properly the portion to be analyzed.

The term "laser ablation" is referred to any micro-removal process in which the formation of a liquid phase is negligible. A distinctive feature of the ablation is that it provides a high energy in a short time interval, so that the removal process can be considered instantaneous and free from heat propagation. In most of the applications known from literature, ultraviolet wavelengths are used. A radiation in the UV field is compatible with the energy levels of electronic transition and consequently causes, only by absorption, the breaking of the bonds. In UV ablation, the dynamic behavior prevails over the thermal one, and the heat that propagates is due exclusively to the release of heat from the excited molecules. The effect of the energy pulse therefore remains confined to the narrow impact area ensuring excellent resolution.

The diameter d of the crater (spot) depends on the wavelength of the laser beam: the shorter the wavelength, the lower the minimum spot of the laser beam. This is why most of the lasers used in the LA-ICP-MS technique have a wavelength belonging to the UV range (Fig. 6.5).

The laser ablation system (LA) is essentially made up of the sample holder, the laser module and then lens system (Fryer et al. 1995).

The sample to be analyzed is vaporized through the laser and then transported by an inert gas (generally a mixture of He and Ar) into the ionization chamber where it interacts with the plasma (Fig. 6.6).

The following steps are identical to those regarding the analytical procedure for nebulization of an aqueous solution.

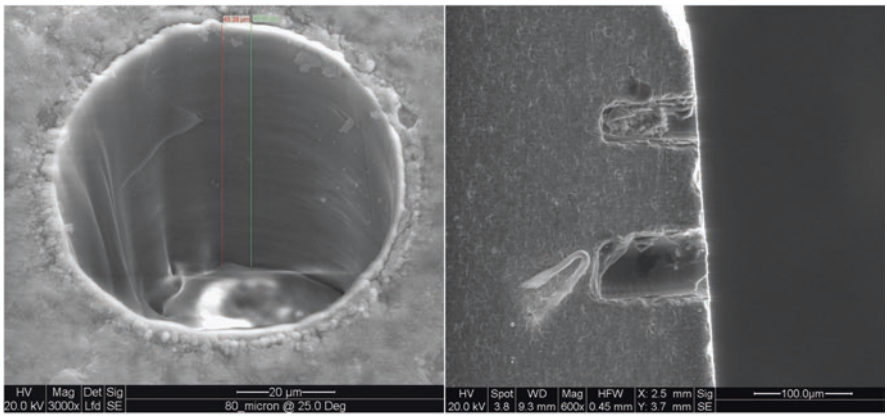

Fig. 6.5 SEM images of the hole produced by the laser ablation

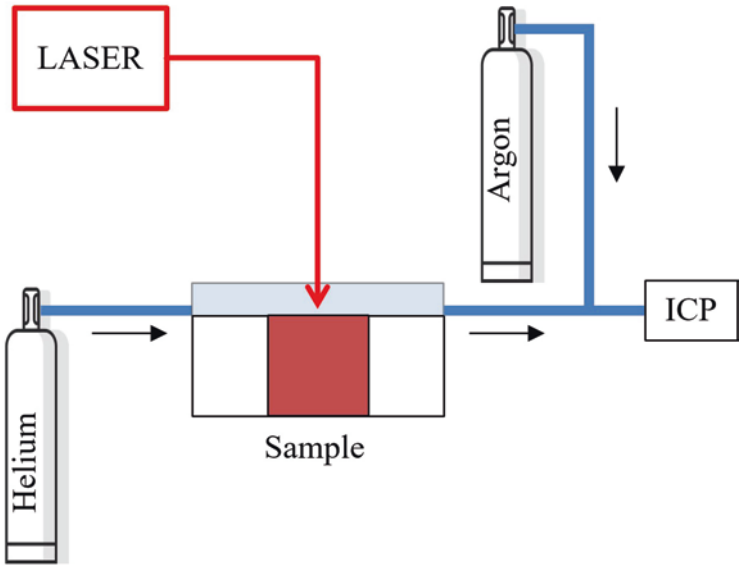

Fig. 6.6 Scheme of the LA-ICP-MS equipment

6.3 Sample Preparation and Analytical Phase

To determine the concentrations of the elements within a sample by ICP-MS technique, the samples must be in aqueous solution (Mester and Sturgeon 2003).

The solution obtained after sample preparation must contain and keep in solution all the elements present in the starting matrix, contains all the analytes of interest at a concentration suitable to be detected by the instrument, produces the lowest

number of non-spectral (chemical-physical) and spectral (isobaric and polyatomic) interferences, and has a low aggressiveness toward the equipment.

In order to analyze aqueous matrices, no special treatment is required, before analysis; the samples must be simply filtered and stabilized with the addition of 1% of ultrapure HNO_3.

On the contrary, to perform the analysis of solid samples, it is necessary to dissolve them, carrying out procedures that vary according to the type of sample.

The procedure is destructive, although the amount of sample required is very limited.

Solid samples to be analyzed must be prepared by following one or more of these steps:

- pulverization;
- weighing;
- acid attack;
- microwave digestion;
- evaporation on plate;
- conservation of samples (if needed);
- analysis

Solid samples (rocks, minerals and soils) must be dried and pulverized before being prepared for analysis.

The samples are weighed in special polytetrafluoroethylene (PTFE – Teflon) vessels, using an analytical balance (sensitivity 0.0001 g). Each vessel corresponds to a sample to be analyzed. The samples, suitably signed, are weighed with an approximately similar quantity, in order to be comparable to each other. Usually, 0.1 g of sample powder is used.

Acids are added to the weighed samples in the vessels, the nature of which depends on the type of sample to be mineralized. Actually, a reagent can be effective and necessary for the digestion of certain mineralogical phases but, at the same time, it can be corrosive for the instrumentation. Generally, for rock samples it is used:

1. nitric acid (HNO_3) that has a strong oxidizing power and a good ability to form soluble salts with most of the elements. Furthermore, it does not generate great interference in ICP-MS;
2. hydrochloric acid (HCl) that is a strong acid, with reducing power in conditions of high temperature and pressure. These characteristics make it capable of attacking oxides, hydroxides, carbonates and sulphates with the formation of water-soluble compounds. Its use, however, involves the formation of important polyatomic interferences such as: $^{40}Ar^{35}Cr$ for the analysis of ^{75}As; $^{37}Cl^{14}N$ for the analysis of ^{51}V; $^{35}Cl^{16}O$ and $^{35}Cl^{16}OH$ for the analysis of ^{52}Cr;
3. hydrofluoric acid (HF) that responds to the need to bring into solution even the most resistant crystalline silicate phases according to the reaction:

$$SiO_2 + 4HF \rightarrow 2H_2O + SiF_4$$

An excessive quantity of this acid implies the formation of insoluble and moderately insoluble compounds (for example precipitates of La, Ce, Mg and Th), and of volatile compounds which mainly affect the alkaline elements, but also the lanthanides and actinides.

Rock and soil samples can be attacked with 6 ml of nitric acid (HNO_3), 6 ml of hydrofluoric acid (HF) and 3 ml of perchloric acid ($HClO_4$).

After the acid attack, the hermetically sealed vessels are placed in microwave oven. The vessels are resistant to high temperatures (~300 °C) and pressures (~ 1500 PSI); moreover, the caps are equipped with a vent mechanism, able to prevent dangerous breakages in the presence of excessive pressures. The microwave oven is usually equipped with a sensor system for automatic temperature and pressure control.

At the end of the microwave cycle, the samples should be totally dissolved. The content of the vessel is poured into PTFE containers with the addition of ultrapure water. The solutions are then placed on a heating plate at about 200–220 °C and brought to evaporation, to allow the complete removal of the acid fumes. The evaporation phase ends when the solution achieves a gel state. When evaporation is complete, 1 mL of ultrapure perchloric acid ($HClO_4$) and 5 mL of nitric acid (HNO_3) diluted to 5% are added to the rock and soil samples.

Once the evaporation phase on the plate is finished, the samples are brought to a defined volume with the addition of ultrapure water. Finally, the solution is poured into special containers, stored in the refrigerator at +4 °C and ready to be analyzed.

6.3.1 Analytical Phase

The analytical phase involves the optimization of the instrument, the preparation of the calibration curves and finally the analysis of the samples and the recalculation of the results according to the initial weight and the performed dilutions.

To calculate the concentration of the elements it is necessary to make a calibration curve; to this end, solutions of known concentration are suitably prepared. Generally, the elemental quantitative information is obtained by comparing the measured signal for a given element with such a reference calibration curve. A set of standards (STD) at different concentrations and a blank (BLK) are required to construct the calibration curve. The BLK sample must not contain the element to be analyzed. Furthermore, BLK and STD must have a matrix as similar as possible to that of the samples to be analyzed.

The BLK is used both for the adjustment of the calibration curve and during the analysis of the samples to verify that there is no contamination.

The detection limit (DL) is used to verify the instrumental sensitivity and is defined as the lowest concentration that can be detected by the instrument for each analyte. This value depends on the calculation of the background fluctuations, considered as instrumental “noise” and represented by the repeated measurements of the BLK. The Routine Detection Limit, on the other hand, represents the real

performance of the instrument and provides more information on the real lowest measurable quantity during an analysis. It is calculated by collecting *n* measurements of a blank at regular intervals during an entire analysis cycle.

To validate the data quality, following the same procedure used for the samples under test, samples of certified standards are prepared which will be analyzed, at regular intervals, together with the BLK during an analysis cycle. It is a good practice to use certified matrices (for example produced by NIST: National Institute of Standard and Technologies), very similar to the unknown samples to be analyzed. In addition, the use of the certified reference material (CRM) guarantees the accuracy of the data obtained. Accuracy is calculated by comparing the measured values with the corresponding certified concentration values.

To obtain the final result, the last step is represented by the recalculation of the values taking into account the weight of the sample and the dilution.

6.3.2 LA-ICP-MS

As previously discussed, analyses by LA-ICP-MS are performed directly on the sample, therefore, no pretreatment is required (Longerich et al. 1996).

However, as previously stated, the preparation of sections at least 100 microns thick with the glossy surface allows a better view of the sample improving the choice of the spot to be analyzed.

Before carrying out the analyses, the instrument has to be calibrated using a standard glass. The most used glasses are those made by the National Institute of Standards and Technology (NIST), (i.e., SRM 610 glass, in which the elements have a concentration of about 500 ppm, or SRM612 glass, in which the elements have a concentration of about 50 ppm).

The first step is the introduction of the sample into the sample holder chamber where the laser ablation takes place. This is followed by the choice of the spot to be analyzed.

The overall time of each analysis is approximately 180 s during which three steps occur: in the first one (about 60 s) the acquisition of the blank takes place, that is the signal acquisition without any ablation; in the second one (about 60 s) the laser ablation takes place as well as the data acquisition; in the last step, after laser ablation, a flow of argon and helium removes from the instrument all residual material from the sample.

The analyses can be performed using different spots (~25–100 microns). The different phases of each analysis (blank, acquisition, and cleaning) can be monitored in real time using a software that shows the trend of the spectra acquired over time, enabling an overall evaluation of the quality of the signal and, therefore, of the analysis.

Within the analysis sequence, two checks are usually performed on the standard sample (the certified glass) which is analyzed as unknown. The data obtained on this

standard will be compared with the corresponding certified values and used to calculate the accuracy and, consequently, the reliability of the analytical data.

In order to obtain the concentration of the analytes, expressed as mg/kg, it is necessary to reprocess the spectra provided at the output of the LA-ICP-MS system. Usually, the elemental quantitative information is obtained by comparing the measured signal for a given element, with an appropriate reference calibration curve. In the case of an analytical sequence carried out with the LA-ICP-MS system, the calibration curve is represented by the spectra of the analyses performed on standard glasses. Usually, the reprocessing of the spectra requires the introduction of a known concentration value for each spectrum to be recalculated. The element imposed in the reprocessing is a major element, at known concentration, which acts as an internal standard.

6.4 Forensic Applications

The ICP-MS technique is very useful in several sectors. For example, in the environmental field, national and international standards describe the use of the ICP-MS technique for the analysis of trace elements in drinking water (i.e. ISO 17294-2), wastewater and sediments (i.e. EPA METHOD 6020B). In the field of sciences applied to cultural heritage, the LA-ICP-MS technique is used to analyze trace elements in materials such as obsidians, mortars, ceramics to determine their origin (Barca et al. 2007). A recent application concerns the analysis of pollutants on architectural surfaces in urban environments. In particular, the LA-ICP-MS technique allows to investigate the distribution of pollutants in the stone material and evaluate their impact (Barca et al. 2010). Another field of application is represented by forensic analysis. Some examples are described below.

6.4.1 Glass

The analysis of glassy materials as physical evidence can provide valuable information in the context of criminal investigations. For example, when glass fragments are found at the scene of a car accident, robbery, or murder, they can be compared with glass residues collected from the victim's body and/or suspected. If the fragments belong to the same object with a high degree of confidence, this can be a scientific evidence to demonstrate, for example, the interaction between individuals (Almirall 1999, 2001).

In order to be valid for a court, scientific results have to be obtained by techniques and methods that offer good discrimination between different objects of glassy material. The measurement of the refractive index is a useful technique for the forensic examination of glass (Suzuki et al. 2000). However, due to the variability of the refractive index within the same object, a simple discrimination is not

sufficient to constitute proof. Consequently, it is necessary to use additional techniques, such as elemental composition analysis, to make the comparison between fragments more reliable (Hughes et al. 1976).

Elemental analysis by ICP-MS increases the value of the evidence, because the method provides high precision and accuracy of element concentration. Furthermore, it has been shown from the analysis conducted with ICP-MS in solution on glasses, that the elemental composition of glass varies considerably between the lenses of glasses from different sources, as well as between automobile glasses with different production dates. At the same time, there is modest compositional variability within the same object. These features make ICP-MS analysis an excellent technique for forensic glass analysis.

Comparisons were made between ICP-MS in solution and LA-ICP-MS by running parallel analyses on numerous samples from different sources. The results showed that, in the context of glass analysis, the LA-ICP-MS technique has a discriminating power very similar to the ICP-MS in solution. The minimum sample size for a good representativeness is about 0.1 mm per side (Montero 2002).

One issue that should be carefully considered are the potential inhomogeneities that usually affect the different types of glasses involved in cases of forensic crimes (Duckworth et al. 2000). In particular, different analytical approaches should be considered if architectural glass, containers, car windshields or tempered glasses need to be analyzed. For example, tempered glass has undergone a hardening process that gives it greater strength and a mode of breaking into small fragments, making it safer. Hardening has been shown to lead to inhomogeneity in the refractive index between the surface and internal parts. In this case, in order to have a reliable sample, the investigated material must be withdrawn in different areas to mediate the natural heterogeneity within the glass. By contrast, the tempering process does not generate any inhomogeneity at the elemental compositional level within the glass fragments, and therefore there is no criticality for the forensic comparison of the recovered fragments (Trejos et al. 2005).

In addition, architectural glass has good chemical homogeneity, therefore, for comparison purposes, it should be sufficient to sample five different glass fragments from the known source (Zurhaar and Mullings 1990).

In the case of windscreens, it is possible to find differences of elemental composition of the two faces of the glass separated by the polymeric film; in this case, it is advisable to take at least five glass fragments on each of the two sides of the known windscreen (Orellana et al. 2013).

In the case of containers (i.e., bottles, jars) it is also necessary to take into account the natural micro-heterogeneity within a single bottle. It is therefore necessary to take glass samples from the upper, middle and lower area of the container. However, if this is not possible, it is appropriate to sample at least five glass fragments from the known source. As a general rule, an unknown glass fragment should be analyzed at least three times in order to get reliable data to compare with the known source (Koons et al. 1988).

Float Glass
90% of the float glass produced in the world is manufactured with the float system, where the molten glass is poured onto a bath of molten tin. For this reason, the tin content is higher on the side that has been in contact with the molten tin during processing. When the recovered fragments are large enough to be seen under UV light, the non-fluorescent side (side not in contact with molten tin) should be used for analysis (Orellana et al. 2013) (Fig. 6.7).

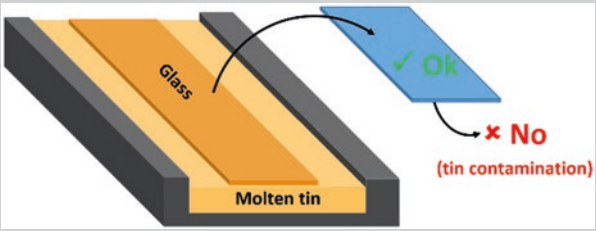

Fig. 6.7 Float glass, the side in contact with molten tin has to be discarded for elemental analysis

6.4.2 Soils

One purpose of forensic investigations of soils is, for example, to compare a sample from an item of clothing (i.e., shoes), with samples taken from known places of interest to the investigation (e.g., a crime scene) or laboratory reference samples. Other cases may be, for example, related to the illegal import of exotic plants or animals, which may bring with them variable quantities of soil from the place of origin, which can be used to hypothesize their origin. In general, there are three possible conclusions that can be drawn from these comparisons: the sample being analyzed (a) certainly does not come from the position of interest; (b) it could come from the position of interest; (c) it almost certainly comes from the position of interest. The reliability of the result depends on a number of factors: the precision and accuracy of the methods used to make the comparisons; the variability that exists in the soil properties considered in the place of interest; the degree of diversity of the place of interest with respect to the surrounding environment (Croft and Pye 2004).

In order to obtain information as reliable as possible, a multi-analytical approach should be adopted, integrating and comparing, for example, data obtained by a particle size distribution, mineralogical and color analysis, pH values and elemental chemical compositions obtained by ICP-MS analyses.

The comparison of the sample under examination with the potential soils of origin have some limitations. For example, in a common situation a portion of soil is

transported by the suspect from the crime scene. Thanks to movement, for example by simply walking, part of the soil is lost, in particular the largest and heaviest particle size fraction, sometimes significantly invalidating the measurements. In more complex situations, there are potentially more crime scenes, in this case a soil mixing may lead to a difficult solution of the problem (Jantzi 2013).

Excluding the aforementioned limitations, it can be generally stated that the elemental analysis provided by the ICP-MS technique represents a solid basis for the comparison of soils. However, it is important to consider the potential errors associated with sampling and analysis procedures. It has been shown that, in the context of soil analysis, when different solutions are prepared from the same soil sample, the standard error is about 2–3% for most of the elements. However, if the solutions are prepared from different samples taken from the same soil, the error is greater (5–6%) for many elements. Some elements are more variable than others (Pye et al. 2006b).

The extent of small-scale (<1 m x 1 m) spatial variability in soil was also investigated. It has been shown that five samples are sufficient to characterize a high percentage (about 90%) of the total variability found on average on a 1 m x 1 m grid of soil, while on average three samples represent about 70% of the total variability (Pye et al. 2006).

Another application of soil analysis, in the forensic field, concerns environmental crimes. For example, the determination of the concentrations of heavy metals, together with the variability within an area, can be useful in identifying pollutants and determining their respective sources. In these cases, the goal is not the comparison between samples, but the determination of the concentrations of each element and the comparison with the regulatory framework on environmental matters.

Bullets

A method for characterizing lead bullets is the evaluation of some physical properties such as weight, size, shape, and distinctive markings (Quatrehomme and Iscan 1998). However, ballistic investigations, which usually compare scratches and characteristic marks left on bullets, do not always provide sufficient information, and bullets may deform in such a way that no physical analysis is possible. Sometimes the only evidence is represented by bullet particles left in the victim's body (Thali et al. 2001). In these cases, the composition of the trace elements and the isotope ratio of lead can be compared with control samples. In a research three parameters were considered (lead isotopes, Sb/Pb ratio and trace element patterns), in order to compare reference bullet samples with fragments and residues sampled on victims (Ulrich et al. 2004). Bullets are usually produced using different lead alloys. The relative abundance of the different isotopes of lead (^{204}Pb, ^{206}Pb, ^{207}Pb, ^{208}Pb) depends on the age of formation of the mineral from which the metal is extracted. The isotope ratios are measurable by ICP-MS. The trace elements

(continued)

typically found in lead alloys are Cu, As, Ag, Cd, Sn, Sb, Te and Bi. Results suggest that the most discriminating element between the types of bullets seems to be the concentration of antimony, while the concentrations of the other elements do not seem to be relevant. In general, the manufacturer does not control the concentration of trace elements (except antimony, which affects the properties of the alloy itself), and uses raw materials that may vary over time. Furthermore, metallurgical phenomena such as segregation, preferential oxidation or stratification can occur, which affect the concentrations of the elements. The isotope ratios of lead, although they seem less variable within samples of bullets from the same manufacturer, may vary when the manufacturer changes supply of the raw material, or uses recycled raw materials. It can be argued that two bullets that have a similar composition might be of the same type, but not that they are definitely the same.

6.4.3 Biological Tissues

Our body contains about 2.5% of metals (the most abundant is calcium), and they are essential for our life (i.e., sodium, potassium, magnesium, zinc, cobalt, selenium). Other metals that have not any active role in human biological pathways, but occurring in our body as ubiquitous in the environment, may exert toxicity when their concentration in our tissues exceeds certain thresholds.

ICP-MS fits the needs in performing a multi elemental analysis in blood, urine, nails and hair (Goullé et al. 2009, 2014). Blood and urine analysis are useful to assess acute and chronic exposure to some elements, while hair and nails are cumulative biomarkers of long-term exposure, each centimeter of hair approximately representing one month of exposure; actually, dating the exposure can provide useful information for forensic purpose (Table 6.1).

Blood, urine and hair specimen are required to differentiate a single exposure from chronic contact by segmentation of the hair for a stated growth period. Fingernails and toenails contain more disulfide chemical groups that retain more metals (Goullé et al. 2009). Moreover, nail growth is more regular than hair and it is less affected by cosmetics and external pollution. Nails are considered better biomarkers than hair to monitor element overall exposure. Arsenic and mercury are two examples of metals studied in body tissues since they can cause poisoning. Arsenic exposure is usually due to contaminated groundwater, while mercury exposure is currently due to seafood, but in the past, it also came from dental amalgams.

Table 6.1 Typical concentration of some metals in blood and nails in healthy individuals

Element	Whole blood (μg/kg)	Fingernail (μg/kg)	Toenail (μg/kg)
^{7}Lithium	<1.2	19	30
^{9}Beryllium	<0.03	5	5
^{51}Vanadium	<0.21	32	29
^{52}Chromium	0.55	420	1140
^{55}Manganese	8.6	360	360
^{59}Cobalt	0.27	17	13
^{60}Nickel	0.80	910	380
^{65}Copper	937	6500	3600
^{66}Zinc	5617	108,000	83,000
^{75}Arsenic	1.87	72	86
^{82}Selenium	110	740	680
^{85}Rubidium	1794	170	480
^{88}Strontium	14.5	540	940
^{98}Molybdenum	0.40	14	7
^{107}Silver	<0.15	170	28
^{111}Cadmium	0.34	31	11
^{118}Tin	0.34	350	100
^{125}Tellurium	0.14	0.3	0.3
^{137}Barium	<0.66	650	560
^{182}Tungsten	<0.03	2	1
^{195}Platinum	<0.008	0.2	0.1
^{202}Mercury	1.72	200	160
^{205}Thallium	0.021	0.3	0.5
^{208}Lead	12.5	720	460
^{209}Bismuth	<0.03	11	4
^{238}Uranium	<0.001	3	2

Adapted from Goullé et al. (2009) and Cesbron et al. (2013)

Thallium Poisoning

The Thallium (Tl) poisoning was very common in the past, especially in murder cases, the authors of such crimes taking advantage of its high toxicity and its peculiar characteristics (colorless, tasteless, odorless). In the biological processes, thallium behaves similarly to potassium, but with an affinity 10 times higher, replacing it in a series of enzymatic complexes. The lethal dose in men is estimated to be between 8 and 12 mg/kg; the lethal plasmatic concentration is considered to be between 0.5 and 11 micrograms/mL.

Thanks to its properties it rapidly disappears from biological fluids, it is of difficult detection during standard toxicological analyses, even though it is rapidly distributed to several organs. Although nowadays Tl is hardly available, a case of thallium poisoning recently took place in Italy. In 2017, eight

(continued)

members of the same family started to show common symptoms, such as dysentery, nausea, vomit, swelling and fever and they were hospitalized (Di Candia et al. 2020). High plasmatic and urinary concentration of thallium were detected, then it was carried out a chelation therapy with Prussian blue. The investigations evidenced a high dosage of thallium sulphate in the infusion that was regularly drunk by the whole family every afternoon. The father and the oldest daughter deceased 2 days after hospitalization, the mother after 14 days while the other 5 members of the family survived (Table 6.2).

The investigators proved that the author of the crime was the grandson of the victims. The high concentrations of thallium in biological matrices (cardiac blood, urine, gastric content and hair) sampled from the three victims during autopsy examination, was assessed by ICP-MS. The presence of thallium in the first 2 cm of hair analyzed suggested that the homicide attempts had started no more than 2 months before the effective death of the three relatives of the murderer.

Table 6.2 Thallium concentrations measured in the victims. Tl concentration in healthy human is about 0.021 μg/kg

Victim	Matrix	Tl dosing at hospital (μg/kg)	Survival time	Post-mortem Tl dosing (μg/kg)
Father	Blood	3400	2 days	2750
	Urine	22,000		1490
	Gastric content	–		1930
	Hair	–		11,110
Daughter	Blood	10,000	2 days	6010
	Urine	42,000		0
	Gastric content	–		3430
	Hair	–		5720
Mother	Blood	5700	14 days	1150
	Urine	16,300		0
	Gastric content	–		1110
	Hair	–		10,380

Adapted from Di Candia et al. (2020)

Printing Inks

The identification of printing inks and its discrimination represents a precious contribution to forensic science (Trejos et al. 2014). In this regard, a careful study was carried out on hundreds of printing inks (belonging to four types:

(continued)

inkjet, toner, offset and intaglio) analyzed directly on the paper substrate by scanning electron microscopy-energy dispersive spectroscopy (SEM-EDS) and LA-ICP-MS (Corzo et al. 2016). The high sensitivity of LA-ICP-MS analyses resulted in excellent discrimination between different ink samples from each of the four ink types and almost 100% correct associations between ink samples known to originate from the same source. Furthermore, when toner and inkjet samples of the same color (cyan, magenta, yellow, or black) were compared, LA-ICP-MS was still able to provide discrimination greater than 97% within each color. SEM-EDS offered both imaging and elemental analysis capabilities, which is particularly important for toner samples as differences in the morphology of the toner particles provided an additional means of differentiation for the set of samples analyzed. A comparison between toners of the same color provided a sample discrimination higher than 94% whereas inkjet samples of the same color gave even better results for cyan, magenta, and yellow inks compared to the very poor values (<50%) of the black inkjets. Although more elements were detectable for the offset samples, compared to inkjet and toner inks, contribution from the paper substrate, as well as the fact that the offset inks penetrate deeply into the paper fibers, led to a relatively poor discrimination (~80%). Interestingly, SEM-EDS provided some complementary information to LA-ICP-MS for the toner, inkjet, and offset samples. Several elements (e.g., K, Fe, Ca, S, Si, Cl) that were difficult to detect by LA-ICP-MS due to polyatomic interferences were easily detected by SEM-EDS and allowed for the differentiation of some pairs that were indistinguishable by LA-ICP-MS.

References

Almirall JR (1999) Elemental analysis of glass fragments. In: Caddy B (ed) Forensic examination of glass and paint. Taylor & Francis, London, pp 65–80

Almirall JR (2001) Glass as evidence of association. In: Houck M (ed) Mute witness; when trace evidence makes the case. Academic, San Diego, pp 139–155

Barca D, Belfiore CM, Crisci GM, La Russa MF, Pezzino A, Ruffolo SA (2010) Application of laser ablation ICP-MS and traditional techniques to the study of black crusts on building stones: a new methodological approach. Environ Sci Pollut Res 17:1433–1447

Barca D, De Francesco AM, Crisci GM (2007) Application of Laser Ablation ICP-MS for characterization of obsidian fragments from peri-Tyrrhenian area. J Cult Herit 8(2):141–150

Cesbron A, Saussereau A, Mahieu L, Couland I, Guerbet M, Goullé JP (2013) Metallic profile of whole blood and plasma in a series of 106 healthy volunteers. J Anal Toxicol 37:401–405

Corzo R, Subedi K, Trejos T, Almirall JR (2016) Evaluation of the forensic utility of scanning electron microscopy-energy dispersive spectroscopy and laser ablation-inductively coupled plasma-mass spectrometry for printing ink examinations. J Forensic Sci 61:725–734

Croft DJ, Pye K (2004) Stable carbon and nitrogen isotope variations in soils: forensic applications. In: Pye K, Croft DJ (eds) Forensic geoscience: principles, techniques and applications. Geological society special publication 232. Geological Society Publishing House, London, pp 257–267

Di Candia D, Muccino E, Battistini A, Boracchi M, Gentile G, Zoja R (2020) Thallium toxicity due to adultered infusion with thallium sulfate in eight members belonging to the same family nucleus: autopsy findings and ICP-MS analysis (inductively coupled plasma mass spectrometry) in a triple homicide. Legal Med 42:101661

Duckworth DC, Bayne CK, Morton SJ, Almirall JR (2000) Analysis of variance in forensic glass analysis by ICP-MS: variance within the method. J Anal At Spec 15:821–828

EPA METHOD 6020B (SW-846): Inductively Coupled Plasma – Mass Spectrometry

Fryer BJ, Jackson SE, Longerich P (1995) The design, operation and role of the Laser -Ablation Microprobe Coupled with an Inductively Coupled Plasma- Mass Spectrometer (LAM – ICP – MS) in the Earth Sciences. Can Mineral 33:303–312

Goullé JP, Saussereau E, Mahieu L, Bouige D, Groenwont S, Guerbet M, Lacroix C (2009) Application of inductively coupled plasma mass spectrometry multielement analysis in fingernail and toenail as a biomarker of metal exposure. J Anal Toxicol 33:92–98

Goullé JP, Saussereau E, Mahieu L, Guerbet M (2014) Current role of ICP-MS in clinical toxicology and forensic toxicology: a metallic profile. Bioanalysis 17:2245–2259

Hughes JC, Catterick T, Southeard G (1976) The quantitative analysis of glass by atomic absorption spectroscopy. Forensic Sci 8:217–227

ISO 17294-2:2016 Water quality -- Application of inductively coupled plasma mass spectrometry (ICP-MS)

Jantzi SC (2013) Elemental Analysis and Forensic Comparison of Soils by Laser-Induced Breakdown Spectroscopy (LIBS) and Laser Ablation Inductively Coupled Plasma Mass Spectrometry (LA-ICP-MS) (2013). FIU Electronic Theses and Dissertations 967

Koons RD, Fielder C, Rawalt R (1988) Classification and discrimination of sheet and container glasses by inductively coupled plasma atomic emission spectrometry and pattern recognition. Forensic Sci Int 33(1):49–67

Longerich HP, Jackson SE, Gunther D (1996) Laser ablation inductively coupled plasma mass spectrometric transient signal data acquisition and analyte concentration calculation. J Anal At Spectrom 11:899–904

Mester Z, Sturgeon R (2003) Sample preparation for trace element analysis, vol 41. Elsevier Science

Montero S (2002) Trace elemental analysis of glass by inductively coupled plasma-mass spectrometry (ICP-MS) and laser ablation-inductively coupled plasma-mass spectrometry (LA-ICP-MS). Ph.D. Dissertation. Florida International University, Florida

Nelms SM (2005) Inductively coupled plasma mass spectrometry. Handbook Blackwell Publishing Ltd

Orellana FA, Gálvez CG, Orellana FA, Gálvez CG, Roldán MT, García-Ruiz C, Roldán MT, García-Ruiz C (2013) Applications of laser-ablation-inductively-coupled plasma-mass spectrometry in chemical analysis of forensic evidence. TrAC – Trends Analyt Chem 42:1–34

Pye K, Blott SJ, Croft DJ (2006) Carter J.F., Forensic comparison of soil samples: Assessment of small-scale spatial variability in elemental composition, carbon and nitrogen isotope ratios, colour, and particle size distribution. Forensic Sci Int 163:59–80

Pye K, Blott SJ, Wray D (2006b) Elemental analysis of soil samples for forensic purposes by inductively coupled plasma spectrometry—precision considerations. For Sci Int 160:178–192

Quatrehomme G, Iscan MY (1998) Analysis of beveling in gunshot entrance wounds. Forensic Sci Int 93:45–60

Russo RE (1994) Laser ablation. In: Holcome J, Hiefte G, Majidi V (eds) Focus on analytical spectrometry: a compendium of applied spectroscopy focal point articles. Society for Applied Spectroscopy, MD, pp 41–55

Sèbastien A, Valladon M, Polvè Duprè M (2000) A routine method for oxide and hydroxide interference corrections in ICP-MS chemical analysis of environmental and geological samples. J Geostand Geoanal 24:19–31

Suzuki Y, Sugita R, Suzuki S, Marumo Y (2000) Forensic discrimination of bottle glass by refractive index measurement and analysis of trace elements with ICP-MS. Anal Sci 16:1195–1198

Thali MJ, Kneubuehl BP, Dirnhofer R, Zollinger U (2001) Body models in forensic ballistics: reconstruction of a gunshot injury to the chest by bullet fragmentation after shooting through a finger. Forensic Sci Int 123:54–57

Trejos T, Almirall JR (2005) Sampling strategies for the analysis of glass fragments by LA-ICP-MS part I. Micro-homogeneity study of glass and its application to the interpretation of forensic evidence. Talanta 67:388–395

Trejos T, Corzo R, Subedi K, Almirall JR (2014) Characterization of toners and inkjets by laser ablation spectrochemical methods and scanning electron microscopy-energy dispersive X-ray spectroscopy. Spectrochim Acta B Atomic Spectrosc 92:9–22

Ulrich A, Moor C, Vonmont H, Jordi HR, Lory M (2004) ICP–MS trace-element analysis as a forensic tool. Anal Bioanal Chem 378:1059–1068

Zurhaar A, Mullings M (1990) Characterization of forensic glass samples using inductively coupled plasma mass spectrometry. J Anal At Spec 5:611–617

Chapter 7
Simultaneous Thermal Analysis (STA): A Powerful Tool for Forensic Investigation of Geomaterials

Mariano Mercurio, Francesco Izzo, Alessio Langella, and Binoy Sarkar

Abstract The use of thermal methods has become common in modern geomaterial analysis laboratories. The simultaneous thermal analysis (STA) represents a valid support for the definition of the physical behavior of concerned samples, once subjected to a temperature variation. This chapter discusses the thermal behaviors of key mineralogical phases present in soils, in order to provide the readers with a valuable tool for optimizing the compatibility and applicability of the STA method in judicial forensic test purposes. To this end, the chapter presents literature evidences and case studies, including those from the authors' own studies, where the STA methods have been successfully used in the judicial forensic field.

Keywords Thermal analyses · Thermogravimetry · Differential scanning calorimetry · Forensic science · Evolved gas analysis · Minerals

Any material subjected to an increase of temperature shows the variation of some of its physical and chemical properties (Table 7.1). The main processes that can occur are: melting, vaporization, crystallization, volume and weight variations, phase transitions (solid-to-solid), as well as changes in the mechanical behaviour and enthalpy. On the other hand, chemical reactions such as oxidation-reduction, corrosion, decomposition, dehydration/dehydroxylation, adsorption/desorption processes can also occur (Robinson et al. 2005; Wagner 2017). There are several factors that can

M. Mercurio
Dipartimento di Scienze e Tecnologie, Università degli Studi del Sannio, Benevento, Italy
e-mail: mamercur@unisannio.it

F. Izzo (✉) · A. Langella
Dipartimento di Scienze della Terra, dell'Ambiente e delle Risorse (DiSTAR), Università Federico II, Napoli, Italy
e-mail: francesco.izzo4@unina.it; alessio.langella@unina.it

B. Sarkar
Future Industries Institute, University of South Australia, Mawson Lake, Australia
e-mail: binoy.sarkar@unisa.edu.au

M. Mercurio et al. (eds.), *Mineralogical Analysis Applied to Forensics*, Soil Forensics, https://doi.org/10.1007/978-3-031-08834-6_7

Table 7.1 Main chemical and physical thermal reactions observable on thermoanalytical curves

Reaction type			DSC/ DTA	TG
Chemical reactions	Thermal decomposition	Dehydration	Endo.	Mass-loss
		Dehydroxylation	Endo.	Mass-loss
		Thermal dissociation	Endo.	Mass-loss
	Oxidation		Exo.	Mass-change
	Reduction		Endo.	Mass-loss
Physical reactions	Structural transition		Endo. or Exo.	–
	Sintering		Exo.	Eventual mass-change
	Phase transition	Melting	Endo.	Eventual mass-change
		Sublimation	Endo.	Mass-loss

Exo. exothermic, *Endo.* endothermic

influence the above phenomena, for example, temperature range, heating rate, temperature/mass calibration, atmospheric conditions of furnace, type of crucible used, and materials examined. Therefore, the use of a technique that simulates thermal cycles is essential, in terms of quality control, for test materials that are thermally stressed and for which a long-lasting shelf life is expected. For these reasons, thermal investigations become very useful for the characterization of substances, such as polymers, ceramics, paints, biomaterials, metal alloys, pharmaceuticals, textiles, cosmetics, glass, and explosives. Geological samples (i.e., minerals, rocks, soils and other geomaterials) are often subjected to this type of stress, representing a class of materials to be characterized from a thermal point of view, not only for scientific purposes but also for their use as industrial raw materials. A correct identification of this category of materials can be interesting also in forensic contexts.

The set of analytical techniques used to study the changes in physical and chemical properties as a function of temperature is generally called "thermal analysis techniques". This family includes, among others, thermogravimetric analysis (TGA) or thermogravimetry (TG) with its derivative (DTG), differential thermal analysis (DTA), differential scanning calorimetry (DSC) and the evolved gas analysis (EGA). The concerned instrumental methods represent one of the most conventional instrumental techniques for the analysis of minerals, especially for thermally reactive minerals (e.g., clay minerals and zeolites) (Bish and Duffy 1990; Bish and Carey 2001).

Nevertheless, all these techniques can be defined as destructive and not repeatable on the same portion of sample material. In addition, they can provide molecular qualitative-quantitative indications with very low concentration ranges, in the order of traces (0.5–1 wt.%).

The contribution of thermal analyses to Earth Sciences and interdisciplinary contexts is well-known (Mackenzie 1991). Nowadays, thermal analysis plays as the

main actor in the process of mineralogical characterization of geomaterials using modern thermal instrumentations, often combined with several other techniques, providing valuable information on the thermal properties of the investigated materials.

Thermal methods differ according to the properties measured and the temperature programs applied. However, thermal analyses generally require long acquisition time, which translates into a careful management of the instrumentation. Hereafter, three of the main thermal methods used in modern laboratories for the characterization of geomaterials and the methods' usefulness in the forensic field, are described.

7.1 Thermoanalytic Techniques and Instrumentation

7.1.1 Thermogravimetric Analysis (TGA)

This technique measures the mass-change of a sample as a function of temperature variations (heating or cooling), generally under isodynamic conditions. Thermal measurements can be carried out under dynamic or static temperature changes. The former generally consists of a linear and constant heating/cooling rate (usually between 5–20 °C/min) where the curve of temperature and time are linearly programmed. Under isostatic conditions, the examined sample undergoes a constant temperature (isothermal) change. It is useful for the specific characterization of some substances but can be combined with dynamic temperature changes. Both in dynamic and isostatic conditions, the weight of the sample is constantly recorded and graphically reported in a weight vs. time/temperature thermoanalytical curve (or thermogram). An example of thermogravimetric curve is given in Fig. 7.1.

During a thermogravimetric analysis, a sample can loss or gain weight. In the first case a decomposition generally occurs with release of gaseous phases, while in the second case (albeit quite rare for minerals), the sample can selectively sorb components from the furnace atmosphere such as, for example, oxygen thus leading to an oxidation process.

A typical example of thermal decomposition of minerals can be observed in the thermogravimetric curve of calcite ($CaCO_3$) when heated up to a temperature of about 900 °C (Fig. 7.1). The recorded weight loss of about 44% is due to the removal of CO_2 from the system, stoichiometrically consistent with the following reaction:

$$CaCO_{3(solid)} = CaO_{(solid)} + CO_{2(gas)} \uparrow \tag{7.1}$$

In general, the instrumentation used for the TGA is mainly composed of a highly sensitive microbalance (i.e., thermobalance), which can detect weight variations up to few micrograms, often placed below a sample holder in top-loading configuration (Fig. 7.2). The latter is surrounded by the furnace connected to a purge gas system

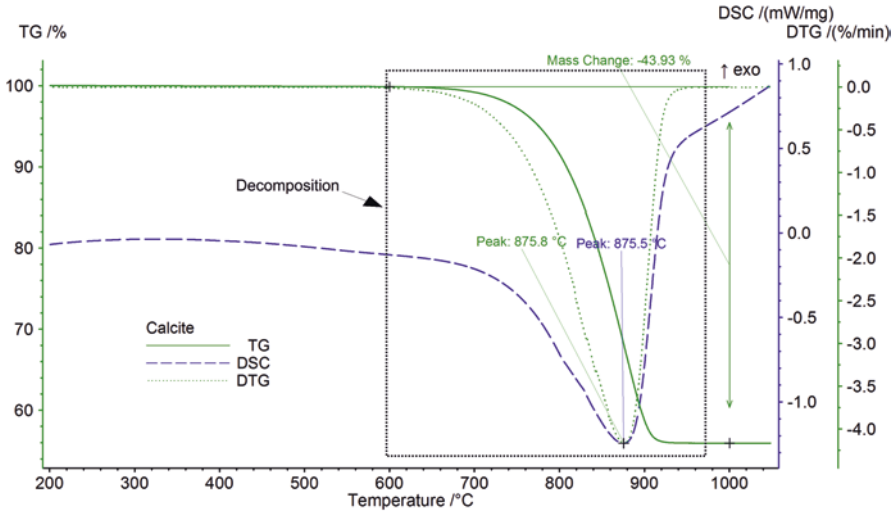

Fig. 7.1 Thermogravimetric (TG) curve of calcite. DTG and DSC curves are also reported in the figure

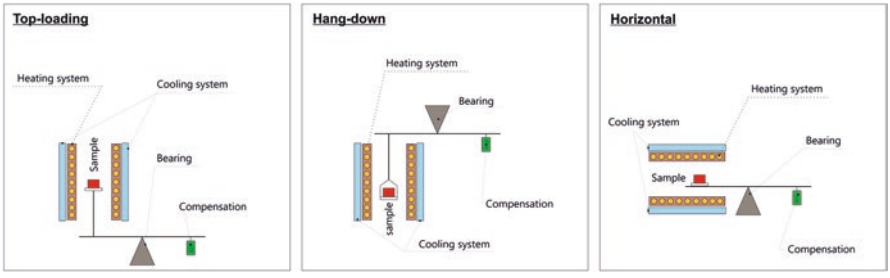

Fig. 7.2 Schematic representation of the three main geometries of thermo-balances

controlling the atmosphere (inert or reactive). Furnace is controlled by a computer that also processes data acquired from thermogravimetry (or other thermal methods). A real-time plot reports the temperature/time on abscissa and the weight variation on ordinates, expressed in milligrams (mg) or as a percentage (%). As shown in Fig. 7.2, there are three types of configurations for thermobalance: top-loading (most common), hang-down and horizontal. The difference between the three lies in the positioning of the sample in relation to the furnace and the arm of the thermobalance itself.

Different types of furnaces can be selected as a function of the maximum heating temperature, the heating/cooling rate, and the type of investigated material. For geological materials a temperature of 1500 °C can be considered a good compromise for an exhaustive thermal characterization.

Samples are usually placed into platinum, aluminium, or corundum (α-Al_2O_3) crucibles. The platinum ones are the most expensive, as they are inert and easy to clean. Nevertheless, α-Al_2O_3 crucibles are those most used for the characterization of geomaterials. Modern TGA instruments are often equipped with an autosampler.

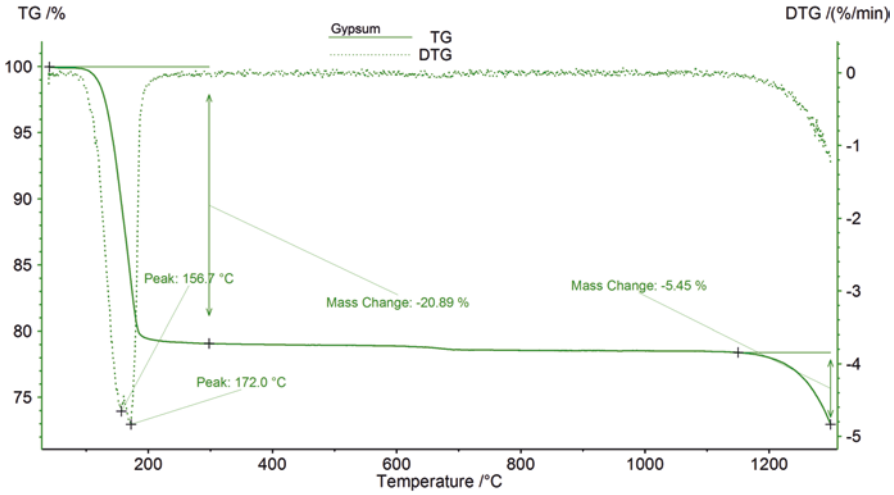

Fig. 7.3 Thermogravimetric and derivative thermogravimetric curves of gypsum

A reliable interpretation of a thermogravimetric analysis requires, in most cases, a processing of TGA curve such as a first derivative (DTG). DTG processing provides useful information about the rate of weight change ($d(w)/dt$) during the heating process and allows to better define the thermal range in which a specific thermal reaction occurs as well as its representative temperature (DTG peak). An example of DTG curve reported for gypsum in Fig. 7.3 well represents the importance of this derivative technique in the study of minerals. The most modern TGA are equipped with software that elaborates the DTG curve for each single acquired thermogram.

Finally, it is necessary to highlight the possible sources of error that normally invalidate the thermogravimetric data. First, the instrument must be placed away from sources of vibration and heat to minimize the fluctuations and/or drifts of the thermobalance, even if the main problem affecting the TGA lies in the floating phenomenon, known as Buoyancy effect, especially in top-loading configuration. This phenomenon is due to the fact that the analysed sample, once placed in an atmosphere that gradually heats up, is subject to an apparent weight increase as a result of the change in the density of the gas medium in the furnace when temperature increases.

Buoyancy effect can be compensated by running a blank (empty crucible with a known composition) at a programmed atmosphere and temperature. The law governing the correction process of the Buoyancy effect can be summarized as follows:

$$M_c = \frac{M_{oss}\left(1-\frac{\rho_a}{\rho_s}\right)}{\left(1-\frac{\rho_a}{\rho_c}\right)} \tag{7.2}$$

Table 7.2 Densities of gaseous substances (expressed in mg/mL) usually used in thermogravimetry at different temperatures (pressure = 1 atm)

Type of gas	ρ at 298 K	ρ at 773 K	ρ at 1273 K
Ultrapure air (N_2/O_2)	1.184	0.457	0.269
Nitrogen (N_2)	1.146	0.441	0.268
Oxygen (O_2)	1.308	0.504	0.306
Argon (Ar)	1.634	0.630	0.383
Helium (He)	0.164	0.063	0.038
Carbon dioxide (CO_2)	1.811	0.698	0.424

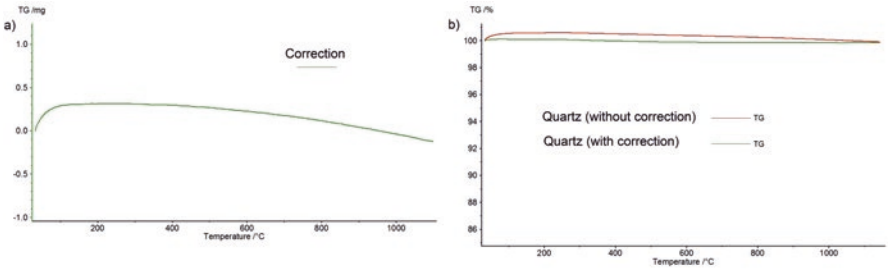

Fig. 7.4 (**a**) Example of TG correction carried out with a heating rate of 10 °C/min in nitrogen atmosphere (60 mL/min); (**b**) effect of the application of TG correction on thermogravimetric analysis of α-quartz

where M_c is the real mass of the unknown sample, M_{oss} is the mass recorded during the measurement of the unknown sample, ρ_a the density of the atmosphere, ρ_s the density of the standard sample, and ρ_c the density of the unknown sample. Furthermore, it must be considered that the density is strictly dependent on the temperature (at constant pressure) as expressed by the following equation:

$$\rho = \rho_0 \frac{T_0}{T} \tag{7.3}$$

where ρ_0 is the density of the gas at the reference temperature (T_0 = 298 K = 25 °C) and T is the temperature expressed in kelvin.

Table 7.2 reports some density values of common purge gases as a function of temperature, whereas Fig. 7.4 shows the thermograms related to (a) a Buoyancy correction carried out at 10 °C/min with a nitrogen flow of 60 mL/min and (b) a representative example of its effect induced on the thermogravimetric curve of quartz. The validity of the correction is given by the observation of a "drumlin-like profile" where the points at the initial and final temperatures should be sited along the same baseline.

Finally, another precautionary procedure concerns the selection of optimized gas flow and heating rates to reduce the turbulence effects deriving from the convective motion of the fluxing gases.

7.1.2 *Differential Thermal Analysis (DTA)*

DTA measures the difference in temperature (ΔT) between a sample and a reference material, symmetrically arranged in a furnace and simultaneously heated by a single heat source.

Figure 7.5 schematically reports the instrumentation used for the DTA experiments where both sample and standard reference with the same weight are loaded in two identical crucibles. DTA compares the temperature of the sample (T_S) and that of the reference (T_R) by continuously detecting the temperature difference between them:

$$\Delta T = T_s - T_R \tag{7.4}$$

Data are then plotted as ΔT *vs* Temperature (°C or K) or time (minutes) providing a thermoanalytical curve as shown in Fig. 7.5. When a thermal event occurs, the temperature of sample changes while the temperature of reference remains almost the same. This is mainly due to changes in enthalpy (ΔH), namely the heat content of sample that can lead to the occurrence of endothermic or exothermic reactions when the heat is adsorbed or given off by the sample, respectively. The result is therefore a curve showing upward and downward peaks which, by convention, respectively represent exothermic and endothermic reactions, schematically described in Table 7.1 and Fig. 7.5.

Endothermic reactions in minerals are, for example, dehydration/dehydroxylation of clay minerals, decomposition of carbonates, orthorhombic to monoclinic phase transition of sulfur, etc. On the other hand, exothermic reactions in mineralogical investigations are mainly represented by oxidation-reduction of iron, most of the polymorphic transition, sintering of clay minerals, etc. It is worthy that some of these physical changes and chemical reactions can occur also without mass changes (e.g., polymorphic transitions). Therefore, DTA can potentially record more thermal events than TG.

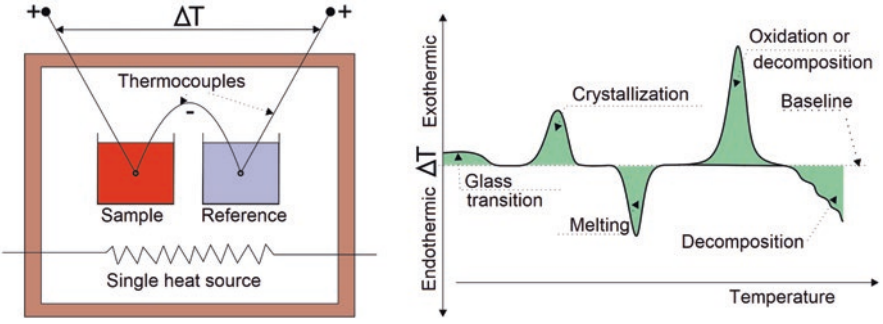

Fig. 7.5 (**a**) Schematic representation of DTA instrumentation and (**b**) some thermal events observable

The area underlying DTA peaks (both endo and exothermic ones) can give useful information on parameters such as: the change in enthalpy ΔH, the mass of the sample (m), and other factors such as the geometry and thermal conductivity of the examined material. These other factors are regulated by a constant K which is related to the peak area (A) using the following formula:

$$A = K(m)(\Delta H) \tag{7.5}$$

Unfortunately, the constant K is strongly dependent on the temperature and requires multiple and time-consuming calibrations. Therefore, DTA is not considered as an elective technique for quantitative measurements, for which the DSC technique is more reliable.

7.1.3 Differential Scanning Calorimetry (DSC)

Unlike the DTA that records temperature differences between sample and reference material, this technique continuously measures the energy differences during the experiment and is generally considered a more reliable method for the measurement of enthalpy changes and heat capacity. The resulting thermogram provides an accurate calorimetric analysis with high precision and sensitivity even in cases where the quantities of sample to be investigated are very small, down to a few milligrams.

There are two types of DSC instrumentation: power-compensated DSC and heat-flux DSC, schematically represented in Fig. 7.6. The power-compensated DSC has two separate heating elements: one for the sample and one for the standard. The detection of a different temperature acts as a signal for one of the two heating elements to be activated to bring the sample and the reference at the same temperature. This happens every time a thermal event occurs in the sample (for example: phase changes, glass transitions, dehydroxylation, etc.) and then the system requires

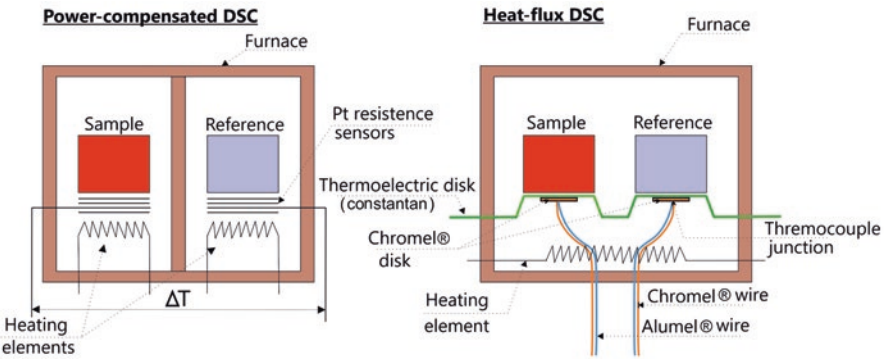

Fig. 7.6 Schematic representation of DSC instrumentation

current to heat again the cooler cell. Therefore, throughout the experiment, the temperatures of both heating elements are always kept the same, and the instrument continuously provides a measure of the power required to rebalance the thermal system. The electrical power-compensation is shown on a diagram (expressed in mW/mg) together with the temperature values.

In the case of heat-flux DSC, the same furnace heats both the sample and the reference and when the heating temperature changes, if thermal events occur, the difference in heat flow generated between the sample and the reference is detected. The crucibles, made up of different materials (corundum, platinum, gold, stainless steel, glass ampoules), are placed onto thermoelectric disks made of constantan (60% copper and 40% nickel). Below them, there are chromel® disks connected to thermocouples made of chromel® and alumel® wires which detect the difference in signal that is generated between the two samples during the reactions, directly proportional to the flow of differential heat generated inside the two crucibles. For this technique, the heat flux dH/dt can be described by the following expression:

$$\frac{dH}{dt} = C_p \frac{dT}{dt} + f\left(T,t\right) \tag{7.6}$$

where H represents the enthalpy in $Jmol^{-1}$, C_p is the specific heat capacity (heat capacity per mole) in JK^{-1} mol^{-1} and f(T, t) is the kinetic response of the sample expressed in $Jmol^{-1}$. It follows that the total heat-flux is closely related to the heat capacity and the kinetic response of the sample. An increase in heat flux suggests an exothermic reaction, while a reduction indicates an endothermic process.

7.1.4 Hyphenated Techniques

STA represents today the most used thermal acquisition system for the characterization of organic and inorganic materials. The most modern thermobalances can operate simultaneously for the acquisition of information related to heat flow DSC or DTA signals. There are several advantages deriving from the use of this combined technique, among which the most important are: i) the decrease in acquisition times and consequent economic/energy saving, ii) the ability to read simultaneously signals concerning thermal reactions that do not involve weight-changes (melting, recrystallization, or glass transitions), iii) more accurate evaluations and processing of signals.

STA provides a correct identification and characterization of unknown materials, and above all quantitative measures of differential heat flows (ΔH) and thermal capacities (Cp). STA instruments can cover a very wide temperature range in the furnace (−150 to 2400 °C), with adequate heating and cooling rates and very accurate resolutions.

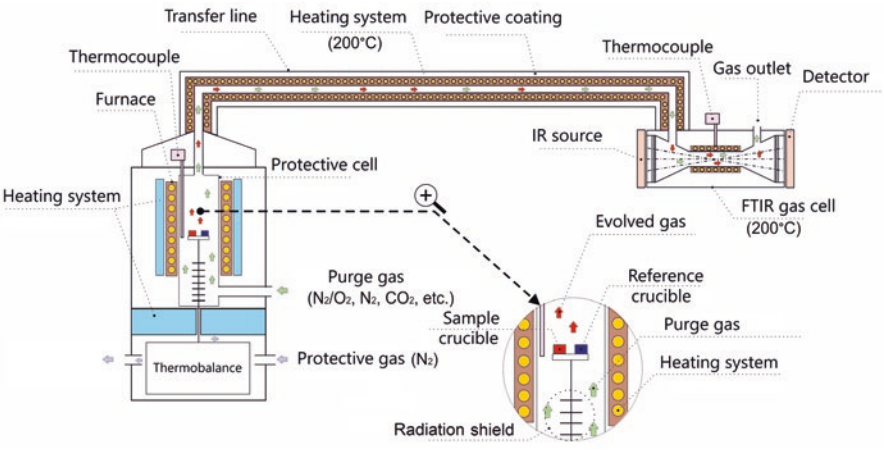

Fig. 7.7 Schematic representation of TG/DSC instrumentation couple to FTIR-EGA

The thermal response of both organic and inorganic material is often characterized by the production of gas phases that can be analysed at various levels of detail using specific techniques such as infrared spectroscopy or mass spectrometry (MS). The latter sometimes combined with gas chromatography (GC).

Evolved Gas Analysis (EGA) is generally performed while the substance under test is subjected to a controlled and well-defined thermal condition. The gaseous products are conveyed from the furnace to the preselected instrument through a transfer line preheated to about 200 °C to avoid condensation phenomena (Fig. 7.7). In modern STA, gas analyser is directly connected to the upper end of the furnace thus limiting any delay in the transfer of gases from the furnace or their excessive dilution. To facilitate the natural upward path of the evolved gas (the so-called "chimney effect") a top-loading thermobalance configuration is usually preferred. This also avoids the condensation of the gases emitted on other components of the system which could in turn cause "memory effects" on subsequent measurements, compromising the reliability of the analysis itself.

EGA-FTIR probably represents one of the most common analytical approaches and is based on the principle that the energy transferred to a molecule, by an incident infrared radiation, is converted into vibrational energy (for further details refer to Chap. 4). The infrared radiation usually used for EGA ranges between 2.5 and 25 μm, i.e., in the wavenumber range between 4000–400 cm^{-1} (medium infrared).

From the interaction of infrared radiation with matter, a selective absorption of the radiation by the investigated material is obtained, which returns a spectrum reporting bands representative of the functional groups contained in the examined gaseous phase. This allows an easy interpretation of the spectra through the graphic comparison with the spectra of substances of known composition, collected in specific databases. A limitation of EGA-FTIR is the impossibility of detecting homonuclear diatomic molecules, such as N_2, O_2, and H_2. However, such a drawback is

advantageously exploited as evolved gases are conveyed into the FTIR cell through purge gases as nitrogen and pure air (mixtures of N_2 and O_2). Finally, it should be noted that quantitative analyses using infrared spectroscopy are rarely used due to the low sensitivity of the instrument.

7.2 Sample Preparation

A reliable comparison of the outputs of thermal analyses performed in different moments and using different methods is deeply influenced by factors, such as, sample preparation, investigation procedure, or by the analysis program set up by the operator. These are factors that, although controllable, require a proper use of these techniques, especially if applied to the forensic field.

Samples for thermal analysis are generally grinded and powdered by means of special micronizing mills or simply by using an agate mortar. Since the samples are often very heterogeneous materials, the quantity usually used (a few tens of milligrams) may not be representative of the sample itself. In this case, the representativeness of the sample can be maximized by sub-sampling procedures, such as the coning and quartering methods. Moreover, in comparative studies, a variable content of water retention (hygroscopic, capillary and film) linked to the different phases occurring in the sample or to the state of conservation of the material itself, should be properly considered. In some cases, it is advisable to eliminate this amount of water with a preheating stage at about 100 °C; any dehydration will be therefore attributable to the intrinsic properties of the sample (mineralogical composition, texture, etc.).

Once a sufficiently homogeneous and representative powder has been obtained, it is important to take into consideration that the repeatability of the test is also greatly influenced by the initial weight of the sample. In fact, even if the weight losses remain unchanged, it is possible to observe a clear difference in the decomposition temperatures (onset) of identical materials under the same operating conditions but with different starting weight. In particular, the greater is the initial mass of the sample, the higher will be the dissociation temperature, as it is controlled by the kinetics.

The particle size of the sample also plays a crucial role in the thermal response of the material examined. In fact, the possibility that a component is released by evaporation, sublimation or decomposition strongly depends on the specific surface area. Consequently, a much finer ground material will exhibit a thermal response at lower temperatures than a sample, representative of the same material, but with a larger grain size.

However, as previously reported, the operating condition that most affects the repeatability of thermal analyses is the heating rate. In general, a rapid increase in temperatures may define a delay in recording the diagnostic temperature of a specific modification which defines a mass-change.

The reactions that can occur by heating in presence of organic components, are deeply influenced by the nature of the gases used in the furnace. In particular, the use of pure air (N_2/O_2) involves the oxidation of the organic matter and therefore its combustion will take place at definitely different temperatures compared to the decomposition of the same material in an inert atmosphere (pyrolysis).

In conclusion, in order to ensure correct repeatability of the test or to make a reliable comparison with the results from other labs, it is necessary to keep constant the operating conditions and methods of sample preparation within the same group of samples. In other words, the heating rate, the nature of the gases in the furnace and their fluxing rate, the calibration of the instrument and the type of crucible used should remain unchanged. Within the limits established by common laboratory practice, it is also necessary that the weight and particle size of the sample be as similar as possible to each other.

7.3 Thermal Behavior of Minerals and Their Mixtures

For a correct interpretation of the thermal curves of a polyphasic mixture it is necessary to have a clear idea of the thermal responses of its individual constituents.

The International Mineralogical Association (IMA) officially approved 5312 of the approximately 5500 mineralogical species discovered and/or hypothesized so far. It appears evident that it is not possible at this stage to provide a complete list and an exhaustive description of each of the existing mineralogical phases, although further investigations can be referred to the specific literature (Bish and Duffy 1990; Robinson et al. 2005; Viczián 2013; Wagner 2017).

Therefore, in this section the thermal behaviours of some of the most common and simple minerals will be described, trying to contextualize their thermal response within a polyphasic mixture of potential forensic interest. The materials and scientific instrumentation used for the realization of this chapter were made available by the Department of Science and Technology of the University of Sannio (Benevento, Italy). STA was performed with a Netzsch Jupiter STA449 F3 instrumentation, while the EGA-FTIR was performed with a Bruker Tensor 27 spectrometer connected to the furnace with a transfer-line heated to about 200 °C. The analyses were carried out in an oxidizing atmosphere (80% N_2 and 20% O_2), with a heating ramp of 10 °C/min.

7.3.1 Clay Minerals

One of the main products resulting from the thermal decomposition of numerous thermally active minerals is certainly water. It is contained in various forms in hydrate minerals and can be released following different kinetics and mechanisms, depending on the type of mineral examined. Following heating, water is released as water vapour and can be easily identified by means of EGA-FTIR (Fig. 7.8).

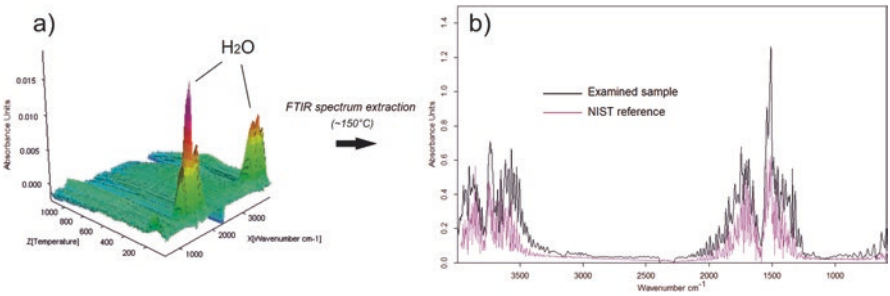

Fig. 7.8 Identification of water vapour, by means of EGA-FTIR, released by dehydration of a smectite during thermogravimetric analysis: (**a**) 3D EGA-FTIR plot; (**b**) Comparison of a FTIR spectrum extracted at ~150 °C and a NIST (National Institute of Standards and Technology) reference spectrum

Excluding the so-called free water, which can be removed by gravity, and capillary retention water, which can be removed by drying at about 100 °C, water in the minerals can be adsorbed on the surface of the crystal or be strongly linked to the crystal lattice, where it coordinates some of the cations contained therein. In the latter case, it is evident that the release process requires greater energy and consequently higher temperatures than those necessary to remove the water adsorbed on the surface of the mineral. By adjourning the discussion to specific literature, we can briefly state that the mineral-bound water can be removed by dehydration and/or dehydroxylation. These reactions involve a reduction in the mass of the sample examined with the consequent formation of a so-called "step" on the thermogravimetric curve. Dehydration and dehydroxylation are typical, but not exclusive, of the clay minerals (Fig. 7.9).

Clay minerals are the main mineralogical constituents of incoherent sediments (soils) with a grain size of less than 2 μm. Clay minerals are phyllosilicates, namely silicates characterized by a layered structure with tetrahedral and octahedral coordination, often affected by isomorphic substitutions that lead to an excess of negative charges on the surface of the mineral. These charges are partially or totally compensated by cation exchange and water adsorption. Clay minerals can be very important from an investigative point of view as they represent the main constituents of forensic soils (Fitzpatrick and Raven 2012). Furthermore, they are widely used in the production of building materials such as, for example, cement, hydraulic lime and bricks, as well as in geotechnical applications (drilling muds). They are also used in the medical-health field as active ingredients or excipients in pharmaceutical and cosmetic formulations, as well as in mud therapy (Carretero and Pozo 2009). Finally, it should be remarked that some clay minerals (for example, chrysotile and palygorskite) have a fibrous habit and belong, like many other fibrous minerals, to the category of asbestos, minerals that are highly harmful to human health.

The correct identification of clay minerals is mandatory for an adequate characterization of the materials, often involved in forensic disputes (infringement of tender conditions, crimes against human health and environment, geotechnical damage of building structures, etc.).

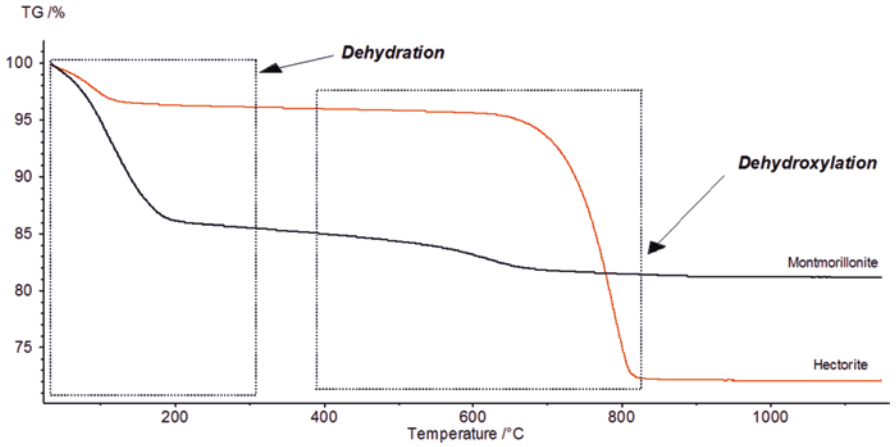

Fig. 7.9 Dehydration and dehydroxylation of a montmorillonite (dioctahedral smectite) and a hectorite (trioctahedral smectite) during thermogravimetric analyses

Given the large number of mineralogical species falling within this subclass of silicates, the interpretation of the thermal behaviour of phyllosilicates can be extremely complex, due to their high chemical variability, and consequently requires the intervention of specialized mineralogists. For the sake of simplicity, we will start describing the thermal behaviour of those phases characterized by a relatively constant structure and chemical composition which reflect in a homogeneous thermal behaviour, such as kaolinite $Al_2Si_2O_5(OH)_4$ and halloysite $Al_2Si_2O_5(OH)_4 \cdot H_2O$ (newly formed minerals typical of soils in humid warm climates). Kaolinite is characterized by just two single thermal events, the first one consisting in a weight loss of about 14% due to the dehydroxylation process (endothermic event), with a maximum reaction rate at about 550 °C (Fig. 7.10). The calcination product is metakaolinite ($Al_2Si_2O_7$), an anhydrous kaolinite widely used as an artificial pozzolana.

The second event consists of an exothermic reaction at about 1000 °C without weight loss, attributable to the polymorphous transition of metakaolinite into other crystalline phases (mainly mullite and amorphous silica). These two events can be summarized through the following reactions:

$$Al_2Si_2O_5\left(OH\right)_4 \overset{\sim 550°C}{\rightarrow} Al_2Si_2O_7 + 2H_2O \uparrow \tag{7.7}$$

$$3Al_2Si_2O_7 \overset{\sim 1000°C}{\rightarrow} Al_6Si_2O_{13} + 4SiO_2 \tag{7.8}$$

Mullite is a mineral with high refractory properties and very resistant to chemical attacks (acids and alkalis). For this reason (but not only), kaolinite is considered as one of the main ingredients in the production of ceramic materials. In addition, kaolinite is widely used in industry for the production of cosmetics, paints and paper, as well as for improving the rheological properties of plastics and rubbers.

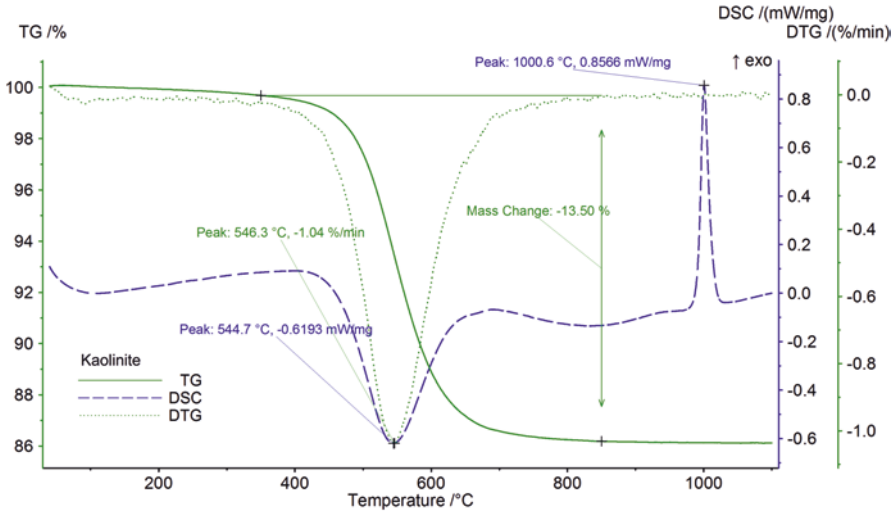

Fig. 7.10 TG, DTG and DSC curves of kaolinite

Halloysite has a thermal behaviour very similar to that observed for kaolinite. However, the presence of interlayer water molecules entails, after dehydration, a greater volumetric contraction, sometimes setting significant limits in its use in the production of ceramics.

Kaolinite and halloysite fall in the category of 1:1 phyllosilicate that is characterized by layers consisting of a superimposition of tetrahedral (T) and octahedral (O) coordination sites (for this reason also known as sheet silicates). The single T-O structures are held together by hydrogen bonds with almost constant or little variable basal distances. The T-O-T structures (i.e., 2:1) are held together by weak bonds (van der Waals) which allow to host greater quantities of cations and water molecules in the interlayer area, with consequent increase in basal distances. Based on these premises, it can be seen that T-O-T clay minerals have, compared to T-O ones, a greater structural and compositional variability, which limits an unambiguous identification of their thermal features. Typical examples of minerals having this structure are smectite and illite.

Among the clay minerals, smectites are those with the greatest swelling ability, thanks to their predisposition to trap considerable water contents in the interlayer area. As reported in the TGA of montmorillonite in Fig. 7.9, a marked dehydration is observed within 200 °C followed, at higher temperatures (~630 °C), by a moderate dehydroxylation. The dehydration temperature is usually a function of the water amount, while the presence of endothermic peaks often depends on the stereochemical features of the interlayer cations. In the case of dehydroxylation, the characteristics of the reaction depend on the stereochemistry of the cations in octahedral coordination and consequently on the bond that is established with the relative hydroxyl groups. In the trioctahedral structures, the presence of magnesium defines a more homogeneous cationic distribution which turns in significantly higher

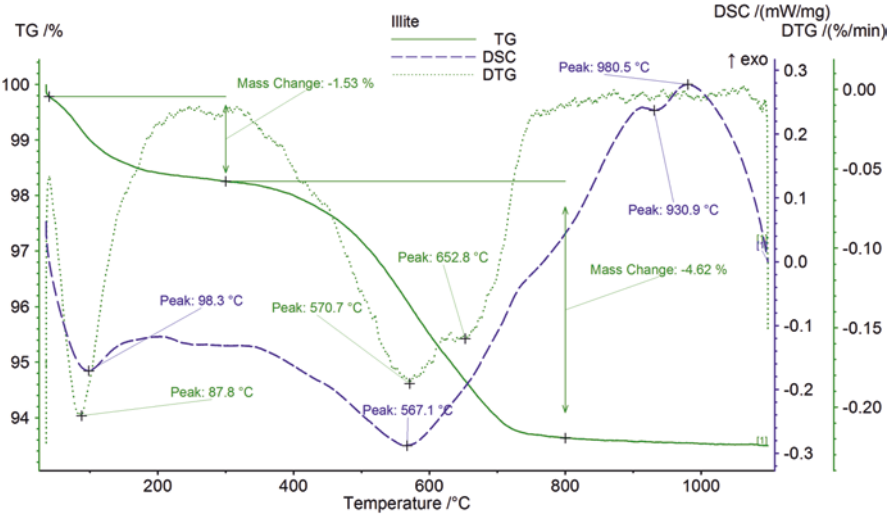

Fig. 7.11 TG, DTG and DSC curves of illite

dehydroxylation temperatures. This is well depicted by the comparison (Fig. 7.9) between a thermal analysis of a dioctahedral smectite (montmorillonite) and of a trioctahedral smectite (hectorite). In the latter, the dehydroxylation is predominant. Other expandable clayey minerals are those belonging to vermiculite group (T-O-T). The thermal analysis of vermiculite shows a double dehydration event: the first one (~100 °C) refers to the loss of surface adsorption water, the second (~185 °C) to the release of interlayer water. In addition, an evident and slow dehydroxylation occurs starting from about 800 °C, accompanied by a succession of endo-exothermic peaks indicating a concomitant recrystallization in enstatite or more generally in *biopyriboles,*[1] up to complete sintering (exothermic peak at ~1000 °C).

Illite is generally much less expandable than smectite and vermiculite. Therefore, water content is usually lower, as highlighted by the first less pronounced endothermic peak in DSC curve (Fig. 7.11). By contrast, dehydroxylation provides a much wider endothermic peak that extends up to about 800 °C. Finally, as in most phyllosilicates, high temperature endo-exothermic reactions are generally attributable to the completion of dehydroxylation and/or collapse of the structure with subsequent recrystallization of new phases.

T-O-T clay minerals such as pyrophyllite do not allow significant cationic substitutions, therefore their structure is simply characterized by alternating tetrahedral and octahedral sheets, with a single and wide dehydroxylation effect. In other phyllosilicates such as micas the dehydroxylation can extend up to ~1000 °C.

[1] The term *biopyribole* was coined by Johannsen (1911) and has been used as acronym for **bio**tite, **pyr**oxene and amph**ibole**. It is a collective noun that generally describe the close kinship between the crystallochemical structures of these minerals (Thompson 1978).

It is worth to note that the thermal analyses seem not to be particularly suitable to distinguish between dioctahedral and trioctahedral species of some clay minerals such as those belonging to the chlorite group, as they are particularly influenced by the particle size of the examined sample. However, chlorites show a peculiar thermal behaviour due to their structure. In fact, chlorite is a 2:1:1 clayey mineral (namely T-O-T + O) or consisting of T-O-T layers with the addition of a brucite sheet (O) in the interlayer area. Consequently, it is possible to observe in the thermoanalytical curves of chlorite two distinct dehydroxylation reactions: the first (~600 °C) attributable to the release of the hydroxyls from the octahedral sheet in the interlayer area and the second (~810 °C) due to the dehydroxylation of the octahedral sheet confined in the T-O-T layers. Recrystallization at higher temperatures almost overlaps the last dehydroxylation reaction.

Chlorite represents a potentially useful marker in forensic investigations, since the genesis of these minerals, unlike many other clay minerals, is often associated with alteration processes in a weakly metamorphic environment.

7.3.2 Zeolites

Zeolites, as well as clay minerals, often derive from post-depositional weathering processes of geological formations usually of pyroclastic origin (Langella et al. 2013). In geological-stratigraphic contexts such as those of the Italian peninsula, these formations are among the youngest ones and therefore placed in direct contact with anthropic activities. Consequently, these minerals are very common in forensic soils and can be important markers in studies on their provenance and origin. They also represent a valuable georesource for solving environmental issues (Izzo et al. 2019, 2022; Mercurio et al. 2019).

The so-called "zeolite water" is mainly contained in molecular form in the zeolite channels and cages and, according to their size and interconnection, they can move freely. Furthermore, depending on the anionic field strength, zeolite water can also be adsorbed in hydroxyl form, and then released at higher temperatures.

Based on the thermal behavior, Bish and Carey (2001) distinguish three categories of zeolites: Category 1 – dehydration is completely reversible and does not involve significant structural or volumetric changes; Category 2 – dehydration is completely or almost completely reversible but significant volume reductions and structural distortions occur; Category 3 – dehydration is completely reversible but only at low temperatures.

Analcime $NaAlSi_2O_6 \cdot H_2O$ is an example of category 1 and is characterized by a low interconnection between the zeolite channels having in turn a kinetic diameter of about 0.26 nm (Viczián 2013). This mineral is often found in volcanic soils due to alteration of leucite. The dehydration of the analcime occurs in a single slow-release event that begins at about 120 °C and ends at about 500 °C (Fig. 7.12). As regards category 2, thermogravimetric analyses of natrolite $Na_2Al_2Si_3O_{10} \cdot 2H_2O$

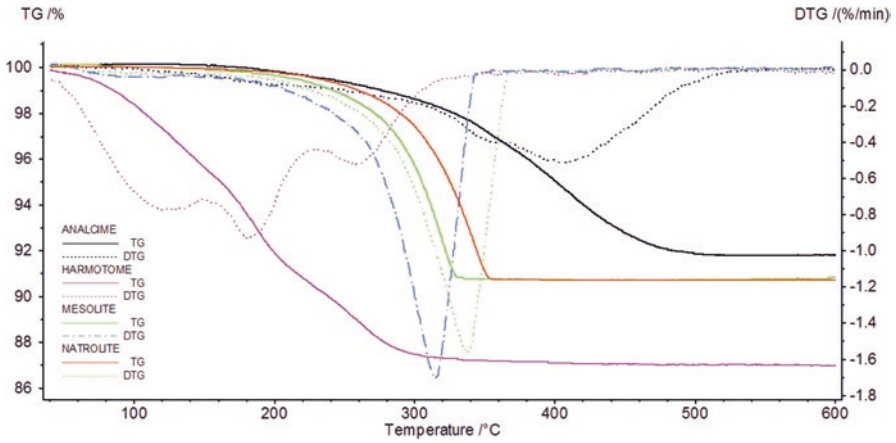

Fig. 7.12 TG and DTG curves of natural zeolites

and mesolite $Na_2Ca_2Al_6Si_9O_{30}{\cdot}8H_2O$ are almost the same and their dehydration occurs in a narrow thermal range with total weight loss approximatively at 9 wt. % (Fig. 7.12).

An example of category 3 is the harmotome $Ba_2Ca_{0.5}NaAl_6Si_{10}O_{32}{\cdot}12H_2O$, displaying a three-dimensional interconnection of the zeolitic channels. In this mineral, dehydration occurs in several stages with an overall release of water vapour of about 14 wt % (Fig. 7.12).

7.3.3 Sulphates

Gypsum ($CaSO_4{\cdot}2H_2O$) is one of the most common sulphates and shows a typical double dehydration within 200 °C with subsequent polymorphic transformations (between 300–600 °C) and dissociation at high temperature (~1220 °C) (Fig. 7.3). These thermal reactions can be summarised as follows:

$$CaSO_4 \cdot 2H_2O_{(s)} \overset{80-200°C}{\rightarrow} CaSO_4 \cdot 0.5H_2O_{(s)} + 1.5H_2O_{(g)} \uparrow \tag{7.9}$$

$$CaSO_4 \cdot 0.5H_2O_{(s)} \overset{80-200°C}{\rightarrow} CaSO_{4(s)} + 0.5H_2O_{(g)} \uparrow \tag{7.10}$$

$$CaSO_{4(\alpha)} \overset{300-600°C}{\rightarrow} CaSO_{4(\beta)} \tag{7.11}$$

$$CaSO_{4(\beta)} \overset{\sim 1220°C}{\rightarrow} CaO_{(s)} + SO_{2(g)} \uparrow + 0.5O_{2(g)} \uparrow \tag{7.12}$$

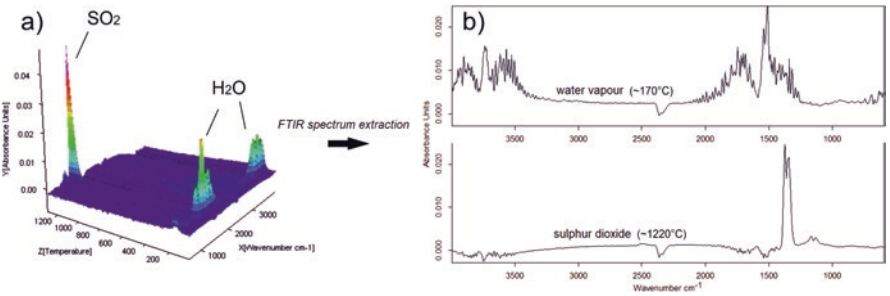

Fig. 7.13 Identification of water vapour and sulphur dioxide, by means of EGA-FTIR, released by dehydration and decomposition of gypsum in thermogravimetric analysis: (**a**) 3D EGA-FTIR plot; (**b**) FTIR spectra extracted at ~170 °C and ~ 1220 °C for water vapour and sulphur dioxide, respectively

In a first phase, gypsum (calcium sulphate dihydrate) is transformed into bassanite (calcium sulphate hemihydrate) and then in soluble anhydrite (anhydrous calcium sulphate). The latter preserves the rehydration capacity which is partially lost only when it is transformed into insoluble anhydrite. The reversibility of the rehydration of the gypsum makes this geological material very suitable to produce binders for plasters and is of considerable interest in the forensic field as it is used in the prevention of fires thanks to its fire-retardant properties. In fact, the water vapour released by the gypsum (Fig. 7.13) inhibits the increase of temperatures, consequently delaying the spread of fire.

7.3.4 Carbonates

The thermal behaviour of carbonates varies significantly as a function of their crystalline composition, their structure, and their degree of crystallinity. Considering the high number of carbonates existing in the nature, only a few didactic examples will be proposed below, referring further information to specific literature.

In water free simple carbonates, the predominant thermal phenomenon is an endothermic decomposition according to the follow reaction:

$$MeCO_3 \rightarrow MeO_{(s)} + CO_{2(g)} \uparrow \tag{7.13}$$

where, M_e is a monovalent cation (for example Na^+ for natrite) or more frequently bivalent ones as, for example, Mg^{2+} (magnesite), Ca^{2+} (calcite), Mn^{2+} (rhodochrosite), Fe^{2+} (siderite), Zn^{2+} (smithsonite), Sr^{2+} (stronzianite), Cd^{2+} (otavite), Ba^{2+} (witherite) and Pb^{2+} (cerussite).

The most widespread carbonate is undoubtedly calcite $CaCO_3$, which dissociates at a temperature between 800–900 °C and a consequent weight loss of about 44% (Fig. 7.1). Such a temperature can vary considerably according to the degree of

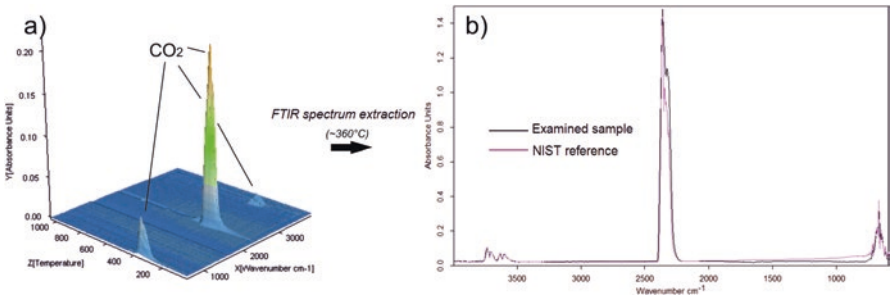

Fig. 7.14 Identification of carbon dioxide, by means of EGA-FTIR, released by decomposition of cerussite during thermogravimetric analysis: (**a**) 3D EGA-FTIR plot; (**b**) Comparison of a FTIR spectrum extracted at ~360 °C and a NIST (National Institute of Standards and Technology) reference spectrum

crystallinity of calcite and according to its origin. For example, decomposition temperature of anthropogenic calcite is generally lower than geological one. The nature of the divalent cation present in the crystal lattice can also lead to variations in the decomposition temperature of carbonates. Generally, it increases as the ionic radius of the cation increases (Smykatz-Kloss 2002), although there are several exceptions. Actually, cerussite $PbCO_3$ decomposes at a much lower temperature than calcite despite the size of its ionic radius. Also, the thermal behaviour of cerussite is quite complex as the release of carbon dioxide (Fig. 7.14) occurs in a relatively low thermal range (300–400 °C) and melts at around 890 °C.

DSC curves allow to distinguish calcite from its most common polymorph, namely aragonite. The DSC of aragonite (Fig. 7.15) shows an endothermic peak just mentioned at about 504 °C, attributable to the polymorphic transition aragonite → calcite. In such circumstances, calcite is often referred to as "paramorphic calcite" (Faust 1950). In the absence of this endothermal peak, aragonite would have the same thermal behaviour as calcite both in terms of decomposition temperature and weight loss. DSC measurements also allow to distinguish double carbonates, such as, for example, dolomite $MgCa(CO_3)_2$, which decomposes in two different thermal ranges.

Pure carbonates in mineralogical mixtures are easily quantifiable by TG measurements based on the constant ratio between the molar mass of the initial compound and the molar mass of the decomposition product removed in gaseous form. This ratio is defined "stoichiometric factor" and for a pure calcite (molar mass = 100.09 g/mol), whose decomposition leads to the release of carbon dioxide (molar mass = 44.01 g/mol), is 2.27. The calcium carbonate content in soils or building materials is usually carried out by calcimetry. Such evaluation is crucial, for example, for the qualification of clayey geotechnical materials used for the construction of artificial confinement barriers for waste landfills.

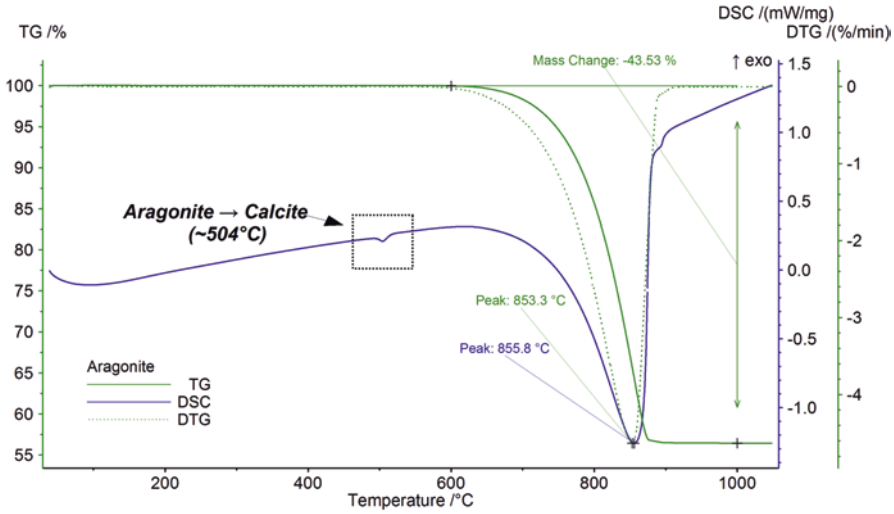

Fig. 7.15 TG, DTG and DSC curves of aragonite

7.3.5 Halides

Halides generally consist of a metal (usually alkaline or alkaline-earth metals) bound to a halogen. Most of these minerals appear to be soluble in water and are usually found in evaporitic deposits. They are often characterized by well-defined melting points, while some hydrated phases show more complex dehydration processes with the consequent formation of acids (for example, bischofite $MgCl_2 \cdot 6H_2O$).

These minerals are rarely studied in thermal analysis. However, a possible future use of thermal analyses for the study of these salts in forensic soils is not excluded, especially if these soils have been affected by contamination by salty or brackish water.

The most common halide is halite NaCl, commonly known as rock salt. The thermal analysis of this mineral (Fig. 7.16) shows a rapid melting at about 810 °C with consequent evaporation.

7.3.6 Other Minerals

Many sediments and rock-forming minerals do not show particular physical changes and/or chemical reactions in the thermal ranges usually used for traditional thermal analyses of geomaterials (40–1100 °C). Examples of these minerals are alkaline feldspar and plagioclases, very common in both effusive and intrusive igneous rocks together with other silicates such as pyroxenes, amphiboles and olivines. Other

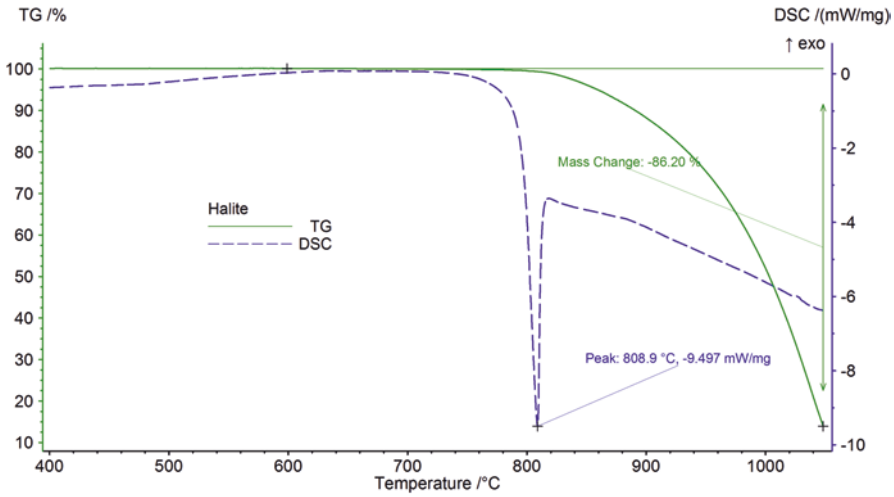

Fig. 7.16 TG, DTG and DSC curves of halite

minerals, on the other hand, can exhibit on DSC curves, evident structural modifications without mass-changes in TGA. A common example is provided by quartz SiO_2, which shows an endothermic peak at about 573 °C, indicative of α-quartz → β-quartz polymorphic transition, namely a structural modification which is not associated to a mass change. The identification of quartz can be fundamental in the mineralogical characterization of polyphasic mixtures such as forensic soils and building materials (bricks, mortars, concrete, etc.).

The thermal behaviour of tourmalines is also noteworthy. They represent a supergroup of boron silicates with a rather complex chemical composition (Mercurio et al. 2018). In fact, tourmalines show an ideal composition $XY_3Z_6T_6O_{18}BO_{33}V_3W$ where X = □, Na, K, Ca, Pb^{2+}; Y = Li, Mg, Fe^{2+}, Mn^{2+}, Cu^{2+}, Al, V^{3+}, Cr^{3+}, Fe^{3+}, Mn^{3+}, Ti^{4+}; Z = Mg, Fe^{2+}, Al, V^{3+}, Cr^{3+}, Fe^{3+}; T = Si, B, Al; B = B; V = OH, O; W = OH^-, F^-, O^{2-}. In thermal analysis, their behaviour is strongly influenced by the actual chemical composition of the sample under examination. Generally, tourmalines do not show evident thermal responses up to about 950 °C, temperature at which a rapid decomposition occurs with consequent weight loss (about 3% for the sample shown in Figs. 7.17 and 7.18).

7.3.7 Soils

One of the main objectives of forensic science is to associate a soil found at a crime scene with another soil sample from a specific place or having a common origin. This approach is based on the "Locard Exchange Principle" according to which the perpetrator of the crime will leave and/or bring with him one or more traces that can be used as forensic evidence from the crime scene (Chisum and Turvey 2000).

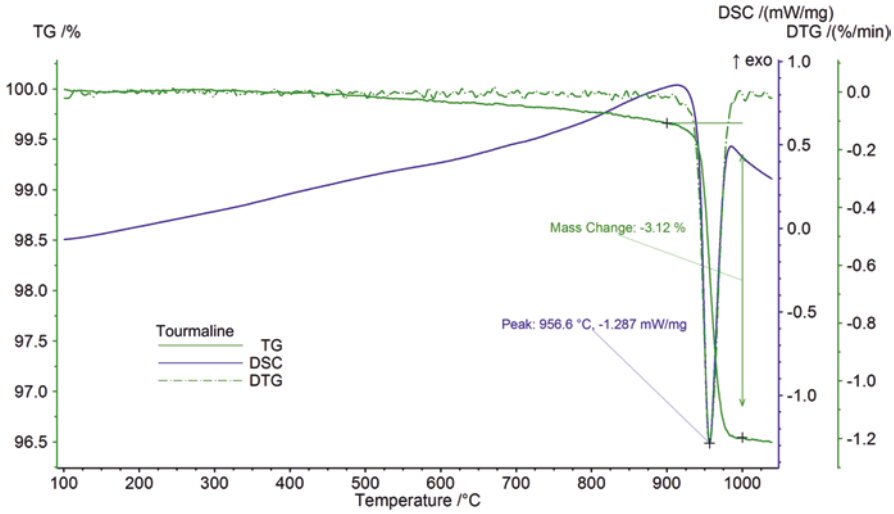

Fig. 7.17 TG, DTG and DSC curves of a tourmaline

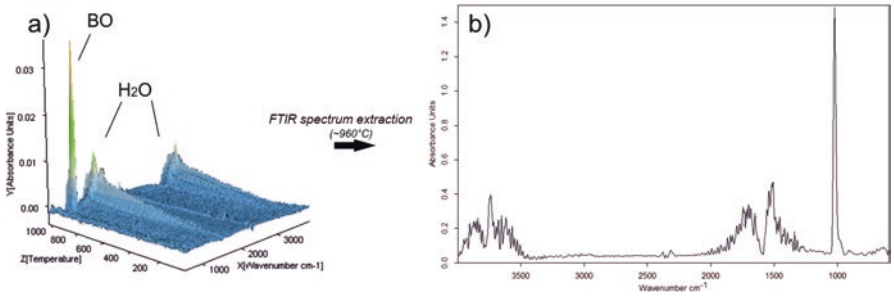

Fig. 7.18 Identification of water vapour and boron monoxide, by means of EGA-FTIR, released by dehydroxylation and decomposition of a tourmaline during thermogravimetric analysis: (**a**) 3D EGA-FTIR plot; (**b**) FTIR spectrum extracted at ~960 °C

However, the term "soil" in the forensic field takes on a very broad meaning and does not necessarily coincide with its scientific definition, as it includes both natural and anthropogenic components (Fitzpatrick and Raven 2012). In fact, in pedology the soil is defined as a natural product of chemical, physical and biological alteration of a starting geological material (parent material). These processes (pedogenesis) determine soil properties and lead to the formation of secondary minerals. Therefore, soil is an open system that tends, according to the second law of thermodynamics, to reach the lowest possible energy configuration, or the maximum degree of disorder (entropy). From a mineralogical point of view, the maximum degree of disorder translates into a reduction in the number of bonds present in the crystalline lattice. Consequently, it is evident that the only traditional techniques of

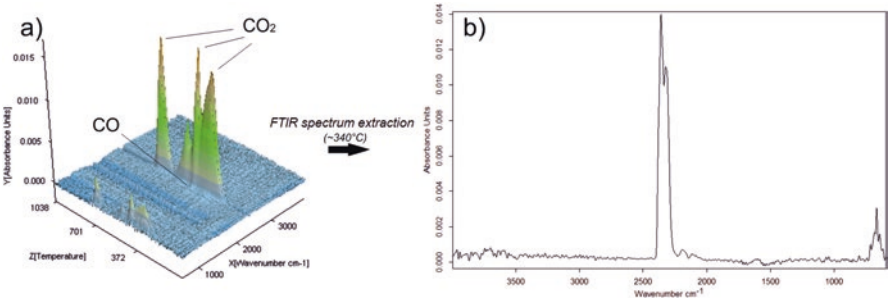

Fig. 7.19 Identification of carbon dioxide and carbon monoxide, by means of EGA-FTIR, released by decomposition of a soil during thermogravimetric analysis: (**a**) 3D EGA-FTIR plot; (**b**) FTIR spectrum extracted at ~340 °C for carbon monoxide and carbon dioxide

mineralogical analysis (for example, X-ray diffraction), based on the crystalline nature of minerals, could not provide enough information about poorly ordered and/or amorphous phases (LO-AP) usually found in forensic soils.

Thermal analyses can provide important information regarding the mineralogical composition of the soils, thanks to the presence of several thermally active phases (phyllosilicates, carbonates, organic substance, etc.). However, considering the compositional complexity of soils, further information are referred to specific literature (Brigatti 2005).

The simultaneous occurrence of both organic and inorganic fractions in the soils makes it particularly difficult to identify and characterize each single constituent, either mineral or amorphous. In an oxidizing atmosphere, the organic substance present in the soils undergoes decomposition and combustion processes in a very wide thermal range (usually up to 550 °C), characterized by weight losses and exothermic reactions superimposed to other thermal events (i.e., dehydration, dehydroxylation, polymorphic transition), as those described in the previous sections. One of the main gases produced by the combustion of organic substance is carbon dioxide (CO_2) often released along with traces of carbon monoxide (CO) (Fig. 7.19). In inert atmosphere (for example, in presence of N_2), pyrolysis of organic substances can change the results of STA in terms of mass-changes and DSC/DTA peak positions. However, the soil organic matter can be removed by treatment with hydrogen peroxide H_2O_2, although this type of chemical oxidation leads to the formation of calcium oxalate, which in turn is thermally active (Brigatti 2005).

7.3.8 Rocks

A rock can be defined as a natural solid aggregate consisting of one or more mineralogical phases deriving from one of the three petrogenetic processes (igneous, metamorphic, and sedimentary). Its thermal response depends on its mineralogical

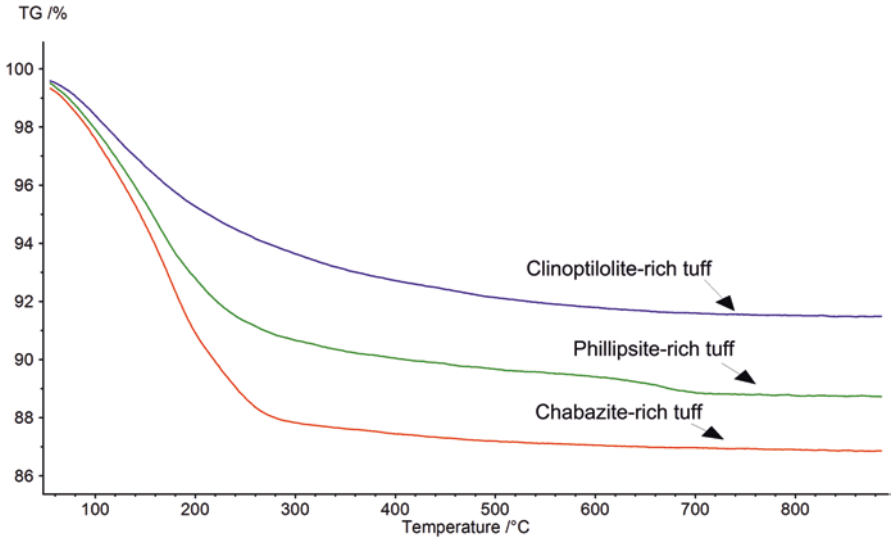

Fig. 7.20 Comparison between TG curves of three zeolitized tuffs. Zeolite contents (wt.%) are 77%, 76% and 56% respectively for phillipsite-, chabazite- and clinoptilolite-rich tuffs

composition. Generally, monomineralic rocks i.e., marble and limestones (calcite) or dunite (olivine), show the typical thermal behaviour of this prevailing mineralogical phase. On the other hand, most of the crystalline phases (i.e., alkaline feldspar, plagioclase, pyroxenes, olivines, etc.), occurring in polyphasic rocks, such as intrusive igneous and many metamorphic rocks, are particularly stable in the standard thermal ranges, and do not show significant thermal responses, except for some polymorphic transitions or weak dehydroxylations (for example, in amphiboles and micas). The greatest thermal activity is expected by effusive igneous, sedimentary and some metamorphic rocks, and in particular by those affected by post-depositional minerogenetic processes (e.g., zeolitization, kaolinization, secondary precipitations). An example can be given by comparing the three zeolite-rich tuffs shown in Fig. 7.20. In this case, it is possible to appreciate the dehydration processes of the zeolitic water, with a small thermal decomposition of carbonate in phillipsite-rich one. The difference between the three TG curves resides first in the different content in zeolite water, which in turn depends on the type of zeolite and its percentage by weight. Notwithstanding the lack of a reliable mineralogical data, it is possible to clearly discriminate these three geomaterials by means of thermal analyses, and to provide useful information about their geological provenance.

The characterization of rocks by thermal analysis can sometimes be useful in legal issues concerning the infringement of tender conditions, for example relating to the exploitation of quarries and mines, engineering works, manufacturing of concrete, and similar contexts.

7.4 Applications of Thermal Analyses to Forensic Sciences

The thermal methods described above can be widely used in the forensic field, as geomaterial samples of judicial disputes require well characterization of both organic and inorganic components. It should be noted however, that thermal analyses often require to be used complementarily to other techniques described in this volume, whenever the origin and nature of a finding needs to be ascertained. In this regard, it is important to mention the studies of Fitzpatrick (2008), Fitzpatrick et al. (2008) and (2009), which provide an exhaustive list of techniques, among which a relevant role is the thermal analysis in the investigation of forensic soils.

A significant number of scientific reports are available concerning the application of forensic techniques, especially with regard to the study of synthetic and natural organic compounds. Among the first approaches, we can mention the work of Hall and Cassel (1975), in which many comparisons of DCS curves, obtained using an inert atmosphere, between different textile materials (yarns) are reported. The authors highlight the clear differences in the thermal shifts as a function of their chemical composition. Other important contributions were later provided by Lombardi (1985) and Hellmiss (1988). The authors report not only the theoretical and technical principles underlying the most common thermal methods (TGA, DSC, DTA and STA/EGA), but also the use of thermomechanical analysis (TMA) for the study of linear mechanical deformation of a material subjected to a controlled variation of the temperature. These contributions also introduce the potential of thermal analyses in the distinction between samples of fibres, paints, and soils, according to their resistance to fire. Furthermore, Hellmiss (1988) highlights how common thermal analyses can be used to study the spontaneous combustion of some materials (for example nitrocellulose), by measuring their specific heat and enthalpy. In 1988, Schwanebeck and Wenz show the importance of associating the analysis of developed gases (using MS) with simultaneous thermal analyses in solving forensic cases.

An important challenge in forensic cases is to establish the origin and age of the bone findings. In this regard, Onishi et al. (2008) carried out experiments on pig bones provided by the Forensic Science Center of the University of Western Australia, using a TG analysis (in an argon atmosphere) coupled with EGA-MS. Pigs (all of the same weight and gender) were slaughtered, and their remains allowed to decompose in a controlled manner under various conditions (burial, atmosphere rich in carbon monoxide) for a variable period between 1 and 5 years. The authors hypothesized an apparent correlation between the TG-MS data and the age of the bone findings, although the work ended with the reference to further investigations.

Based on expertise of the authors of this chapter, particular emphasis here is given to the study of georesources in forensic field, focusing on the thermal behaviour of some of the most common mineral phases. Six case studies concerning thermal studies of forensic geomaterials are described in the following boxes:

Fire at the Polymers Factory (Tsukame et al. 1999)

Another reliable approach to the use of thermal analyses was undertaken by Tsukame et al. (1999) that identified, by means of DSC measurements, an unknown forensic sample collected from the scene of a fire of a factory. To determine the cause of the fire, the forensic sample was compared with two types of polymers involved in the manufacturing processes, labelled as sample A and B (Fig. 7.21). FTIR spectroscopy and GC/MS analyses confirmed that the three samples were made of polyethylene. Samples were also examined combining heating (from 50 °C to 200 °C) and cooling (from 200 °C to 50 °C) program at the same rate (10 °C/min) and atmospheric condition (N_2, 50 mL/min). DSC curves of evidence and reference samples showed the occurrence of two endothermic peaks linked to a melting process of low-density polyethylene (LDPE) (lower-temperature peak) and linear low-density polyethylene (LLDPE) (higher-temperature peak). The result of this investigation was that the samples were made of a mixture of these two polymers, but the best fit of DSC curve of forensic unknown sample was provided by reference sample A. The accuracy of these results was not achieved by any other analytical techniques.

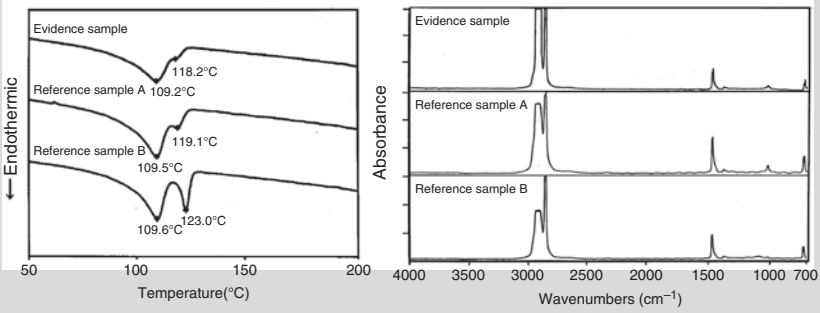

Fig. 7.21 DSC curves and FTIR spectra of forensic sample and reference samples collected from the scene of a fire of a factory. Modified after Tsukame et al. 1999

Identification of Human Hair Samples (Ionashiro et al. 2004)

The potential of thermal analyses (and of DSCs) in the study of human tissues such as, for example, hair, cannot be ignored. As an example, Ionashiro et al. (2004) took hair from the nape of some students and officers of the Institute of Chemistry of Araraquara (University of Sao Paulo, Brasil) and analysed them by DSC; although there were no obvious differences between the responses of the selected ethnic groups (Caucasoid, Negroid and Asian), the comparison between the DSC curves could give important suggestions on the identification of the single sample (Fig. 7.22).

(continued)

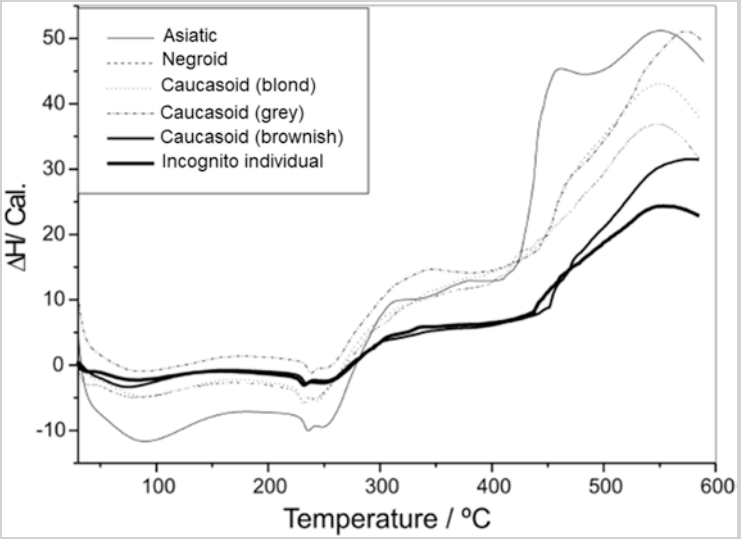

Fig. 7.22 Comparison of human hair DSC curves of different ethnic group and incognito individual. Modified after Ionashiro et al. 2004

Identification of Glove Fragments (Causin et al. 2009)

Another interesting application was proposed by Causin et al. (2009) who applied TG analyses (both in nitrogen and in air) for the characterization and differentiation of latex gloves which, as well known, are often used by criminals at the crime scene in order not to leave fingerprints. Although it is now possible (in some cases) to track DNA traces released inside the gloves, many criminals are unaware of it and naively leave the used gloves on the scene (or in the immediate vicinity) of the crime. Causin et al. (2009) have shown that by comparing the TGA curves it is possible to discriminate about 99.5% of the gloves examined (about 28 types), as each of them returns a particular thermogravimetric response as a function of their complex chemical composition (Fig. 7.23) (natural rubber) and various manufacturing.

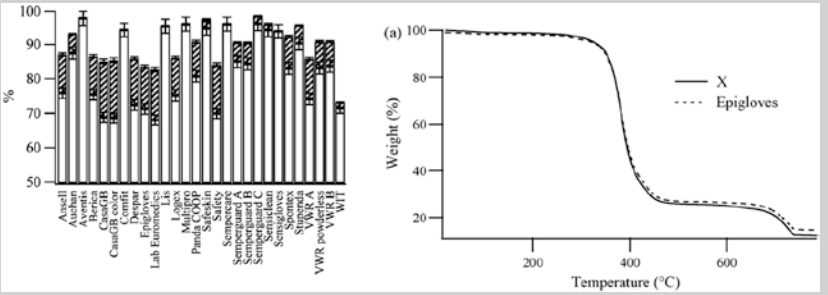

Fig. 7.23 Thermogravimetric analyses of latex gloves (modified from Causin et al. 2009) On the left: Weight losses of the 28 examined samples. On the right: Comparison between TGA curves of an unknown sample (X) with a reference (Epigloves)

Forensic Soils ENFSI APST (Mercurio et al. 2017)

Despite the obvious limitations of thermal analysis in identifying the individual mineralogical phases, the graphic comparison between the thermograms of soil samples allows for rapid and effective feedback in the forensic investigative field. In this regard, we can mention the results of a comparison exercise between forensic soils that involved several European research institutes in 2017 (Mercurio et al. 2017). This exercise is promoted every year by the European Network of Forensic Science Institutes - Animal, Plant and Soil Traces (ENFSI APST) and in 2017, considered the comparison between a soil sample found on the tyres of a vehicle and three samples of soil from three different locations, sites of possible contamination. The TG/DSC thermal analyses combined with the EGA-FTIR allowed to establish the exact correspondence between the sample found on the vehicle and reference sample # 1 (Fig. 7.24) (Mercurio et al. 2017).

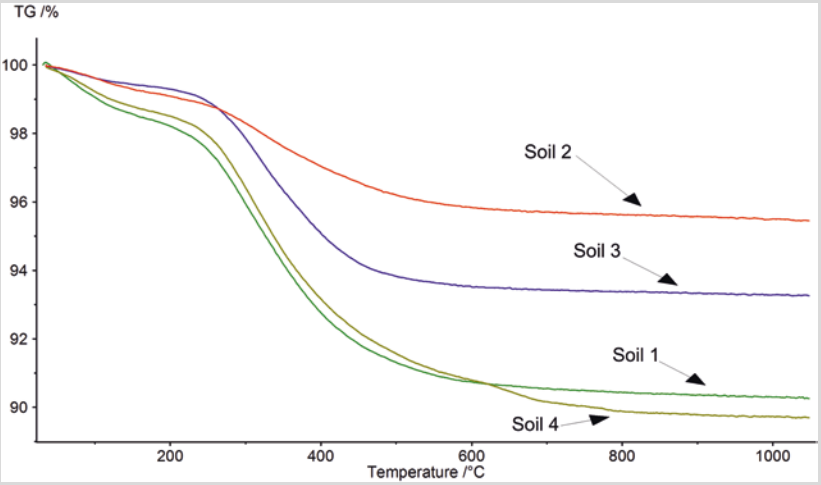

Fig. 7.24 ENFSI APST (Mercurio et al. 2017): comparison between thermogravimetric curves of forensic soils. The correspondence between Soil 4 (found at the crime scene) and Soil 1 (place of contamination) was also confirmed by further analytical evidence

Salt Crystals in Victim's Clothes

This case study concerns the hypothetical suicide of a young man whose body was found on the street of an Italian city, early in the morning. The young man, after a long night at disco and then on the beach, allegedly committed suicide by jumping off a building. However, as the victim was wearing wet clothes presumably bathed with sea water, investigators decided to analyze

(continued)

victim's jeans in order to reconstruct his last hours. In Fig. 7.25 is reported the simultaneous thermal analysis of a representative portion of the clothes worn by the victim. Apart from the initial weight loss (ca. 92 wt.%, 40–550 °C) due to decomposition and combustion of synthetic fibers forming the examined textiles, an additional weight loss (ca. 2.4 wt.%) can be observed at higher temperatures. Such a loss, due to decomposition of halite (see Sect. 7.3.5), confirms data obtained by Stereomicroscopy and SEM/EDS analyses which attest the presence of NaCl crystals in the fabric (cfr. Chapter 1). STA could provide an accurate quantitative information (Fig. 7.25) about the concentration of NaCl crystals into the different portions of the examined cloth. One of the key information for investigators was a higher amount of salt in the external portions of the jeans, thus suggesting that the victim entered the sea fully clothed before he died.

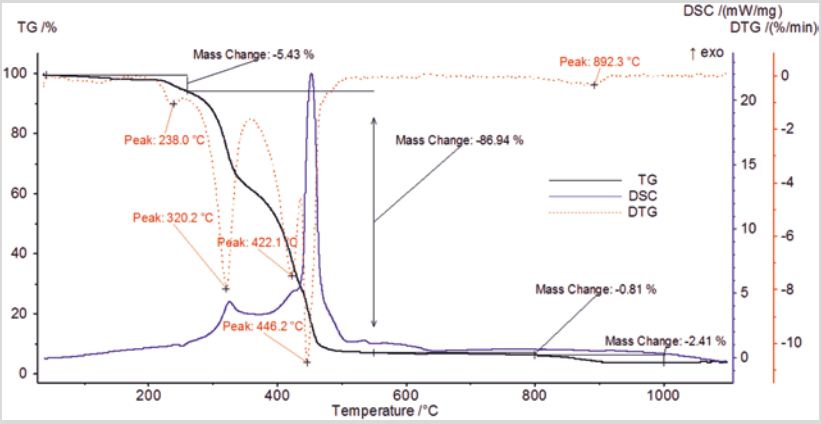

Fig. 7.25 TG, DTG and DSC curves of a representative portion of the examined clothes

The Kidnapping and Murder of Aldo Moro (Lombardi 1999)

A unit of the Red Brigades kidnapped the Italian Prime Minister Aldo Moro on March 16th, 1978. The ambush took place just one kilometer from his house and five bodyguards were killed after a violent fire attack. The corpse of Aldo Moro was then found on May 8th, 1978, in a trunk of a car parked not far from the headquarters of the Italian Communist Party, in the center of Rome. Prof. Gianni Lombardi (Università degli Studi di Roma "La Sapienza") carried out a forensic investigation on the evidences found on Moro's clothes, shoes and on the car, using a multi-analytical approach based on conventional mineralogical and petrographic techniques. A particular attention was paid on

(continued)

bitumen and polyester fragments found below Moro's shoes, inside and outside the car, that were characterized by means of DSC measurements.

Thanks to this investigation, which results were published twenty years later (Lombardi 1999), very interesting information on the potential provenance of sediments were carried out. As a whole, the evidences found on crime scene were high comparable with the textural and compositional characteristics of the sands coming from a limited number of roads leading to a tract of seashore close to the Capital city.

The applicability of thermal analyses to the study of geomaterials is strictly influenced by the thermal activity of the minerals themselves. However, only some of them show an effective physical or chemical response as a function of temperature. For this reason, thermal analyses can hardly completely replace the more traditional and consolidated techniques of mineralogical analysis such as X-ray diffraction and scanning electron microscopy, especially in the identification and quantification of natural mineralogical components and synthetic ones. Nevertheless, for those minerals exhibiting very characteristic thermal behaviours, it is possible to make important evaluation and comparison among materials of unknown or uncertain compositions, as often required in forensic investigations.

References

Bish DL, Carey JW (2001) Thermal behavior of natural zeolites. Rev Mineral Geochem 45:403–452

Bish DL, Duffy CJ (1990) Thermogravimetric analysis of minerals. Therm Anal Clay Sci 3:96–157

Brigatti MF (2005) Analisi Termica, Capitolo IX. In: Metodi di Analisi Mineralogica del Suolo. FrancoAngeli Edizioni, Milano

Carretero MI, Pozo M (2009) Clay and non-clay minerals in the pharmaceutical industry. Part I. Excipients and medical applications. Appl Clay Sci 46:73–80

Causin V, Marega C, Marigo A et al (2009) A method based on thermogravimetry/differential scanning calorimetry for the forensic differentiation of latex gloves. Forensic Sci Int 188:57–63

Chisum WJ, Turvey B (2000) Evidence dynamics: Locard's exchange principle & crime reconstruction. J Behav Profiling 1:1–15

Faust GT (1950) Thermal analysis studies on carbonates I. Aragonite and calcite. Am Mineral 35:207–224

Fitzpatrick RW (2008) Nature, distribution, and origin of soil materials in the forensic comparison of soils. In: Soil analysis in forensic taphonomy, 1st edn. CRC Press, Boca Raton (FL), pp 13–40

Fitzpatrick RW, Raven MD (2012) How pedology and mineralogy helped solve a double murder case: using forensics to inspire future generations of soil scientists. Soil Horizons 53:14–29

Fitzpatrick RW, Raven MD, Forrester ST (2008) A criminal case study involving transference of acid sulfate soil material from a crime scene to forensic evidence. In: Inland acid sulfate soil systems across Australia. CRC LEME, Perth, pp 151–156

Fitzpatrick RW, Raven MD, Forrester ST (2009) A systematic approach to soil forensics: criminal case studies involving transference from crime scene to forensic evidence. In: Criminal and environmental soil forensics. Springer, Switzerland, pp 105–127

Hall JH, Cassel B (1975) In: Davies G (ed) Forensic applications of differential scanning calorimetry. Forensic Science. ACS Publications, Washington DC, pp 114–133
Hellmiss G (1988) Thermal analysis methods in forensic science. In: Forensic science Progress. Springer, pp 1–30
Ionashiro EY, Hewer TSR, Fertonani FL et al (2004) Application of differential scanning calorimetry in hair samples as a possible tool in forensic science. Eclética Química 29:53–56
Izzo F, Mercurio M, de Gennaro B et al (2019) Surface modified natural zeolites (SMNZs) as nanocomposite versatile materials for health and environment. Colloids Surf B Biointerfaces 182
Izzo F, Langella A, de Gennaro B et al (2022) Chabazite from Campanian Ignimbrite tuff as a potential and sustainable remediation agent for the removal of emerging contaminants from water. Sustainability 14:725
Johannsen A (1911) Petrographic terms for field use. J Geol 19:317–322
Langella A, Bish DL, Cappelletti P et al (2013) New insights into the mineralogical facies distribution of Campanian Ignimbrite, a relevant Italian industrial material. Appl Clay Sci 72:55–73
Lombardi G (1985) Thermal analysis in forensic science. Thermochim Acta 93:313–315. https://doi.org/10.1016/0040-6031(85)85080-2
Lombardi G (1999) The contribution of forensic geology and other trace evidence analysis to the investigation of the killing of Italian Prime Minister Aldo Moro. J Forensic Sci 44:634–642
Mackenzie RC (1991) Geosciences in thermal analysis development. Therm Anal Geosci 18:1–15
Mercurio M, Di Maggio RM, Grifa C, et al (2017) Forensic mineralogy: the case study of the ENFSI-APST collaborative exercise “Soil 2017”. Congress SIMP-SGI-AIV-SoGeI 2017, Pisa, September 4 - 6, 2017, p 225
Mercurio M, Rossi M, Izzo F et al (2018) The characterization of natural gemstones using non-invasive FT-IR spectroscopy: new data on tourmalines. Talanta 178:147–159
Mercurio M, Sarkar B, Langella A (2019) Modified clay and zeolite nanocomposite materials: environmental and pharmaceutical applications. Elsevier, Amsterdam
Onishi A, Thomas P, Stuart B et al (2008) TG-MS analysis of the thermal decomposition of pig bone for forensic applications. J Therm Anal Calorim 92:87–90
Robinson JW, Frame EMS, Frame GM et al (2005) Undergraduate instrumental analysis. M. Dekker, New York
Schwanebeck W, Wenz HW (1988) Simultaneous thermogravimetry/mass spectrometry: a new TG-MS interface for forensic science applications. Fresenius’ Zeitschrift für Anal Chemie 331:61–64
Smykatz-Kloss W (2002) Differential thermal analysis of Mg-bearing carbonates and sheet silicates. J Therm Anal Calorim 69:85–92
Thompson JB (1978) Biopyriboles and polysomatic series. Am Mineral 63:239–249
Tsukame T, Kutsuzawa M, Sekine H et al (1999) Identification of polyethylene by differential scanning calorimetry: application to forensic science. J Therm Anal Calorim 57:847–851
Viczián I (2013) Földvári, Mária: handbook of the thermogravimetric system of minerals and its use in geological practice. Occasional Papers of the Geological Institute of Hungary, Budapest
Wagner M (2017) Thermal analysis in practice: fundamental aspects. Carl Hanser Verlag GmbH Co KG, Munich

Chapter 8
X-Ray Fluorescence: Chemical Characterization of Materials by X-Ray Spectrometry

Pasquale Acquafredda and F. Javier Huertas

Abstract X-ray fluorescence techniques are widespread since the half of the last century for chemical investigation on rocks, minerals, industrial products, construction materials, precious materials, environmental pollutants, metals, paints, etc. Actually, they can be used to analyse almost every kind of solids and in many cases also liquid or gelatinous substances. XRF allows to obtain chemical analyses, in elements or in oxides, expressed as percent atoms or atoms in percent weight, alternatively as oxides, stoichiometrically binding the oxygen to the dosed cation. Depending on the accuracy of the desired data and on the sample characteristics, the XRF can be used as partially destructive or as absolutely non-destructive technique; consequently, the sample required for an analysis varies from few tens of milligrams up to about 12 g, depending on the selected analytical procedure and the type of instrumentation. In the last decades, the diffusion of the ED silicon drift detectors, together with the development of very accurate and high specialised software for quantitative analysis, increased the diffusion of portable spectrometers offering new possibilities for *in-situ* and very rapid specimen characterizations, useful during forensic investigations, particularly on samples that cannot be removed for legal reasons or difficult to transport as being too large. The theoretical physical principles and the main components of X-ray spectrometers, in energy dispersion (ED) and wavelength dispersion (WD), are described also comparing the advantages and disadvantages of each analytical technique. Some forensic case studies are also presented.

P. Acquafredda (✉)
Dipartimento di Scienze della Terra e Geoambientali, Università degli Studi di Bari Aldo Moro, Bari, Italy

Centro Interdipartimentale "Laboratorio di Ricerca per la Diagnostica dei Beni Culturali", Campus Universitario, Bari, Italy
e-mail: pasquale.acquafredda@uniba.it

F. J. Huertas
Instituto Andaluz de Ciencias de la Tierra, CSIC – Universidad de Granada, Granada, Spain
e-mail: javierhuertas@csic.es

M. Mercurio et al. (eds.), *Mineralogical Analysis Applied to Forensics*, Soil Forensics, https://doi.org/10.1007/978-3-031-08834-6_8

Keywords X-ray fluorescence · Chemical analyses of materials · Non-destructive analyses · Anthropology · Cultural heritage · Forensic science

The spectrochemical analysis technique by X-ray fluorescence (XRF) allows to obtain the chemical analyses, in elements; such analyses can be expressed as atoms per cent or as atoms by weight per cent or as oxides by weight per cent.

The X-ray fluorescence spectrochemical technique uses, in the most common cases, a process of irradiation of the sample by primary X-rays in order to subsequently analyze the spectrum of secondary X-rays emitted by the sample itself. The technique will therefore involve the use of a primary X-ray source that will irradiate the specimen and a detection system for the X-rays produced on the sample; this apparently very simple system involves the use of *energy dispersion* X-ray detectors. Conversely, the use of detectors in *wavelength dispersion* accounts for an X-ray disperser interposed between the X-rays emitted from the sample and the X-ray collection system, similarly to what happens in a Newton's prism for the dispersion of light.

XRF can be used as a destructive technique or even as an absolutely non-destructive technique; in the first case, wavelength dispersion spectrometers are preferably used, while in the second case those in energy dispersion are more appropriate. The use of one type of spectrometer or the other will also depend on the accuracy and repetitiveness of the data to be obtained, on the shape and size of the object, and above all if the analyses can be done in the laboratory or if they must be carried out "*in situ*".

The quantity of sample required for a chemical analysis using XRF varies from about 12 g down to a few tens of milligrams (about 40 mg, Acquafredda et al. 2018), depending either on the qualitative or quantitative result to be obtained or on the method and instrumentation used.

The samples that can be analyzed in XRF are the most diverse, from rocks, minerals, industrial artifacts, construction materials, metals, paints, etc. Actually, it is possible to analyze almost any solid substance as well as many liquid or gelatinous substances.

One of the major advantages of XRF analyses, as in the case of powdered samples treated with a binder, is that the same specimen can be re-analyzed, with another XRF spectrometer or other analytical instruments such as scanning electron microscopy, even after many years, as long as it remains intact and well preserved. Even after more than 20 years it was proved that the same analytical results are obtained using the same specimens as experimented for some natural glasses (obsidians) of the central-eastern Mediterranean basin (Acquafredda et al. 2018).

The preparation of the sample will depend on the analytical procedure to be used; as far as non-destructive analyses are concerned, samples can be tested without any preventive treatment or even without being moved from its natural location. An *in situ* investigation opens up a very wide range of applications, especially in the forensic field, where it may be necessary to analyze samples that cannot be removed

for legal reasons or that are difficult to transport because of their large size; the same goes for the characterization of precious objects whose partial destruction would significantly decrease the value of the object to be analyzed.

In recent years, the use of portable XRF spectrometers is definitely improving the ability to detect pollutants in the environment. Reliability of these *in situ* analyses could be confirmed, after appropriate sampling, by more accurate measurements in qualified laboratories.

To understand the processes of generation and detection of X-rays are required some basic knowledge which will be hereafter briefly summarized.

8.1 Processes That Can Generate X-Rays

X-rays are electromagnetic radiations with a wavelength (λ) between 0.01 nm and 10 nm; their energy is proportional to its vibration frequency and its wavelength according to the relationship:

$$E = h \cdot \nu = h \cdot c / \lambda$$

where

h is Planck's constant,
ν is the frequency of the X-rays,
λ is X-ray wavelength,
c is the speed of light in vacuum, and
E is the X-ray energy.

The most intense characteristic X-rays, are formed by the appearance of a gap in the innermost orbitals of atoms. These gaps are formed by:

(i) bombardment of the atom with particles such as electrons, neutrons, ions, etc.
(ii) irradiation of the atom with electromagnetic radiation such as X-rays, γ rays, etc.
(iii) irradiation with radioactive isotopes, such as ^{55}Fe, ^{109}Cd and ^{241}Am.

The formation of gaps in the innermost electronic orbits (ionization of the atom) is followed by a process of rearrangement of the atom which also emits its characteristic X radiations.

The simplest way to produce X-rays is through a so-called X-ray tube. It consists of:

(i) A tungsten filament (Fig. 8.1) that is heated by the passage of direct electric current: it produces electrons by thermionic effect.
(ii) A part of the electrons generated on the filament are accelerated, thanks to a high potential difference, towards a metal plate which is called anode.

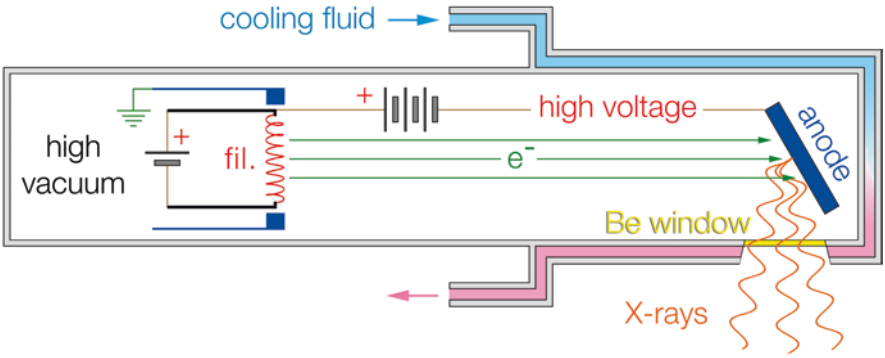

Fig. 8.1 Schematic section of an X-ray tube; deionized water is usually the cooling fluid

(iii) The electrons hitting the anode cause its X-rays emission, both as characteristic lines and as a continuous background (*bremsstrahlung*). Much of the energy due to the abrupt deceleration of electrons is converted into thermal energy which must be dissipated through efficient cooling systems, generally a flow of deionized water.

(iv) The X-rays come out from the tube through a window of a light element, generally beryllium, which does not greatly attenuate their intensity; the beryllium window is also necessary as it is able to endure the high X-ray tube vacuum conditions (about 10^{-5} Pa) required to allow acceleration voltages of the electrons in the order of 10–50 kV.

8.2 The Spectrum of X-Rays

The emission spectrum of an X-ray tube consists of two fundamental components: continuous radiation, or braking radiation (*bremsstrahlung*) and characteristic radiation or Rayleigh lines.

The bremsstrahlung is due to the deceleration of the incident electrons that are braked by the atoms of the anode of the X-ray tube.

The characteristic radiations are consequent to the energetic rearrangement process of the atom that has been excited and are independent of the cause that generated them; their wavelength depends on the type of atom that has been ionized and on the type of electronic transition that leads to the energetic rearrangement of the atom that is emitting them. The wavelength of the characteristic radiation of a given chemical element increases progressively passing from $K\beta_1$ to $K\alpha_1$ to $L\gamma_1$ to $L\beta_1$ to $L\alpha_1$ to $M\gamma_1$ to $M\beta_1$ to $M\alpha_1$, and so on (Fig. 8.2). Furthermore, it is good to keep in mind that the intensity of the different characteristic lines depends on the probability with which each electronic transition can occur with consequent emission of the corresponding X-ray line. In particular, within the spectral series K, the transition from M to K is much less probable than the transition from L to K and therefore the Kβ line is less intense than the Kα line. The $I_{K\alpha}/I_{K\beta}$ ratio increases as the atomic number of the element decreases: it is about 3 for tin, about 5 for copper and about

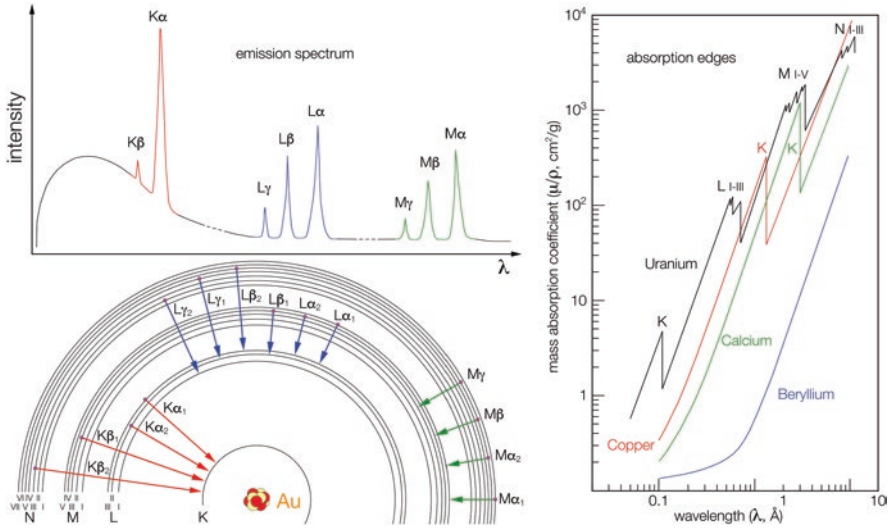

Fig. 8.2 Above: schematic representation of the continuous background and of the distribution of the main characteristic radiations of an element as a function of λ. Bottom: energy levels (orbital) of the atom between which the electrons move, generating the characteristic X lines. On the right are the absorption edges of some chemical elements. (Modified from Bertin 1975)

25 for aluminum. A conspicuous alteration of these intensity ratios must warn about interference between spectral lines of different chemical elements.

These two types of radiation, *bremsstrahlung* and characteristic, contribute to the excitation of the atoms to be analyzed and therefore both have to be considered for an appropriate choice of the X-ray tube to be used for an analysis.

It will be possible to excite the characteristic lines of a chemical element very effectively if the incident radiation has high intensity in correspondence with the wavelengths of those that the excited element re-emits, even better if very close to its absorption peaks.

For example, to make uranium emit a K radiation which has its "absorption edge" at 115.62 eV, the incident radiation must be produced by an X-ray tube that has an electron acceleration voltage of at least 120 kV; this causes heavier elements to excite the lower energy spectral lines such as the L series or even the M series, even if at the expense of a lower intensity of the emitted radiation.

The sample can be excited both with the characteristic lines of the X-ray tube and with its continuous background, so the choice of the anode of the X-ray tube is very important for more effective excitation and detection of the elements to be analyzed.

For W the L characteristic lines constitute 25% of the intensity of the entire spectrum and therefore the bremsstrahlung has a very high intensity; for Cr the K characteristic lines represent 75% of the intensity of the entire spectrum and therefore the bremsstrahlung has a lower intensity.

Actually, it can be said that for the analysis of heavy elements it is more appropriate to use X-ray tubes with an anode of heavy elements and that for the analysis

of light elements it is more appropriate to use X-ray tubes with an anode of light elements.

8.3 Absorption of X-Rays

The absorption of X-rays by a given sample depends on its **mass absorption coefficient** μ/ρ, where ρ is the density of the material expressed in g/cm^3 and μ is its linear absorption coefficient. The value of μ/ρ is defined by the Bragg-Pierce law:

$$\mu / \rho = KZ^4 \lambda^3$$

where

λ is the wavelength expressed in centimeters,
Z is the atomic number of the chemical element,
K is a proportionality factor as a function of the electron orbits.

For the same chemical element, the mass absorption coefficient μ/ρ differs according to the discontinuity considered (K, L, M); in particular μ/ρ increases passing from the discontinuity K to those of the outermost orbitals. Furthermore, with the same energy considered (λ = constant), the mass absorption coefficient μ/ρ is higher for elements with a higher atomic number (Fig. 8.2).

It is important to consider the mass absorption coefficient of the sample because the quantity of X-rays emitted, once it has been subjected to irradiation, will depend on it: a sample that is made up, on average, of heavy elements, absorbs X radiation (both the incident ones and those of fluorescence emitted by the sample) much more than a sample made up of light elements; the consequence is that the quantitative relationships between incident radiation and emitted radiation do not depend only on the element being analyzed but also on the other elements with which the element in question is associated. Chlorine can provide a very exhaustive example. Actually, when chlorine is measured in sodium chloride (halite, NaCl) the radiation emitted by chlorine will be little absorbed by the surrounding atoms of sodium but, in the case of a lead chloride (cotunnite, $PbCl_2$) it will be strongly absorbed by the lead atoms which will act as a screen for the X radiation emitted by chlorine.

It will also be necessary to pay extreme attention not only to the shielding effect of some heavy chemical elements, as in the case just described of lead, but also to the particular position of the absorption peaks of one element with respect to another: as an example, reference can be made to nickel which is used as a monochromator for the K radiation of copper, because its absorption peak K (1.49 Å) is in an intermediate position between the CuKα (1.54 Å) and CuKβ (1.39 Å) radiations. The interaction between the various elements that make up the sample, which is defined as the "matrix effect", is extremely important during the analyses conducted using XRF because it conditions the response in quantitative terms and can also severely limit its detectability. Bearden (1967) and Bearden and Burr (1967)

carefully detailed the wavelengths of the characteristic lines emitted by chemical elements and the wavelengths of their absorption peaks.

8.4 Detection and Measurement of X-Rays

The discovery of X-rays (W.C. Röntgen, 8 November 1895) was casually ascertained as they impressed a thin photographic plate; this system has remained, until very recent times, one of the most used systems for their detection such as, for example, radiographs used in medical analysis.

The possibility of obtaining accurate measurements of the quantity and X-rays emitted but above all of their energy, and therefore of their wavelength, have led to the development of different types of detectors that are more or less efficient if used to collect energy or wavelength of X-rays.

8.4.1 X-Ray Detection by Energy Dispersion (ED = Energy Dispersive)

X-rays can be detected in energy dispersion with solid state detectors (Fig. 8.3) consisting of a semiconductor. The most used semiconductors are silicon crystals, doped with various elements such as P, Al, B, Li; other semiconductors used are germanium or diamond.

Doping involves the replacement of some atoms in the crystal lattice of a crystal with other atoms; when a photon X hits one of these semiconductors, it generates an "electron-electron hole" pair inside the material (Fig. 8.3). The energy required to generate the e-h pairs is proportional to that of the incident radiation and therefore

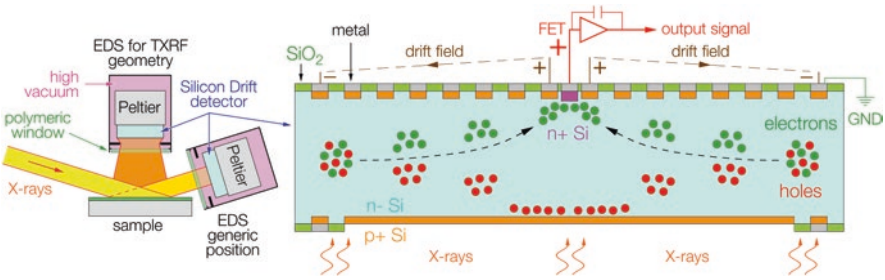

Fig. 8.3 Scheme of an Energy dispersive (ED) spectrometer: the ED detector can collect X-rays in any position relative to the sample; for low X-rays incident angle (about 0.1°) the X-rays can be collected just above the sample, as in Total reflection X-Ray Fluorescence (TXRF) spectrometers. On the right, the detail of an ED Silicon Drift detector; n+, n- and p+ indicate the type of doping of the Si crystal. (Modified from Acquafredda 2019)

it is possible to know the type of incident radiation and, by integrating the signal over time, its intensity.

The ED detectors allow to analyze almost simultaneously the entire spectrum of the X-rays emitted by the sample and this makes them irreplaceable for rapid qualitative chemical analyses or to obtain X-ray maps of the sample. They also have simple geometries: they can be positioned in various ways with respect to the sample, as long as they collect a sufficient quantity of X-rays coming from its surface.

ED systems show three weak sides at the same time:

(i) the detector must be refrigerated to keep the semiconductor structure intact during operation; the old detectors had to be refrigerated even with liquid nitrogen (−196 °C) while for the new detectors a Peltier cooler is sufficient which, similarly to those used in portable refrigerators for cars, works with direct electric current and reaches about −60 °C.
(ii) the resolution in energy, at best 115 eV, often does not allow to sufficiently separate some lines of the X spectrum emitted by the sample.
(iii) solid-state detectors cannot collect particularly high quantities of X-rays (generally less than 250,000 counts per second on the total spectrum) because as the counts increase also the so-called "dead time" increases, that is the discarded counts. Having fewer counts coming out of the detector is equivalent to a greater error in the X-ray measurement.

Portable or transportable ED instruments have the problem that for the detection of very light elements, whose radiations would be drastically absorbed by the air, it is necessary to work: (i) with systems that allow to create a vacuum between the sample and the detector; (ii) with the flow of a gas, such as helium, between sample and detector; (iii) greatly reducing the distance between sample and detector.

A particular use of ED detectors is that for X-ray fluorescence spectrometry in total reflection geometry (TXRF: Total reflection X-Ray Fluorescence); these spectrometers provide that the X-rays affect the sample at an angle close to the critical angle of reflection (about 0.1 °) so as to avoid penetrating the substrate of the sample itself. The detector will collect the X radiation produced on the sample by the incident beam with a grazing angle (Fig. 8.3); it will therefore be possible to obtain a quantitative analysis of the surface of the sample, free from matrix effects, using only an internal standard.

TXRF is particularly useful for the analysis of liquids (wastewater, environmental contaminants, body fluids, etc.) but it is also used effectively for solids treated as thin films (pigments of works of art, atmospheric particles, etc.), so much so that it is often used in forensic investigations of glass, soils, drugs, inks, etc. (Roux et al. 2013).

8.4.2 X-Ray Detection by Wavelength Dispersion (WD = Wavelength Dispersive)

In order to disperse the X radiation in its components of the electromagnetic spectrum it is necessary that these interfere with an object that can allow the spectral separation: this object, organic or inorganic, is a crystalline lattice which is called an analyzer crystal or a scattering crystal.

The diffraction process is regulated by Bragg's law:

$$2d \sin\theta = n\lambda$$

where

d is the distance between the lattice planes of the crystal,
θ is the angle of incidence and diffraction (reflection according to Bragg),
n is the order of reflection,
λ is the wavelength of the incident and reflected (diffracted) radiation.

The XRF analysis in wavelength dispersion provides for the determination of the value of λ, characteristic for each chemical element, by measuring the θ angle as long as the d value of the diffracting crystal is known.

In order to correctly observe the dispersion according to Bragg's law, the source of the X-ray signal (in this case the sample that emits X-rays of secondary fluorescence), the diffracting crystal and the X-ray detector must necessarily be on a circle, called focusing circle. To scan the entire spectrum of X-rays emitted by the sample, the detector must be rotated by a θ angle, gradually increasing, towards which the diffracting crystal will direct the X radiation by rotating by a θ/2 angle. As the θ angle varies, the X-ray source, the diffracting crystal and the detector will not always be on the same focus circle but on focus circles with different radii. The condition is that of a non-perfect focusing geometry depending on whether crystals are used: flat diffracting crystal coupled to auxiliary collimators generate a parafocusing geometry; curved diffracting crystals coupled to collimation slits generate a semi-focus geometry (Fig. 8.4). The use of auxiliary collimators or collimation slides generates a loss of the X-ray signal.

Alternatively, by providing a more complex geometry of the spectrometer, in addition to the normal rotation of the dispersing crystal and the detector, it will also be necessary to move them so that, as the θ angle varies, they are always on the same focusing circle (perfect focusing); this configuration allows the least loss of signal.

During the scanning of the X-ray spectrum emitted by the sample, it will also be necessary to change the diffracting crystal: for short radiations we will use crystals with small 2d (1.801 Å for LiF 420) and for larger radiations we will use crystals with increasing 2d values (up to over 100 Å for multilayer organic crystals).

Detectors used in WD spectrometers must allow both large and small λ radiation to be read efficiently. The detectors usually used for this purpose are generally 2: one using flow gas, for large λ radiation, typical of light elements, and a solid-state scintillator, for small λ radiation, typical of intermediate and heavy elements.

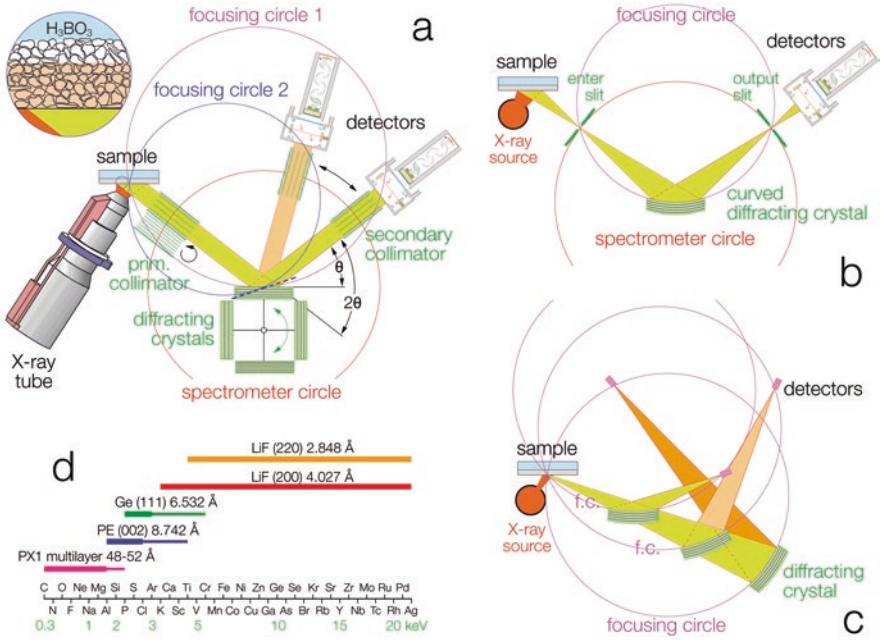

Fig. 8.4 (**a**) scheme of a plane diffracting crystal WD spectrometer, in parafocusing geometry, with the magnification of the X-ray irradiated sample in the upper left corner; (**b**) scheme of a curved diffracting crystal spectrometer, in semi-focusing geometry; (**c**) scheme of a curved diffracting crystal spectrometer: the simultaneous angular movement of the diffracting crystal and detectors, also associated with a translation, allows the spectrometer to work in perfect focusing geometry; (**d**) diffracting crystals commonly used during the analysis of chemical elements with different atomic numbers. (Modified from Acquafredda 2019)

Flow-gas detectors use the ionization process of a gas (Fig. 8.5) produced by X-rays; the X radiation penetrates the detector through a window consisting of a thin sheet of a material particularly transparent to this type of radiation (a polymeric sheet of Mylar©), and causes the ionization of the gas atoms which, under the influence of the electric field, are conveyed towards the central filament (negative charged ions), and towards the walls (positive charged ions) of the detector. The electrical signal generated in the detector, proportional to the X-rays, can be amplified and quantified.

The scintillation detectors are crystals, generally consisting of sodium iodide activated with about 1% of thallium, which, when hit by X-rays, emit a number of photons proportional to the energy of the absorbed X-rays. A photocathode reads the *quanta* of light produced and converts them into electrons which, through a chain of dynodes, generate a signal proportional to the *quantum* X that has hit the detector. The signal can be further amplified and quantified.

Unfortunately, the two detectors just described, flow counter and scintillator, are not particularly efficient in the wavelength range between about 2 and 0.75 Å, in which elements commonly dosed such as Mn, Fe, Co, Ni, Cu, Zn, As, etc., emit

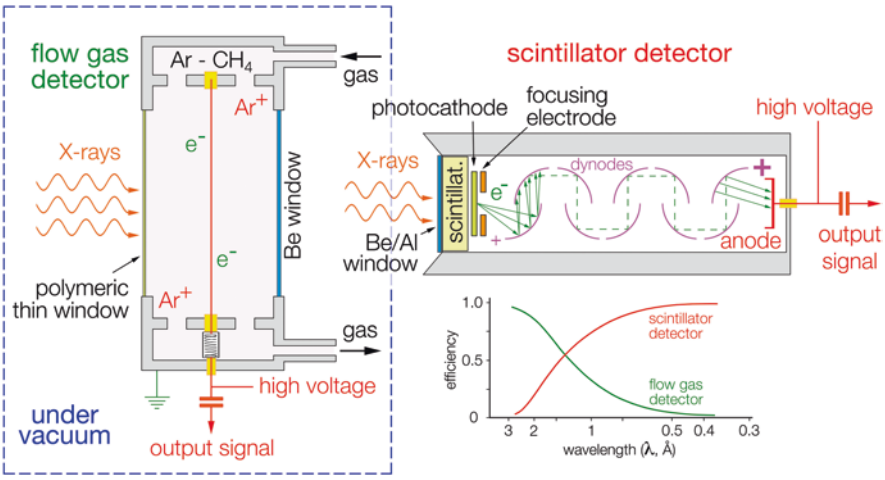

Fig. 8.5 Flow gas detector (Flow Counter), on the left, and scintillator detector on the right. At bottom right the different efficiency of the two detectors as a function of the incident radiation

their K X-ray lines. The most recent spectrometers also mount gas-sealed meters, such as Neon, Krypton and Xenon ones, which, coupled to traditional flow gas and scintillation detectors, make the collection of the entire X-ray emission of a sample to be analyzed more efficiently.

To allow the detection of very light elements (up to Be) whose radiations would be drastically absorbed by the air, the WD spectrometers accommodate the X-ray source, the scattering crystal and at least the detector for large wavelengths, in a bin held at a vacuum of about 2 Pa (Fig. 8.5).

8.5 XRF Qualitative Analysis

Qualitative analyses will be performed with an X-ray source that can better excite the chemical elements present in the sample. In this case it should be remembered that the incident radiation must have an energy that is at least 1.5 times greater than that of the absorption edge of the radiation that must be emitted by the element. For this reason, in recent years there is a tendency to use X-ray tubes with anode of a heavy element, e.g. Rh which is considered a "wide range purpose", as it can excite the emission spectrum of the sample either with its characteristic lines (both the K and L lines) or with its continuous background (the intensity of the continuous background increases as the atomic number of the anode in the X-ray tube increases).

ED spectrometers allow to obtain a complete qualitative analysis of the sample in a few seconds, from 50 to 100, but it will be necessary to pay attention to the

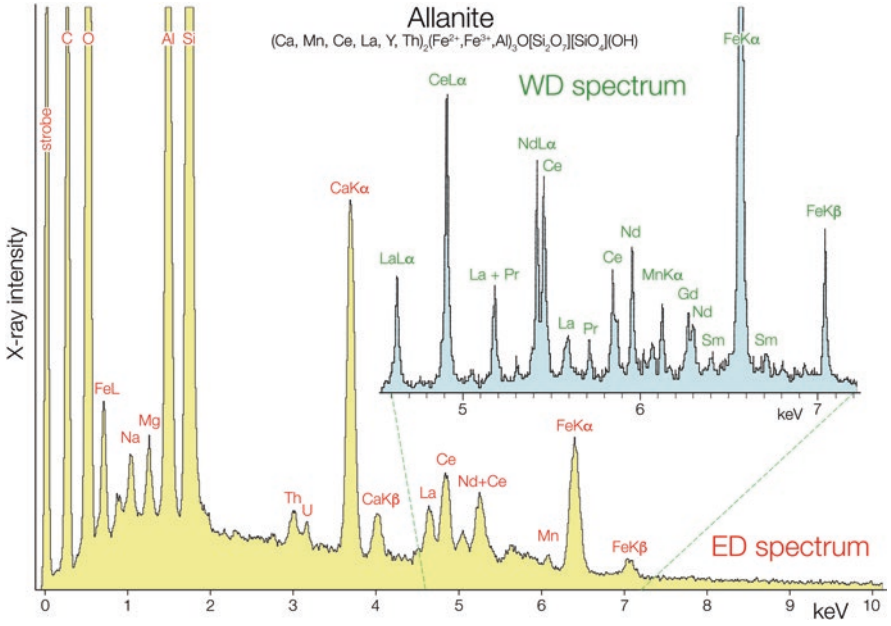

Fig. 8.6 Allanite ED spectrum: in this case, a qualitative analysis of a silicate mineral rich in rare earth elements, can be very demanding due to the presence of strong overlaps of the L lines of elements such as La, Ce and Nd; the strobe is the reference peak of the system for zero energy. An aid to the identification of rare earths elements can be given by a WD scan in the energy range 4.55–7.25 keV, performed using a LiF 200 diffracting crystal, as visible in the enlarged detail present in the top right part of the figure. (Modified from Acquafredda 2019)

overlap of the L or M lines of heavy elements on the K lines of light elements (Fig. 8.6).

For WD spectrometers it will be necessary to choose the most appropriate diffracting crystals to better separate the different emission lines of the elements: this implies that a great experience of the operators is necessary along with longer times of acquisition of the spectral scan that can even exceed 15 min. The considerable advantage of WD analyses is that they enable a better separation of the different spectral lines emitted by the sample, and therefore an easier and more reliable recognition (Fig. 8.6).

The identification of the different elements present in the sample, once its X-ray emission spectrum has been obtained, can be done with specific software supplied with the instruments. It is possible to use conversion tables or to use the literature data that provide, for each chemical element, the energy and wavelength of the X emissions and the relative absorption peaks (Bearden 1967; Bearden and Burr 1967).

8.6 XRF Quantitative Analysis

Quantitative chemical analyses using ED and WD X-ray fluorescence spectrometry must consider a calibration of the spectrometer: the calibration can be supplied with the instrumentation or carried out by the operator. This operation is absolutely necessary as, from the measurement of the X-rays emitted by the sample, it is possible to obtain the elemental concentrations taking into account the "matrix" of the sample: if the sample matrix is not properly considered, any output data on the investigated element can significantly vary from the real concentration.

Nowadays, most spectrometers are supplied with software that suggests the optimal conditions for dosing an element or a series of chemical elements, namely: anode of the X-ray tube to be preferably used, electron acceleration voltage, X-ray lines to be collected (K series, L series or M series), type of diffraction crystal (for WD spectrometers), type of detector (for WD spectrometers).

Other aspects, however, must always be kept in mind, such as those hereafter listed:

(i) Error in the measurement of X-ray counts.

When measuring the intensity of an X-ray emission, the measurement error (ε) is directly proportional to the number of counts itself, namely:

$$\varepsilon = \sqrt{N}$$

namely, the more X-ray counts can be read, the lower is the percentage error ($\pm\varepsilon$), due to the counting statistics, compared to N that is the real value of X-ray counts.

(ii) Measure of the background and therefore of the net peak.

The signal that represents both qualitatively and quantitatively the element to be dosed emerges from a background that must be taken into account; this background is sometimes linear and constant (its value is similar on the left and right side of the peak), other times it is linear but not constant (its value is different on the left and right side of the peak), in other cases it is described by an exponential function (Leoni and Saitta 1976; Acquafredda et al. 2018). It is extremely important to know the background value with great precision: if the peak value is not at least twice the error of the background reading value (2ε), the peak itself is confused with the measurement error of the background.

(iii) Counting statistics

The optimal time to acquire X-rays will depend on the irradiation power of the sample and the concentration of the element to be determined; it can be chosen by calculating the relative standard deviation (σ), which takes into account all these parameters including the peak/background ratio:

$$\sigma\% = \frac{100}{\sqrt{time}} \frac{1}{\sqrt{peak} - \sqrt{background}}$$

the higher the counting time and/or the net intensity of the peak, the smaller the standard deviation σ.

(iv) Problems related to the shape of the sample

The shape of the sample, as for many other analytical procedures, requires a perfectly flat surface; this allows the source-sample-detector and source-standard-detector geometry to be the same both during the analysis of an unknown sample and during calibration.

If WD spectrometers are used, a flat shape of the sample is almost always a prerequisite in order to keep each point of the sample surface on the same focusing circle on which the diffracting crystal and detector lie. This constraint of the plane surface of the sample, when working with WD spectrometers, can be bypassed if the intensity ratios of elements that are contiguous in the Mendeleev Periodic Table of Elements are used to characterize a sample instead of their elemental concentrations (De Francesco et al. 2008; Acquafredda et al. 2018; Acquafredda 2019).

The shape of the sample surface, on the other hand, does not pose too many limitations if ED spectrometers are used; in fact, these spectrometers do not have constraints like those of the focusing circle and are less affected by reading errors induced by an irregular geometry of the sample surface (Ruste 1979; Acquafredda and Paglionico 2004; Acquafredda et al. 2018).

(v) Analytical problems related to the operator

The operator, in any laboratory, is a variable that absolutely must not be neglected. The sensitivity of this person in understanding the analytical problem and his operational correctness, will decisively affect data accuracy. The same attention should be taken in choosing the instrumentation to be used, whether it is WD or ED, large and extremely versatile or small and portable. However, it is always important to identify rigid protocols to be followed, especially in the forensic field where each case can make its own story, although a high qualification and experience of the operator must be privileged to obtain reliable data.

(vi) Optimal use of the equipment purchased

For quantitative chemical analyses, almost all the instruments are now equipped with software which transform the intensity of the X-rays into elemental concentrations, taking into account the background generated by the X-ray tube, the background of the sample and the interelementary effects due to the "matrix" of the sample. Software often refers to a calibration made by the manufacturers (analysis in standardless conditions), with an instrumentation that is therefore sold as a "turn-key car". The software adapts calibration to the particular conditions set by the operator such as the power supply conditions of the X-ray tube.

If you do not want to use the closed-box packages provided by the manufacturers, you can build your own calibration straight line with special international standards that take into account the compositional differences of reference samples with different "matrices"; the use of these regression straight lines will allow to obtain

the elementary concentrations, as a function of the X-ray intensities, for samples with matrices similar to those of the reference standards.

Other analytical procedures that can solve the problem of interelemental effects due to the matrix, such as the addition procedure, the internal standard procedure, the infinite dilution procedure or the mathematical matrix correction procedures (Acquafredda 2019), can be used for rather complex calibrations that not all laboratories can afford and that are not always easy to implement, especially on portable instruments.

8.7 Use of Portable Equipment

The use of portable or transportable instrumentation is becoming more and more widespread; this diffusion has been facilitated by the production of low-power X-ray micro-tubes, generally less than 50 W in power, which have replaced radionuclide sources (radioactive sources) which require special permits to be transported; a particular impulse to the use of these instruments came above all from the diffusion of refrigerated ED detectors with Peltier systems that do not require liquid nitrogen. A wide range of products are marketed, from X-ray handguns (Hand-Held portable XRF: HHpXRF), to slightly more complex systems to be mounted on tripods (Field-portable X-ray Fluorescence: FpXRF) up to small transportable spectrometers (Bench-portable X-ray Fluorescence: BpXRF). All these systems generally work in the air, therefore they allow the intermediate and heavy elements to be read normally; the light elements are detectable down to magnesium or, if you work with helium flow or even with small vacuum chambers, down to sodium or in some cases even down to fluorine.

Some of these instruments can be fitted with special optics, the polycapillaries, which, by exploiting the phenomenon of total reflection, focus the incident X-ray beam on a very small area (up to about 20 μm); this allows to obtain chemical analyses of extremely small areas of the preparation, with a detectability of down to tens of parts per million, and the possibility of acquiring, by means of X-ray maps, the elemental distribution of the sample surface.

These portable units are now irreplaceable for measurements on large objects (surfaces of buildings or machinery, paintings, statues, etc.), which obviously cannot be placed in the measurement chamber of an X-ray spectrometer, or for which it is difficult or impossible, even due to limits set by institutions such as the State Offices for Justice or for Cultural Heritage, to take a representative fragment.

The typology of these analyses, carried out on samples that often have irregular geometries, hardly guarantees quantitative data that are reproducible; the goodness of these data will depend a lot, once again, on the operator's experience, on a correct calibration of the spectrometer and finally on a rigorous control of the results with appropriate reference standards or with analyses carried out in certified XRF laboratories.

8.8 Preparation of the Samples

The preparation of the samples will depend on the type of spectrometer to be used, whether in wavelength dispersion or energy dispersion, and on the type of analytical procedure that will be adopted.

For forensic investigations, in most cases, as already mentioned, absolutely non-destructive methods will be preferred, which therefore do not require any treatment of the sample. For analyses with a greater degree of accuracy and which allow greater reproducibility, it will be necessary to address those methods, such as the standard addition procedure, the internal standard procedure, the infinite dilution procedure or the mathematical matrix correction procedure. For these procedures the sample must be destroyed, generally by pulverizing it, and that it must be treated with binders (standard addition procedure, internal standard procedure, mathematical matrix correction procedure) or with low melting components (infinite dilution procedure). The use of binders or low melting components requires a particularly experienced operator to prepare the samples before analysis and above all to refer to extremely rigorous analytical procedures (Acquafredda 2019).

8.9 Examples of Use of the XRF in Forensic Investigations

The use of X-ray spectrometry in forensic field is widespread and varies from the analysis of polluting or dangerous substances (heavy or radioactive metals such as chromium, mercury, arsenic, uranium, thorium, etc.; compounds containing sulfur, nitrates, phosphates, fluorinated compounds, etc.; particular substances such as inks, drugs, atmospheric particles, etc.), to the characterization of building materials (crushed stone, cements, mortars, etc.), paints, oils and fuels, minerals, rocks, jewelry and precious pigments or also all the materials interesting the Cultural Heritage.

However, any approach to geoforensic investigations, among which also those using X-ray fluorescence, cannot ignore the scientific protocols typical of chemical, physical, Earth Sciences, etc.

Before deciding on any analytical procedure or scientific technique to be adopted, some assumptions must be taken into account:

1. Desired results:
   (a) accuracy and precision of the data;
   (b) costs;
   (c) sample loss.
2. Isotropy of the sample and therefore representative quantity:
   (a) qualitative results;
   (b) quantitative results.

In the following section, as examples, are reported some cases in which different types of X-ray spectrometers are used for particular forensic investigations, also depending on the desired results and the isotropy of the sample.

8.9.1 Materials for Industry

The certification of raw materials is important, such as in the glass or steel industry, because this document goes deeply on any disputes regarding supplies from companies that have to deliver them. In this case, the tolerances regarding accuracy (approximation to the real value) and precision of the data (data repeatability) limit the choice of the equipment for X-ray fluorescence analyses only to wavelength dispersion spectrometers (WD) operating on specimens prepared as powdered pellets or as glass beads.

The analysis of samples used as raw material in the glass industry, such as siliceous sands, quartzarenites, etc., must also reach accuracies of the part per million, especially for chromophore elements (Fe, Co, etc.).

These surveys can foresee costs of up to one thousand euros, quite sustainable for the interested parties, considering that these certifications are required to validate industrial productions. In these specific cases, a loss (destruction) of the sample certainly is not an issue; rather, it will be necessary to pay particular attention to the isotropy or anisotropy of the sample itself, especially if the analysis is quantitative and not just qualitative. In the case of particularly anisotropic samples, it will be necessary to perform a quartering (a cone-shaped granulate is divided into 4 equal parts and the 2 opposite quarters are sampled) in order to get a representative sample.

Materials for Industry

In the case of raw materials for the metallurgical industry, the accuracy can also be of the order of a few thousand parts per million but the precision must be particularly high: for raw materials that can generally have very different levels of Fe_2O_3 between 55% and 93%, of SiO_2 between 3% and 42% and of Al_2O_3 between 1% and 5% the relative error of determination, between two different measurements, must not exceed 0.5% (these unpublished data refer to a research on the characterization of raw materials in the steel industry carried out about fifteen years ago, by the University of Bari, Italy, in collaboration with the ILVA steelworks in Taranto and Genova, Italy).

In the last 20 years, in the stone materials industry for the production of concretes, it has become essential to certify the possible presence of amorphous silica or of microcrystalline silica (calcedony) that could lead to fracturing and popout of the concrete due to the alkali-silica reaction (ASTM C 1260). Further than a simple observation of concrete rock fragments in optical

(continued)

microscopy, an XRF-ED analysis can be very important, e.g. even with an X-ray handgun, to detect even small silica particles due to the presence of siliceous fossils, as frequently happens in the carbonates, or of very little chert fragments.

It should be noted that WD-XRF spectrometers, especially if used with standard addition procedure or mathematical matrix correction procedures, allow to obtain very accurate and precise data, with a detection limit that can reach, for some trace elements, parts per million or even fractions (Acquafredda et al. 2018). It is important to underline that the use of correct analytical procedures and of performing equipments protects, especially the suppliers of raw materials, from any disputes with the customers.

8.9.2 Precious Materials (Metals and Stones) and Cultural Heritage Materials

Whenever a characterization of jewels or of objects of Cultural Heritage is required it is often mandatory to foresee non-destructive X-ray fluorescence investigations carried out using energy dispersion spectrometers (ED) which are less affected by errors induced by an irregular geometry of the sample surface (Ruste 1979;

Precious Materials
During the analyses of some pieces of the Treasure of Saint Nicholas, safeguarded in the Basilica of Saint Nicholas in Bari (Italy), in addition to an usual gemological analysis, an investigation using a portable XRF may be crucial to distinguish different minerals with similar colors; actually, it is not uncommon that very precious minerals such as ruby, emerald and sapphire, stolen from jewels of religious worship, have been replaced by imitations of much lower value such as garnet, quartz of various colors or even colored glasses (Tempesta et al. 2009).

In some situations, it might be useful to analyse different portions of a jewel to understand if it is authentic or an imitation. This is the case of a necklace made up of very old-looking glass beads linked together by a gold thread (Fig. 8.7); the "Carabinieri Department for the Protection of Cultural Heritage" in Italy seized the precious object from people linked to criminal activities.

The EDS analysis of these glass beads (Table 8.1) revealed a chemical composition compatible with that of the Roman glasses (Janssens et al. 2000; Genga et al. 2008), in particular the "low-magnesia low-potassium oxide glass" (LMLKG) with SiO_2 = 66–72%, Na_2O = 16–18%, CaO = 5–8%, MgO

(continued)

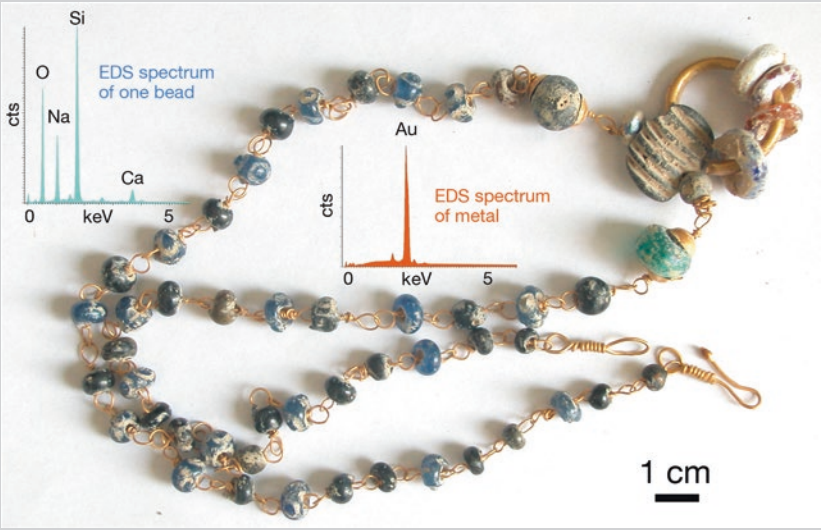

Fig. 8.7 Necklace made up of very old-looking glass beads joined together by a pure gold thread; in green the ED spectrum of one bead and in orange the ED spectrum of the gold thread

Table 8.1 ED-XRF analyses of the surface of a glass bead of a necklace (the necklace of Fig. 8.7)

	1	2	3	Mean	St. dev.
SiO_2	70.55	70.50	70.65	70.65	0.08
Al_2O_3	1.76	1.81	1.78	1.78	0.03
FeO	0.30	0.24	0.43	0.32	0.10
MgO	0.37	0.34	0.37	0.36	0.01
CaO	7.76	7.84	7.77	7.79	0.05
Na_2O	18.05	17.99	17.72	17.92	0.17
K_2O	0.48	0.47	0.47	0.48	0.00
PbO	0.73	0.82	0.81	0.78	0.05

and $K_2O < 1\%$. Furthermore, the glass beads were joined together by a pure gold thread and not by a gold alloy such as those currently used in jewelry. Also, the shape of the glass beads and their aging forms, controlled by researchers expert in the History of Art, suggested that the necklace was a very ancient piece.

Only the careful examination of the gold threads, by a goldsmith, revealed the presence of cutting signs due to modern shears; the forger, therefore, had imitated the composition of an ancient glass and had used a pure gold thread, as it was done in Roman times: only the use of modern cutting tools has revealed the falsification.

Paint, Pigments and Inks

Analysis of chemical composition of writing materials (e.g., inks, toners) is important in forensic examination of documents for their authentication or age determination. Chemical methods frequently require sample preparation to isolate the ink or pigment from the substrate, leading to partial deterioration of the document. ED-XRF does not alter the sample and provide chemical composition. Zieba-Palus and Kunicki (2006) examined inks from ballpoint pens and gels, using XRF along with Raman and FTIR spectrometry, obtaining a good discrimination.

Inks on cultural heritage objects as paper, papyrus or tissues are other fields of application of non-destructive ED-XRF, frequently combined with other noninvasive techniques. For example, Festa et al. (2019) reported an investigation on the black ink used in 19 Egyptian inscribed textiles from the tomb of the royal architect Kha and his wife, dated to the fifteenth century BCE. In addition to XRF, analyses were also performed using untraviolet, near infrared and Raman spectroscopies, and prompt gamma activation analysis. At present, the inks have brownish color and have produced a corrosion of the linen fibers (Fig. 8.8). This evidence may suggest the use of iron gall ink, usually obtained by mixing iron sulphate with oak galls (containing gallotannic

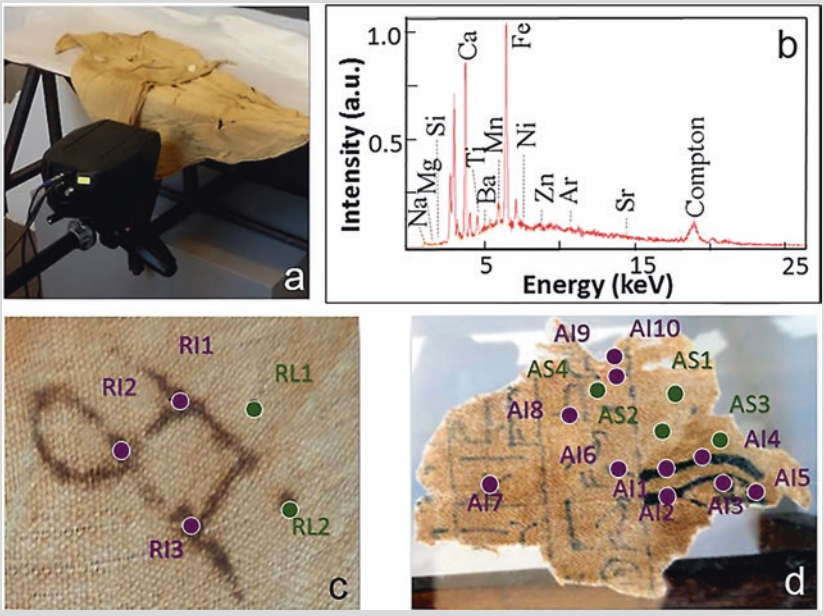

Fig. 8.8 XRF analysis of the inks in the textile. (**a**) visible light picture during XRF analysis, (**b**) ED spectrum of a point, (**c**) and (**d**) XRF measurement points. (Modified from Festa et al. 2019)

(continued)

acid). The oldest evidence of the uses of iron gall inks were dated to the third century BCE, being the technology for producing this kind of inks older than expected. The characterization of the tissues with several spectroscopies shows the presence of Fe and Mn as iron oxides and oxyhydroxides. This suggested that the ink was likely an ocher type, based on a combination of carbon and Mn-Fe oxy(hydro)xides, and thus the use of iron-gall ink should be excluded.

Acquafredda et al. 2018). Anyway, chemical investigations must be carried out on a surface of the sample that can be considered sufficiently flat; data obtained must represent the average of three or more points of analysis, so that its repeatability can be checked also by calculating the standard deviation (Table 8.1). In these situations the most useful spectrometers are those that also include the use of polycapillary lenses, so as to concentrate the incident X-ray beam on a very small area of about 20 μm: such a small area, with an appropriate positioning sample with respect to incident X-rays, can be considered suitably flat thus providing sufficiently reproducible chemical data (Acquafredda 2019).

8.9.3 Characterization of Paint, Pigments and Inks

A third example can be represented here by cases in which analyses are required on samples that cannot be moved from their seat or that cannot be introduced into X-ray spectrometers: this would be the characterization of pigments in paintings, inks, paints, which often have also an extremely thin thickness, that is that of the atmospheric particulate matter (PM10, etc.) deposited on celluloid or cellulose filters. In all these cases it is better to use energy dispersion spectrometers, preferably the latest generation silicon drift (SDD) ones, both in variable geometry configuration, decided by the operator, and in total reflection geometry (TXRF).

8.9.4 Analysis of Evidence in Criminal Scenes in Forensic Anthropology and Archaeology

One of the fields where XRF is most versatile is the investigation of evidence from crime scenes. In principle, it can be applied to any material whose elemental chemical composition must be analyzed, using destructive, non-destructive, microscopic and portable techniques, which allow the analysis of evidence with very different characteristics, both *in-situ* or in laboratory. However, XRF is revealed as a very powerful technique to characterize evidence that cannot be altered.

Criminal Scenes in Forensic Anthropology and Archaeology

A number of studies have been performed to constraint the capacity of XRF to identify skeletal remains, to distinguish human and non-human rests, as well as differentiating bone from tooth tissues. For example, Christensen et al. (2012) reported XRF analysis as a valid technique for determining bone or dental origin of unknown material. The investigation was performed with a micro XRF spectrometer, with the X-ray collimated down to a spot of 0.05–1 mm, on a variety of tissues (bones and teeth) from human and non-human origin, as well as other biological hard tissues (e.g., horn, beak, coral, etc.) and materials that can resemble osseous or dental fragments, as minerals, wood, plastic, glass, etc. They considered various degrees of deterioration as burning, weathering, aging by exposure to chemical agents. Osseous and dental fragments were accurately identified based on Ca and P levels; materials with similar Ca/P ratio have different structural characteristic from bone and tooth. They concluded that XRF is a routine and reliable method for elemental analysis, nondestructive, easy to use and straightforward to interpret.

Portable XRF (pXRF) spectrometers are becoming more and more common. Byrnes and Bush (2016) evaluated the device utility and limitation to analyze osseous materials. An important limitation is that light elements are not accurately detected, being phosphorus affected. pXRF devices use low-energy X-rays that limit their analytical performance. The depth of the analyzed area on cortical bone and the effect of removing its surface layer were carefully tested. The results show that, for example, Sr was not uniformly distributed in the bone and that signal should be corrected for depth. Furthermore, diagenesis of bone surface may represent a source of error.

On the other hand, Nganvongpanit et al. (2016) reported comparative analyses based on elemental profile that allowed to differentiate bones from humans and other mammal species with an accuracy rate higher than 92%. Furthermore, Nganvongpanit et al. (2017) applied a similar methodology based on elemental analysis performed with a handheld XRF spectrometer to a large set of human and nonhuman teeth. The results showed a high accuracy to identify human teeth from other animal or hard tissues, although the technique does not permit sex discrimination. Gonzalez-Rodriguez and Fowler (2013) applied the technique to discriminate bone fragments from different individuals.

All these examples show the potential of XRF for forensic analysis, for direct determinations or as a screening previous to more costly and time-consuming techniques as DNA analysis.

There is an increasing number of situations where human remains need to be identified, such as natural disasters, accidents, terrorist attacks, mass graves, etc. The principal method applied to this process is DNA analysis, but it can be constrained by a number of factors such as large cost of processing, condition of the remains, or availability of relatives to supply DNA samples. Bones and teeth are mineralized tissues than can be suitable for elemental analysis by XRF. The development of portable XRF spectrometers permit forensic scientists to take it to remote areas. Analysis cost is almost inexpensive compared with DNA, is very fast and non-destructive. These advantages present XRF as an ideal technique for alternative fast identification or screening technique previous to DNA.

8.9.5 Analysis of Soils, Earth Materials and Environmental Samples

XRF is a widely and routinely applied technique for chemical analysis of soils, sediments, rocks, as well as derived materials. It can be applied for the analysis of major and trace elements, by destructive and non-destructive methods. As already indicated, in the case of ED-XRF equipments, both desktop and portable, the precision and accuracy in the analysis of light elements (Na, Mg or even lighter) is low or even impossible to achieve. Also taking into account these constraints, XRF still appears to be a very versatile technique, with a wide range of use cases in geosciences.

Forensic examination of earth material can be complex because of diversity and complexity of samples. In addition to rock fragments or soil remains, earthy materials can contain materials of anthropogenic origin such as plastic fragments, brick, cement, etc. In general, an evidence of a soil may consist of a mixture of materials of diverse nature and origin. This makes quite difficult their characterization and,

Soils

Rawlings and Cave (2004) tested discrimination of soil samples based on their individual and multi-element geochemical signature (19 elements). The geochemical and statistical study was supported by a regional soil survey in eastern England (513 sample sites). The success rate was of 80% and 99.8%, respectively, for individual elements and multi-elemental analysis. However, they stressed there exist some difficulties in forensic work if compared with soils survey sampling methods such as, for example, the sample size or the type of support of typical forensic samples (i.e. the shoes of a victim).

Woods et al. (2014) analyzed 29 soils samples from East Australia. XRF elemental profile was used as a screening technique prior to being forwarded to more sophisticated analysis. XRF provides a simple and fast elemental analysis of soils. They achieved 99.5% discrimination in Australian soils samples

(continued)

using a micro-XRF device. On the other hand, Uitdehaag et al. (2017) combined element concentration by XRF analysis with a database and a discriminative model to compare soil samples from The Netherlands (50 sites). They paid special attention to the field sampling procedure and nondestructive sample preparation. De Cariat et al. (2019) also contributed to develop tools for provenance analysis of soil evidences. They produced a workflow using digital soil grids (CSIRO, Australia) that used several soil attributes that includes elemental chemical analysis obtained by XRF. They reported how their approach had several advantages compared with traditional empirical procedures: applicable to wide regions, high spatial resolution, and being transparent, reproducible and objective. These examples show that XRF is an analytical technique able to characterize soil samples in a simple and non-destructive way. However, the complexity of criminal evidences requires a further analysis of the obtained results, by applying complementary analytical techniques, as well as data and statistical analysis. The collaboration of earth science scientists with forensic analysis experts contributes to developing robust soil sample identification tools and their practical application to forensic cases.

XRF is used to determine the concentration of trace elements in numerous materials, with high sensitivity and spatial resolution, which makes it a suitable technique for environmental analysis. A very interesting case is the combination of dendrochronology and XRF analysis in forensic analyses. In particular, the detection methods applied to dendrochronology is called dendrochemistry and in forensic investigation it may contribute to resolve timing and sources of environmental incidents (Balouet et al. 2009). In the case of elements that are not normally present in wood, their mere presence in any part of the growth rings may indicate the exposure of the plant to an unusual process or chemical event. The elements most commonly analyzed are Pb as a marker for gasoline, S and Cl for fossil fuels, or Cl for solvents. ED-XRF was used to scan a single-core of *liriodendron tulipifera* (Smith et al. 2008), observing anomalies in wood formed in 1978 and early 1970s, which indicate potential exposure to contamination in mid-1970. Balouet et al. (2012) described a groundwater pollution case by dendrochemical investigation. ED-XRF was used to identify Cl as a marker derived from chlorinated solvent degradation in cores from 9 trees from Verl (Germany). Figure 8.9 shows the scan of tree 2 core with chlorine anomalies, likely interpreted as a plant response to a solvent plume.

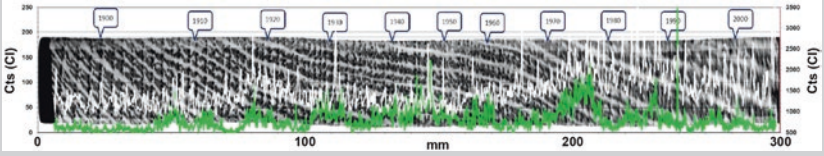

Fig. 8.9 Cl (green) and Ca (white) profiles of a tree core from Verl (Germany). The direction of growth is from left to right. Year corresponds to Cl anomalies, interpreted as response to a solvent plume. Elemental profiles are superimposed on an X-ray image of the core. (Modified from Balouet et al. 2012)

above all, the identification of their origin (Fitzpatrick and Donnelly 2021). Therefore, the analysis of a soil sample is not straightforward and requires that the geologist or soil scientist adopt the perspective of a forensic geologist or forensic soil scientist, respectively.

Forensic soil provenance is defined as the capability to spatially constraint the potential source area of an evidential sample of earth material. The use of soil samples to investigate the validity of evidence is one of the main objectives of forensic analysis of soil samples. However, the value of this evidence in establishing a source area is not obvious to police or law enforcement. If no particular or exotic geological materials occur, it is very difficult to identify the precise origin of an earth sample. To facilitate this identification task, it is necessary to have high-resolution and large-scale geological or soil databases, together with the application of data analysis and statistics techniques to the elemental analyses.

References

Acquafredda P (2019) XRF technique. In: Sabbatini L, van der Werf ID (eds) Chemical analysis in cultural heritage. Physical Sciences Reviews [Online]. De Gruyter, pp 31–61

Acquafredda P, Paglionico A (2004) SEM-EDS microanalyses of microphenocrysts of Mediterranean obsidians: a preliminary approach to source discrimination. Eur J Mineral 16:419–429

Acquafredda P, Muntoni IM, Pallara M (2018) Reassessment of WD-XRF method for obsidian provenance shareable databases. Quat Int 468:169–178

Balouet JC, Smith KT, Vroblesky D, Oudijk G (2009) Use of dendrochronology and dendrochemistry in environmental forensics: does it meet the *Daubert* criteria? Environ Forensic 10:268–276

Balouet JC, Burken JG, Karg F, Vroblesky D, Smith K, Grund H, Rindby A, Beaujard F, Chalot M (2012) Dendrochemistry of multiple releases of chlorinated solvents at a former industrial site. Environ Sci Technol 46:9541–9547

Bearden JA (1967) X-ray wavelengths. Rev Mod Phys 39:78–124

Bearden JA, Burr F (1967) Reevaluation of X ray atomic energy levels. Rev Mod Phys 39:125–142

Bertin EP (1975) Principles and practice of X-ray spectrometric analysis. Plenum Press, New York

Byrnes JF, Bush PJ (2016) Practical considerations in trace element analysis of bone by portable X-ray fluorescence. J Forensic Sci 61:1041–1045

Christensen AJ, Smith MA, Thomas RM (2012) Validation of X-ray fluorescence spectrometry for determining osseous or dental origin of unknown material. J Forensic Sci 57:44–51

De Cariat P, Simpson T, Woods B (2019) Predictive Soil Provenancing (PSP): an innovative forensic soil provenance analysis tool. J Forensic Sci 64:1356–1369

De Francesco AM, Crisci GM, Bocci M (2008) Non-destructive analytic method using XRF for determination of provenance of archaeological obsidians from the Mediterranean area: a comparison with traditional XRF methods. Archaeometry 50:337–350

Festa G, Christiansen T, Turina V, Borla M, Kelleher J, Arcidiacono L, Cartechini L, Ponterio RC, Scatigno C, Senesi R, Andrean C (2019) Egyptian metallic inks on textiles from the 15th century BCE unraveled by non-invasive techniques and chemometric analysis. Sci Rep 9:7310

Fitzpatrick RW, Donnelly LJ (2021) An introduction to forensic soil science and forensic geology: a synthesis. In: Fitzpatrick RW, Donnelly LJ (eds) Forensic soil science and geology. Geological Society, London, pp 1–32. Special Publications

Genga A, Siciliano M, Tepore A, Mangone A, Traini A, Laganara C (2008) An archaeometric approach about the study of medieval glass from Siponto (Foggia, Italy). Microchem J 90:56–62

Gonzalez-Rodriguez J, Fowler G (2013) A study on the discrimination of human skeletons using X-ray fluorescence and chemometric tools in chemical anthropology. Forensic Sci Int 231:407.e1–407.e6

Janssens K, Vittiglio G, Deraedt I, Aerts A, Vekemans B, Vincze L, Wei F, Deryck I, Schalm O, Adams F, Rindby A, Knochel A, Simionovici A, Snigirev A (2000) Use of microscopic XRF for non-destructive analysis in art and archaeometry. X-Ray Spectrom 29:73–91

Leoni L, Saitta M (1976) X-ray fluorescence analysis of 29 trace elements in rock and mineral standards. Rendiconti Società Italiana Mineralogia e Petrologia 32(2):497–510

Nganvongpanit K, Buddhachat K, Klinhom S, Kaewmong P, Thitaram C, Mahakkanukrauh P (2016) Determining comparative elemental profile using handheld X-ray fluorescence in humans, elephants, dogs, and dolphins: preliminary study for species identification. Forensic Sci Int 263:101–106

Nganvongpanit K, Buddhachat K, Piboon P, Euppayo E, Mahakkanukrauh P (2017) Variation in elemental composition of human teeth and its application for feasible species identification. Forensic Sci Int 271:33–42

Rawlins BG, Cave M (2004) Investigating multi-element soil geochemical signatures and their potential for use in forensic studies. In: Pye K, Croft DJ (eds) Forensic Geoscience: principles, techniques and applications. Geological Society, London, pp 197–206. Special Publication

Roux C, Taudte RV, Lennard C (2013) X-ray fluorescence in forensic science. In: Meyers RA (ed) Encyclopedia of analytical chemistry. Wiley, pp 1–16

Ruste J (1979) X-ray spectrometry. In: Maurice F, Meny L, Tixier R (eds) Microanalysis and scanning electron microscopy. Les Editions de Physique, pp 215–267

Smith KT, Balouet JC, Oudjk G (2008) Elemental line scanning of an increment core using EDXRF: from fundamental research to environmental forensics applications. Dendrochronologia 26:157–163

Tempesta G, Santigliano M, Nsaka JM, Scandale E (2009) Analysis and characterization of the material composition of medieval artefacts. In: Scandale E (ed) Lo scrigno del tesoro di San Nicola di Bari. The Treasure Crest of Saint Nicholas of Bari. Adda Editore, Bari, pp 39–52

Uitdehaag S, Wiarda W, Donders T, Kuiper I (2017) Forensic comparison of soil samples using nondestructive elemental analysis. J Forensic Sci 62:861–868

Woods B, Kirkbride KP, Lennard C, Robertson J (2014) Soil examination for a forensic trace evidence laboratory – part 2: elemental analysis. Forensic Sci Int 245:195–201

Zieba-Palus J, Kunicki M (2006) Application of the micro-FTIR spectroscopy, Raman spectroscopy and XRF method examination of inks. Forensic Sci Int 15:164–172

Chapter 9
Isotopic Analysis Techniques Applied to Forensics: New Frontiers of Isotope Geochemistry

Massimo D'Antonio, Valeria Di Renzo, Ilenia Arienzo, and David Widory

Abstract The isotope composition of chemical elements is an invaluable investigation tool widely used in Earth Sciences. Rocks, waters and gases acquire specific radiogenic (e.g., $^{87}Sr/^{86}Sr$) and stable (e.g., $\delta^{18}O$) isotope ratios due to geological processes such as magmas' genesis and evolution, past climatic changes, mixing among distinct reservoirs. The power of these tracers bears in the particular isotope signature any geological material acquires due to both its history and specific processes undergone. Isotope approaches have recently been applied to track air, soil and water pollutants, to identify the provenance of archaeological artifacts, and to reconstruct diet and migration paths of past animals and humans. In this framework, isotope tracers can be efficiently coupled to more traditional investigation techniques to solve forensic issues, including linking a suspect to a crime scene, identifying crime victims and the guilty of an environmental crime, tracking the provenance of drugs, identifying explosives. In this chapter, laboratory techniques for the preparation of variable materials aimed at their isotope analysis are illustrated. Examples of application of isotope analysis techniques are described for a variety of forensic problems.

Keywords Radiogenic and stable isotope ratios · Isotope ratios in forensic investigations · Samples preparation techniques · Isotopic ratios determinations

M. D'Antonio (✉) · V. Di Renzo
Dipartimento di Scienze della Terra, dell'Ambiente e delle Risorse (DiSTAR), Università Federico II, Napoli, Italy
e-mail: masdanto@unina.it

I. Arienzo
Sezione Osservatorio Vesuviano, Istituto Nazionale di Geofisica e Vulcanologia (INGV), Sez. Osservatorio Vesuviano, Napoli, Italy

D. Widory
Département des Sciences de la Terre et de l'Atmosphère, Université du Québec à Montréal, Montréal, Canada

M. Mercurio et al. (eds.), *Mineralogical Analysis Applied to Forensics*, Soil Forensics, https://doi.org/10.1007/978-3-031-08834-6_9

Most chemical elements include two or more isotopes, i.e., atoms with a specific *atomic number* Z (number of protons in the nucleus), but with a different *mass number* A (sum of protons and neutrons in the nucleus). Therefore, isotopes of the same chemical element are distinguished by their number of neutrons. There are two categories of isotopes: stable and radioactive. Isotopes subject to radioactive decay spontaneously transform over time by emitting high-energy particles to form other isotopes, which can in turn be stable or radioactive. On the other hand, isotopes that do not decay are stable, even over geological timescales; some of them can also be produced by the decay of radioactive isotopes, either directly or as intermediate or final terms of a decay series. These are then called *radiogenic*.

Radiogenic isotope geochemistry uses the isotope ratios of natural elements either to perform absolute dating of samples of geological material (rocks and minerals) or as a tracer of geological processes. The isotope ratios of these elements vary because of their more or less long permanence in the Earth' mantle or crust. During this time, the abundance of the radiogenic isotopes increases due to the radioactive decay of their parent isotopes. For example, ^{87}Sr increases over time due to radioactive decay of ^{87}Rb. *Stable isotope geochemistry* uses the fractionation existing between isotopes of a chemical element generally with a low atomic number, such as hydrogen, carbon, nitrogen, oxygen, and sulfur (light elements). Isotope fractionation is the enrichment, resulting from various natural processes, of a lighter isotope of a given element with respect to a heavier one, or vice versa. Therefore, *isotope geochemistry* offers efficient tools to investigate many geological processes, including variations in climatic conditions in marine and oceanic environments; assimilation of crustal rocks by a crystallizing magma; mixing between distinct magmas; mixing between waters from different sources; mixing of different clast types in sedimentation basins. For all these purposes, the isotope composition of the elements of interest is reported as ratio between the abundance of two isotopes of the same element, since these ratios are determined using specific analytical tools (Sect. 9.3). In the case of heavy elements such as Sr, Nd and Pb, the ^{87}Sr/^{86}Sr, ^{143}Nd/^{144}Nd and ^{206}Pb/^{204}Pb ratios are used, where the radiogenic isotope, placed in the numerator, is related to a stable and non-radiogenic isotope of the same element placed in the denominator (White 2015, and references therein). In the case of light elements such as B, C, N and O, the so-called δ notation is used, in which the measured values of the isotope ratios are normalized to those of a standard, for example δ^{11}B, δ^{13}C, δ^{15}N and δ^{18}O (White 2015, and references therein).

9.1 Sample Preparation

When facing a crime scene, investigators might need characterizing a great variety of both inorganic and organic materials. Moreover, other contexts besides crime scenes may offer additional investigation materials. More specifically, inorganic materials of interest may include soil, sand, clay, rock/mineral fragments, and parts from building constructions such as mortar, plaster, bricks, concrete, all derived

from natural raw materials. On the other side, organic materials of interest span among human or animal remains such as hair, bones, teeth, as well as food, beverages, plants including those cultivated for obtaining drugs such as *Cannabis* for marijuana, *Papaver somniferum* for opium, and *Erythroxylum coca* for cocaine.

Depending on the chemical nature and physical state of the find under investigation, and on the type of element(s) to be analyzed for its isotope composition, a specific preparation procedure suitable for the measurement must be followed. Furthermore, isotope analysis may be carried out either on simple compounds containing large amounts of the element of interest, or on chemically complex matrices where the element of interest is dispersed into trace amounts. This is important because there are some analytical techniques capable of analyzing a single element in a complex matrix, and others needing this element to be isolated from its matrix through specific separation techniques. The latter allow obtaining a single element in an ionic form in either aqueous or acid solution, an easily solubilized simple compound (a salt) of the element of interest, or a gaseous element or compound.

The element of interest may be in many cases a trace metal such as Sr or Pb dispersed in a solid. In these cases, sample preparation must be carried out in a *clean room* laboratory (Fig. 9.1), to minimize any possible contamination of the sample from external sources such as air, dust or water.

For isotope analysis, an ISO 6 class (i.e., <10,200 particles per m^3 with ≥0.3 μm diameter) clean room is desirable. The filtered air is introduced into the clean room with an overpressure of a few pascals and then extracted to the outside to assure an exchange of at least 50 air volumes per hour. As a further precaution aimed at minimizing sample contamination, the employed laboratory glassware is made up of either Teflon (PTFE, *Polytetrafluoroethylene*) or PFA (*Perfluoroalkoxy alkanes*) due to their chemical resistance and anti-stick properties. High-purity chemical reagents of *Suprapur*® and/or *Ultrapure* grades, diluted with Milli-Q® deionized water (18.2 MΩ cm^{-1} resistivity) are utilized for glassware cleaning, sample dissolution and the other chemical processes described in the following section. The latter procedures require using strongly corrosive and toxic reagents and must be carried out under a laminar flow hood (Fig. 9.1), capable of extracting and reducing their fumes.

9.1.1 Preparation Techniques for Inorganic Samples

Inorganic samples (*rocks*, *minerals*, *amorphous material*) of interest for forensic investigations are extremely variable in chemical composition. In several cases, they are constituted of variable amounts of minerals, namely natural solid substances where the constituent atoms are ordered in a tridimensional crystal lattice. Most minerals on Earth are silicates and carbonates, whereas other species such as oxides, phosphates, sulfides, and pure metals are less common.

Inorganic samples can be treated as a whole or might need to be subdivided into their constituting phases, including various minerals and amorphous fraction. The element of interest can occur in one or more of the separated phases. The separated

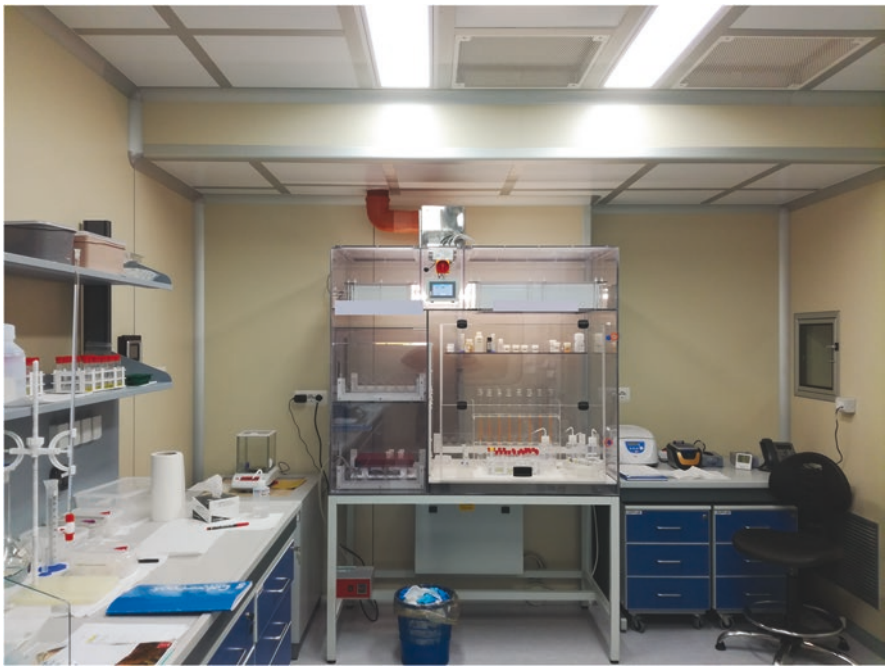

Fig. 9.1 ISO 6 class clean room. Notice the High Efficiency Particulate Air (HEPA) filters on the ceiling from which clean air enters the room and, in the background, a Perspex laminar flow hood equipped with two HEPA filters located on top, to achieve ISO 5 class. (Source: Clean Room, Department of Earth, Environmental and Resources Sciences (DiSTAR), University Federico II, Naples, Italy. Photo by M. D'Antonio)

fraction(s) of the sample will have a certain grain-size; the latter should be on the order of a few tens of microns for the sample to be efficiently treated during the following chemical procedures. Should the grain-size be too large, it can be reduced to the desired value by means of suitable pulverization techniques and devices, such as planetary ball mills.

9.1.1.1 Extraction with a Solvent

Based on the type of compound and its solubility, a variety of solvents can be used including simple water, diluted acid solutions of HCl, HNO_3, CH_3COOH, and organic solvents like CH_2Cl_2. One useful application is the extraction of a protein from food (Sect. 9.1.2.5). If the element of interest represents the main component of a simple, soluble compound such as a chloride or sulfide, it can be easily extracted using a suitable solvent. However, extraction with a solvent has a limited applicability because isotope analysis is carried out on mostly insoluble inorganic materials. Such

compounds are complex matrices where the element of interest does not form its own mineral but is dispersed in trace amounts. Therefore, the sample must be solubilized through dissolution with a mineral acid, as described in the following section.

9.1.1.2 Dissolution with Mineral Acids

A trace element of interest can be extracted from complex matrices utilizing various techniques depending on the chemical nature and physical state of the sample. A typical dissolution procedure of a solid inorganic sample, using *Suprapur*® grade reagents, includes several steps:

- Weighing 50–100 mg of the powdered sample in a PTFE crucible using a high-precision analytical balance (Fig. 9.2a).
- Leaching: based on the alteration state of the sample it may be useful to pre-treat the powder with 1–2 mL of a diluted HF or HCl, at either room or higher temperature, for few minutes to tens of minutes. The acid solution is then removed using a pipette with a sterilized tip, and the procedure repeated once or more times. At the end, the powder is rinsed several times with 1–2 mL of Milli-Q® water, every time removed with a pipette. This procedure can effectively remove secondary carbonates, chlorides and/or undesired silicate glass, that may contain significant amounts of trace elements that might interfere with the measured isotope ratio.
- First acid dissolution, finalized to the disaggregation of chemical bonds in most silicates: it is achieved by adding a mixture of 40 vol.% HF (the only mineral acid capable of dissolving silicates) and 14 M HNO_3 (5:1), for a total of 1.5 mL per 50 mg of powder, closing tightly the vial and leaving it on a hot plate (Fig. 9.2b) at a temperature of ~120 °C for a time variable from 12 h to 4–5 days, depending on the type of sample. At the end, the vial is left open on the hot plate under a laminar flow hood until complete evaporation is achieved (generally 3–4 h). The resulting solid will be made up of very reactive fluoride compounds.
- Second acid dissolution, aimed at transforming these fluorides into nitrates: 0.5 mL of 14 M HNO_3 are added to the sample in the vial, and left open on hot plate under a laminar flow hood until complete dryness. The resulting nitrates are almost completely soluble in diluted acid solutions. However, for isolating the element of interest for the isotope analysis, chlorides are the preferred chemical form (see Sect. 9.1.3).
- Third acid dissolution, to transform the nitrates back into chlorides: 2 mL of 6 M HCl are added to the sample in the vial and left open on the hot plate under laminar flow hood for the time required to reach complete evaporation.

The described procedure may vary depending on specific characteristics of the sample and on its chemical response to the different types of acid solutions employed. Adaptations may include (i) adding 30% H_2O_2 to the powder to remove organic matter; (ii) putting the closed vials with the mixture acid + sample in an

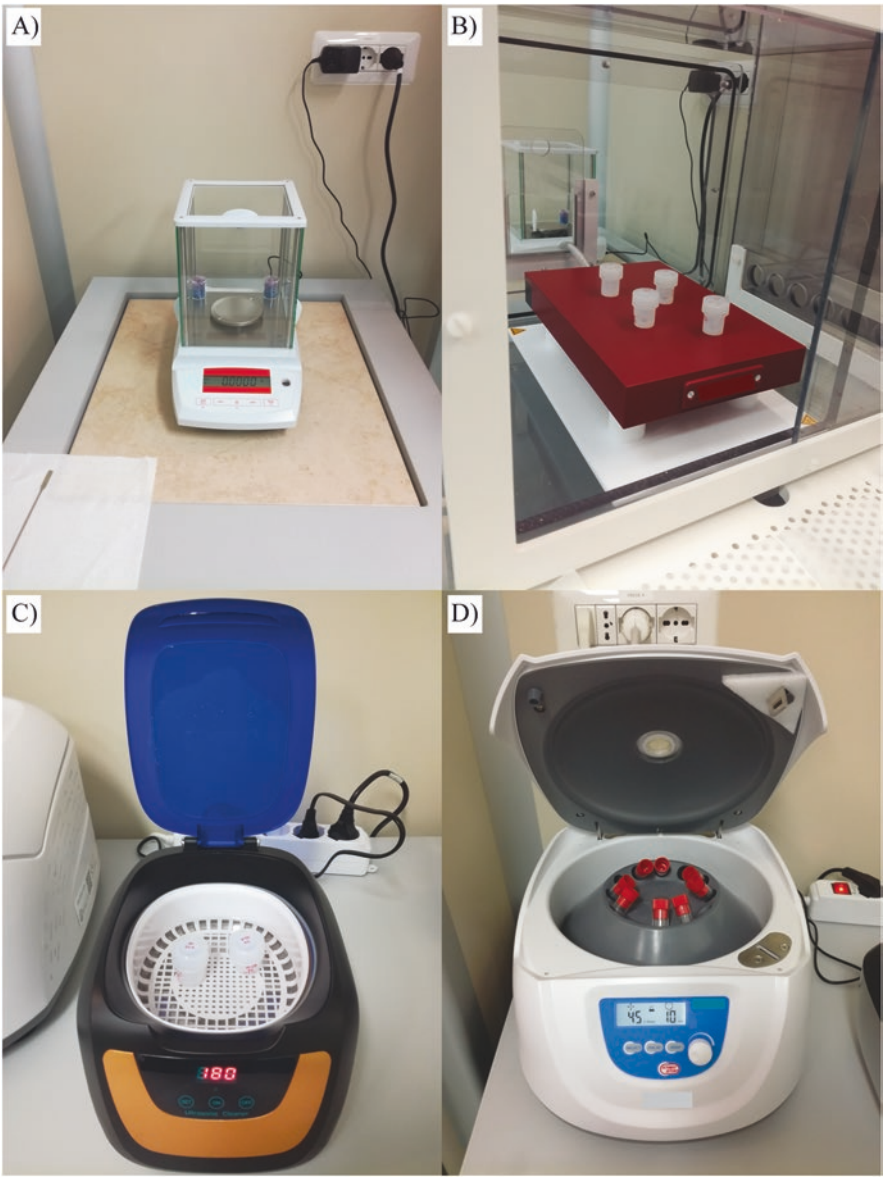

Fig. 9.2 Equipment commonly employed for sample preparation in a clean room. (**a**) high-precision analytical balance placed on an antivibration table; (**b**) PFA-coated, acid-resistant hot plate, with Savillex® vials on top for sample digestion; (**c**) ultrasonic bath; (**d**) centrifuge. (Source: Clean Room, DiSTAR, University Federico II, Naples, Italy. Photos by M. D'Antonio)

ultrasonic bath (Fig. 9.2c) for 5–10 min at the initial step of the acid dissolution to facilitate fragments' disaggregation; (iii) varying the residence time of the mixtures on the hot plate before opening the vials.

At the end of the acid dissolution, the chloride residue is generally fully soluble. It is then retaken with 1–2 mL of 2.5 M HCl, transferred into a pre-cleaned centrifuge tube, and centrifuged at 5000 rpm for 10 min (Fig. 9.2d). This latter procedure aims at separating possible insoluble matter that would have accumulated at the bottom of the tube, as samples may include a variable amount of accessory mineral phases that are poorly sensitive to the described acid dissolution (e.g., metal oxides, magnetite). The supernatant solution is ready to undergo chromatographic separation (Sect. 9.1.3); it contains virtually all the chemical elements of the original sample, except for silicon, which bonded with the anion F^- during the first dissolution and escaped from the solution as SiF_6 upon evaporation. Further details on the described procedures are provided by Arienzo et al. (2013).

9.1.1.3 Fusion with a Flux

When the matrix includes a significant amount of insoluble mineral phases, melting the sample at high temperature and then quenching it to obtain an easily soluble glass bead may be required. The laboratory should be thus equipped with the following: a muffle reaching temperatures of at least 1000 °C; crucibles made of noble metals or metal alloys (e.g., Pt, Pt-Ir, Au-Pd); some *fluxes*, namely low-melting compounds (e.g., anhydrous sodium carbonate, Na_2CO_3; sodium or potassium hydroxides; lithium metaborate – boric acid, $LiBO_2$), to be added to the powdered sample to lower its melting point. Complete fusion shall be achieved within 30–60 min; once cooled down, the glass bead will easily dissolve in diluted nitric acid solutions. *Contamination* of the sample by the flux itself, which adds significant amounts of chemical elements such as lithium, boron and especially alkalis plus a variety of trace elements may happen and heavily affect the result of the isotope measurement.

9.1.2 Preparation Techniques for Organic Samples

9.1.2.1 Teeth and Bones

Human or animal teeth and bones found on a crime scene must be cleaned in an ultrasonic bath (Fig. 9.2c) for several minutes with a suitable solution, such as methanol and chloroform (CH_4O:$CHCl_3$ = 2:1; Meier-Augenstein and Fraser 2008), or deionized water and hydrogen peroxide (H_2O:H_2O_2 = 3:1; Arienzo et al. 2020). A small piece of the tooth enamel or bone, both mostly made of hydroxyapatite, can be cut with a dental drill equipped with a diamond-coated saw (Fig. 9.3). The organic fragment is then washed again in the ultrasonic bath, followed by dissolution (like that described in Sect. 9.1.1.2), though simplified because teeth and bones dissolve in nitric and hydrochloric acids with no need for hydrofluoric acid (Arienzo

Fig. 9.3 Cutting of a tooth using a dental drill equipped with a diamond-coated saw. (Source: Radiogenic Isotope Laboratory, National Institute of Geophysics and Volcanology, Section of Naples Osservatorio Vesuviano, Naples, Italy (Photo by M. D'Antonio))

et al. 2020). Hydroxyapatite can be extracted through a buffer solution of 0.75 M ammonium hydroxide (NH_4OH) and silver nitrate ($AgNO_3$). Further details may be found in Meier-Augenstein (2010).

9.1.2.2 Hair

Made of keratin, a fibrous protein, hair must be treated with specific procedures. Among metals, Sr and Pb isotope ratios of hair from mummies and modern humans have been widely used as tracers for anthropological investigations (e.g., Font et al. 2012; Lugli et al. 2018) (see Discussion). The procedure includes several steps, using Milli-Q® water to remove surface dust and dirt, and Ultrapure grade reagents for dissolving 50–100 mg of hair cut in small pieces. Both archaeological and modern hair samples are immersed in a 2:1 chloroform:methanol solution ultrasonicated for 10 min, followed by rinsing with Milli-Q® water. The whole step is repeated three times. Then, a leaching procedure is carried out with cold 2 M HNO_3 for 30 min, repeated 2–3 times, followed by rinsing with Milli-Q® water. The dissolution is achieved by: (1) adding 2 mL of *aqua regia* (14 M HNO_3:8 M HCl = 3:1) in a PFA vial kept closed on hot plate at 110 °C for 24 h, followed by opening for complete evaporation; (2) adding 1 mL of 14 M HNO_3 at 110 °C for 24 h, followed by opening for evaporation; (3) removing organic matter adding alternated 100 μL aliquots of H_2O_2 and 14 M HNO_3 leaving the vial open on hot plate at 105 °C for evaporation. The residue is taken up in 3 mL of 3 M HNO_3. The obtained solution is ready for chromatographic separation (Sect. 9.1.3.1).

9.1.2.3 Soil

Soil being produced by the degradation of rocks exposed to the surface (bed-rock) is made up of an inorganic fraction, including variable amounts of minerals and non-crystalline material, and an organic fraction. The amount of soil needed for

determining the isotope ratio of a metal such as Pb, Cr, etc. is in the order of a few grams to tens of grams, significantly higher than for rock samples. This comes because, rather than their metal content in the bulk soil, it is important to analyze their labile, or "bioavailable" content. This corresponds to the metal content mostly retained at the soil's surface in its inorganic fragments and that is released in a diluted acid solution and thus available to the plants and other organisms. Any polluting metal added to a soil, for example either as deposited aerosols or wastewater, will also adsorb on the soil fragments surface. Once the amount of soil is weighed in a suitable beaker, there are many ways to extract its bioavailable fraction. One is leaving the sample immersed in 100 mL of 1 M ammonium acetate ($C_2H_3O_2NH_4$) overnight, slowly agitating the solution for the entire period. The solution is then filtered through a 0.45 μm filter, acidified with concentrated HNO_3 and left on a hot plate until complete dryness. The final residue is retaken in ~20 mL of 2.5 M HCl and, after being centrifuged for 10 min at 5000 rpm, is ready for chromatographic separation (Sects. 9.2.3 and 9.3). A different procedure can be adopted to extract bioavailable strontium from soil samples (Mercurio et al. 2014): adding a 1 M ammonium nitrate (NH_4NO_3) solution to 20 g of 2 mm size sieved soil, and agitating the solution for 2 h at 50 rpm, followed by filtration and acidification with a HNO_3:H_2O 1:1 solution.

9.1.2.4 Plants

Leaves can be crumbled in a mortar with a pestle and dissolved in methanol (Galimov et al. 2005) and analyzed (Sect. 9.2.3). The preparation of plant samples for analyzing the isotope ratios of their heavy metals is more complex because the organic fraction must be removed to isolate the element(s) of interest. According to Petrini et al. (2015), 2 mL of must can be left drying slowly at 70 °C; the residue is dissolved in 0.2 mL of concentrated Ultrapure HNO_3 for 2 h until the solution becomes clear. After dilution in 13 mL of Milli-Q® water, the solution is ready to be analyzed by ICP-MS techniques (Sect. 9.2.1). For analysis by TIMS (Sect. 9.2.2), a high temperature mineralization process (*thermal ashing*) is required to preconcentrate trace elements. The procedure starts with drying 5 g of sample, pretreated as previously described for ICP-MS, in a Nickel crucible at 60 °C; then, the sample is calcinated at temperature increasing up to 700 °C for 1 h in a muffle. The residual powder is dissolved in 2.5 M Ultrapure HCl, and the resulting solution is ready for separating the element of interest through liquid chromatography (Sect. 9.1.3.1). Mercurio et al. (2014) carried out the dissolution of branches, leaves, grapes and wine by acid leaching (HNO_3:H_2O_2 6:1 solution) in a microwave oven. The residue was then acidified with a HNO_3:H_2O 1:1 solution and kept at 4 °C before separating Sr by liquid chromatography (Sect. 9.1.3.1).

Leaves and inflorescences were treated by West et al. (2009b) as follows: an aliquot of the dried sample is crumbled in a mortar with a pestle; the coarse fraction is then eliminated with a 250 μm opening stainless-steel sieve. The finest part is thermally ashed by increasing temperature every 2 h to 80, 200 and 600 °C. The

dissolution of the obtained powder is accomplished using concentrated HNO_3 in a PTFE vial on hot plate, until complete evaporation. 30% H_2O_2 is finally added at 80 °C to remove organic matter residues. The dried sample is retaken in a 3.5 M HNO_3 solution that can be utilized for separating the element(s) of interest through liquid chromatography techniques (Sect. 9.1.3.1).

9.1.2.5 Food

Various types of food can be isotopically analyzed for both light and heavy atomic number elements. The sample preparation strictly depends on the type of material and the specific analytical technique to be utilized. $\delta^{18}O$ and δD can be measured directly on water extracted from frozen meat. For the oxygen isotopes, water is equilibrated with a reference sample of known $\delta^{18}O$. For hydrogen isotopes, water goes through *pyrolysis*, i.e., combustion in absence of oxygen, and then reduction in a hot furnace containing chromium at 1075 °C, allowing the release of hydrogen. Isotope analysis can also be carried out on protein extracted from food dry residues obtained with dichloromethane (CH_2Cl_2) in a *Soxhlet extractor*, successively homogenized in a vibrating ball mill. A weighed amount of the protein placed in a tin capsule undergoes pyrolysis in a furnace filled with tungsten and cobalt oxides at 590 °C. The released CO_2 and NO_x are then separated by gas chromatographic techniques for determining their $\delta^{13}C$ and $\delta^{15}N$ (Boner and Förstel 2004).

The isotope composition of light elements, e.g., H, C, N, O, can be measured on casein and/or glycerin extracted from 4 g of frozen and dried cheese by means of petroleum ether (pure or mixed with ethylic ether in 2:1 ratio) in a *Soxhlet* device, (e.g., Pillonel et al. 2005; Camin et al. 2012). The extracted protein is then homogenized and centrifuged to separate ether, cleaned twice with deionized water, and centrifuged again. The residue is lyophilized and kept at room temperature. An aliquot is combusted or pyrolyzed, if analyzed by gaseous source mass spectrometry techniques (IRMS; Sect. 9.3.3). If ICP-MS techniques (Sect. 9.3.1) are used, 0.65 g of the sample are weighed in a quartz crucible and placed in a microwave oven with 4 mL of 14 M HNO_3 and 2 mL of H_2O_2, both of *Suprapur*® grade.

For rice samples, the preparation is similar to that of cheese. If the isotope analysis is made by ICP-MS techniques (Sect. 9.2.1), the sample is digested with concentrated HNO_3 in a microwave oven. For IRMS techniques (Sect. 9.2.3), the sample is dried, pulverized, and homogenized. Then, a 0.5–2 mg aliquot is weighed in a tin or silver capsule and subjected to pyrolysis (Kelly et al. 2002; Suzuki et al. 2008).

Liu et al. (2014) analyzed Sr and B isotopes in unroasted coffee beans from the main production zones worldwide. Beans were first dried and frozen, then 5 g were pulverized, from which 50 mg were dissolved in a HNO_3 – H_2O_2 solution in a PTFE vial left for 2 h on hot plate at 120 °C. The obtained solution, diluted in Milli-Q® water, was in part utilized for determining the trace element content by ICP-MS (Sect. 9.2.1), and in part subject to chromatography to separate Sr and B (Sect. 9.1.3), before analysis by TIMS (Sect. 9.2.2).

9.1.2.6 Beverages

Wine is one of the key beverages isotopically investigated with the purpose of authenticating its terroir and identifying adulterations. $\delta^{13}C$ can be determined on: (i) ethanol isolated by distillation; (ii) sugars isolated by lyophilization after precipitation of other components with $Ca(OH)_2$; (iii) organic acids isolated by liquid chromatography (e.g., Rossmann et al. 1996; Weber et al. 1997). Combustion of its sugars allows the release of a gaseous compound from which CO_2 is separated and purified (Sect. 9.1.2.7).

$\delta^{18}O$ is determined on the water extracted from wine through complex distillation procedures carried out under vacuum, followed by freezing in liquid nitrogen (−195.8 °C) and re-heating (West et al. 2007). Similar procedures can be applied to beer, whisky, champagne, and even on carbonated non-alcoholic beverages for determining $\delta^{13}C$ (Meier-Augenstein 2010, and quoted references).

Strontium isotope ratios in wine has recently developed as one frontier application in food isotope geochemistry (Saar de Almeida et al. 2022). Marchionni et al. (2016) determined $^{87}Sr/^{86}Sr$ on 5–10 mL of wine, must and grape juice left to dry at 90 °C. Residues were digested with 3 mL of high-purity 30% H_2O_2 leaving the vial closed for 1 day at 40 °C, then opening it until complete evaporation at 90 °C. A second dissolution step was achieved with 2 mL of high-purity concentrated HNO_3, left closed for 1 day at 150 °C and then opened to evaporation. The residue was taken up in 1 mL of 3 M HNO_3 from which Sr was separated by chromatography (Sect. 9.1.3). Similar preparation techniques to those described for the analysis of must and grape in Sect. 9.1.2.4 were also used (Mercurio et al. 2014; Petrini et al. 2015).

For Sr isotopes in olive oil by TIMS (Sect. 9.2.2), Medini et al. (2015) proposed a specific protocol. Up to 100 g of oil is dissolved in an Ultrapure 7 M HNO_3:H_2O_2 7:1 solution; the residue is calcinated in a quartz crucible left for 2 h in a muffle at 650 °C; the residue is taken up in 2 M HNO_3; lastly, Sr purification is carried out by chromatography (Sect. 9.1.3.1).

9.1.2.7 Extraction of a Gas from a Solid

Light elements' (H, C, N, O, S) stable isotopes must be analyzed under gaseous form (Sect. 9.2.3). However, the element(s) of interest is (are) often hosted in a solid compound, either organic or inorganic, requiring specific protocols for extraction as a gas. In most cases, the material to be analyzed is animal or vegetal tissue fragments that can be solubilized through various techniques as described in the previous sections. For inorganic solid materials, conversion is carried out through one or more of the following techniques: isotope exchange, acid dissolution, oxidation, reduction, combustion, under vacuum pyrolysis, fluorination combined with laser ablation. One reason for combining more than one technique is that the gas of interest can be a component of a gaseous solution, from which it needs to be isolated. To this purpose, ad-hoc extraction/purification lines (Fig. 9.4) are available,

Fig. 9.4 An example of gas extraction and purification line. (Source: Geowissenschaftliches Zentrum, Abteilung Geochemie, Georg-August-Universität, Göttingen, Germany. Photo courtesy by R.S. Iovine)

assembling several cold and hot "traps" connected by metal hairline tubes and valves, and including a vacuum pumps system and a gas-chromatographer (Sect. 9.1.3.2). Cold traps are held at −195.8 °C by liquid nitrogen to capture condensable gases (e.g., H_2O, CO_2, SO_2), whereas non-condensable gases (e.g., O_2, N_2, noble gases) are either pumped out by the vacuum system, if undesired, or let go further to enter the gas chromatographer. Hot traps, held at high temperature, are designed to either oxidize or reduce gaseous species. At the end of the extraction/purification line, a gas chromatographer separates the gaseous species of interest that will be analyzed individually, as described in Sect. 9.2.3.

9.1.3 Chromatographic Separation Techniques

Chromatographic separation is needed when the chemical element of interest must be isolated from the hosting matrix prior to its isotope analysis. Chromatography is based on the different affinities that chemical elements have when they interact with certain materials. A chromatography device is composed of (i) a *stationary phase* capable of selectively trap and then sequentially release chemical elements, and (ii)

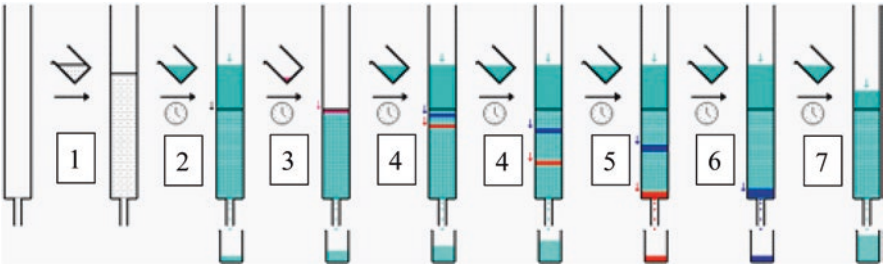

Fig. 9.5 Sketch of chromatographic columns illustrating the sequence of steps to separate compounds (or single ionized elements) from a complex matrix. (1) ion exchange resin (stationary phase); (2) conditioning of the resin with a fixed molarity acid solution; (3) loading of the sample (mobile phase) containing two different compounds (red and blue); (4) discarding of the eluates, during which the two compounds are physically separated by the resin; (5) collection of the eluate containing the red compound; (6) collection of the eluate containing the blue compound; (7) cleaning and reconditioning of the resin for a future use. (Source: Wikipedia, modified, https://en.wikipedia.org/wiki/Chromatography#/media/File:Column_chromatography_sequence.png)

a *mobile phase* containing the element of interest within its matrix. The stationary phase can be placed in a column (Fig. 9.5), on paper, etc. Depending on the physical state of the mobile phase, either liquid or gaseous phase chromatography can be employed.

9.1.3.1 Liquid Phase Chromatographic Separation

To analyze metals such as alkalis and alkaline earths including Sr, Rare Earth Elements (REE) including Nd, heavy metals such as Cr, Pb, etc., liquid phase ion-exchange chromatography is employed on already liquid samples or samples solubilized with one of the techniques described in Sects. 9.1.1 and 9.1.2. Figure 9.6 illustrates chromatographic columns employed to separate Sr and REE from both inorganic and organic samples. Such columns are made of hot-molded 22 cm high cylindric quartz tubes with inner diameter of ~0.5 cm. The total volume of the column is ~20 mL including the top cylinder reservoir. The stationary phase is made up of a cation exchange resin bed (AG 50 W X-8, 200–400 mesh, BioRad®), held by a 20 μm porous filter (*Teflon frit*) at the bottom. The *column volume, CV*, i.e., the effective volume of resin, is usually 2 mL. For samples whose concentration of the element of interest is low, microcolumns (Fig. 9.6b) with a reduced column volume (100–200 μL) can be used to achieve an efficient separation, with the advantage of reducing the reagents to be used and, hence the total *blank* of the analysis. The column is loaded with usually 0.5 mL of the solubilized sample for CV = 2 mL. Since the AG 50 W X-8 resin is conditioned in 2.5 M HCl for an efficient separation of alkalis and alkaline earth metals, the sample solution must have the same form at the end of the preparation procedure (see Sects. 9.1.1 and 9.1.2).

Each column needs to be pre-calibrated to establish the correct volume of eluent to use before passing the volume of eluent containing Sr. A careful calibration of

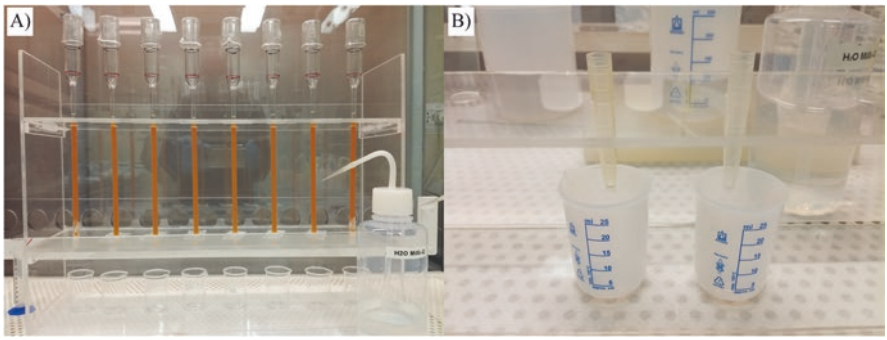

Fig. 9.6 (**a**) Chromatographic columns filled with cation exchange resin (see text for details), used to separate Sr and REE from both inorganic and organic samples. (**b**) Microcolumns built from 1 mL sterile pipette tips to be filled with Sr-Spec® cation exchange resin, used to separate Sr and Pb for samples with low concentrations of these elements. (Source: Clean Room, DiSTAR, University Federico II, Naples, Italy. Photo by M. D'Antonio)

each column will prevent collecting Rb, a metal showing affinity with Sr, that isobarically interfere with Sr during analysis (see Sect. 9.2). The eluate containing Sr, collected in a PTFE vial, is then left to evaporate on hot plate under laminar flow hood until complete dryness.

After the collection of Sr, from the same sample aliquot it is possible to separate the light Rare Earth Elements (LREE) all together, including neodymium for determining its isotope ratio. The eluent must be stronger than the one used for collecting Sr, usually 6 M HCl, and the right volumes to be discarded and collected with the LREE must be established with a calibration as well. The eluate containing the LREE, after evaporated to complete dryness, will be introduced in chromatographic columns filled with LN Spec® resin for separating Nd. All Sr and Nd dry fractions are nitrified with a few droplets of 14 M HNO_3, before loading onto a metal filament that will be introduced into the mass spectrometer (Sect. 9.2.2.1).

After purification, the resin can be regenerated through cleaning with several CVs of 6 M HCl, rinsing with 1.5 CVs of Milli-Q® water, and finally reconditioning with a few CVs of 2.5 M HCl.

9.1.3.2 Gas Phase Chromatographic Separation

The separation of light elements, such as H, C, N, O, S from a gaseous mixture is achieved through *gas-chromatography* (GC). The typical scheme of a *gas-chromatographer* (Fig. 9.7) includes: an injection system for the gas sample (1 in Fig. 9.7a) that uses an inert carrier gas such as Helium or Argon (2); a small, temperature-controlled oven (3 in Fig. 9.7a, b) hosting a thin chromatographic column of variable length, from a few dm (*packed column*; Fig. 9.7c) to a few tens of meters (*capillary column*; Fig. 9.7d). In the column, the various gaseous species of the sample interact differently with the stationary phase, made of a *zeolite* or

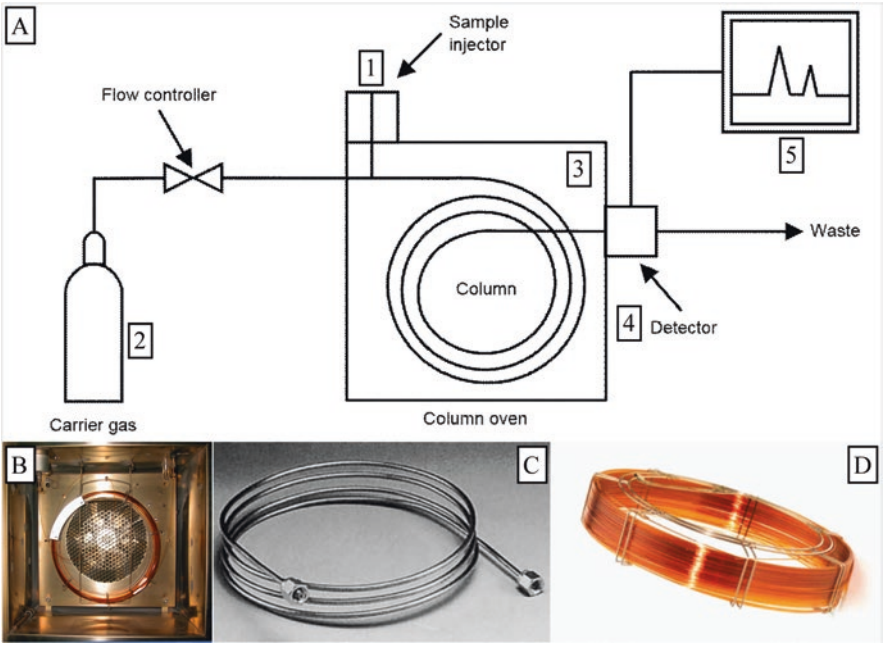

Fig. 9.7 Scheme of a gas-chromatographer. (**a**) instrument parts: (1) sample injector; (2) reference (carrier) gas reservoir; (3) oven hosting the chromatographic column; (4) detector; (5) schematic chromatogram; (**b**) inner part of the oven; (**c**) packed chromatographic column; (**d**) capillary chromatographic column. (Source: Wikipedia, modified)

polystyrene adhering by a few tens of μm on the inner walls of the column, and are separated before they reach the detector (4 in Fig. 9.7a). The detector is either an ionizing flame or a thermal conductivity device or a reduction photometer. Lastly, the signals out of the detector are converted into a chromatogram (5 in Fig. 9.7a) where each gas is distinguished by a gaussian-shaped peak, whose area is proportional to its amount in the mixture. Quantitative measurements are possible by means of calibration curves obtained by analyzing reference samples with known composition (standards). The gas-chromatographer is interfaced with the gas source mass spectrometer (Sect. 9.2.3).

9.2 Instrumentation

Mass spectrometry is the main analytical technique for determining the isotope ratios of elements. It separates charged particles (i.e., ions) based on their mass or, more correctly, based on their mass/charge ratio. Therefore, it allows both distinguishing isotopes of a single element and calculating ratios between their abundances (isotope ratios). Samples of all physical states of matter can be analyzed but

must be treated to be introduced as a solid, liquid or gas in the differently designed spectrometers, summarized below. For the isotope ratios of heavy elements (Pb, Sr, REE), either inductively coupled plasma-mass spectrometry (ICP-MS), in which the sample is analyzed as a liquid, or thermal ionization mass spectrometry (TIMS), as a solid, exist. For both techniques, the sample is transformed, by high temperature heating, into free atoms and, partially, into positive or negative ions. Isotope ratio mass spectrometry (IRMS) is used for light elements (H, C, N, O, S), where samples are introduced as a gas, obtained from a gas, solid or liquid sample through appropriate preparation (Sect. 9.1). Alpha (α) and gamma (γ) spectrometry are specifically used for measuring the radioactivity of unstable isotopes.

9.2.1 Inductively Coupled Plasma-Mass Spectrometry

9.2.1.1 Principles and Instrumentation

ICP-MS combines mass spectrometry with an inductively coupled plasma source and consists of (Fig. 9.8): a sample injection system, an ion source, called ICP torch, where ions are generated and then extracted; a mass analyzer; an ion detection apparatus; a data acquisition and processing system (computer). The sample is a liquid

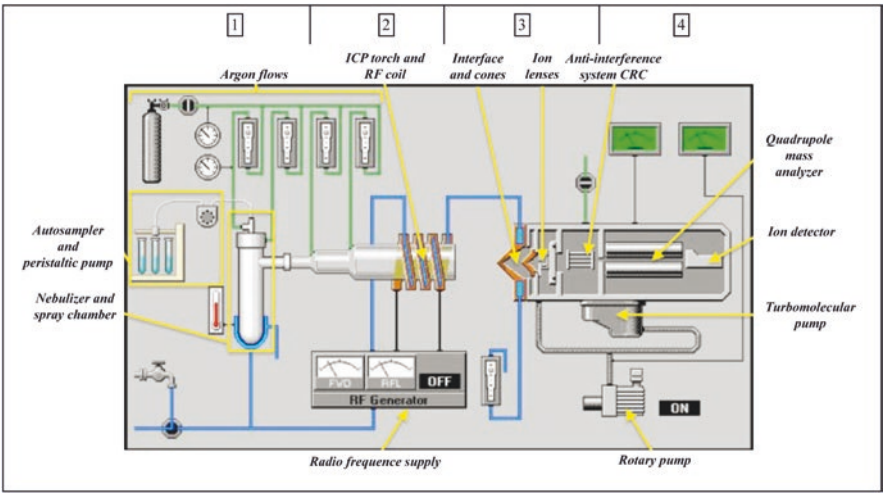

Fig. 9.8 Schematic of an inductively coupled plasma-mass spectrometer. Instrument parts: (1) sample gas injection system; (2) ICP torch; (3) interface between plasma and mass spectrometer, including a *sampling cone* and a *skimmer cone*; (4) mass spectrometer consisting of a *quadrupole mass analyzer* and an *ion detector*. (Source: The University of Texas at Austin, Department of Geological Sciences, Jackson School of Geosciences, TX, U.S.A., http://www.jsg.utexas.edu/icp-ms/icp-ms/, modified)

solution that may even be a complex matrix, such as that resulting from the dissolution techniques described in Sect. 9.1.

The liquid sample is aspirated through a peristaltic pump and introduced into a nebulizer, which converts it into an aerosol. The nebulizer rarely produces a uniform aerosol consisting of droplets of the same size. To prevent the largest droplets from reaching the plasma, a spray chamber is placed between the nebulizer and the ICP torch. The gas carrying the aerosol enters the chamber where it undergoes a change of direction. The largest drops are eliminated by being blocked along the walls of the spray chamber and are drained off, whereas the smallest ones reach the plasma.

The ICP torch consists of three concentric quartz tubes inside which argon circulates. The plasma is obtained with an inductively coupled radiofrequency generator (Fig. 9.8). A water-cooled copper coil, powered by a radio frequency (RF) generator, creates an intense magnetic field wrapping the ICP torch. The ionization of argon gas is triggered by a spark produced by a Tesla coil, and the resulting cations (Ar^+) and electrons are accelerated by the magnetic field produced by radio frequencies. Collisions between charged particles and argon atoms generate a plasma, an ionized gas stable at very high temperatures. The sample entering the plasma is rapidly volatilized at 6000–10,000 kelvins, and most of its compounds are dissociated into their constituent elements, partially ionized. These ions produced at atmospheric pressure are extracted from the plasma thanks to the high vacuum of the mass spectrometer. The interface between the plasma source and the mass spectrometer consists of two opened nickel cones, the *sampling cone* and the *skimmer cone*, which allow ions to pass, deflecting most of the molecules and atoms in the neutral state. Ions focusing after the skimmer cone is obtained through electrostatic lenses. A *photon stop* placed along the direction of the beam, prevents light reaching the ion detector reducing the background signal. The ion beam is deflected around the photon stop and moves towards the mass analyzer. The most common mass analyzer is a mass filter called *quadrupole*. It allows only ions having a certain mass/charge ratio to reach the detector, by varying potentials applied to two opposite pairs of metal cylinders. The resolution of the quadrupole is sufficient to separate masses of elements showing adjacent peaks. The ability to count the ions individually and the low background signal give the instrument a good sensitivity. Indeed, ICP-MS allows quantifying a great variety of chemical elements, including trace elements, either sequentially or simultaneously. More sophisticated than quadrupoles, multi-collector ICP-MS are equipped with Faraday Cups and/or secondary ion multipliers (SEM), corresponding to those installed on TIMS spectrometers (Sect. 9.2.2). They allow determining the isotope ratios of many chemical elements from complex liquid matrices.

9.2.1.2 Measurement Procedures

The analytical sensitivity of mass spectrometers varies as a function of (i) isobaric interferences caused by the superposition of the peak(s) of the target element with those generated by other chemical species with similar masses, and/or (ii) effects

resulting from the matrix composition. The ability to investigate all mass signals during a series of scans can be used to do a purely qualitative analysis of the sample. The spectrum can be visually examined to check for the analyte presence or absence.

Since many instruments give a sensitivity vs. mass plot, it is possible to build a curve that gives information on the ionization degree and the isotope abundance. This response curve can be used to calibrate the instrument and to provide semi-quantitative data when indicative analyte concentration values only are required. The most common and widespread calibration method involves the use of standards, usually three plus a blank. In this case, numerous standard solutions are prepared that cover a wide range of concentrations. Least squares regression methods are then used to build calibration curves for each element. To avoid signal fluctuations due to the instrument sensitivity decrease between one series of measurements and the next, two different approaches are used: correction of the instrumental drift and internal standardization. The range and combination of elements that can be determined by ICP-MS are very large. The instrument provides the possibility for the simultaneous determination of many chemical elements including trace elements. Some volatile trace elements, such as Hg and As, may be lost during the preparation of the solution, so their determination is impossible. This means that a successful analysis depends mostly on a survey to be carried out on the matrix in advance. Indeed, before a quantitative analysis, the sample should be qualitatively known to identify its major and trace elements, and evaluate possible interferences, especially related to acid dissolution. The final dilution of the sample should only be done after it has been decided whether or not to include certain elements in the survey.

9.2.2 Thermal Ionization Mass Spectrometry – Solid Source Mass Spectrometers

9.2.2.1 Principles and Instrumentation

TIMS can separate charged particles (positive or negative ions) through the combined use of an electric field and a magnetic field. According to the original scheme proposed by the physicist Alfred Nier in 1940, it consists of (Fig. 9.9): an ion source; a magnetic analyzer crossed by a flight tube along which ions move; a detection apparatus (collector array in Fig. 9.9b); an acquisition system, i.e., a PC. In order not to disturb the ion motion by collisions with other particles, the whole system is kept under high vacuum through: an oil bath rotary pump and a liquid nitrogen cryogenic pump for pre-vacuum, that reach pressures of up to 10^{-3} mbar; a turbomolecular pump and two ion pumps for reaching higher vacuum, up to 10^{-9} mbar. The ion source of *solid source* mass spectrometers consists of a vacuum chamber ($P \leq 10^{-7}$ mbar) hosting a turret containing several samples that are analyzed individually (Fig. 9.9). The solid sample is retaken with a micro-drop of diluted acid solution and loaded onto a previously outgassed pure metal (Re, W, Ta) filament

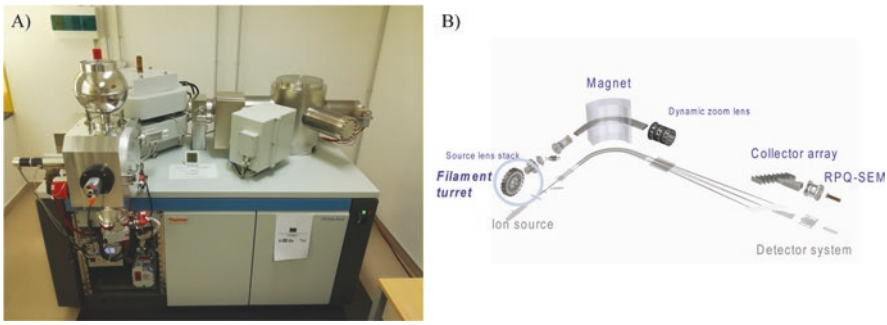

Fig. 9.9 (**a**) Triton Plus® thermal ionization mass spectrometer. (Source: Mass Spectrometry Laboratory, DiSTAR, University of Naples, Italy). (**b**) Technical scheme of the Triton Plus®. (Source: Permission by Thermo-Fisher Scientific, April 2018)

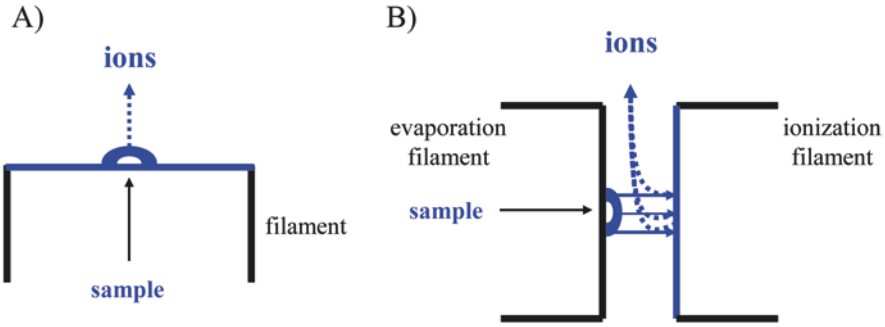

Fig. 9.10 Schematic of (**a**) single filament configuration, and (**b**) double filament configuration. (Source: M. D'Antonio)

(Fig. 9.10), welded on a steel support. In the source, the filament is heated at high temperature by an electric current and emits electrons by *thermionic emission*. The thermionic emission is such that only a part of the atoms to be analyzed is ionized. Elements with ionization energies lower than the *work function* of the filament (a parameter related to type of metal of the filament) will produce many ions at low temperatures, whereas elements with higher ionization energies will require a high filament temperature which causes a rapid loss of the sample. This can be avoided with the use of two (or three) filament systems (Fig. 9.10b), where only one of them, called evaporation filament, is loaded with the sample. The ionization filament is brought to high temperatures (~1700 °C), whereas the evaporation filament is heated at lower temperatures (~1100 °C).

The ions produced by thermo-ionization are accelerated to high voltage (10 kV) in the analyzer tube, held at high vacuum (10^{-9} mbar), and focused through a system of electrostatic lenses, to form a high-energy ion beam entering the flight tube of the magnetic analyzer (Fig. 9.9b). The flight tube forms an arc, with a radius of curvature r, that passes through a magnetic field of intensity B generated by an external

electromagnet with variable intensity. The ions of the beam are charged particles q with mass m and velocity v. Their kinetic energy due to the voltage V acceleration is $E = ½mv^2 = qV$. It comes that $v^2 = 2qV/m$. In the magnetic field of intensity B and perpendicular to the beam trajectory, ions will be deviated by the Lorentz force ($F = qvB$) following a curvilinear trajectory of radius r, resulting from the balance between the aforementioned force and the centripetal force mv^2/r. Combining the previously determined equations of forces' equilibrium and of ion velocity gives: $2qV/m = B^2q^2r^2/m^2$. Expressing the ratio m/q as a function of the intensity of the magnetic field B, the acceleration voltage V and the radius of curvature r, yields: $m/q = B^2r^2/2$ V, so that the magnetic field can separate ions with different mass/charge ratios.

To unambiguously identify the isotopes being analyzed, the magnetic field needs to be calibrated to assign a known value of B to each m/q ratio value, specific to a given isotope. The mass spectrometer must be able to distinguish ion beams with similar but still distinct m/q ratios, i.e., ions that differ by a single atomic mass unit (amu) and send them separately to the detectors. The detection apparatus consists of one or more ion collectors (Fig. 9.9b) which convert charged particles into an electrical signal. Each collector is connected to an amplifier, which renders the signal processable. The most common collectors are Faraday Cups, carbon-coated metal boxes. The ion beam enters the Faraday Cup through a slit, hits a positively charged electrode, which creates a current flow from the ground through a strong resistance (10^{-11} ohm or less). The potential difference ($V = RI$) across the resistance represents the signal that will be subsequently amplified and processed to give the isotope ratio of interest, being proportional to the charge deposited by the ion beam on the electrode. Another detection device, used for ion beams of low intensity, is the secondary ion multiplier (Secondary Electron Multiplier), generally coupled to a quadrupole mass filter (Retarding Potential Quadrupole). The last part of the TIMS spectrometer is the acquisition system, consisting of one or two computers that manage most of its functions (only some are performed manually, such as introducing the samples into the source and liquid nitrogen into the cryogenic pump) and the software for processing the acquired data.

9.2.2.2 Measurement Procedures

The isotope ratios measurement procedure involves several steps: the right ionization temperature of the filament is reached by heating it by supplying current at increasing amperage; the value of magnetic field suitable for the measurement of a given isotope ratio is selected and the ion beam is focused; then the spatial configuration of the Faraday Cups suitable for detecting the various ion beams of the element to be analyzed is chosen and the automatic calculation procedure of the isotope ratios starts. Measurements can be carried out in static or dynamic mode: the former uses several collectors at the same time to measure various isotopes of a given element while keeping the magnetic field constant, whereas the latter involves the use of one or more collectors at a time where selected isotopes of the element are

measured by varying the magnetic field. The calculation of the isotope ratios of a given element requires appropriate corrections for the baseline (background signal or background noise), isobaric interferences and within-run mass fractionation. The baseline results of both ions diffused by the ionized sample and the electronic noise of the detection system, whereas the isobaric interferences are due to isotopes of other elements with the same mass number as the one of interest. The correction is made by monitoring an interference-free isotope. For example, ^{87}Rb interferes isobarically with ^{87}Sr. To correct this interference, ^{85}Rb can be used as it is not isobaric with any Sr isotope. The correction is made as: $^{87}Sr_{corr} = {}^{87}Sr_{meas} - (^{87}Rb/^{85}Rb)\ ^{85}Rb_{meas}$, where ^{87}Rb/^{85}Rb is the average natural isotope ratio of rubidium. Mass fractionation is observed when the sample is held at high temperatures for long times causing the thermal ionization of lower mass isotopes, which over time leads to their depletion in the sample, compared to higher mass isotopes. To correct this effect in the case of strontium, it is necessary to consider that one of the isotopes of interest, ^{87}Sr, is radiogenic and variable in nature. Therefore, it is necessary to normalize the ^{87}Sr/^{86}Sr ratio using a stable and non-radiogenic isotope, usually ^{86}Sr, to a value assumed for a ratio between non-radiogenic isotopes that does not vary in nature (e.g., ^{86}Sr/^{88}Sr = 0.1194), considering that it is known how much the fractionation degree changes with mass difference. An exponential correction law has been shown to well describe the mass fractionation of strontium and other elements. Current TIMS spectrometers provide automatic corrections for both within-run mass fractionation and isobaric interferences during measurement of the element of interest, reaching accuracies of 10^{-6} (e.g., Avanzinelli et al. 2005; Arienzo et al. 2013).

9.2.3 Thermal Ionization Mass Spectrometry – Gas Source Mass Spectrometry

9.2.3.1 Principles and Instrumentation

IRMS presents a lower sensitivity but much higher resolution and precision compared to solid source mass spectrometry. Compared to the latter, IRMS mainly differ in the sample introduction system and the source, as well as in the mass analyzer, as the electromagnet generally generates a magnetic field of fixed intensity. The gas source mass spectrometer (Fig. 9.11) includes an ion source, a mass analyzer consisting of a flight tube and a magnetic sector, and ion detectors.

The instrument is kept under high vacuum (P = 10^{-8} mbar) to prevent collisions between ions and residual gas molecules. The source consists of a chamber into which the sample/reference gas is injected and ionized by an electron beam (energy between 50 and 100 keV). Electrons are produced by a filament heated at high temperature and follow a helical path within a magnetic field. The source also includes two electrodes, one with a positive potential (ion accelerator, Fig. 9.11), which accelerates the created ions towards the inlet slit of the flight tube, and the other with

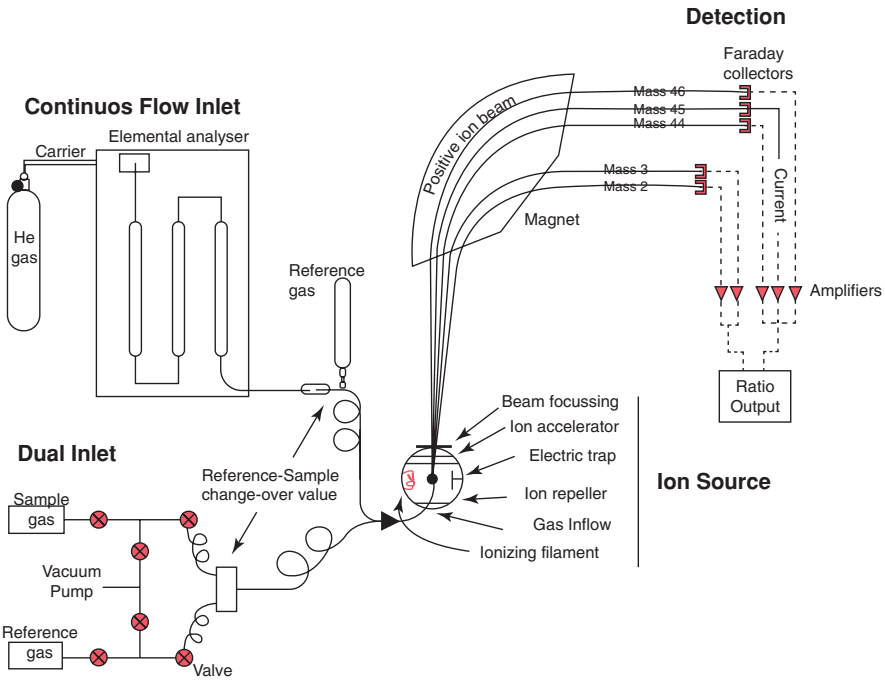

Fig. 9.11 Schematic of a gas-source mass spectrometer for the measurement of stable elements in gaseous form. (Source: Sustainability of semi–Arid Hydrology and Riparian Areas (Tucson, AZ, U.S.A.). http://web.sahra.arizona.edu/programs/isotopes/methods/gas.html)

a negative potential (electric trap, Fig. 9.11) that traps the ionizing electron beam. The beam of positive ions of the gas, repelled by a third positive potential electrode (ion repeller, Fig. 9.11), exits from the source, is focused through a series of electrostatic lenses of variable potentials, and finally enters the flight tube. There the ion beam crosses the magnetic field, which separates ions into distinct ion beams based on their mass/charge ratio, as described in Sect. 9.2.2.1. A series of fixed Faraday Cups arranged along an oblique focal plane to the incident ion beams, collect their respective charge and convert them into an electrical signal. Following amplification, this signal serves as the basis for calculating the isotope ratios of interest of the gas being measured. The isotope ratios determination of a light element involves the comparison with a standard of the same element of known isotope composition. The sample-standard comparison process is controlled by the gas injection system. The most used configurations are (Fig. 9.11): (1) double injection (Dual Inlet, DI-IRMS) and (2) continuous helium flow (Continuous Flow inlet, CF-IRMS). The DI-IRMS includes two tanks, one for the sample gas and one for the standard gas, connected by means of capillaries to a system of valves (changeover valve) which allows to alternately inject the sample and the reference gas into the source. Flow velocities for the two gases in the capillaries are equalized thanks to a variable volume system (metal bellows) that regulates the pressure, ensuring a non-turbulent flow, limiting

possible isotope fractionation. The continuous flow injection system uses helium as a carrier gas. The helium flow is maintained at 0.2 ml per minute and the background pressure in the instrument at ~10^{-5} mbar. In the Dual Inlet configuration, samples are prepared and purified (converted into an elementary gas or simple gaseous compound isolated from other unwanted gases) off-line by a vacuum line that may include compression pumps, concentrators, reaction furnaces and microdistillation apparatuses (extraction/purification line; Sect. 9.1.2.7). In the continuous helium flow configuration, the sample preparation and purification line is interfaced with the mass spectrometer, making the analysis simpler and faster. The mass spectrometer may be coupled to peripherals such as liquid or gas-chromatographers, used for separating the liquid(s)/gas(es) of interest from the matrix (Sect. 9.1.3.2). The last part of the instrument is the acquisition system, consisting of a PC that controls most of the functions, including opening and closing valves, as well as processing the data.

9.2.3.2 Measurement Procedures

Gas mass spectrometers combine different techniques for introducing, separating and purifying the gaseous species of interest. Gas-chromatography (GC) is used for the separation of small gas quantities (down to a few micromoles) and is linked to a combustion system (C) to convert solid samples into gases that can be analyzed by the mass spectrometer. For example, C-GC-IRMS can measure C, N and S stable isotopes: samples disposed in tin capsules are placed in a furnace filled with oxygen and carried by helium, creating a flash combustion at high temperature (1800 °C). Catalyzed by the presence of oxygen, the combustion reaction converts samples into CO_2, NO_x, SO_x and H_2O. Therefore, this technique is referred as Continuous Flow Isotope Ratio Mass Spectrometry (CF-IRMS). Following oxidation, gases pass through a reduction column containing copper heated to 650 °C, transforming formed nitrogen oxides into N_2. Gases are then separated by gas-chromatography before being split between a thermal conductivity detector that quantifies each gas produced, and the mass spectrometer. For the analysis of the C isotopic composition, the latter can be present in different forms (organic carbon, carbonates, CO_2-bearing fluid inclusions, etc.) even in the same sample, such as geological materials. In these cases, combustion at different temperature intervals (step-heating) is used by energizing the surface of the sample with a laser ablation system interfaced with the mass spectrometer, so that the various molecular components of carbon are released and measured separately. For DI-IRMS, samples are converted into a simple gas via either an off-line procedure and subsequently introduced into the mass spectrometer, or an interfaced laser ablation device as described above. Off-line sample preparation procedures require a longer time and larger samples (millimoles), with the risk of contamination and isotope fractionation during the processing steps. While DI-IRMS is generally more accurate when measuring isotope ratios of light elements, CF-IRMS offers advantages including: online sample preparation and purification; ability to analyze smaller samples; simultaneous analysis

of multiple gas species (N, C, S…); higher throughput; better cost/benefit ratio. The main drawback is a lower accuracy in the determined isotope ratio.

For all IRMS techniques, direct comparisons are made between the intensity ratios of the ionic beams of the sample gas and those of gases of known isotope ratios (either reference gas or certified standards) to determine the ‰ value of the δ parameter (Sect. 9.1). Data must eventually be corrected for the effects of instrumental drift and for the isobaric interferences through suitable factors that are adjusted for each gas being measured.

9.2.4 Alpha and Gamma Spectrometry

The alpha and gamma spectrometric techniques are used to quantify radioactive isotopes that emit alpha particles, i.e., an ^{4}He atom, or gamma photons, i.e., very short wavelength electromagnetic radiation. In both cases, their emission occurs at specific energy values (in MeV) characteristic of each isotope species, which therefore can be identified and, with particular techniques, quantitatively analyzed. Measurements can be carried out both on the field, through portable meters that measure radioactivity, but do not allow identifying isotopes, or in the laboratory using spectrometers that allow both identification and quantification of the radionuclides. The main part of these instruments is a detector sensitive to ionizing particles, constituted in its modern versions of a semiconductor crystal (e.g., silicon, Si or germanium, Ge).

9.3 Application of Isotope Forensics

Although isotope geochemistry was originally developed for research in geology after its discovery by Harold Urey in 1934, the evolution of its analytical techniques has allowed to vastly extend its application fields: from mining exploration to biogeochemical cycles, or the human impact on our environment. Since recently, isotope geochemistry has also demonstrated its added value when trying to tackle key forensics issues (e.g., Muccio and Jackson 2009; Matos and Jackson 2019): e.g., food adulteration, drugs, illicit pharmaceuticals, microbiology, doping, explosives, ammunitions. The application of isotope geochemistry to forensic investigations was historically limited to the study of stable isotope systematics. During the 90's, in the US where forensic science was born, C ($\delta^{13}C$) and N ($\delta^{15}N$) isotope compositions were first used to characterize seized drugs or adulterated wines. Building on these promising results, the US and UK created the "Forensic Isotope Ratio Mass Spectrometry Network" (FIRMS), a still active today scientific network regarded as the standard benchmark for stable isotope forensic practitioners. FIRMS aims at developing the scope of stable isotope techniques in forensic applications, with the ultimate goal of raising awareness of the relevance and importance of isotope

geochemistry in forensic science, crime detection and reduction. To further push the limits of the forensic isotope geochemistry it became necessary to characterize materials of inorganic nature containing, among others, heavy metals (e.g., fragments of soil, rocks, illegally transported radioactive material). This marked a step increase in the analysis of radiogenic isotopes, in combination or not with the then classical analysis of stable isotopes, opening new routes to forensic investigations.

In the following sections we are presenting a series of examples of application of isotope forensics, taken from the current literature.

9.3.1 Placement of a Suspect at the Crime Scene

At the scene of a crime numerous artifacts can be suitable for isotopically identifying their origin, by making comparisons with materials of known locations. This can then be used to place a suspect at the crime scene. For example, the origin of wood fragments can be inferred through the analysis of H, C, and O isotopes. Other examples include soil or rock fragments, found on the crime scene that can isotopically be related to precise locations. These isotope characteristics can then be compared to those measured in shoe soles, car or motorcycle tires, or from the home surroundings of suspected individuals. Farmer et al. (2007) used $\delta^{13}C$ and δD, in a case of an individual suspected of attempting to burn materials potentially related to a murder case. Characterizing safety matches seized at the suspect's house and those recovered from a crime scene, the authors showed that they were (isotopically) different, which was also confirmed by XRD and microscopy analysis.

9.3.2 Human Provenancing

The large scope of available literature detailing the effective application of isotope analysis techniques to the identification of unidentified human remains include examples such as the deaths related to the crossing of the Mexico-United States border, reported by Aggarwal et al. (2008), or the recent migration events from Africa and the Middle East to Europe, involving hundreds of victims each year.

The added value of stable or radiogenic isotope systematics resides in the fact that their study in human tissues allows determining the provenance of human beings or of their remains. A particular attention is made on human tissues that once formed will not, or slightly, be modified, such as the tooth enamel, hair or bones. Paraphrasing the old adage "we are what we eat", one can state that isotopically-speaking "we are what we eat plus or minus a few ‰" (DeNiro and Epstein 1976). In fact, isotope (^{2}H, ^{13}C, ^{15}N, ^{18}O or ^{34}S among others) abundances in the different human tissues reflect what the person ate and drunk during her/his recent life, also including her/his recent geographical mobility. To put it differently, diet and geolocation of a human being influence the isotope compositions of her/his tissues,

including hair, nails, teeth or bones. One of the basic principles on which the reconstruction of a person's geographical history is based is that food is the sole source for carbon and nitrogen in the human body. Similarly, the water we drink and take from cooked food is an important source of hydrogen in our body (~30%).

The mean annual $\delta^{13}C$ for terrestrial plants is determined by their photosynthetic pathway: C_3 and C_4 plants, and CAM (Crassulacean Acid Metabolism) plants. These different photosynthetic pathways reflect in their distinct $\delta^{13}C$ ranges: −33 to −24‰ for C_3 plants, −16 to −10‰ for the C_4 ones and −20 to −10‰ for the CAM ones (O'Leary 1988). The δD and $\delta^{18}O$ of drinking water is controlled by those of the meteoric recharge. It has to be noted that isotope compositions of rainwater are subject to seasonal variations originating from variations in its temperature and evaporation rate (Bowen 2008, 2010). Coupling isoscape maps of local/national/international precipitations with computational models it is thus possible to identify, or more precisely to exclude, areas of geographical provenance. Chesson and Berg (2021) provided an in-depth review of the selection of appropriate human tissues samples and gave guidance on the available options for the isotope analysis preparation, analysis and data handling.

Strontium Isotopes in Human Provenancing

Studies have shown that the strontium (Sr) isotope ratios measured in bones and/or teeth can successfully be used for the identification of human remains (e.g., Rauch et al. 2007). Living beings do not biologically use Sr but it is a key biomineral constituent of bones and teeth as it enters their mineral structure by substitution with calcium. Sr is thus taken up early in people's life and is fixed in bones and teeth, recording the average $^{87}Sr/^{86}Sr$ ratio of the "bedrock" of the locality where people were born and raised during the early stages of their life. Sr isotope ratios have carved their niche as proxies of dietary habits and migratory routes of ancient populations, in the certification of different food types and more generally in forensic sciences. Coelho et al. (2017) report a useful collection of literature works on these topics. To increase even more the identification power of Sr isotopes, it can be coupled to those of other heavy and light elements.

The Sr isotope approach required the creation of isotope base maps (also known as isoscapes, see Fig. 9.12; Bowen 2010) that allow a direct comparison of a given isotope parameter from a certain geographical area to that of a sample of water, hair, drug or plant grown in that area. This was synthetized by Bataille and Bowen (2012) and Chesson et al. (2012) who modeled $^{87}Sr/^{86}Sr$ in bedrocks by developing GIS-based models for Sr isotopes in rock and water that included the combined effects of lithology and time. However, given the variable bedrock of each area, the above methodology is not without some uncertainty, which can be reduced only by making detailed studies of a given area.

(continued)

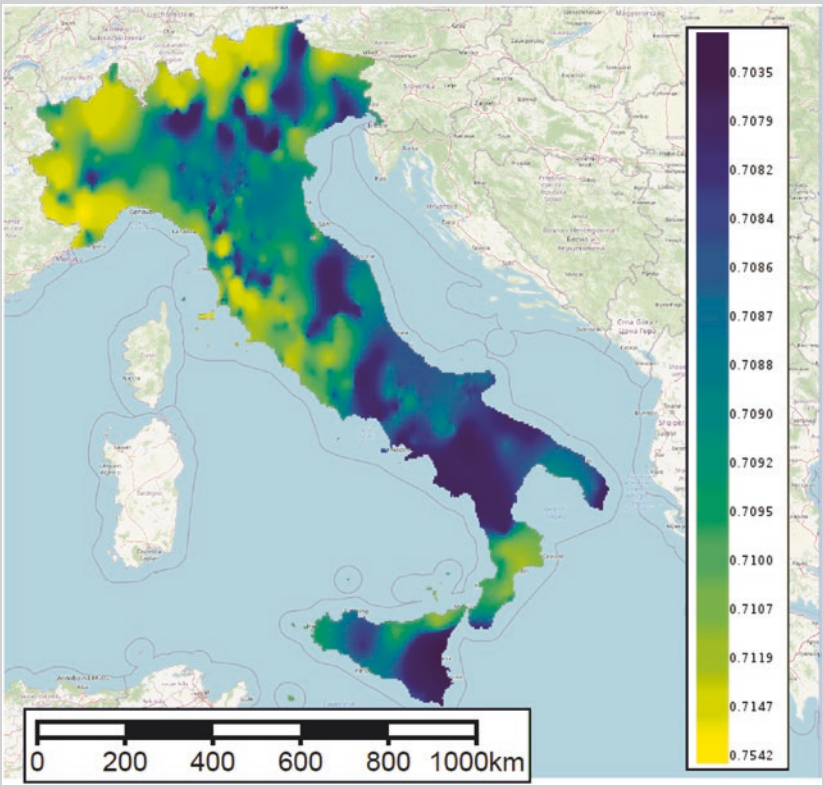

Fig. 9.12 $^{87}Sr/^{86}Sr$ isoscape map of Italy. (Downloaded from https://www.geochem.unimore.it/sr-isoscape-of-italy/; Lugli et al. 2021)

9.3.3 Drugs

In 1997, C and N isotope compositions measured on cannabis samples seized from a truck were brought to the Australian Supreme Court of the Northern Territories as evidence in a drug trafficking trial: the case of Queen versus Thomas Ivan Brettschneider. The values were identical (at 95% confidence level) to those measured on samples seized from a suspect plantation. This constituted the first official use of isotope forensic techniques to solve a drug trafficking case. Tracking the geographical origin of different drug types, either natural (cannabis, marijuana, cocaine) or semisynthetic (amphetamine, methamphetamine, morphine, heroin) by means of C and N isotopes has been one of the most popular applications in forensic science in USA, Brazil and Asia since the 1990s. Interestingly, these forensic applications is that it is possible to infer the geographic location where the plants were

grown and whether the cultivation took place "indoor" or "outdoor". For example, as C and N isotope compositions in marijuana are very sensitive to climatic conditions and variations in latitude (Shibuya et al. 2007), it was possible to discriminate Brazilian marijuana grown in the arid regions of Bahia and Pernambuco ($\delta^{13}C = -26.28 \pm 1.55‰$ and $\delta^{15}N = 1.51 \pm 3.11‰$, respectively) from that grown in humid regions such as Mato Grosso do Sul and Para ($\delta^{13}C = -29.77 \pm 1.05‰$, and $\delta^{15}N = 5.89 \pm 1.73‰$, respectively). The combination of isotope systematics is extremely useful when trying to reconstruct the path of illicit drug trafficking. This approach can be implemented to other types of narcotics. Since the first study of Mas et al. (1995), $\delta^{13}C$ and $\delta^{15}N$ have been used to trace the origin of Ecstasy tablets (MDMA; 3,4-methylenedioxymethamphetamine). This pioneer study was followed by many others (Carter et al. 2002a, b, 2005; Palhol et al. 2003, 2004; Billault et al. 2007; Buchanan et al. 2008).

Like natural processes, illicit manufacturing processes, that use different chemical transformation techniques (e.g., the acetylation of morphine to create a heroin base that is then transformed into heroin hydrochloride) may be accompanied by significant isotope fractionations during the different processing steps. These can ultimately be used to discriminate between different origins of the same type of narcotic (Carter et al. 2005). They were first described by Desage et al. (1991) on heroin samples. Still, the authors reported a narrow range of $\delta^{13}C$ values, from $-31.5‰$ to $-33.5‰$ for samples covering a wide geographic area. Similarly, Casale et al. (2005) reported no C isotope fractionation during the conversion of cocaine base to cocaine HCl but a N isotope fractionation of 1‰. The authors also demonstrated that there was a kinetic carbon isotope fractionation of $-1.8‰$ during the acetylation of morphine to heroin that is depleting the end-product in ^{13}C. Acetylation is also accompanied by an isotope fractionation against ^{15}N. Building on this, Hurley et al. (2010) proposed to add the H isotope systematics. The authors developed stable isotope-based models incorporating $\delta^{13}C$ and δD to predict geographic origin and growth environment for marijuana trafficking in the USA. When tested, the model predictions were 60–67% reliable for the determination of the region of origin and 86% accurate for the cultivation environment.

Recently, studies have proposed Sr isotope ratios as another useful tool in forensic drug provenancing. Unlike light elements, $^{87}Sr/^{86}Sr$ ratios are not fractionated by natural processes. They are thus directly linked to the parent material. West et al. (2009a) first analyzed the $^{87}Sr/^{86}Sr$ ratios of marijuana samples grown in 79 counties across the US, trying to relate them to the isotope signal of the geology they were grown on. The authors concluded that there was some remaining unexplained variability in their dataset, though marijuana Sr isotope ratios do retain a primary geological signal based on the bedrock age. This means that the primary geological footprint, which differs in different geographical areas, leaves a recognizable trace in the Sr isotope ratios of plants. More recently, DeBord et al. (2017) published the first use of $^{87}Sr/^{86}Sr$ ratios for the geographic origin of 186 illicit heroin samples of known origin. The authors demonstrated that the technique showed 77–82% discrimination between South American and Mexican heroin.

9.3.4 Explosives

With the increasing threat of terrorism in our modern lives and the broad range of explosive devices available, sourcing explosives has become a growing interest for government sectors. The very first published isotope analysis of explosives dates back to 1975 (Nissembaum 1975), where the author discriminated 2,4,6-Trinitrotoluene (TNT) samples from different countries based on their $\delta^{13}C$, showing that the observed variations were linked to both the isotope composition of the starting materials and the country of origin. The manufacturer Thermo reported in 1995 that 3 samples of TNT explosives from different countries could be distinguished when coupling their $\delta^{13}C$ and $\delta^{15}N$, concluding that further research was needed to determine whether these resulted of different production sites, of substrate lots in the production process, or of post-production adulteration (Thermo 1995). After that, isotope geochemistry demonstrated its efficiency at discriminating other types of explosives: RDX or T4; plastic explosives, such as Semtex; TNT (e.g., Benson et al. 2009a, b, 2010; Widory et al. 2009; Brust et al. 2015; Bezemer et al. 2016). Reported values mostly include O and N isotopes but also, to a lesser extent, C and H ones. Phillips et al. (2002) showed that Pentaerythritol Tetranitrate (PETN) based explosives produced by the same manufacturer fall within a tight cluster of stable isotope compositions, distinguishable from others. Lott et al. (2002) tested whether isotopes were useful in determining the "point of origin" of explosives, specifically whether differences in production processes or substrates used in the manufacturing process might lead to difference in their corresponding isotope ratios. Historically, the UK Forensic Explosive Laboratory (FEL) is probably the first laboratory that included the isotope geochemistry of explosives in its research scope. Since, the technique has spread worldwide with new dedicated laboratories being implemented in Europe, the US, China and elsewhere.

Fractionation of Stable Isotopes for Discriminating Explosives

As most of the chemical procedures involved in the preparation of explosives do not proceed in a quantitative fashion and generate product yields that are generally <100%, isotope fractionations of light elements occur. Lock and Meier-Augenstein (2008) reported average fraction factors (α) of 1.0087 ± 0.0003 and of 0.9860 ± 0.0005 between hexamine (precursor) and its RDX product for $\delta^{13}C$ and $\delta^{15}N$, respectively. These distinct α values can then be used to characterize differently treated explosives. Benson et al. (2009a) discriminated the starting materials and/or manufacturing processes samples of TATP and PETN samples based on their C, N and O isotope compositions. These authors published a second article focusing more specifically on a multi-isotope approach (N, O and H isotopes) to discriminate lots of ammonium nitrate (AN), a common oxidizer used in improvised explosive mixtures (Benson et al. 2009b). They also compared pre- and post-blast samples and showed a N isotope fractionation, resulting in a ^{15}N enrichment of the

(continued)

post-blast samples that was explained as the likely result of both a kinetic isotope fractionation effect and also of the breakdown of the nitrate ion into nitrite. Going further, Brust et al. (2015) combined IRMS (Sect. 9.2.3.1) and ICP-MS (Sect. 9.2.1.1) to augment the discrimination power of this approach. The authors successfully discriminated between samples from different manufacturers and between different types of AN, combining their $\delta^{15}N$ and $\delta^{18}O$ to elements such as Mg, Ca, Fe and Sr. Measuring $\delta^{13}C$ and δD they concluded that the added value of these last two isotope systematics was negligible for differentiating the origin of AN. More recently, Can et al. (2021) reviewed the different isotope techniques that have been reported in the literature to isotopically characterize common explosives such as ammonium nitrate, black powder, TNT, pentaerythritol tetranitrate (PETN) and cyclotrimethylene trinitroamine (RDX).

Howa et al. (2016) proposed a new method for separating components of plastic explosives based on their solubility: binder, oil, explosive, and insoluble. These fractions produced isotope compositions of individual compounds, such as RDX and HMX for the explosive fraction, and Sudan I and N-phenyl-2-naphthaleneamine for the oil fraction. The authors show that adding the isotope characteristics of non-explosive materials (e.g., binder) allowed discriminating between chemically and isotopically indistinguishable C-4 samples if only raw material or the RDX component were analyzed. Two-ways radio transmitter are generally employed to initiate improvised explosive devices (IEDs). Combining the δD and $\delta^{13}C$ analysis of five sampling points taken in commercially supplied radios Quirk et al. (2009) found that it provided a pattern that was characteristic of a given radio. Those same radios were then subjected to detonation and analyzed similarly. The authors concluded that when 3 or more post-blast fragments were recovered it was isotopically possible to associate these with the undamaged radio with a high degree of certainty.

Environmental contaminations due to the presence of nitroaromatic compounds (NACs) are a common problem at military training installations, abandoned production facilities or munition disposal sites (e.g., Kalderis et al. 2011). As NACs are present in different phases and may undergo competing degradation pathways, assessing their fate is challenging but can be achieved by a compound-specific multi-isotope approach (C, N and H isotopes; Wijker et al. 2013).

9.3.5 Radioactive Materials

The isotope analysis of heavy elements is also used in investigations of radioactive material trafficking and is usually referred as nuclear forensics. This is a relatively young discipline, with a steady increase in the scientific publications within the last two decades (Burk 2005; Aggarwal 2016). Radioactive materials (e.g., actinides)

emit radiations that can be harmful to human health, even at extremely low levels (i.e., microgram amounts). The main objective of nuclear forensic and investigations is to find out the origin of interdicted, stolen, or lost material to eliminate its accessibility to illicit traffickers. Nuclear fuel generally consists of uranium enriched in its ^{235}U and plutonium, but other radioactive elements can be used in so-called radiological dispersal device (RDD). RDDs consist of a non-fissile radioactive material, that cannot explode through a nuclear reaction but could ignite if metallic, that is treated to make it very volatile. A RDD is defined as a weapon designed to disperse radioactive material, consisting either of nuclear power plant or hospital waste, over an area using either conventional explosives, of even modest power, or more covert dispersion methods to contaminate objects and people (Hanson 2008). The recognition of low-level radioactive weapons as part of the class of atomic weapons could lead to the inclusion of depleted uranium weapons in this category (Ahn and Seo 2021).

In these cases, isotope analysis can be used to identify the nature and origin of radioactive material or weapons based on them, and to monitor their illicit trafficking (Wallenius et al. 2006; Mayer et al. 2007; Fahey et al. 2010; Kristo and Tumey 2013). To prevent the fabrication of eventual dirty bombs, radioactive materials need to be precisely and rapidly identified. The Geiger-Muller counter (GM counter) is usually the most conventional radiation detector used. However, it cannot distinguish the different radiation types. Secondary-Ion Mass Spectroscopy (SIMS), TIMS, alfa and gamma spectrometry (Sects. 9.2.2 and 9.2.4) are used for isotope analysis, but they will take longer for obtaining results. In 2018, Beals et al. showed that the study of fission products' properties helps eliminate ambiguity in identifying low-yield nuclear detonation in its early stages, by allowing to discriminate three categories of explosive devices: (i) RDD, (ii) a failed nuclear device where nuclear material is scattered by conventional devices and (iii) a nuclear device that scatters nuclear material producing a very low-yield from nuclear fission. More recently, Kim et al. (2019) evoked the feasibility for laser-induced breakdown spectroscopy (LIBS) to identify radioactive materials in dirty bomb terror scenes.

9.3.6 Environmental Forensics

Environmental forensics has emerged as a discipline directed towards determining parties liable for causing spills of contaminants into the environment. It has thus become important to be able to determine the source(s) of these contaminants as well as to characterize their transportation and potential degradation history. Isotope geochemistry has widely demonstrated its added value as one of the most refined and promising techniques in this sense. As early as in 1947, J.H. Sterner evoked the possibility to use tracer isotopes in industrial toxicology (Sterner 1947). The author then predicted that the use of radioactive and stable isotopes was "likely to extend" in the following decades, which seems to have been correct, but also concluded that "the radioactive isotopes have advantages over the stable isotopes", which should be open to debate in the present section. Environmental forensics cover a broad range

of contaminants, which complexifies the use of a single technique to track their respective sources and fate in the environment. It is thus usually necessary to use a variety of analytical techniques to resolve this issue. Bulk and compound-specific isotope ratio analysis of light and heavy isotope systematics have been vastly documented as well as advances and remaining challenges when applied to environmental contamination (Elsner and Imfeld 2016).

Schmidt et al. (2004) published a review of the isotope analysis of organic contaminants that included the identification and quantification of biodegradation processes and corresponding isotope fractionations on a range of environmental matrices. The contamination of soils, aquifers and groundwater bodies is an important issue that has relied a lot on isotope geochemistry to identify particular emission sources. Many different isotope systematics have been employed, including N and O isotopes in nitrates (e.g., Chen et al. 2020; Peters et al. 2018), C isotopes in tracking the provenance of hydrocarbons and related refinery products and wastes (e.g., Wang et al. 2018; Humez et al. 2019; Liu et al. 2021). Air pollution issues have been tackled by the study of atmospheric gases and aerosols (e.g., Xiao et al. 2020) but also through the indirect study of bioindicators (e.g., Kousehlar and Widom 2020; Soba et al. 2021).

Heavy metal isotope systematics have also been investigated and showed that they can help identify sources of contamination, and even more to characterize the extent of environmental contamination when combined with multi-element screening (e.g., Pontér et al. 2016). Non-conventional isotope systematics may as well provide key information about environmental contamination. For example, Tieman et al. (2020) employed barium isotopes to track the source of dissolved solids in produced water from the unconventional Marcellus Shale Gas Play, and Li et al. (2021) used the mercury isotope signature of residential coal combustion to discuss its impact on air quality in rural areas in China. This can be achieved as most contaminants of anthropogenic origin display an isotope profile that significantly differs from that of their corresponding natural sources.

9.3.7 Food Adulteration

The certification of food products, their authenticity and origins has become a growing priority amongst consumers and producers. Counterfeited products do not meet safety standards, leading to various levels of health risks for consumers. A number of European food products are now protected with specific geographical origin (Protected Designation of Origin; PDO) and production (Protected Geographical Indications; PGI) labels. The European Union adopted the regulation No. 1169/2011 that requires the provision of food information to consumers by identifying the origin of a food as being either its country of origin or its place of provenance (e.g., Monahan et al. 2018). This arose the need for developing authentication techniques to prevent the mislabeling of PDO and PGI foods. As early as in 2003, stable isotope analysis was already performed on a regular basis in Europe and the USA to authenticate wines, certain liqueurs, olive oil and other vegetable oils, natural flavors, and honey (Ogrinc et al. 2003).

The foundation of the isotope approach relies on the fact that during their growth, plants absorb bioavailable elements that are present in the soil. These inherited elements can provide information about the geological substratum on which plants grew and can transfer this information to the food and beverages that are produced from them (e.g., Vinciguerra et al. 2016). This soil-plant connection reflects in the isotope ratios of their respective constituting elements, creating "isotope fingerprints" that can be used to trace their origin (e.g., Allen et al. 1994; Asfaha et al. 2011; Zhao and Zhao 2020). Historically, light isotopes were majorly analyzed, but recent studies demonstrated the added value of heavier isotope systematics, such as Sr isotopes, as effective tracers of the "bedrock" on which, for example, olive trees and grapevines grow, opening new perspectives in the field of viticulture (e.g., Mercurio et al. 2014; Guibourdenche et al. 2020). Several factors can contribute to the final isotope ratios measured in animal-based foods. For example, the $\delta^{13}C$, $\delta^{15}N$ and $\delta^{34}S$ of animal tissues are highly influenced by its diet, usually consisting of different plant species for herbivorous animals such as cattle and sheep (e.g., Camin et al. 2017). For $\delta^{18}O$ and δD, isotope compositions in animals' tissues are driven by drinking water and food (e.g., Hobson and Koehler 2015). GIS driven isotope maps and isotope footprints were thus developed for food products including beer, honey, cereal crops, cheese, fruit juices, tea, coffee, olive oil, peppers, soft fruit, tiger prawns, crab, rice, tomato-based products, vinegar, wine and asparagus (e.g., Cabanero et al. 2006; West et al. 2007; Flores et al. 2013; Zhao et al. 2013; Carter et al. 2015; Stevenson et al. 2015; Zhao et al. 2016; Chen et al. 2016; Luo et al. 2016, 2019; Chiocchini et al. 2016; Camin et al. 2017; Perini et al. 2018; Gopi et al. 2019; Richter et al. 2019). Isotope comparison of these with pre-defined isoscapes allows demonstrating the provenance and thus authenticity of food products (e.g., Danezis et al. 2016).

Following the increasing demand for centralized and certified data in the domain of isotopes for food science, Eftimov et al. (2019) recently proposed an ISO-FOOD ontology to link and harmonize the existing different knowledge repositories. As stated by the authors, "such an ontology will help stable isotope scientists, data managers, educators and trainers as well as producers, control agencies and policy makers to more easily answer questions concerning quality of measurements in food commodities, the main stable isotope characteristics of food of plant and animal origin, geographical location, and authenticity".

Isotope Geochemistry in Doping

Doping represents one of the major issues in sports, mostly through the use of synthetic steroids. Before 1982, xenobiotic steroids were the only class of steroids that had been banned. Following the prohibition of testosterone administration by the International Olympic Committee and subsequently by the World Anti-Doping Agency (WADA 2022), the need for the implementation of new tools to maximize the detection of synthetic steroid doping

(continued)

violations arose. Historically, molecular spectrometry techniques, such as GC-MS, were the reference methods to detect and quantify the administration of synthetic steroids (Thevis et al. 2020). This steroid profile, based on the analysis of several urinary steroids that are generated by the athlete's endocrine system, serves as a screening method for urine samples entering the laboratory and allows eliminating those of nonsuspicious nature. For those of suspicious nature, isotope geochemistry revealed its added value by characterizing the origin and metabolic pathways undergone by metabolites in biological fluids (e.g., Montes de Oca Porto et al. 2020; Iannella et al. 2021). Southan et al. (1990), using the example of gonadal and pharmaceutical testosterone, first demonstrated that the distribution of C stable isotopes was distinguishable between endogenous and exogenous (i.e., synthetic) metabolites.

Studies demonstrated that the administration of steroids, particularly testosterone, resulted in a ^{13}C depletion in the corresponding steroid diol metabolites: $\delta^{13}C$ values are shifting from their endogenous values towards exogenous isotope compositions (e.g., Shackleton et al. 1997; Aguilera et al. 1999). Cawley and Flenker (2008) thus proposed a two-stage protocol to ensure a precise and reliable certification of steroid abuse in urine samples.

A preliminary screening based on the measurement of the $\delta^{13}C$ of androsterone and etiocholanolone, the terminal androgen metabolites that are excreted in urinary concentrations, helped to identify suspicious samples with C isotope compositions that would fall outside of the reference intervals such as those reported by Ueki and Okano (1999) and de la Torre et al. (2001) for endogenous steroid metabolites ($-25 < \delta^{13}C < -15‰$) and commercially available steroids ($-36 < \delta^{13}C < -26‰$).

For samples classified as suspicious, the authors recommend that the doping action is confirmed by a second $\delta^{13}C$ analysis on the aab- and bab-diols (i.e., steroid diol metabolites) and/or testosterone.

While most of the literature available is focusing on the use of C isotopes, recent studies have turned their attention to other isotope systematics such as H isotopes (e.g., Piper et al. 2009; Putz et al. 2020).

References

Aggarwal SK (2016) Nuclear forensics: what, why and how? Curr Sci 110(5):782–791

Aggarwal J, Habicht-Mauche J, Juarez C (2008) Application of heavy isotopes in forensic isotope geochemistry: A review. Appl Geochem 23:2658–2666

Aguilera R, Catlin DH, Becchi M et al (1999) Screening urine for exogenous testosterone by isotope ratio mass spectrometric analysis of one pregnanediol and two androstanediols. J Chromatogr B Biomed 727:95–105

Ahn J, Seo H (2021) Material attractiveness of unirradiated depleted, natural and low-enriched uranium for use in radiological dispersal device. Nucl Eng Technol 53(5):1652–1657

Allen MS, Lacey MJ, Boyd S (1994) Determination of methoxypyrazines in red wines by stable isotope dilution gas chromatography–mass spectrometry. J Agric Food Chem 42(8):1734–1738

Arienzo I, Carandente A, Di Renzo V et al (2013) Sr and Nd isotope analysis at the Radiogenic Isotope Laboratory of the Istituto Nazionale di Geofisica e Vulcanologia, Sezione di Napoli – Osservatorio Vesuviano. Rapporti Tecnici INGV 260:1–18

Arienzo I, Rucco I, Di Vito MA et al (2020) Sr isotopic composition as a tool for unraveling human mobility in the Campania area. Archaeol Anthropol Sci 12:157

Asfaha DG, Quétel CR, Thomas F et al (2011) Combining isotopic signatures of n(^{87}Sr)/n(^{86}Sr) and light stable elements (C, N, O, S) with multi-elemental profiling for the authentication of provenance of European cereal samples. J Cereal Sci 53(2):170–177

Avanzinelli R, Boari E, Conticelli S et al (2005) High precision Sr, Nd, and Pb isotopic analyses using the new generation thermal ionisation mass spectrometer thermofinnigan triton–Ti©. Per Mineral 74:147–166

Bataille CP, Bowen GJ (2012) Mapping ^{87}Sr/^{86}Sr variations in bedrock and water from large scale provenance studies. Chem Geol 304–305:39–52

Beals D, Dunlop W, Niemeyer S et al (2018) Categorizing an explosive device by its nuclear signature. Report LLNL-TR-761906, Lawrence Livermore National Laboratory, USA

Benson SJ, Lennard CJ, Maynard P et al (2009a) Forensic analysis of explosives using isotope ratio mass spectrometry (IRMS) – preliminary study of TATP and PETN. Sci Justice 49(2):81–86

Benson SJ, Lennard CJ, Maynard P et al (2009b) Forensic analysis of explosives using isotope ratio mass spectrometry (IRMS) – discrimination of ammonium nitrate sources. Sci Justice 49:73–80

Benson SJ, Lennard CJ, Maynard P et al (2010) Forensic analysis of explosives using isotope ratio mass spectrometry (IRMS), Part 2: forensic inter-laboratory trial: bulk carbon and nitrogen stable isotopes in a range of chemical compounds (Australia and New Zealand). J Forensic Sci 55:205–212

Bezemer KDB, Koeberg M, van der Heijden AEDM et al (2016) The potential of isotope ratio mass spectrometry (IRMS) and gas-chromatography-IRMS analysis of triacetone triperoxide in forensic explosives investigations. J Forensic Sci 61(5):1198–1207

Billault I, Courant F, Pasquereau L et al (2007) Correlation between the synthetic origin of methamphetamine samples and their N–15 and C–13 stable isotope ratios. Anal Chim Acta 593:20–29

Boner M, Förstel H (2004) Stable isotope variation as a tool to trace the authenticity of beef. Anal Bioanal Chem 378:301–310

Bowen GJ (2008) Spatial analysis of the inter-annual variation of precipitation isotope ratios and its climatological corollaries. J Geophys Res Atmos 113:ARTN. D05113

Bowen GJ (2010) Isoscapes: spatial pattern in isotopic biogeochemistry. Annu Rev Earth Planet Sci 38:161–187

Brust H, Koeberg M, van der Heijden M et al (2015) Isotopic and elemental profiling of ammonium nitrate in forensic explosive investigations. Forensic Sci Int 248:101–112

Buchanan HAS, Nic Daéid N, Meier-Augenstein W et al (2008) Emerging use of isotope ratio mass spectrometry as a tool for discrimination of 3,4–methylenedioxymethamphetamine by synthetic route. Anal Chem 80:3350–3356

Burk DE (2005) Forward model calculations for determining isotopic compositions of materials used in a radiological dispersal device. Doctoral dissertation, Texas A&M University

Cabanero AI, Recio JL, Ruperez M (2006) Liquid chromatography coupled to isotope ratio mass spectrometry: a new perspective on honey adulteration detection. J Agric Food Chem 54:9719–9727

Camin F, Wehrens R, Bertoldi D et al (2012) H, C, N and S stable isotopes and mineral profiles to objectively guarantee the authenticity of grated hard cheeses. Anal Chim Acta 711:54–59

Camin F, Boner M, Bontempo L et al (2017) Stable isotope techniques for verifying the declared geographical origin of food in legal cases. Trends Food Sci Technol 61:176–187

Can H, Hongcheng M, Hongling G et al (2021) Recent advance in stable isotope ratio analysis of common explosives. Chin J Chromatogr 39(4):376–383

Carter JF, Titterton EL, Grant H et al (2002a) Isotopic changes during the synthesis of amphetamines. Chem Commun 21:2590–2591
Carter JF, Titterton EL, Murray M et al (2002b) Isotopic characterization of 3,4–methylenedioxyamphetamine and 3,4–methylenedioxymethylamphetamine (ecstasy). Analyst 127:830–833
Carter JF, Sleeman R, Hill JC et al (2005) Isotope ratio mass spectrometry as a tool for forensic investigation (examples from recent studies). Sci Justice 45:141–149
Carter JF, Yates HSA, Tinggi U (2015) A global survey of the stable isotope and chemical compositions of bottled and canned beers as a guide to authenticity. Sci Justice 55(1):18–26
Casale JF, Ehleringer JR, Morello DR et al (2005) Isotopic fractionation of carbon and nitrogen during the illicit processing of cocaine and heroin in South America. J Forensic Sci 50:1–7
Cawley AT, Flenker U (2008) The application of carbon isotope ratio mass spectrometry to doping control. J Mass Spectrom 43:854–864
Chen T, Zhao Y, Zhang W et al (2016) Variation of the light stable isotopes in the superior and inferior grains of rice (Oryza sativa L.) with different geographical origins. Food Chem 209:95–98
Chen F, Lao Q, Zhang S et al (2020) Nitrate sources and biogeochemical processes identified using nitrogen and oxygen isotopes on the eastern coast of Hainan Island. Cont Shelf Res 207:104209
Chesson LA, Berg GE (2021) The use of stable isotopes in postconflict forensic identification. WIRE Forensic Sci 2021:e1439. https://doi.org/10.1002/wfs2.1439
Chesson LA, Tipple BJ, Mackey GN et al (2012) Strontium isotopes in tap water from the coterminous USA. Ecosphere 3(7):67
Chiocchini F, Portarena S, Ciolfi M et al (2016) Isoscapes of carbon and oxygen stable isotope compositions in tracing authenticity and geographical origin of Italian extra-virgin olive oils. Food Chem 202:291–301
Coelho I, Castanheira I, Moura Bordado J et al (2017) Recent developments and trends in the application of strontium and its isotopes in biological related fields. Trends Anal Chem 90:45–61
Danezis GP, Tsagkaris AS, Camin F et al (2016) Food authentication: techniques, trends & emerging approaches. Trends Anal Chem 85:123–132
de la Torre X, Gonzalez JC, Pichini S et al (2001) $^{13}C/^{12}C$ isotope ratio MS analysis of testosterone, in chemicals and pharmaceutical preparations. J Pharm Biomed Anal 24:645–650
DeBord J, Pourmand A, Jantzi SC et al (2017) Profiling of heroin and assignment of provenance by $^{87}Sr/^{86}Sr$ isotope ratio analysis. Inorg Chim Acta 468:294–299
DeNiro MJ, Epstein S (1976) You are what you eat (plus a few permil): the carbon isotope cycle in food chains. Geol Soc Am Abstr Programs 8:834–835
Desage M, Guilly R, Brazier JL et al (1991) Gas chromatography with mass spectrometry or isotope-ratio mass spectrometry in studying the geographical origin of heroin. Anal Chim Acta 247:249–254
Eftimov T, Ispirova G, Potočnik D et al (2019) ISO-FOOD ontology: a formal presentation of the knowledge within the domain of isotopes for food science. Food Chem 277:382–390
Elsner M, Imfeld G (2016) Compound-specific isotope analysis (CSIA) of micro- pollutants in the environment – current developments and future challenges. Curr Opin Biotechnol 41:60–72
Fahey AJ, Zeissler CJ, Newbury DE et al (2010) Postdetonation nuclear debris for attribution. PNAS 107(47):20207–20212
Farmer NL, Ruffell A, Meier-Augenstein W et al (2007) Forensic analysis of wooden safety matches – a case study. Sci Justice 47:88–98
Flores P, López A, Fenoll J et al (2013) Classification of organic and conventional sweet peppers and lettuce using a combination of isotopic and bio-markers with multivariate analysis. J Food Compos Anal 31(2):217–225
Font L, van der Peijl G, van Wetten I et al (2012) Strontium and lead isotope ratios in human hair: investigating a potential tool for determining recent human geographical movements. J Anal At Spectrom 27:719
Galimov EM, Sevastyanov VS, Kulbachevskaya EV et al (2005) Isotope ratio mass spectrometry: $\delta^{13}C$ and $\delta^{15}N$ analysis for tracing the origin of illicit drugs. Rapid Commun Mass Spectrom 19:1213–1216

Gopi K, Mazumder D, Sammut J et al (2019) Combined use of stable isotope analysis and elemental profiling to determine provenance of black tiger prawns (Penaeus monodon). Food Control 95:242–248

Guibourdenche L, Stevenson R, Pedneault K et al (2020) Characterizing nutrient pathways in Quebec (Canada) vineyards: insight from stable and radiogenic strontium isotopes. Chem Geol 532:119375

Hanson JT (2008) Radiological dispersal device primer: from a terrorist perspective. Report, Air War College, Maxwell AFB, AL, 36112, 56 pp

Hobson KA, Koehler G (2015) On the use of stable oxygen isotope ($\delta^{18}O$) measurements for tracking avian movements in North America. Ecol Evol 5:799–806

Howa JD, Lott MJ, Chesson LA et al (2016) Isolation of components of plastic explosives for isotope ratio mass spectrometry. Forensic Chem 1:6–12

Humez P, Osselin F, Kloppmann W et al (2019) A geochemical and multi-isotope modeling approach to determine sources and fate of methane in shallow groundwater above unconventional hydrocarbon reservoirs. J Contam Hydrol 226:103525

Hurley JM, West JB, Ehleringer JR (2010) Stable isotope models to predict geographic origin and cultivation conditions of marijuana. Sci Justice 50:86–93

Iannella L, Colamonici C, Curcio D et al (2021) Detecting the abuse of 19-norsteroids in doping controls: a new gas chromatography coupled to isotope ratio mass spectrometry method for the analysis of 19-norandrosterone and 19-noretiocholanolone. Drug Test Anal 13(4):770–784

Kalderis D, Juhasz AL, Boothpathy R et al (2011) Soils contaminated with explosives: environmental fate and evaluation of state-of-the-art remediation processes (IUPAC Technical Report). Pure Appl Chem 83:1407–1484

Kelly S, Baxter M, Chapman S et al (2002) The application of isotopic and elemental analysis to determine the geographical origin of premium long grain rice. Eur Food Res Technol 214:72–78

Kim H, Lee Y, Choi S (2019) Identifying radioactive materials in dirty bomb terror scene using laser-induced breakdown spectroscopy. Proceed Korean Radioact Waste Soc Conf, pp 43–44

Kousehlar M, Widom E (2020) Identifying the sources of air pollution in an urban-industrial setting by lichen biomonitoring – a multi-tracer approach. Appl Geochem 121:104695

Kristo MJ, Tumey SJ (2013) The state of nuclear forensics. Nucl Instr Meth Phys Res B 294:656–661

Li X, Li Z, Chen J et al (2021) Isotope signatures of atmospheric mercury emitted from residential coal combustion. Atmos Environ 246:118175

Liu HC, You CF, Chen CY et al (2014) Geographic determination of coffee beans using multi–element analysis and isotope ratios of boron and strontium. Food Chem 142:439–445

Liu H, Wu M, Gao H et al (2021) Hydrocarbon transformation pathways and soil organic carbon stability in the biostimulation of oil-contaminated soil: implications of ^{13}C natural abundance. Sci Total Environ 788:147580

Lock CM, Meier-Augenstein W (2008) Investigation of isotopic linkage between precursor and product in the synthesis of a high explosive. Forensic Sci Int 179:157–162

Lott MJ, Howa J, Ehleringer JM (2002) Locating the origins of explosives through stable isotope ratio analysis. Forensic isotope ratio mass spectrometry (FIRMS) conference 2002. https://www.forensic-isotopes.org/2002.html

Lugli F, Cipriani A, Tavaglione V et al (2018) Transhumance pastoralism of Roccapelago (Modena, Italy) early-modern individuals: inferences from Sr isotopes of hairstrands. Am J Phys Anthropol 167:470–483

Lugli F, Cipriani A, Bruno L et al (2021) A strontium isoscape of Italy for provenance studies. Chem Geol. https://doi.org/10.1016/j.chemgeo.2021.120624

Luo D, Dong H, Luo H et al (2016) Multi-element (C, N, H, O) stable isotope ratio analysis for determining the geographical origin of pure milk from different regions. Food Anal Methods 9:437–442

Luo R, Jiang T, Chen X et al (2019) Determination of geographic origin of Chinese mitten crab (*Eriocheir sinensis*) using integrated stable isotope and multi-element analyses. Food Chem 274:1–7

Marchionni S, Buccianti A, Bollati A et al (2016) Conservation of $^{87}Sr/^{86}Sr$ isotopic ratios during the winemaking processes of 'Red' wines to validate their use as geographic tracer. Food Chem 190:777–785

Mas F, Beemsterboer B, Veltkamp AC et al (1995) Determination of common–batch members in a set of confiscated 3,4–(methylendioxy) methylamphetamine samples by measuring the natural isotope abundances: a preliminary study. Forensic Sci Int 71:225–231

Matos MPV, Jackson GP (2019) Isotope ratio mass spectrometry in forensic science applications. Forensic Chem 13:100154

Mayer K, Wallenius M, Fanghänel T (2007) Nuclear forensic science – from cradle to maturity. J Alloys Comd 444–445:50–56

Medini S, Janin M, Verdoux P et al (2015) Methodological development for $^{87}Sr/^{86}Sr$ measurement in olive oil and preliminary discussion of its use for geographical traceability of PDO Nîmes (France). Food Chem 171:78–83

Meier-Augenstein W (2010) Stable isotope forensics: an introduction to the forensic application of stable isotope analysis. Wiley, Chichester

Meier-Augenstein W, Fraser I (2008) Forensic isotope analysis leads to identification of a mutilated murder victim. Sci Justice 48:153–159

Mercurio M, Grilli E, Odierna P et al (2014) A "Geo–Pedo–Fingerprint" (GPF) as a tracer to detect univocal parent material–to–wine production chain in high quality vineyard districts, Campi Flegrei (Southern Italy). Geoderma 230–231:64–78

Monahan FJ, Schmidt O, Moloney AP (2018) Meat provenance: authentication of geographical origin and dietary background of meat. Meat Sci 144:2–14

Montes de Oca Porto R, Fernandez Hormiga MA, Correa Vidal MT et al (2020) Carbon isotope ratio of endogenous urinary steroids of the Cuban population of athletes studied for doping purposes. Drug Test Anal 12(10):1501–1507

Muccio Z, Jackson GP (2009) Isotope ratio mass spectrometry. Analyst 134:213–222

Nissenbaum A (1975) The distribution of natural stable isotopes of carbon as a possible tool for the differentiation of samples of TNT. J Forensic Sci 20:455–459

O'Leary MH (1988) Carbon isotopes in photosynthesis. Bioscience 38(5):328–336

Ogrinc N, Košir IJ, Spangenberg JE et al (2003) The application of NMR and MS methods for detection of adulteration of wine, fruit juices, and olive oil: a review. Anal Bioanal Chem 376:424–430

Palhol F, Lamoureux C, Naulet N (2003) ^{15}N isotopic analyses: a powerful tool to establish links between seized 3,4–methylenedioxymethamphetamine (MDMA) tablets. Anal Bioanal Chem 376:486–490

Palhol F, Lamoureux C, Chabrillat M et al (2004) $^{15}N/^{14}N$ isotopic ratio and statistical analysis: an efficient way of linking seized ecstasy. Anal Chim Acta 510:1–8

Perini M, Giongo L, Grisenti M et al (2018) Stable isotope ratio analysis of different European raspberries, blackberries, currants and strawberries. Food Chem 239:48–55

Peters BD, Lam PJ, Casciotti KL (2018) Nitrogen and oxygen isotope measurements of nitrate along the US GEOTRACES Eastern Pacific Zonal Transect (GP16) yield insights into nitrate supply, remineralization, and water mass transport. Mar Chem 201:137–150

Petrini R, Sansone L, Slejko FF et al (2015) The $^{87}Sr/^{86}Sr$ strontium isotopic systematics applied to Glera vineyards: a tracer for the geographical origin of the Prosecco. Food Chem 170:138–144

Phillips SA, Doyle S, Philp L et al (2002) Proceedings: network developing forensic applications of stable isotope ratio mass spectrometry conference 2002. Sci Justice 43:153–160

Pillonel L, Badertscher R, Casey M et al (2005) Geographic origin of European Emmental cheese: characterisation and descriptive statistics. Int Dairy J 15:547–556

Piper T, Thevis M, Flenker U et al (2009) Determination of the deuterium/hydrogen ratio of endogenous urinary steroids for doping control purposes. Rapid Commun Mass Spectrom 23(13):1917–1926

Pontér S, Sutliff-Johansson S, Engström E et al (2016) Evaluation of a multi-isotope approach as a complement to concentration data within environmental forensics. Fortschr Mineral 11(1):37
Putz M, Piper T, Thevis M (2020) Identification of trenbolone metabolites using hydrogen isotope ratio mass spectrometry and liquid chromatography/high accuracy/high resolution mass spectrometry for doping control analysis. Front Chem 8:435
Quirk AT, Bellerby JM, Carter JF et al (2009) An initial evaluation of stable isotope characterization of post-blast plastic debris for improvised explosive devices. Sci Justice 49:87–93
Rauch E, Rummel S, Lehn C et al (2007) Origin assignment of unidentified corpses by use of stable isotope ratios of light (bio–) and heavy (geo–) elements – a case report. J Forensic Sci 168:215–218
Richter B, Gurk S, Wagner D et al (2019) Food authentication: multi-elemental analysis of white asparagus for provenance discrimination. Food Chem 286:475–482
Rossmann A, Schmidt HL, Reniero F et al (1996) Stable carbon isotope content in ethanol of EC data bank wines from Italy, France and Germany. Z Lebensm Unter Forsch 203:293–301
Saar de Almeida B, Fedele L, D'Antonio M et al (2022) Characterizing wine terroir using strontium isotope ratios: a review. Earth-Sci Rev (Submitted)
Schmidt TC, Zwank L, Berg MEM et al (2004) Compound-specific stable isotope analysis of organic contaminants in natural environments: a critical review of the state of the art, prospects, and future challenges. Anal Bioanal Chem 378:283–300
Shackleton CHL, Roitman E, Phillips A et al (1997) Androstane-diol and 5-androstenediol profiling for detecting exogenously administered dihydrotestosterone, epitestosterone, and dehydroepiandrosterone: potential use in gas chromatography isotope ratio mass spectrometry. Steroids 62:665–673
Shibuya EK, Sarkis JES, Negrini-Neto O et al (2007) Carbon and nitrogen isotopes as indicative of geographical origin of marijuana samples seized in the city of São Paulo (Brazil). Forensic Sci Int 167:8–15
Soba D, Gámez AL, Úriz N et al (2021) Foliar heavy metals and stable isotope ($\delta^{13}C$, $\delta^{15}N$) profiles as reliable urban pollution biomonitoring tools. Urban For Urban Green 57:126918
Southan G, Mallet A, Jumeau J et al (1990) Program and abstracts of the 2nd international symposium of applied mass spectrometry in the health sciences. Barcelona, pp 306
Sterner JH (1947) Tracer isotopes in industrial toxicology. Occup Med 3(6):552–559
Stevenson R, Desrochers S, Hélie JF (2015) Stable and radiogenic isotopes as indicators of agri-food provenance: insights from artisanal cheeses from Quebec, Canada. Int Dairy J 49:37–45
Suzuki Y, Chikaraishi Y, Ogawa NO et al (2008) Geographical origin of polished rice based on multiple element and stable isotope analyses. Food Chem 109:470–475
The World Anti-Doping Agency (WADA) Prohibited List 2022. http://www.wada-ama.org/en/resources/science-medicine/2022-prohibited-list-documents
Thermo (1995) $^{15}N/^{14}N$ and $^{13}C/^{12}C$ by EA/IRMS forensic studies using the ConFlo II interface. Application Flash. Report 15:12/1995 PL 0/1177
Thevis M, Kuuranne T, Geyer H (2020) Annual banned-substance review: analytical approaches in human sport drugs testing 2019/2020. Drug Test Anal 13:8–35
Tieman ZG, Stewart BW, Capo RC et al (2020) Barium isotopes track the source of dissolved solids in produced water from the unconventional Marcellus Shale Gas Play. Environ Sci Technol 54:4275–4285
Ueki M, Okano M (1999) Analysis of exogenous dehydroepiandrosterone excretion in urine by gas chromatography/combustion/isotope ratio mass spectrometry. Rapid Commun Mass Spectrom 13:2237–2243
Vinciguerra V, Stevenson R, Pedneault K et al (2016) Strontium isotope characterization of wines from Quebec, Canada. Food Chem 210:121–128
Wallenius M, Mayer K, Ray I (2006) Nuclear forensic investigations: two case studies. Forensic Sci Int 156:55–62
Wang Y, Liang J, Wang J et al (2018) Combining stable carbon isotope analysis and petroleum-fingerprinting to evaluate petroleum contamination in the Yanchang oilfield located on loess plateau in China. Environ Sci Pollut Res 25(3):2830–2841

Weber D, Rossmann A, Schwarz S et al (1997) Correlations of carbon isotope ratios of wine ingredients for the improved detection of adulterations. 1. Organic acids and ethanol. Z Lebensm Unters Forsch 205:158–164

West JB, Ehleringer JR, Cerling TE (2007) Geography and vintage predicted by a novel GIS model of wine $\delta^{18}O$. J Agric Food Chem 55(17):7075–7083

West JB, Hurley JM, Dudàs FO et al (2009a) The stable isotope ratios of marijuana. II. Strontium isotopes relate to geographic origin. J Forensic Sci 54:1261–1269

West JB, Hurley JM, Ehleringer JR (2009b) Stable isotope ratios of marijuana. Carbon and nitrogen stable isotopes describe growth conditions. J Forensic Sci 54:84–89

White WM (2015) Isotope geochemistry. Wiley, West Sussex

Widory D, Minet JJ, Barbe-Leborgne M (2009) Sourcing explosives: a multi-isotope approach. Sci Justice 49:62–72

Wijker RS, Bolotin J, Nishino SF et al (2013) Using compound-specific isotope analysis to assess biodegradation of nitroaromatic explosives in the subsurface. Environ Sci Technol 47:6872–6883

Xiao HW, Zhu RG, Pan YY et al (2020) Differentiation between nitrate aerosol formation pathways in a southeast Chinese city by dual isotope and modeling studies. J Geophys Res Atmos 125(13):e2020JD032604

Zhao S, Zhao Y (2020) Application and preparation progress of stable isotope reference materials in traceability of agricultural products. Crit Rev Anal Chem. https://doi.org/10.1080/10408347.2020.1768359

Zhao Y, Zhang B, Chen G et al (2013) Tracing the geographic origin of beef in China on the basis of the combination of stable isotopes and multielement analysis. J Agric Food Chem 61:7055–7060

Zhao Y, Yang S, Wang D (2016) Stable carbon and nitrogen isotopes as a potential tool to differentiate pork from organic and conventional systems. J Sci Food Agric 96:3950–3955

Chapter 10
Image Analysis in Forensic Mineralogy

Chiara Germinario and Celestino Grifa

Abstract The analysis of digital images represents a valuable tool in the field of forensic sciences. With the advancements in imaging technologies, the digital images are becoming a concrete information source. The computational techniques that aid in the measurement or quantification of features visible within an image have been used for several years in biology and metallurgy, as well as in the military field, in remote sensing and medicine. However, in the last decades, they started to find wide use in the areas of Geological Sciences, especially in mineralogy and petrology where the use of macroscopic and microscopy images has always represented a valid tool for scientific investigation.

In forensic sciences, the technological advancement (i.e., advent of high-performing computers and comparatively large memories), coupled with digital microscope cameras, has brought about a revolution in computer-assisted image analysis. Macroscopic images, photomicrographs of sections either in transmitted or reflected light and images from scanning electron microscope of materials from crime scenes can be analysed by image analysis, representing an effective methodology able to provide significant clues for the resolution of a judicial case.

Keywords Image analysis · Digital images · Image processing · Measurements

The term 'Image analysis' is generally referred to computational techniques which permit the extraction of quantitative information from images captured in digital form. The potential that these techniques provides in data acquisition, their processing and statistical approach, permitted their large use in the field of mineralogy and petrology (Francus 1998).

C. Germinario · C. Grifa (✉)
Department of Sciences and Technologies, University of Sannio, Benevento, Italy
e-mail: chiara.germinario@unisannio.it; celestino.grifa@unisannio.it

M. Mercurio et al. (eds.), *Mineralogical Analysis Applied to Forensics*, Soil Forensics, https://doi.org/10.1007/978-3-031-08834-6_10

Nevertheless, when the more conventional imaging systems are applied to the study of rocks and sediments, difficulties may arise in data processing and interpretation, often related to the correct definition of the geometric and dimensional features of the elements recognizable from digital images (Francus 1998).

During the last decades, the application of image analysis has significantly increased, in an attempt to overcome the described difficulties by improving the quality of image acquisition.

Therefore, the choice of the most appropriate image analysis technique is carefully made according to the characteristics of the material to be analyzed, the information to be obtained and the amount of sample available; the latter is a crucial point in the forensic field.

In any case, the typical sequence of operations includes image acquisition, image processing, measurements, data processing, and interpretation (Francus 1998). Such an operational approach will be detailed in the next paragraphs.

10.1 Digital Images and Acquisition Systems

By definition, an image is a representation of objects or a scene according to independent spatial coordinates. In particular, it can be defined as a distribution (two- or three-dimensional) of a physical entity. Images can be either *analog* or *digital*. A digital image is composed of a two-dimensional array of *pixels* (PICture ELements), a portion of the image with particular color or shade of gray, arranged according to a predefined ratio of columns and rows. Thus, a digital image may be defined as a two-dimensional function, $f(x, y)$, where x and y are spatial (plane) coordinates, and the amplitude of f at any pair of coordinates (x, y) is called the *intensity* or gray level of the image at that point (x, y, and the intensity values of f are all finite, discrete quantities) (Gonzalez and Woods 2018).

The pixel represents the smallest self-contained element of the image itself; the pixel dimensions of an image define the information content of the image: the more pixels in an image, the more information it contains (Stern and Richardson 2003).

Digital images are generated by the combination of an energy source and the reflection of energy emitted from the source by objects in a scene. The light from the scene passes through the lens system inside the acquisition system (camera), which directs it towards a sensor, a system sensitive to the impulses radiated by objects that captures the energy of light and converts it into an electrical current, thus determining the brightness value of each pixel (Battiato et al. 2013).

The digital images can be divided in four basic types (McAndrew 2021):

- ***Binary***. Each pixel is just black or white. Since there are only two possible values for each pixel, we only need one bit per pixel (Fig. 10.1a).
- ***Grayscale***. Each pixel is a shade of gray, normally from 0 (black) to 255 (white). This range means that each pixel can be represented by eight bits, or exactly one byte (Fig. 10.1b).

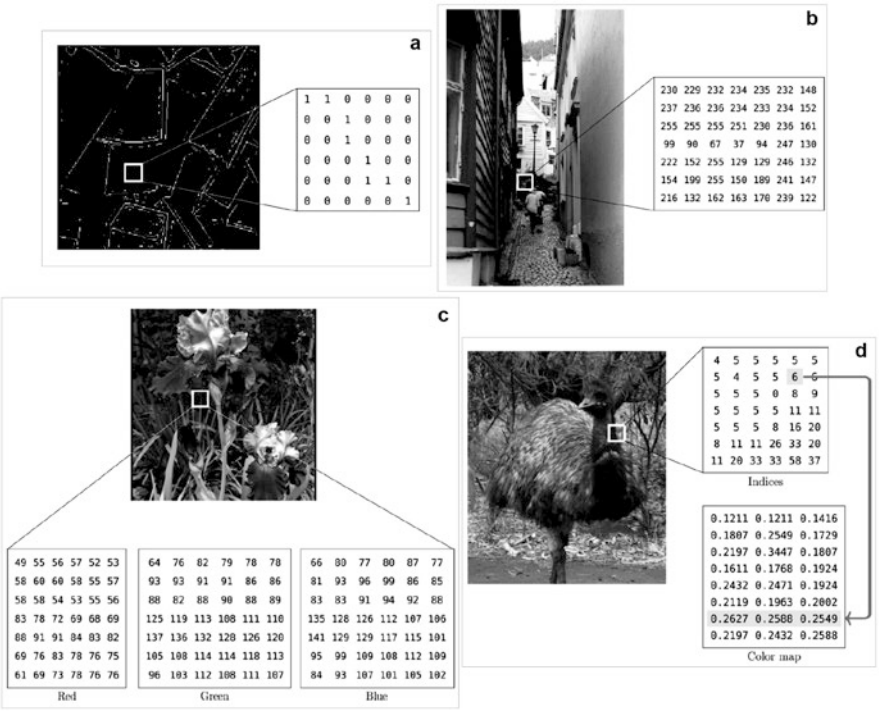

Fig. 10.1 Types of digital images. (**a**) Binary image; (**b**) Gray scale image; (**c**) True color, or RGB image; (**d**) Indexed image. (Modified after McAndrew 2021)

- ***True color, or RGB***, in which each pixel has a particular color; that color is described by the amount of red, green, and blue in it. If each of these components has a range 0–255, this gives a total of 255^3 = 16,777,216 different possible colors in the image. Since the total number of bits required for each pixel is 24, such images are also called 24-bit color images. Such an image may be considered as consisting of a "stack" of three matrices, representing the red, green, and blue values for each pixel (Fig. 10.1c). This means that for every pixel there are three corresponding values.
- ***Indexed.*** Most color images only have a small subset of the more than 16 million possible colors. For convenience of storage and file handling, the image has an associated color map, or color palette, which is simply a list of all the colors used in that image. Each pixel has a value which does not give its color (as for an RGB image), but an index to the color in the map (Fig. 10.1d). It is convenient if an image has 256 colors or less, for then the index values will only require one byte each to store.

As the images, also the image acquisition systems can also be analog or digital; the first ones (traditional cameras) allow to capture the image that will be later digitized. For the second ones (digital cameras and video cameras, scanners), instead, the

digitalization process is carried out simultaneously to the acquisition. They are often connected to other equipment (e.g. digital microscopes with reflected light, video microscopes, optical microscopes with transmitted light, scanning electron microscopes, etc.) for acquiring microphotographs at higher magnifications and definitions.

Digital cameras have a range of resolutions which vary from camera to camera. Image resolution is the ability of a digital system to represent fine details. Different types of resolution can be distinguished (i.e., spectral, radiometric, temporal) but the measure of the smallest discernible detail in an image is represented by *spatial resolution*. It can be defined as the density of pixels over the image and varies with the number of pixels occurring in an image (the more pixels are used to display the image, the greater the spatial resolution) (Gonzalez and Woods 2018; McAndrew 2021); it is measured in *dots per inch* (*DPI*).

10.2 Image Processing

After the acquisition, a digital image can be processed with dedicated software that permit the improvement of its quality and facilitate the interpretation, in an automatic or semi-automatic way. The applications of digital image processing range from medicine to entertainment, passing by geological processing and remote sensing (da Silva and Mendonça 2005).

The processing consists in applying one or more operations to the digital image in order to change the photometric or structural characteristics of the image, thus obtaining a new image, which is more easily "readable" and "interpretable" (Tuba et al. 2016). The processing of digital images can be divided into different classes, as *image enhancement, image restoration, image analysis,* and *image compression* (da Silva and Mendonça 2005).

The ***image enhancement*** consists in a set of procedures by which an image is manipulated so that it can be better displayed or improved for extracting useful information from it. There are many techniques that can be applied for the image enhancement, including, for example:

- *Histogram manipulation*

The histogram of an image is a function that maps each gray level of an image to the number of times it occurs in the image (da Silva and Mendonça 2005). Modifications made to histogram produce variation of the image, because the value of the pixels of the processed image will be different from those of the original one. The manipulation of histogram can result in a more uniform distribution of image's gray level (*histogram equalization*) (Fig. 10.2), a modification of the same to make it as similar as possible to a given image (*histogram specification*), or make the histogram of one image correspond to that of another one, for example, of the same scene taken from different sensors (*histogram matching*).

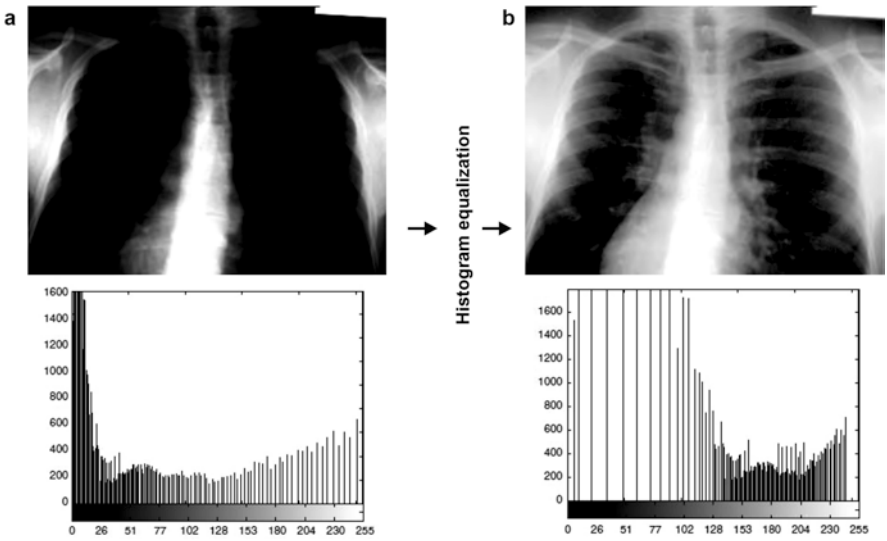

Fig. 10.2 Histogram of an original image (**a**) and of the equalized image (**b**). (Modified after da Silva and Mendonça 2005)

- *Image filtering*

The improvement of the images quality can be carried out by manipulating pixels inserting filters or masks (Gonzalez and Woods 2018). Linear filters modify a pixel based on its value and that of a set of pixels in a surrounding (mask). The intensity value of the pixel will then be equal to the weighted average of the intensity of the pixels in the mask.

Linear filtering is one of the most powerful image enhancement methods. Linear filters can, for example, reduce noise in images but at the same time worsen the definition of details, especially edges (*low-pass filter* or *blur filter*), highlight differences in intensity between pixels, especially the contours of objects, reducing the definition of background details (*high-pass filter*), accentuate contours, inevitably increasing noise in the image (*sharpen filter*), or identify edges with a particular orientation (*horizontal and vertical contour filters*).

Non-linear filters, on the other hand, permit to obtain a new, improved image applying statistic methods or mathematical formulas to the values of a matrix of pixels around the pixel under consideration. For example, they replace the value of the pixel considered with the median of the matrix values (*median filter*), with the maximum value (*dilation filter*) or with the minimum value of the matrix (*erosion filter*), respectively expanding or reducing the objects or enhancing only the pixels that belong to the contour, zeroing the others (*differentiation filters*). Moreover, filters can transform an image according to the shape properties of the objects in the image itself (*morphological filters*), for example, by removing contour pixels,

reducing the object to a skeleton (*skeletonization*) (Gonzalez and Woods 2018; McAndrew 2021).

The ***image restoration*** techniques aim at processing corrupted images from which there is a statistical or mathematical description of the degradation so that it can be reverted (McAndrew 2021). The reversion of the image can be done, for example, by:

- removing of noise (i.e., any degradation in the image signal, caused by external disturbance);
- removing of blur caused by linear motion;
- removing optical distortions;
- removing periodic interference.

The ***image analysis*** processes an image (or a sequence of images) so that information can be automatically extracted from it. An example of image analysis is:

- *Image segmentation*

Image segmentation algorithms separate the images into different, homogeneous regions. The identified regions must be distinct (two regions must not share any pixel), complete (all pixels in the image must be assigned to at least one region of the partition), connected (all pixels belonging to a region are connected), and homogeneous (all pixels in a region are characterized by the same property (e.g., color, intensity, etc.)) (da Silva and Mendonça 2005; Gonzalez and Woods 2018; McAndrew 2021).

The identification of regions, and thus segmentation, can occur by discontinuity (edge-based method), i.e., by identifying areas of discontinuity between the objects to be isolated (e.g., isolated points, lines, edges) and by similarity (Gonzalez and Woods 2018; McAndrew 2021). This second methodology can be performed, for example: (a) aggregating adjacent regions that should prove to be compatible according to a merging criterion (*region merging*); (b) aggregating unallocated pixels to one of the adjacent regions according to a certain criterion (*region growing*); (c) repeatedly partitioning an image up to uniform components are obtained (*region splitting*) and subsequently aggregating adjacent regions that should prove to be compatible according to a merging criterion (*region merging*); (d) applying thresholds of intensity, arbitrarily or automatically according to a statistical criterion, in order to distinguish the objects and the background, which will have, respectively, higher or lower intensity values (*thresholding*) (Gonzalez and Woods 2018; McAndrew 2021) (Fig. 10.3).

The ***image compression*** includes those techniques that remove the data redundancy in the digital images by reducing the number of bits needed in their representation. These operations are practical to store and transmit digital images (da Silva and Mendonça 2005).

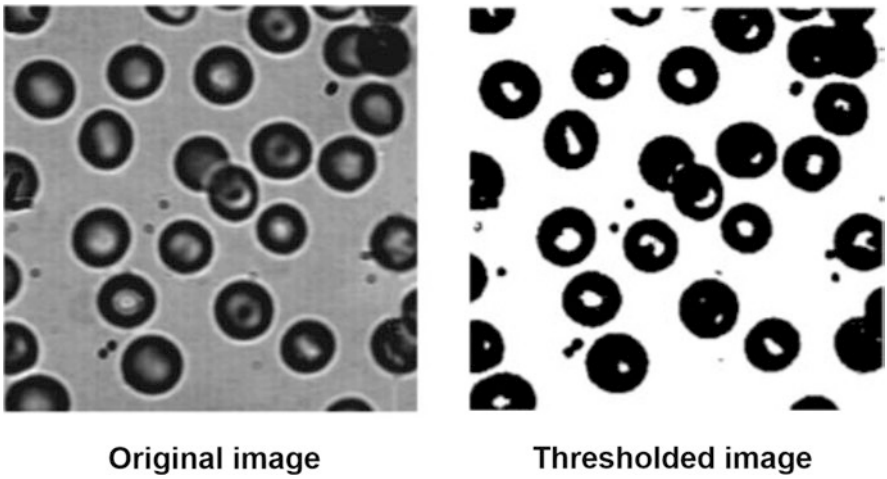

Fig. 10.3 Red blood cells original (**a**) and thresholded image (**b**). (Modified after Zhang et al. 2020)

10.3 Measurements

In the field of forensic mineralogy, the main applications of image analysis techniques are related to the determination of specific properties of analyzed samples. Actually, after an appropriate processing of digital images, measurements can be performed on them. In particular, very useful are the analyses permitting to determine morphological and textural features of materials, whether natural or artificial. Image analysis techniques, in fact, quantitatively evaluate the morphological and textural characteristics of materials that, otherwise, are merely estimated in a qualitative way.

Generally, they are determined by using comparison tables that, for example, permit to estimate, with a fair degree of subjectivity, the abundance of the granular component and/or macropores in the analyzed material (Fig. 10.4).

To overcome these drawbacks, software using appropriate algorithms for the quantitative calculation of each parameter are dedicated to the analysis of digital images. Image analysis, in fact, permits to calculate, automatically or semi-automatically, dimensional and morphological parameters of the particles, to obtain a quantitative and statistically significant measure of grain size distributions (hereafter GSD) and morphological parameters.

For the GSD description, dimensional parameters such as perimeter, area, minor axis and major axis of the particles are commonly used; in particular, major axis is used to calculate the φ (phi) value, a dimensional parameter introduced in the Udden-Wentworth dimensional scale to express the grain-size of the particles (Krumbein phi scale) (Krumbein and Sloss 1963). It is a logarithmic value equal to:

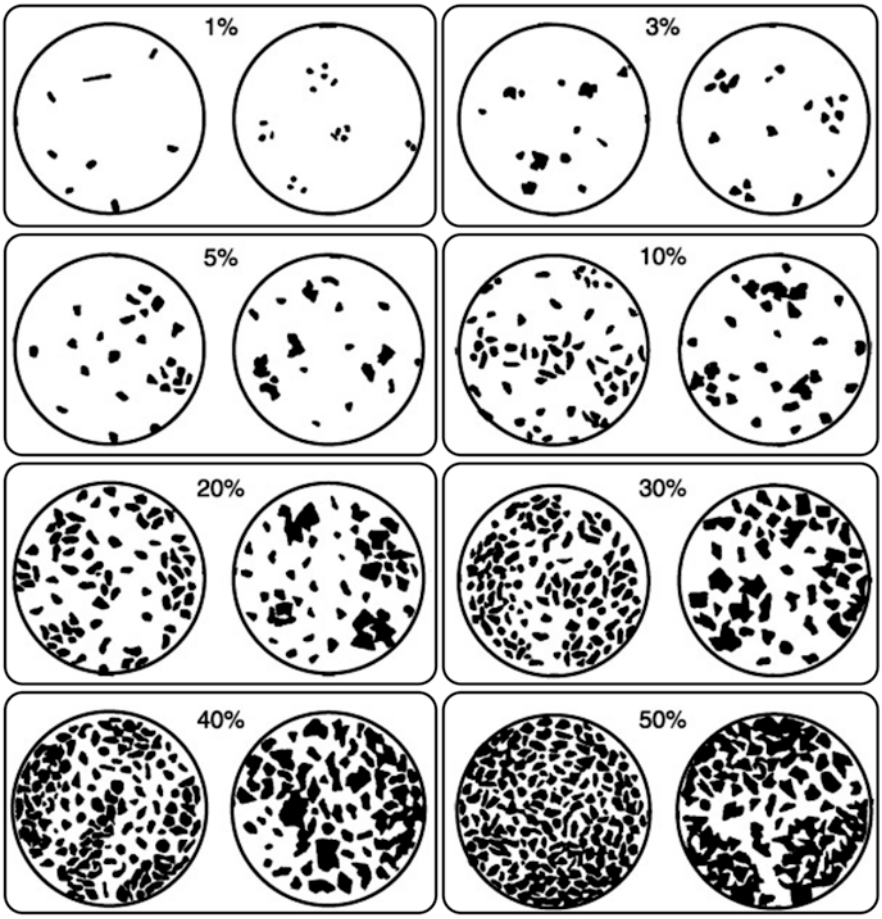

Fig. 10.4 Comparison chart for the estimation of the abundance of the granular component. (Modified after Terry and Chilingar 1955)

$$\varphi = -\log_2 \left(major\ axis\ /\ reference\ diameter \right)$$

where the reference diameter is equal to 1 (used to make the equation dimensionally homogeneous).

Another dimensional parameter frequently used to describe particle grain-size is the Feret diameter (dF), defined as the distance between two parallels tangent to the particle contour in a well-defined orientation (Fig. 10.5).

The maximum Feret diameter is the maximum diameter considering all possible orientations (0° – 180°) of a particle with an irregular shape while the minimum Feret diameter is the minimum diameter considering all possible orientations of the particle (Fig. 10.5). The average Feret diameter, on the other hand, is the average value of the Feret diameters with respect to all orientations.

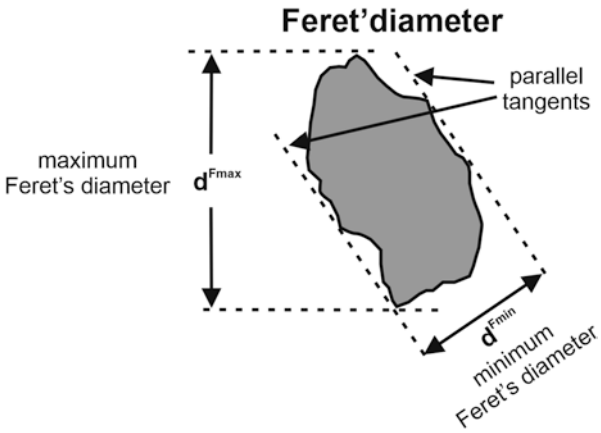

Fig. 10.5 Feret's diameter. (Modified after Gawenda et al. 2020)

The minimum Feret is the best value for describing particle size, as it yields size values comparable to those from a sieving particle size in which particles tend to orient preferentially along this direction (Fig. 10.5).

From the distribution of these parameters it is possible to obtain other information on texture and structure of the analyzed material, related, for example, to the distribution of the particles (homogeneous, banded, etc.), to the orientation (absent, weak, moderate, strong, etc.) or to the sorting (S), defined as the degree of particle size selection of the material, which can also be expressed as a diffusion of the distribution of particle sizes around the average diameter; this is expressed quantitatively as:

$$S = \sigma(\varphi)$$

where σ is the standard deviation.

Morphological parameters, on the other hand, are expressed by shape-factors, dimensionless quantities that numerically describe the shape of a particle regardless of its size. One of the principal shape factors used to describe the morphological features of particles is the sphericity, a measure of how much a particle's shape deviates from spherical, defined as:

Sphericity = Surface area of a sphere of the same volume as the particle / Actual exterior surface of the particle

The sphericity is 1 for spheres and <1 for all other particle shapes. The measurement of particle volumes and particle exterior surface areas permit the accurate determination of such a parameter. Thus, in practice, it is very difficult to correctly evaluate it. As a result, its two-dimensional analogue, namely the circularity (C), is often measured, assuming it to be equal to the sphericity (Grace and Ebneyamini 2021).

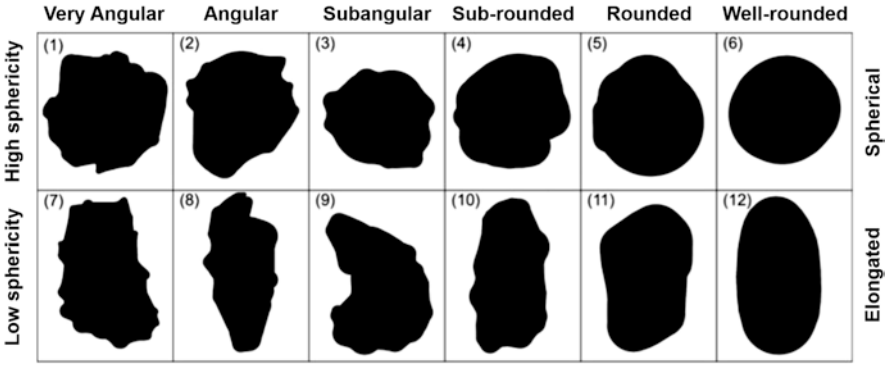

Fig. 10.6 Visual comparison chart for estimating the roundness and sphericity of grains. (Modified after Sun et al. 2019)

The circularity indicates how much a particle fits a perfect circle. It is a parameter that depends on the area and perimeter of the particle and is mathematically expressed as:

$$C = \left(4\pi^{*} area\right) / \left(perimeter \wedge 2\right)$$

Values vary from 0 to 1; a circularity value of 1.0 indicates a perfectly circular particle, while a value close to 0.0 indicates a particle with an increasingly elongated shape (Fig. 10.6).

Aspect ratio, on the other hand, indicates the ratio between the long axis and the short axis of a particle, and is expressed as

$$AR = major\ axis\ /\ minor\ axis$$

The inverse value of the aspect ratio defines the roundness of the particles. This parameter indicates the degree of curvature of the contour of the element examined and decreases, within crystalline phases, with the increase of the regularity of crystalline habits that, as is well known, are manifested by a rigid geometric arrangement of faces, vertices and edges. Roundness can also be numerically expressed as:

$$Roundness = \left(4^{*} area\right) / \left(\pi^{*} majoraxis \wedge 2\right)$$

The dimensional and morphological parameters that describe the characteristics of the materials can be directly measured by software dedicated to image analysis. These permit to calculate areas, measure distances and angles, plot graphs and histograms in relation to regions (ROI = Region of Interest) selected by the user.

Among those, the most widely used software for applications in the geological field is ImageJ (Rasband 1997–2018) an open source software, programmed in JAVA, dedicated to image processing, portable on different platforms, which allows to view, edit, analyze, process and save 8-, 16- and 32-bit images in different formats.

ImageJ characteristics well respond to the potentialities of image analysis techniques in the field of forensic mineralogy. The software, in fact, found large applications in mineralogy and petrography for the detailed analysis of texture and structure of sediments and clastic rocks, as well as of artificial geomaterials (Lewis et al. 2010).

Grain size and morphometric parameters of materials can be analyzed either semi-automatically, by manually identifying and circumscribing each particle, or automatically. Automatic particle detection is directly performed by the software, following an automated procedure (Fig. 10.7).

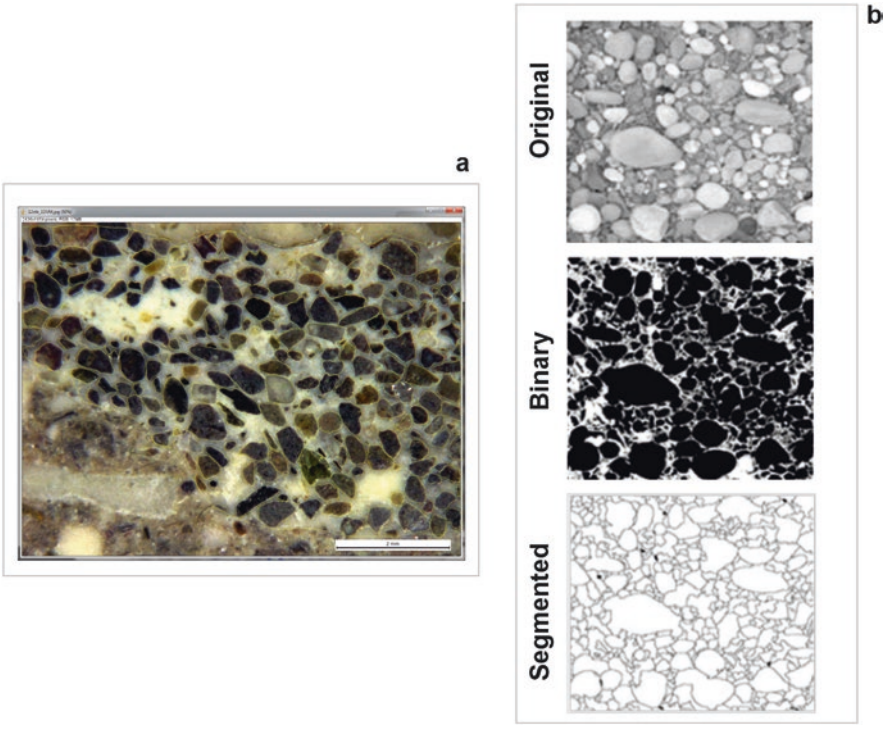

Fig. 10.7 Areal measurement method. (**a**); Image analyses with a manual contouring of particles; (**b**) Image-processing that permit to obtain, from the original image, a binary image from which the software, after segmentation, automatically identifies the particles. (Modified after Chang and Chung 2012)

Theoretically, obtaining information on the dimensional and morphological characteristics of a material in an automatic way is less laborious and faster than the manual detection of the single particle; for this reason, during the last decades several algorithms have been developed to process an image so that the software can automatically detect the particles and derive the information related to grain-size or morphology (Buscombe 2008). Most of these, process a binary image (i.e., containing only black and white pixels) by applying thresholds and filters to an 8-bit image, and extract information about the texture and structure of the analyzed material (Fig. 10.7).

Numerical data on dimensional and morphological parameters obtained by image analysis allow the construction of frequency histograms to define, for example, GSD or the morphometric characteristics of the material.

Image analysis also permits the quantification of each phase constituting the studied material, whether natural or artificial. This type of analysis, called modal analysis, is commonly used in geology to estimate relative proportions of each mineralogical phase in a rock. It is based on the relation which states that the ratio of the area occupied by a mineral (A) to the area occupied by all minerals (the total measurement area) is a consistent estimate of the volume percentage of mineral A in the rock (Goins and Reedy 2000).

It is a type of investigation that is usually carried out on thin-section images acquired by optical microscopes and scanning electron microscopes and is mainly based on two types of approach: the point-counting method and areal measurement.

The point counting method estimates the relative proportions of phases by identifying and counting minerals located at grid intersections or points.

The areal measurement method, on the other hand, calculates, through a manual or automatic selection by the image analysis software, the actual area occupied by each phase within the total measured area. In the automatic method, the software analyzes the image and picks out areas of different intensity or color values (Goins and Reedy 2000).

In order for the estimate to be statistically effective, it is necessary to analyze a quantity of material that can be considered representative, both in compositional and textural terms; nevertheless, modal analyses include errors in the estimation of the percentages of each phase, which can, however, be evaluated analytically and/or graphically (Germinario et al. 2019 and references therein).

Assuming that the sample is statistically relevant, often the enhancement of the image is required before starting the image analyses, for better define the particles constituting the sample. Different filters and algorithms may be applied to the images in order to enhance features of interest. Once the features of interest can be separated reliably by the software, the analysis can begin and data collected, either in a manual or automatic way, can be exported into a spreadsheet (Goins and Reedy 2000).

10.4 Fields of Application of Image Analysis in Forensic Geology

Image analysis turns out to be a useful support in the field of forensic science, since it can be applied on digital images of both natural (geological) (e.g., soil residues or rock fragments) and artificial materials (e.g., residues of construction material).

Regarding geological materials, the main applications concern quantitative analysis of morphological features of soil particles, rock fragments, or fragments of building material found on a crime scene, even if in small quantities (few grams of material).

Forensic analysis of sediments found beneath the soles of shoes, for example, is an important tool for understanding a person's movements before, during, and after that a crime has been committed (Bull and Morgan 2007; Morgan et al. 2009). Granulometric, morphological and mineralogical study of sediments and their possible mixing with other materials, different from those present in the crime scene, is, in fact, one of the most effective methodologies to obtain significant clues for the resolution of a judicial case.

Some of this information can be obtained observing and comparing the characteristics of the materials using image analysis, the results of which can then be used for further analysis using more in-depth investigation techniques.

In the following paragraphs, the possible applications of image analyses (on both macroscopic and microscopic images, acquired with stereo microscopes, optical microscopes and scanning electron microscopes) are better detailed.

10.4.1 Applications on Macroscopic Images

Image analysis for the study of natural or artificial materials in forensic science finds its first application on macroscopic images. They can be acquired: (a) directly on the scene of the crime when the amount of sample to analyze is scarce and the collection may prove difficult and cause a dispersion of the material to be analyzed (Baptista et al. 2012); (b) whenever the information on the material to be analyzed (e.g., grain size, grain sorting, etc.) are directly obtainable without further preparation of the sample for observations via microscopy.

Images can be acquired using a camera *in situ* or in the laboratory (if it is possible to collect the material), and directly processing digital images without further sample preparation.

The advantages of this type of analysis consist precisely in the rapidity of data acquisition, and in the possibility to analyze a sample for which a specific preparation is not required.

The main applications regard the study of loose clastic material, for which the analysis of particle size allows to obtain information on grain-size distribution, a relevant opportunity to better understand the nature of the analyzed material. As

demonstrated for the study of fluvial or marine sediments (Baptista et al. 2012; Buscombe 2008; Chang and Chung 2012), the analysis of digital images acquired directly *in situ*, and therefore at the crime scene, has the advantage of not causing disturbance of the state in which the material is located, allowing, also, to have information on its grain-size and morphology.

If the information sufficient for the investigation concerns precisely these two parameters (grain size and morphology), the images captured with the camera at the crime scene can then be analyzed without the need to collect the sample and processed by dedicated software. On the other hand, samples can be collected and analyzed in laboratory, where new and interesting insights can be revealed from the analysis of macroscopic images (see Procter et al. 2019).

Although advantageous, this type of approach can be addressed only to materials visible to the naked eye. Morphological features and grain-size of particles can be obtained but other information that better defines the origin of the material such as, for example, the mineralogical assemblage of the material or the texture of the grains (Bull and Morgan 2007), remains obscure.

Analysis of Macroscopic Images of Soils on Clothing (Procter et al. 2019)

Soil forensics has proven helpful in assisting criminal investigation, and there is an increasing demand for experimental studies on such trace evidences.

In forensic scenarios, soils are frequently recovered from artefacts and clothing that may be used to link or eliminate potential scenes of crime from suspects and victims. At the scene of a crime, in fact, soil can transfer on clothing materials of the victim or perpetrator. In the specific case of clothing, trace soil evidence including pollen and mineralogical profiles have been recovered from clothing and shoes, even after cleaning in a washing machine and dry cleaning.

This highlights the importance of understanding soil as a forensic trace evidence, and its relationship with evidentiary materials such as clothing. However, there is a complex relationship between soil transfer and clothing material type; soil moisture content and soil type were found to have a greater influence on the transfer of soils overall.

Image analysis can be used to quantitatively determine the amount of soil transferred to different materials (i.e., cotton, denim, fleece, nylon, leatherette) by calculating the total percentage cover of soil on the fabric (Fig. 10.8).

Adjusting the threshold of macroscopic images of experimental replicas (Fig. 10.8), it was highlighted the soil from the background clothing material. Pixels containing transferred soil were counted, enabling to calculate the total area of soil-stained material, as a percentage of the total area of material in contact with the soil. The image threshold was adjusted manually, with the user determining when the software had picked up all of the transferred soil and excluded background noise.

(continued)

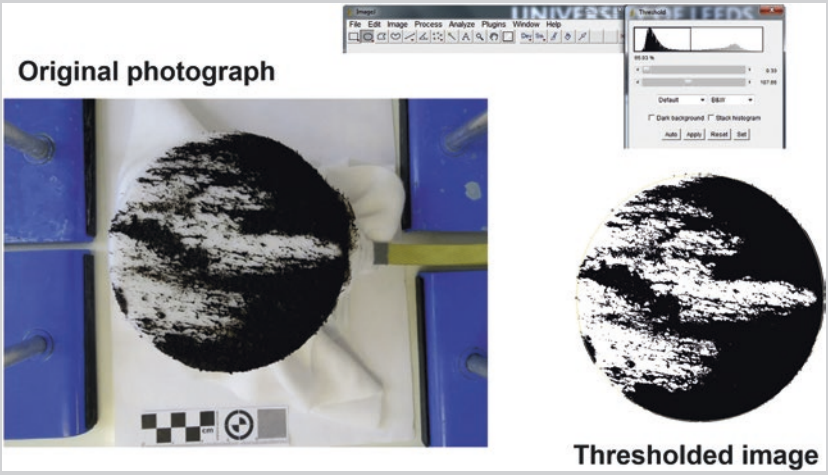

Fig. 10.8 Original photograph and adjusted image threshold (in ImageJ), which highlighted only the soil on the photograph (Modified after Procter et al. 2019)

10.4.2 Applications on Images Acquired in Stereomicroscopy

In order to obtain a "realistic" view of the analyzed material at higher magnifications without any specific preparation, sample can be observed by using a stereo microscope, which allows to evaluate the characteristics of the sample not visible to the naked eye.

Whenever the material can be taken from the scene of the crime, in fact, it can be subjected to the analysis in stereoscopy without any preliminary treatment that could modify or even destroy the sample. A stereo microscope is equipped with objectives with fixed magnification that allow to obtain detailed images of the observed sample, acquired by cameras directly connected to the microscope (Di Maggio 2019).

The advantage of stereomicroscopy is the possibility to acquire images of the sample "as it is" at higher magnifications, obtaining more detailed information than those acquired with the naked eye. Moreover, repeatability in the execution of the analysis, represents another important aspect.

Applications of image analysis on images acquired in stereomicroscopy mainly concern the study of morphological features of particles present in the geological material and/or artificial geomaterial (e.g., the aggregate in mortars or plasters). In addition, observations in stereomicroscopy can be performed on material subjected to washing and/or sieving. In this way, it is possible to observe each particle size fraction and analyze its characteristics.

However, stereomicroscopy does not allow to precisely investigate the mineralogical nature of the sample under examination, for which, however, is necessary a specific procedure of preparation of the sample (i.e., thin sections).

10.4.3 Applications on Images Acquired in Optical Microscopy

More detailed information can be provided if suitable and representative quantity of material is investigated by means of optical microscopy. However, this type of analysis requires a specific sample preparation by making a thin section, a procedure that irreversibly compromises the integrity of the sample itself. Therefore, it is advisable to carry out this type of analysis if the amount of sample is sufficient to replicate experiments with other analytical techniques or if it is strictly necessary to know the mineralogical composition of a sample.

Optical microscopy is an elective technique for the identification of minerals present in the examined material (Cucciniello et al. 2019). As specified in the Chapter dedicated to the Optical Microscopy, the images are captured by a camera placed after the objectives of a polarizing microscope; it is possible to acquire multiple photos and then make a collage, in order to view a surface as large as possible.

After acquiring the images, they can be imported by the software dedicated to the image analysis (e.g., ImageJ) and, through manual contouring procedures or semi-automatic filtering/segmentation/editing, it is possible to measure all the necessary parameters described in the paragraph 10.3.

The limitation of this technique consists in the approximation of the two-dimensional (actually three-dimensional) object that is observed.

10.4.4 Applications on Images Acquired in Scanning Electron Microscopy

The scanning electron microscopy is certainly among the most elective analytical techniques for observation of samples because it allows to obtain detailed images at very high magnifications.

In a scanning electron microscope, the sample (even in thin section) is subjected to a line-by-line scan by the electron beam. The sample re-emits different types of signals, namely backscattered electrons (BSE), secondary electrons (SE), X-rays and other signals that, if picked up with dedicated detectors, permit the investigations of textural and micro-structural features of the sample, as well as its chemical (EDS/WDS) and mineralogical composition (EBSD – electron backscattered diffraction) (Petrosino et al. 2019).

The preparation of the sample is relatively easy: sample requires appropriate metallization with graphite or other conductive material (e.g., gold). It is worth to note that VP-SEM (Variable Pressure-SEM) and E-SEM (Environmental-SEM) are

able to investigate and analyze uncoated and even wet samples by creating a gaseous environment in the specimen chamber. These instruments allow observation of specimens in their natural state.

Since the wavelength of electrons is shorter than that of photons, the resolution of a SEM is significantly higher than that of an optical microscope. In addition, high depth of field of SEM also permits acquisition of perfect images, even for three-dimensional samples.

The topographic (SE) and compositional (BSE) images are in gray scale; for the former, grey shades are due to the intensity of the secondary electron signals released by the three-dimensional samples (areas in relief release very strong SE signals, so they appear lighter). By contrast, for BSE images the penetration of the electron beam depends on atomic number of the elements present in the sample (the lighter is the element, the darker is the material containing it and vice versa). Thus, BSE images obtained by SEM show a gray scale that is a function of the chemical composition of the material itself.

Numerous studies have been conducted in order to automate the recognition of the mineralogical phases of a natural specimen and to determine its textural characteristics. These procedures range from acquisition to gray-level reduction, noise elimination, threshold selection, and grain contouring (Peregrina-Barreto et al. 2013).

Images acquired using SE provide greater definition and depth of field on unprepared samples and, therefore, allow more accurate measurement on shape and morphology of particles. An interesting applications concerns quartz crystals from soils recovered from hypothetical crime scenes (Morgan et al. 2019).

Analysis of SEM Images for Investigating Quartz Grain Textures (Morgan et al. 2019)

The value of environmental evidence for reconstructing journey histories has significant potential given the high transferability of sediments and the interaction of footwear with the ground.

In this perspective, experimental studies were designed to address the transfer and persistence of sediments on the soles of footwear in forensically relevant scenarios, by means of quartz grain surface texture analysis; this technique has been demonstrated to be able to distinguish between samples of mixed provenance. Soil traces adhering to sole portions, removed by a careful brushing, have been compared with sediment samples taken from three sites exhibiting different geological features within the United Kingdom representing hypothetical pre-, syn- and post-forensic event locations (Fig. 10.9a).

Site A is an area composed of undifferentiated Triassic sediments of a fine–grained nature. Site B, the hypothetical crime scene, was an area geologically different from Site A, consisting in complex sedimentary belts including conglomerates, sandstones, and shales with occasional thin impure limestones and beds of chert (i.e., Millstone Grit series). Site C was a walking area where predominantly outcrop clays and bands of sandy soils.

(continued)

All these sediments contain quartz grains that were prepared for a careful evaluation of their surface textures on SEM. Images analyses of these surfaces revealed different morphological features, representative of different sedimentary processes (Fig. 10.9b–e).

These results provide insights on the dynamics of sediment transfer and persistence in forensically relevant contexts and enable inferences to be made about mixed source sediments that were identified on footwear. Such information may represent an empirical basis for assessing the significance of such sediment particles for a specific forensic reconstruction.

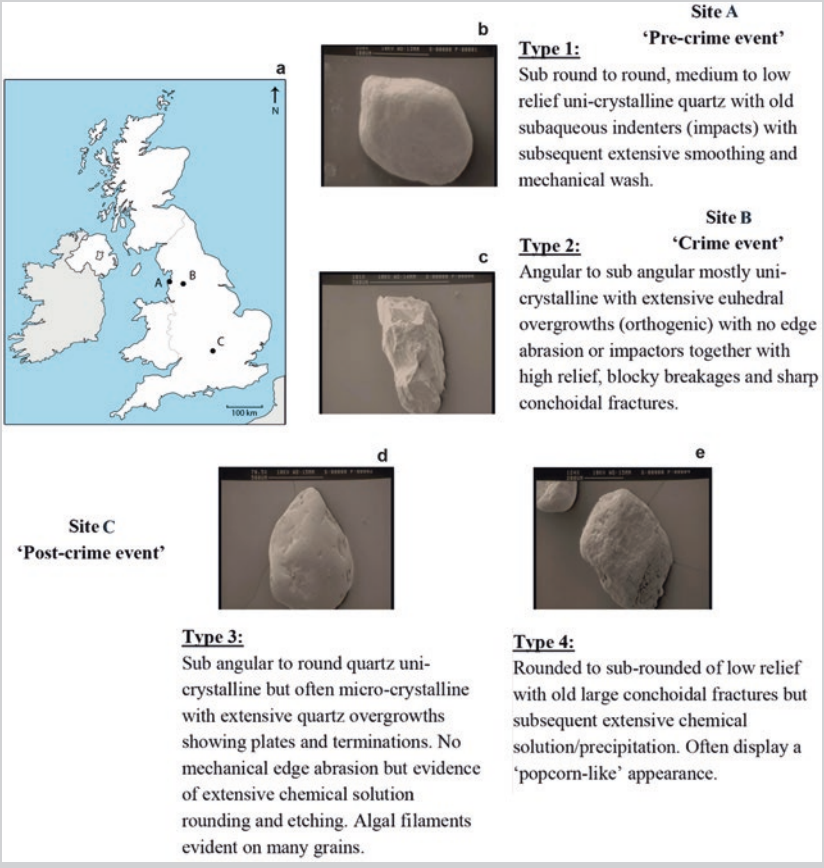

Fig. 10.9 (**a**) Map of three sites. Site A: coastline of Lytham St. Annes, north-west UK; Site B: Sunnyhurst Woodland, North West Pennines in Blackburn, Lancashire, UK; Site C: Shotover Hill park and woodland, Oxford, UK; (**b**) Quartz grains from site A; (**c**) Quartz grains from site B; (**d**, **e**) Quartz grains from site C. (Modified after Morgan et al. 2019)

Another interesting application in forensic since deriving from SEM analyses concerns the investigation of morphological features of gunshot residues, which present specific morphological and chemical peculiarities (Brozek-Mucha 2014).

Analysis of Gunshot Residues (Brozek-Mucha 2014)

A suspect was apprehended within 10 h after the shooting incident. Specimens of gunshot residues were collected from his hands and additionally his clothing was secured as the evidence. Items were analyzed with the question, whether gunshot residue is present on them.

Gunshot residue produced when a firearm is discharged disperses in the close vicinity of the firearm, and settles on, e.g., the skin and clothing of the person carrying out the shooting. Revealing both uncommon chemical and physical properties, organic and inorganic residue, whenever detected, can be used in forensic reconstructions of incidents involving firearms. For this reason, gunshot residues belong to the criminalistic traces of the greatest evidential value.

The application of a specific analytical method suitable for chemical and morphological examinations of the primer residue particles, such as scanning electron microscopy coupled with energy dispersive X-ray spectrometry (SEM-EDS) is of great importance for forensic science examiners.

Whereas for specimens collected from the suspect's hands the results obtained with SEM-EDS analysis were negative, small numbers of particles revealing spherical morphology and containing lead, antimony and barium were found in the specimens collected from the surface of the clothing (Fig. 10.10).

This evidence enabled to attest the persistence of gunshot residue particles showing that, although they can be lost from hands after few hours, they may remain for longer times on clothing.

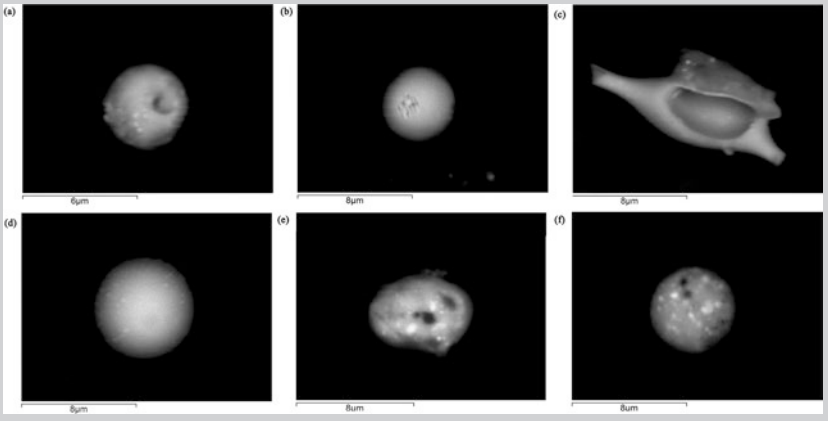

Fig. 10.10 The backscattered electron images of particles revealed in the specimens collected from clothing of the suspect: jacket (**a**, **b**), trousers (**c**, **d**) and baseball cap (**e**, **f**). (Modified after Brozek-Mucha 2014)

Coupling SEM equipment with special detectors has also made it possible to develop procedures suitable both for a more precise geometric and morphological definition of the particles and also for their quantification. This is the case of coupling SEM with EDS and WDS detectors, which allows chemical characterization (qualitative and quantitative) of investigated substances. This equipment is able to perform punctual chemical analysis, along lines or on areas of the sample; this last application allows to obtain images in false colors of the distribution of the chemical elements present in the observed particles.

In particular, an evolution of chemical mapping is the QemSCAN (see Chap. 3) system that, applied in forensic science, can offer interesting results on soils or powders, developing a fully automated system that overcomes the general problems of identification of minerals when small quantities of material are available, providing useful morphological and textural parameters.

References

Baptista P, Cunha TR, Gama C, Bernardes C (2012) A new and practical method to obtain grain size measurements in sandy shores based on digital image acquisition and processing. Sediment Geol 282:294–306. https://doi.org/10.1016/j.sedgeo.2012.10.005

Battiato S, Galvan F, Jerian M, Salcuni M (2013) Linee guida per l'autenticazione forense di immagini. In: IISFA Memberbook, pp 125–176

Brozek-Mucha Z (2014) On the prevalence of gunshot residue in selected populations – an empirical study performed with SEM-EDX analysis. Forensic Sci Int 237:46–52. https://doi.org/10.1016/j.forsciint.2014.01.020

Bull PA, Morgan RM (2007) Sediment fingerprints: a forensic technique using quartz sand grains – a response. Sci Justice 47:141–144. https://doi.org/10.1016/j.scijus.2007.08.001

Buscombe D (2008) Estimation of grain-size distributions and associated parameters from digital images of sediment. Sediment Geol 210:1–10. https://doi.org/10.1016/j.sedgeo.2008.06.007

Chang FJ, Chung CH (2012) Estimation of riverbed grain-size distribution using image-processing techniques. J Hydrol 440–441:102–112

Cucciniello C, Fedele L, Morra V (2019) Microscopia ottica. In: Mercurio M, Langella A, Di Maggio RM, Cappelletti P (eds) Analisi Mineralogiche in Ambito Forense. Aracne Editrice, Latina, pp 43–82

da Silva EAB, Mendonça GV (2005) Digital image processing. In: Chen W-K (ed) The electrical engineering handbook. Academic, Burlington, pp 891–910. https://doi.org/10.1016/B978-012170960-0/50064-5

Di Maggio RM (2019) Stereomicroscopia. In: Mercurio M, Langella A, Di Maggio RM, Cappelletti P (eds) Analisi Mineralogiche in Ambito Forense. Aracne Editrice, Latina, pp 23–42

Francus P (1998) An image-analysis technique to measure grain-size variation in thin sections of soft clastic sediments. Sediment Geol 121:289–298. https://doi.org/10.1016/S0037-0738(98)00078-5

Gawenda T, Krawczykowski D, Krawczykowska A, Saramak A, Nad A (2020) Application of dynamic analysis methods into assessment of geometric properties of chalcedonite aggregates obtained by means of gravitational upgrading operations. Fortschr Mineral 10:180. https://doi.org/10.3390/min10020180

Germinario C, Grifa C, Di Maggio RM (2019) Analisi d'immagine. In: Mercurio M, Langella A, Di Maggio RM, Cappelletti P (Eds.), Analisi Mineralogiche in Ambito Forense. Aracne Editrice, Latina, pp 429–452. https://doi.org/10.4399/9788825522358X

Goins E, Reedy CL (2000) Digital image analysis in microscopy for objects and architectural conservation. Obj Spec Gr Postprints 7:122–137

Gonzalez RC, Woods RE (2018) Digital image processing, 4th edn. Pearson

Grace JR, Ebneyamini A (2021) Connecting particle sphericity and circularity. Particuology 54:1–4. https://doi.org/10.1016/j.partic.2020.09.006

Krumbein WC, Sloss LL (1963) Stratigraphy and sedimentation, 2nd edn. Freeman, San Francisco

Lewis T, Francus P, Bradley RS, Kanamaru K (2010) An automated system for the statistical analysis of sediment texture and structure at the micro scale. Comput Geosci 36:1374–1383. https://doi.org/10.1016/j.cageo.2010.03.018

McAndrew A (2021) A computational introduction to digital image processing. Chapman and Hall/CRC

Morgan RM, Freudiger-Bonzon J, Nichols KH, Jellis T, Dunkerley S, Zelazowski P, Bull PA (2009) The forensic analysis of sediments recovered from footwear. In: Ritz K, Dawson L, Miller D (eds) Criminal and environmental soil forensics, pp 253–269. https://doi.org/10.1007/978-1-4020-9204-6_16

Morgan RM, Scott KR, Ainley J, Bull PA (2019) Journey history reconstruction from the soils and sediments on footwear: an empirical approach. Sci Justice 59:306–316. https://doi.org/10.1016/j.scijus.2018.11.002

Peregrina-Barreto H, Terol-Villalobos IR, Rangel-Magdaleno JJ, Herrera-Navarro AM, Morales-Hernández LA, Manríquez-Guerrero F (2013) Automatic grain size determination in microstructures using image processing. Measurement 46:249–258. https://doi.org/10.1016/j.measurement.2012.06.012

Petrosino P, de Gennaro R, Mondillo N (2019) Microscopia elettronica a scansione. In: Mercurio M, Langella A, Di Maggio RM, Cappelletti P (eds) Analisi Mineralogiche in Ambito Forense. Aracne Editrice, Latina, pp 169–217

Procter FA, Swindles GT, Barlow NLM (2019) Examining the transfer of soils to clothing materials: implications for forensic investigations. Forensic Sci Int 305. https://doi.org/10.1016/j.forsciint.2019.110030

Rasband WS (1997–2018) ImageJ. U. S. National Institutes of Health, Bethesda, Maryland, USA. https://imagej.nih.gov/ij/

Stern EJ, Richardson ML (2003) Preparation of digital images for presentation and publication. Am J Roentgenol 180:1523–1531. https://doi.org/10.2214/ajr.180.6.1801523

Sun Q, Zheng J, Coop MR, Altuhafi FN (2019) Minimum image quality for reliable optical characterizations of soil particle shapes. Comput Geotech 114:103110. https://doi.org/10.1016/j.compgeo.2019.103110

Terry RD, Chilingar GV (1955) Summary of "Concerning some additional aids in studying sedimentary formations" by M.S. Shvetsov. J Sediment Petrol 25:229–234. https://doi.org/10.1306/74D70466-2B21-11D7-8648000102C1865D

Tuba M, Jordanski M, Arsic A (2016) Improved weighted thresholded histogram equalization algorithm for digital image contrast enhancement using the bat algorithm. In: Yang X-S, Papa JP (eds) Bio-inspired computation and applications in image processing. Academic, pp 61–86. https://doi.org/10.1016/B978-0-12-804536-7.00004-1

Zhang H, Chiu Y-J, Fan J (2020) A novel relative homogeneity thresholding method with optimization strategy. Neural Comput & Applic 32:8431–8449. https://doi.org/10.1007/s00521-019-04333-3